Assessing Radarsat-2 Polarimetric SAR for Mapping Shoreline Cleanup and Assessment Technique (SCAT) Classes in the Canadian Arctic

by

Sarah N. Banks

A thesis submitted to the Faculty of Graduate and Postdoctoral Affairs in partial fulfillment of the requirements for the degree of

Master of Science

in

Geography

Carleton University
Ottawa, Ontario

Library and Archives Canada

Published Heritage Branch

395 Wellington Street
Ottawa ON K1A 0N4
Canada

Bibliothèque et Archives Canada

Direction du Patrimoine de l'édition

395, rue Wellington
Ottawa ON K1A 0N4
Canada

Your file Votre référence
ISBN: 978-0-494-93624-5

Our file Notre référence
ISBN: 978-0-494-93624-5

Abstract

With the potential for a greater human presence and increased development of natural resources, culturally and biologically sensitive shorelines in the Arctic may face increasing risk of environmental emergencies. To establish response contingency plans it is necessary to improve upon available shoreline maps. This study assessed the potential for automated classification of Arctic shore and nearshore land covers using polarimetric Radarsat-2 imagery. Repeatability and optimal acquisition parameters (incidence angle and polarization) were evaluated through comparison of multiple incidence angle images acquired over two study areas in the southern Beaufort Sea, Northwest Territories, Canada. Analyses of backscatter coefficients and decomposition parameters showed that shallow angles are generally preferred, and that discrimination of a number of land covers (including: sand, mixed sediment, herbs, shrubs, and wetlands) is possible.

Acknowledgements

Support for this thesis was provided by Carleton University and the National Wildlife Research Centre, as part of the Emergency Spatial Pre-SCAT for Arctic Coastal Ecosystems (e-SPACE) project. I would like to thank those providing this support, as well as all of my committee members, family and friends.

Table of Contents

List of Tables

List of Figures

1. Introduction

In recent years the need for better monitoring and protection of the Arctic has been a concern at the international level. This is in part due to rising interests in the economic potential of the North, which may result in increased shipping traffic and natural resource development, including: minerals, fish, oil and gas (Carnaghan & Goody, 2006). A greater human presence in the Arctic is also expected due to issues related to sovereignty and increasing global temperatures that may permit greater accessibility, with longer open water seasons. This places culturally and ecologically significant shorelines at risk of environment emergencies, such as oil spills.

In order to establish emergency response contingency plans, as well as monitor environmental conditions and map species habitat, it is necessary to establish basic land cover maps of Arctic shorelines. In the event of a spill, these could be used to define priority protection areas as well as improve response efficiency in order to reduce long term impacts. In Canada, this information is required by federal government bodies to meet legislative requirements, since in the event of a spill it is the responsibility of Environment Canada's Environmental Emergencies Branch to monitor cleanups and provide guidance to responsible parties.

To do this, they typically rely on pre-spill databases or shoreline sensitivity maps, which by convention are consistent with the Shoreline Cleanup Assessment Technique (SCAT). SCAT is a survey method implemented following spills to map shoreline types, and assess oiling conditions in order to determine cleanup strategies. Mapping shorelines that are consistent with this technique allows responders to readily allocate some cleanup

and or protection method for each shoreline segment. Shoreline type in this sense refers to the overall geomorphology and or primary substrate, including: human-made surfaces, sand beach, peat beach, marsh, etc. (Owens & Sergy, 2004).

While these and similar indices and maps exist for many areas throughout North America, including Alaska, major information gaps remain for Arctic Canada. This is largely a result of logistical issues associated with the current mapping method, which is based on the manual interpretation of low altitude, oblique helicopter videography. Not only can map accuracy be affected by video quality and interpreter bias, but these methods are also costly and labour intensive, especially along complex or sinuous shorelines. Flights are also limited to ideal weather conditions, low tides, and the flight range of the helicopter. In the Arctic for example, fuel caching is commonly required to travel a substantial distance, since there are few refueling stations. Additionally, dynamic shorelines such as those present in the outer Mackenzie Delta, also require frequent updates.

There is potential to improve the efficiency of mapping these dynamic and remote Arctic shorelines through the use of Earth Observation data. This study focuses on assessing the potential for mapping SCAT land cover classes using data that are available at an operational level to federal government agencies; specifically, fine-quad Radarsat-2 imagery. Radar imagery provides a number of benefits over optical imagery, and this is primarily based on the type of sensors used, which actively transmit their own energy source to illuminate the surface. This allows for acquisitions at any time of day or night. Sensors also use longer wavelengths (defined subsequently) that are not affected by clouds or haze. This is significant for Arctic coastlines, which are subject to persistent

cloud cover, as well as non-existent to low lighting conditions during the winter months.

Establishing, and or improving existing pre-spill indices and maps are also especially beneficial in Arctic environments because response efforts are complicated by harsh environmental conditions and limited accessibility. As an example, it is harder to detect and map the extent of an oil spill in ice covered water, making it difficult to allocate personnel and equipment, as affected areas may be far from the spill source (DF, 2004). Low lighting conditions, low temperatures, and high winds also pose greater risk to personnel that have to be in the field for extended periods of time. Colder temperatures also slow the natural biodegradation of oil (Atlas, 1981).

Earth Observation data are well suited to broad scale mapping, since imagery can be acquired remotely over large areas, and with automated processing techniques can be used to generate products more cost-effectively than helicopter videography, with less bias also, than manual interpretation. The use of radar imagery is also more cost effective than conventional shoreline mapping methods as it is readily available to the Canadian federal government. Radar is also well suited to the identification of some important land cover classes based on its sensitivity to roughness (Baghdadi et al., 2002) and moisture (Henderson & Lewis, 2008).

As an example, for the SCAT classification process it is important to differentiate beaches and flats on the basis of grain size (e.g. sand versus mixed sediment) since oil tends to penetrate porous materials, making it more difficult to clean (Owens & Sergy, 2000). There is a substantial basis in the literature for substrate mapping using radar, since differences in texture have been shown to have a significant impact on backscatter, with rougher surfaces typically showing higher values than smoother surfaces (Derion et

al., 1997; Singhroy & Saint-Jean, 1999; Dong & Leblon, 2004; Paradella, et al., 2009).

Additionally, there is typically an increase in backscatter over wet compared to dry surfaces, which is a major physical difference between wetlands and other vegetated areas. These land cover types are some of the most sensitive to the effects of oil, since they typically provide important species' habitat and are also low energy environments (Owens & Sergy, 2000). This can increase the residence time of oil, since natural removal by wave action is negligible in comparison to shoreline features such as a beach. There is also a substantial basis in the literature for the use of radar for wetlands mapping (Henderson & Lewis, 2008).

1.1 Research Goal and Objectives

The overall goal of this research was to assess Radarsat-2 polarimetric SAR for discrimination of SCAT land cover classes in the Arctic. The specific objectives were to:

1) Determine optimal image acquisition parameters, including incidence angle and polarization.
2) Determine optimal image processing techniques and parameters to discriminate classes.
3) Determine dominant scattering mechanisms, average backscatter coefficients and the polarimetric behaviour of classes.
4) Assess potential for broad scale mapping by comparing results from objectives 1 to 3 between two study areas.
5) Determine potential for land cover mapping with the Wishart-entropy/alpha and Wishart-entropy/anisotropy/alpha classifiers.
6) Determine optimal parameters for classification from: a) HH, HV, and VV

backscatter coefficients, and b) incoherent decomposition parameters derived from the Freeman-Durden and Cloude-Pottier decompositions.

7) Assess the potential for classification of a) optimal radar parameters, b) pan sharpened SPOT-4 spectral bands, and c) combined radar and SPOT-4 data as inputs to the Maximum Likelihood Classifier.

The results were intended to inform research related to Environment Canada's Emergency Spatial Pre-Scat for Arctic Coastal Ecosystems (e-SPACE) project, designed to improve methods of mapping SCAT classes before an emergency event, and the major source of funding and logistical support for this research. Additionally, this study addresses a gap in the literature as these types of analyses have not been widely conducted in Arctic environments.

1.2 Thesis Structure

The following section (Chapter 2) provides a background of the SCAT method and shoreline sensitivity mapping, radar polarimetry, and a summary of the literature on radar remote sensing, focussing on studies of relevance to the SCAT land cover types of this research. Chapter 3 outlines the methods used in this analysis. Results and discussion are presented in Chapters 4 and 5, while study limitations and conclusions are summarized in Chapters 6 and 7.

2. Background

2.1. Shoreline Sensitivity Mapping and the Shoreline Cleanup and Assessment Technique (SCAT)

In the wake of the Exxon Valdez oil spill off the coast of Alaska and Nestucca spill off the Coast of Washington state in 1989, specific protocols were developed to document and describe oiled shorelines. With contributions from Environment Canada these would later develop into the Shoreline Cleanup and Assessment Technique (SCAT). By 1994, a standardized field guide was developed so methods could be applied consistently, regardless of location and response team (Owens & Sergy, 1994). Since then, a number of agencies throughout North America have adopted the SCAT approach and have worked towards continued method standardization (Owens & Sergy, 2000). This work is motivated by the following: 1) oil deposits are typically non-uniform in the affected area, 2) the affected area can be extensive, making logistical requirements difficult to assess, 3) if identified, the most sensitive shorelines in terms of biological and or human resources can be prioritized for protection and cleanup, and 4) responders require specific information for operational level decisions (Lamarche et al., 2007).

Many organizations have also moved towards maintaining and establishing pre-spill databases, which reduce environmental impacts by making response and cleanup efforts more efficient (Lamarche et al., 2003). For almost 30 years, audio commentaries and helicopter videography acquired at 60 to 80 knots and 100 m altitude have been used for this purpose (Owens, 1983). Pre-spill databases (as well as SCAT surveys), may also be based on field data or a combination of field data and aerial surveys. Initially these databases were stored as paper atlases, but today most agencies use Geographic

Information Systems (GIS) (Percy et al., 1997; Laflamme & Percy, 2003; Lamarche et al., 2007). This enables quick access and ready dissemination of data to all responsible parties. There still remain a number of limitations associated with current mapping methods however, including: 1) it is expensive and time consuming, 2) the experience of the videographer largely determines video and map quality, and 3) acquiring videography is difficult to plan logistically, as it requires the timing of acquisitions with tides (Lamarche et al., 2007).

To generate a pre-spill database, Environment Canada's Environmental Emergencies Branch typically transfers information recorded during helicopter videography surveys into a GIS, using the hydrographic vector layers provided with Canvec products (cartographic products in digital format, freely available from Natural Resources Canada). To do this, the interpretation of videography relies heavily on the ability to link video segments with precise ground locations. Ideally this is achieved through continuous collection of GPS waypoints during flights, which can then be overlaid onto Canvec layers. Based on this association of video segments with portions of the vector, the interpreter manually cuts the shoreline into homogeneous segments by substrate type and physical features, or overall geomorphology. This allows response and cleanup efforts to be tailored to individual areas (Owens & Sergy, 2004).

To populate the attribute table associated with each vector, the interpreter must also consider the shoreline in terms of across shore units. The first three are within the inter-tidal zone or the area which is exposed at low tide and covered by water at high tide, including: 1) the lower intertidal zone, representing the bottom third of the inter-tidal zone, 2) the mid intertidal zone, representing the middle portion of the intertidal zone,

and 3) the upper intertidal zone, which ends at the mean high water line. Beyond the upper intertidal region is the supratidal zone. This area is affected by wave action and spray, and in the Beaufort Coastland, periodic storm surges as well. Beyond this is the backshore, which is not affected by marine processes, but may be of importance for access to a coastal site in the event of an environmental emergency (Lamarche et al., 2007).

For each shoreline vector representing a homogeneous area, the two most important descriptors are the shoreline type and character. The former usually refers to the primary substrate type of the upper intertidal zone, while the latter is typically used to describe the physical characteristics of the shoreline, which is used in decision making processes related to access and staging for cleanup. In some databases and where the information is available, each across shore zone is also given a shoreline type; however, it is most important to have this information for the upper intertidal zone, since this is the most likely place where oil will become stranded, and the substrate type is important as it affects surface penetrability.

19 different shoreline types are currently used by Environment Canada (Table 1), three of which have been recently added to describe Arctic shorelines specifically, including: Tundra Cliffs, Peat Shorelines, and Inundated Low Lying Tundra (Owens & Sergy, 2004). Other data that are typically included in pre-spill databases are related to environmental sensitivity and logistical information such as: road access, amount and type of debris present, as well as zone width and length (Owens, 2010).

Table 1: The primary shoreline types and characters utilized in pre-spill databases by Environment Canada's Environmental Emergencies Branch. Recreated after Lamarche et al. (2007).

Shoreline Types	
1) Human-made Solid	11) Sand Tidal Flat
2) Bedrock	12) Mixed and Coarse Sediment Tidal Flat
3) Glacier Ice	13) Intertidal Boulder Barricade
4) Ice Shelf	14) Salt Marsh
5) Sand Beach	15) Wetland
6) Mixed Sediment Beach	16) Peat Shoreline
7) Pebble Cobble Beach	17) Ice-Rich Tundra Cliff
8) Boulder Beach	18) Ice-Poor Tundra Cliff
9) Mud Tidal Flat	19) Inundated Low Lying Tundra
10) Fine-Grained Scarred or Ridged Shore	
Shoreline Characters	
1) Human-made	8) Beach
2) Cliff/Hill	9) Delta
3) Sloped	10) Dune
4) Raised Beach Ridges and Sloped	11) Lagoon
5) Low Lying Tundra	12) River Inlet/Channel
6) Eroding Tundra	13) Wetland
7) Flat/Lowland	

2.2. Radar Remote Sensing and Radar Polarimetry

Radar remote sensing may be well suited to detecting and differentiating a number of SCAT land cover classes, as well as contributing to the development of an automated process that could be used for broad scale mapping. To demonstrate this, this section first summarizes some theory of radar remote sensing and polarimetry.

2.2.1. Radar Remote Sensing

Radio detection and ranging or radar is a method of remote sensing, whereby electromagnetic radiation (EMR) within the microwave portion of the spectrum is transmitted from a sensor to illuminate a surface, and record that which is scattered back in the direction of the sensor (known as backscatter). In contrast, optical sensors rely on

the sun as an illumination source and passively record radiance that is reflected (or for thermal infrared, emitted) from the surface. Optical sensors also operate at smaller wavelengths (~0.3 - 12 μm) compared to microwave sensors (~1 mm - 1 m), resulting in different but complementary information being record about the surface. Since sine waves are typically used to approximate the propagation of EMR, wavelength can be defined as the distance between crests or troughs within the same wave cycle. While most optical sensors record energy from multiple wavelengths, most microwave sensors transmit and receive energy that is within one narrow region of the EM spectrum, known as a band. C-band radars for example, utilize EMR around 5.6 cm in wavelength, whereas L-band radars utilize EMR around 23.5 cm in wavelength (Henderson & Lewis, 1996).

A number of other elements separate optical and microwave sensors. As active radar sensors provide their own EMR source, imaging may be done at night and users can optimize acquisition geometry to highlight certain features. An image taken at steep incidence angle for example, typically shows greater sensitivity to soil moisture than one taken at a shallow incidence angle (Ramsey, 1998). Because sensors operate at longer wavelengths, images are also not significantly affected by clouds. Thus, they are well suited to studies along coastal environments, which are subject to persistent cloud cover. The radar signal may also penetrate into certain other media, such as very dry soil or vegetation canopies, providing information on the characteristics within the medium (Sletten & Mc Laughlin, 2005). It is also of interest to note that most sensors today are Synthetic Aperture Radars (SARs). This has allowed for improved spatial resolutions compared to traditional Real Aperture Radars (RARs), through synthesis of longer antennas (Henderson & Lewis, 1996).

2.2.2. Electromagnetic Waves and Wave Polarization

The following section will describe electromagnetic waves and wave polarization theory, which unless otherwise indicated, is largely summarized from Sletten and McLaughlin (2005) and Woodhouse (2006).

Though typically approximated by a single sine wave, EMR is actually made up of both electric (E) and magnetic (M) field waves that oscillate orthogonally to one another. Since E is typically only affected through interactions with natural surfaces, and can be used to approximate M, it is often the only component that is considered. It is also convenient to represent the propagation of EMR on a right-handed Cartesian coordinate system, where the z-axis represents the direction of propagation and lies between the sensor and the surface of interest. The x and y axes can then be used to measure other elements about the wave cycle. To do this E is typically represented by a vector that rotates about the z axis (Figure 1), where the wave amplitude (A) or power, is represented by the length of the vector, and the wave polarization is represented by the shape and orientation that the vector traces (Born & Wolf, 1999).

Figure 1 also shows that two additional sine waves can be fitted to the wave cycle (E_x^o) and (E_y^o), and these are used to characterize movement along the horizontal (x) and vertical (y) axes, respectively. By considering the relative phase between them it is possible to determine the specific polarization state, which can be one of: linear, circular or elliptical. For linearly polarized waves both E_x^o and E_y^o are completely in phase, have the same amplitude and the E vector traces a single line, normal to the direction of propagation. For circularly polarized waves, E traces a circle along the direction of propagation, and both E_x^o and E_y^o components have the same amplitude, with a 90° phase

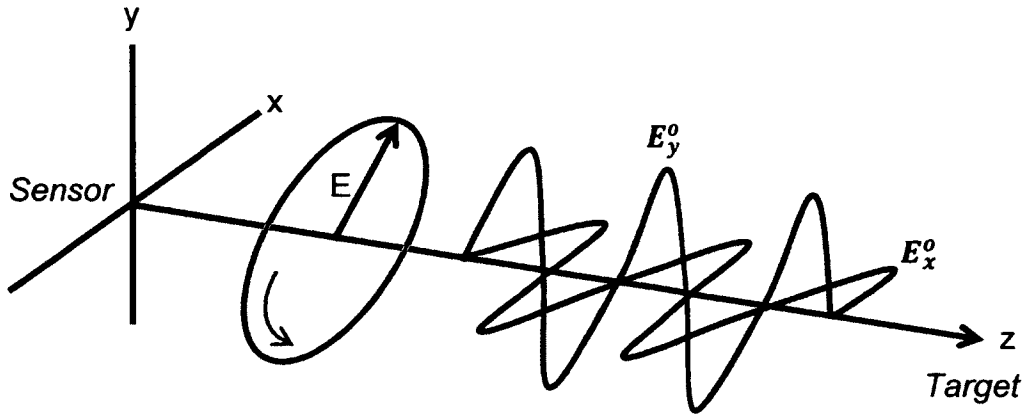

Figure 1: Representation of a the propagation of a microwave, showing the full cycle that the E vector traces (red circle). Two sine waves that can additionally be fitted to the entire wave cycle to characterize movement along the horizontal axis (E_x^o) and vertical axis (E_y^o) are also displayed. Recreated after CCRS (2011a).

difference. Under the Backscattering Alignment (BSA) convention, when the difference is negative the rotation is counter-clockwise if looking from the sensor to the ground, and the polarization is considered right-handed. When the phase difference is positive, the rotation is clockwise and the polarization is considered left-handed (Born & Wolf, 1999). For elliptically polarized waves, E_x^o and E_y^o components have phase differences of between 0° and 90°, as well as different amplitudes.

If the complete wave cycle is projected onto a flat two dimensional surface (Figure 2) a number of parameters can be used to describe the wave: 1) the maximum length of the horizontal component (E_x^o), 2) the maximum length of the vertical component (E_y^o), 3) the orientation angle or psi (Ψ), and 4) the ellipticity or chi (χ). Both Ψ and χ vary based on amplitude and the relative phase of E_x^o and E_y^o. For a linearly polarized wave χ is 0 and Ψ is either 90° for a vertically polarized wave or either 0° or 180° for a horizontally polarized wave. For a circularly polarized wave only χ is needed

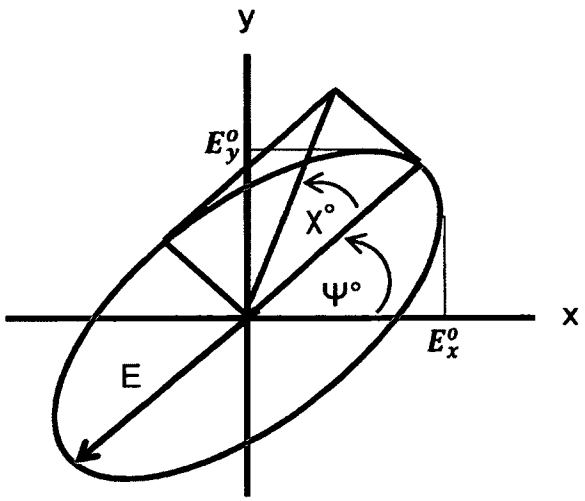

Figure 2: Elliptically polarized wave projected onto a flat two dimensional surface, with the entire wave cycle shown in red. Recreated after CCRS (2011a).

to characterize polarization (χ = -45° for right handed and χ = 45° for left handed), and E_x^o and E_y^o have equal amplitudes. For an elliptically polarized wave both χ and Ψ are needed to characterize the wave cycle and amplitude varies for both E_x^o and E_y^o components.

Early satellite SARs transmitted and recorded energy using one band and polarization. Radarsat-1 for example acquires images at C-band, with linear horizontal polarization for signal transmission and recording. By convention this is denoted as HH, where the first H represents the transmit polarization and the second H represents the receive polarization. Many SARs today are capable of acquiring fully polarimetric imagery, where all possible transmit-receive combinations are recorded for two orthogonal polarization sets, typically linear HH and linear VV. This produces four image bands where HV and VH represent cross-polarizations and HH and VV represent co-polarizations (Touzi et al., 2004). One of the benefits of acquiring fully polarimetric imagery is that it is also possible to characterize inter-channel phase information. These

are the time delays between the transmission and reception of channels due to different surface interactions, which vary depending on the transmitted polarization type, as well as sensor parameters, and surface characteristics (Ulaby et al., 1987). When phase is considered in terms of a wave cycle and 360° degrees represents one full rotation, two waves are considered in phase when both begin at 0° and end at 360° at the same time (Figure 3).

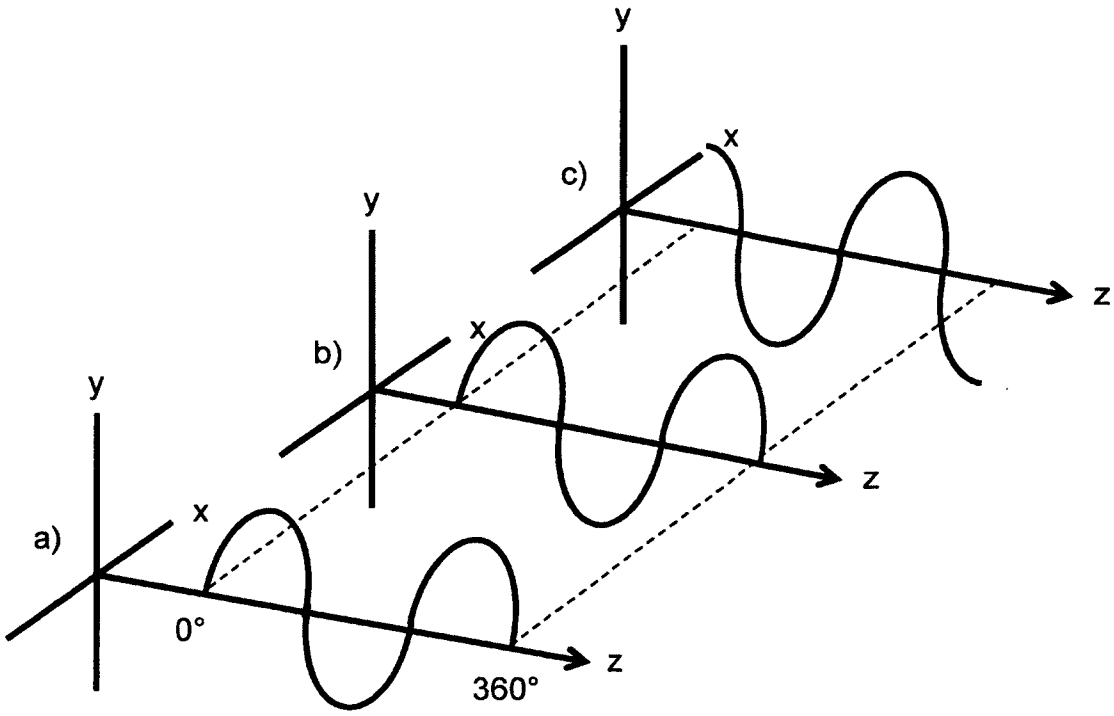

Figure 3: Complete wave cycles (360°) shown for two waves that are in phase (a and b), and one that is out of phase with them (c). Recreated after CCRS (2011a).

2.2.3. Measuring Wave Amplitude and Phase

The scattering matrix is used to store information about the four channels acquired by a fully polarimetric sensor. This includes information about each transmit and receive combination (HH, HV, VH and VV), with both amplitude and phase

information for each wave stored together as complex numbers (Sletten & Mc Laughlin, 2005):

$$S = \begin{bmatrix} S_{hh} & S_{hv} \\ S_{vh} & S_{vv} \end{bmatrix} \quad (1)$$

where h and v represent the wave amplitude and phase, for the transmitted (first subscript) and received (second subscript) waves, respectively. As such, the scattering matrix describes the transformation of the transmitted wave to the backscattered or received wave. Amplitude is also measured in units of voltage and represents the strength or height of the wave. Under most conditions, and when the radar system is monastic (having one antenna for transmitting and receiving); the scattering matrix has only three independent parameters (Henderson & Lewis, 1996). This is known as the reciprocity principle, which assumes $S_{hv} = S_{vh}$. As a result, it is commonplace to average the HV and VH components, which can provide a more reliable estimate of the cross-polarized signal because backscatter coefficients are generally low, and therefore more likely to be affected by instrument and background noise (Woodhouse, 2006).

It is important at this point to note that EMR is typically composed of multiple waves, and as a result can be described as: 1) fully polarized, 2) partially polarized, or 3) completely unpolarized. For fully polarized waves the shape that the E vector traces remains constant over time, and both amplitude and phase information contain little noise. The energy that is transmitted by a sensor for example, is filtered so that only waves of a specific polarization are able to reach the surface. Additionally, some natural surfaces like buildings can backscatter fully polarized waves. These are considered coherent, point targets. Unpolarized waves on the other hand have a completely random

shape and orientation through time. As such, both amplitude and phase information are random. Most natural surfaces produce backscattered waves that are partially polarized. These are considered incoherent, distributed targets, for which amplitude and phase information can be characterized using statistics.

The scattering matrix specifically, can only be used to describe coherent waves and as a result, can only be used to describe backscatter from coherent, point targets. Since this is not typically the response observed over natural surfaces, it is common to generate local statistics through some type of spatial averaging of neighbouring pixels, and convert elements of the scattering matrix to the power domain (amplitude^2, measured in units of watts). Two common matrices used for power representations are the covariance (C) matrix, and the coherency (T) matrix. For details refer to (Cloude, 1985; Cloude & Pottier, 1996). The C matrix is commonly used because the powers recorded from the four possible transmit-receive polarization combinations can be easily extracted, as they are represented on the main diagonal. The sum of these also represents the total power or span of the matrix. Amplitude and power values are also commonly converted to decibels. These represent a ratio of power to some reference. In this case this represents the strength of the backscattered signal recorded by the sensor, to the strength of the incident wave (Henderson & Lewis, 1996):

$$P_{dB} = 10\ log_{10}(\frac{P}{P_{ref}}) \quad (2)$$

where P represents the scattered wave power and P_{ref} represents the transmitted wave power. Decibels specifically are useful for representing a wide range of values and are unitless.

2.2.4. Surface Interactions

Not all energy transmitted from the sensor to the surface is returned as backscatter. It is also possible that upon contact, energy is specularly reflected and or diffusely transmitted to lower layers of the surface. The physical properties of the surface that largely determine surface-microwave interactions, and subsequently the characteristics of backscattered waves, include: 1) surface roughness, 2) sensor parameters, defining sensor to surface geometry, and 3) the complex dielectric constant of the surface (Henderson & Lewis, 1996).

Surface roughness describes height variations of objects at the surface and greatly impacts the amount of energy scattered back in the direction of the sensor. This is a result of roughness largely determining the degree to which reflection is specular or diffuse. Figure 4 shows that over smooth surfaces reflectance is mostly specular, resulting in very little energy being received by the sensor. This produces dark image tones. As roughness increases, reflection becomes more diffuse. This increases the amount of energy backscattered in the direction of the sensor and as a result image tone is intermediate, as there is still some element of specular reflection. Over very rough surfaces reflection is mostly diffuse resulting in bright tones and a substantial amount of energy being scattered in the direction of the sensor (Henderson & Lewis, 1996).

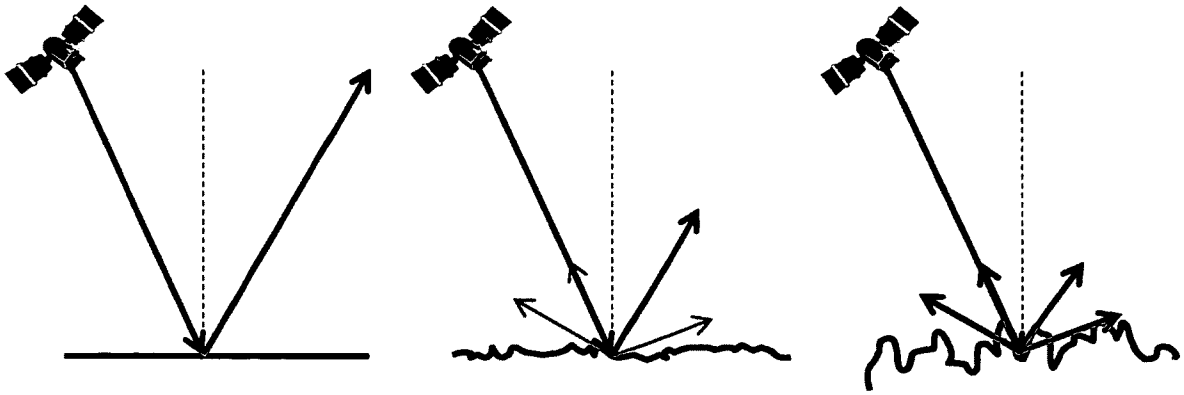

Figure 4: Varying degrees of specular reflection and diffuse scattering with increasing roughness. Left shows mostly specular reflection, the middle shows some specular and some diffuse, and the right shows mostly diffuse scattering. Here blue arrows represent transmitted energy from the sensor, where red arrows represent scattered energy. Recreated after Trevett (1986).

In addition to being related to the orientation and size of physical objects, the impact of roughness is also dependent on wavelength, and sensor-surface geometry, or the angle at which microwaves strike the surface. The latter is measured from nadir and is known as the incidence angle. Perceived image roughness can be approximated using the Peake and Oliver Criterion (Peake & Oliver, 1971):

a) Surfaces appear smooth in radar images if,

$$h_{rms} > \frac{\lambda}{25 \cos \phi} \tag{3}$$

b) Surfaces appear rough in radar images if,

$$h_{rms} > \frac{\lambda}{4.4 \cos \phi} \tag{4}$$

h_{rms} or root mean square of height is often represented as the standard deviation of height. Whether h_{rms} is rough or smooth also depends on wavelength (λ) and incidence angle (ϕ)

as shown in Equations 2 and 3. For example, for a C-band image (λ ~5.6 cm) acquired at an incidence angle of 40°, rms surface variations of less than 0.29 cm would be considered "smooth", while those greater than 1.65 cm would be considered "rough", and values in-between these would be considered "intermediate". These equations show that with increasing wavelength (i.e., from C-band to L-band for example) there is a decrease in the roughness effect on backscatter. It is also important to note that because energy is actively transmitted at some angle to the surface, roughness effects on backscatter are also dependent on the orientation of objects relative to the radar line of sight (Peake & Oliver, 1971). As a result, objects or slopes facing towards the sensor will generally produce more backscatter and be brighter in image tone, than those facing away from the sensor.

The electromagnetic properties of surface materials also affect backscatter. If a material has a high electrical conductivity, incident microwaves cannot significantly penetrate into the surface and as a result, they will not lose a significant amount of energy since they are mostly reflected from the surface. In other words, the more microwaves propagate through a medium; the more energy is lost through wave attenuation and or absorption by the medium. This is typically characterized by the dielectric constant, which for non-perfect conductors, measures the ratio of the relative permittivity of the material to that of free space. Values typically range from 80 for water, representing highly conductive materials, to around 3 for dry soil. (Henderson & Lewis, 1996). As a consequence, the dielectric constant and image brightness for media such as soils generally increase with increasing volumetric moisture content.

For unconsolidated surfaces such as vegetation canopies, penetration of the signal

through small gaps results in interactions with multiple layers, known as volume scattering. Over vegetated areas for example, backscatter contributions may be from the ground surface, trunks, branches and leaves (Henderson & Lewis, 1996). Volume and surface scattering, which can be described as scattering from a medium without much penetration to sub-surface layers, resulting in a relatively direct return towards the sensor, make up two important scattering mechanisms described in radar remote sensing. Another is dihedral or double bounce.

This type of scattering is caused by the incident microwave striking a smooth surface, upon which it is specularly reflected towards another surface that lies about 90° to the first. As an example, this is often observed with over buildings when they are oriented about perpendicular to the radar line of sight (Henderson & Lewis, 1996). Another important scattering mechanism is Bragg scattering, which occurs over periodically rough surfaces. This for example is typically observed over water bodies where periodic waves are present and are oriented perpendicular to the radar line of sight, as well as spaced at about half the wavelength of incidence microwaves. This can enhance backscatter, due to the coherent combination of waves within a resolution cell (Henderson & Lewis, 1996). These and other common scattering processes (described previously) are represented in Figure 5 and should be considered typical responses observed over natural surfaces.

2.2.5. Processing and Analysis of Radar Imagery

2.2.5.1. Image Speckle

Raw radar images have a grainy, "salt and pepper" appearance due to the presence

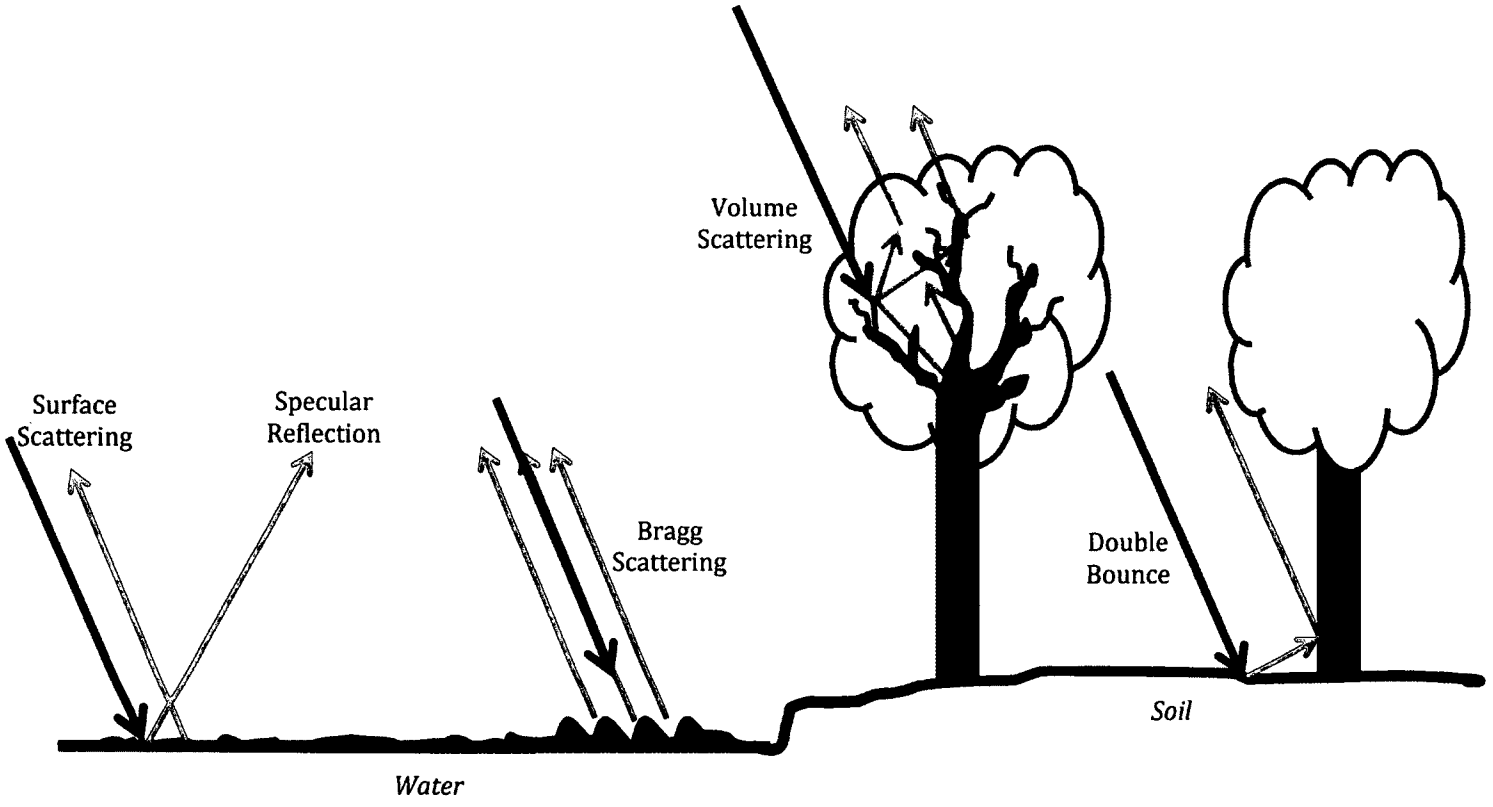

Figure 5: The main scattering mechanisms described in radar remote sensing. Blue arrows represent transmitted energy from the sensor, and red arrows represent scattered energy (Henderson & Lewis, 1996).

of speckle. Speckle results from multiple elements within a resolution cell that, when illuminated by the sensor can produce a number of waves of varying amplitudes and phases that contribute to the total backscatter recorded for that cell. When the amplitudes and phases of these waves are coherently summed, the effect can be a substantial increase in amplitude when backscattered waves are in phase. This is known as constructive interference. Destructive interference on the other hand, results in lower intensity values and occurs when waves are out of phase. As a result of speckle, there is a great degree of pixel to pixel variation in radar image brightness, even over homogeneous surfaces. While this may actually represent information, speckle is commonly treated as "noise" (Woodhouse, 2006).

To reduce the effects of speckle, multiple "looks" can be acquired over the same area and averaged. This results in greater radiometric accuracy, but at a reduced spatial resolution. This type of data is known as multi-look complex (MLC). If only one image is taken during the acquisition, known as single look complex (SLC) data processing, multiple looks can also be synthesized by for example, averaging pixels within a window of a specified size that is passed through the image. It is important when applying speckle filtering that an appropriate window size is selected, as there needs to be a compromise between "noise" reduction and preservation of texture and edges. A window size that is too small for example, will not remove enough speckle, whereas a window that is too large will blur edges and reduce contrast between land covers (Touzi & Lopes, 1994; Lee & de Grandi, 1999).

2.2.5.2. Target Decompositions

Target decompositions are commonly applied to polarimetric imagery to relate observed scattering behaviour to idealised responses. More specifically, the total power of the matrix is partitioned into contributions from a number of different scattering mechanisms. There also exist both coherent and incoherent methods. Coherent methods assume that the backscattered wave is fully polarized, and scattering mechanisms can therefore be characterized by what are known as canonical targets (Kennaugh, 1951; Huynen, 1965; Cameron, 1996). As an example, the response from a dihedral corner reflector (double bounce) is commonly ascribed to the response observed over buildings.

Incoherent decompositions are commonly applied to natural surfaces (as in this thesis), where local statistics (i.e.,, C or T matrix elements) are used to identify scattering mechanisms and other properties about backscattered waves, such as how random the scattering process is (Cloude & Pottier, 1996). Two commonly used incoherent decomposition methods, which are implemented in this thesis, are the Freeman-Durden and Cloude-Pottier decompositions (described subsequently). Due to space limitations the complete theory of these decompositions is not presented here, though can be found in (Cloude & Pottier, 1996; Freeman & Durden, 1998).

Freeman-Durden Decomposition

The Freeman-Durden method, which is a model-based decomposition that was developed as an extension of the van Zyl decomposition, is based on the symmetrized C matrix (van Zyl J. J., 1989; Freeman & Durden, 1998). Where the van Zyl decomposition assigns each pixel in an image one of three scattering mechanisms (surface, double bounce, and volume scattering) represented by physical models, the Freeman-Durden

decomposition divides the total power observed over each pixel into respective contributions from each scattering mechanism. This is done using three separate C matrices, the sum of which is equal to the total power of the matrix.

This provides three individual outputs representing the proportion of each scattering mechanism in the scene, and can be used to create colour composites typically with double bounce scattering in the red, volume scattering in the green, and surface scattering in the blue. For the surface scattering component, a slightly rough, Bragg surface is modelled where contributions from HV and VH are small (Lee & Pottier, 2009). A dihedral corner reflector is used to model double bounce scattering, and cylindrically shaped and randomly oriented scatterers are used to represent volume scattering.

Cloude-Pottier Decomposition

Cloude and Pottier introduced both the T matrix and three useful and independent parameters that can be derived from it (Cloude & Pottier, 1996; Cloude & Pottier, 1997). The first two parameters are based on the eigenvalues, which in a symmetrized matrix are representative of three scattering mechanisms, where the first is the dominant, and the second and third are less dominant.

Entropy characterizes the degree of randomness of scattering, where $H = 0$ represents a single mechanism, and $H = 1$ represents multiple scattering types, indicating high signal depolarization and or noise (Cloude & Pottier, 1997).

Anisotropy is the normalized difference between the second and third eigenvalues, representing the second and third scattering mechanisms. It is used to indicate the relative importance of these, where $A = 0$ shows contributions from the

second and third mechanism are equal. For A > 0, low values indicate that the third scattering mechanism contributes significantly to total power, and if values are high, only the second contributes significantly to total power (Cloude & Pottier, 1997).

Alpha angle (α) is based on the eigenvectors of the T matrix, and can be used to determine the dominant scattering mechanism observed for individual pixels (Cloude, 1986; Van Zyl, 1992; Cloude & Pottier, 1996; Cloude & Pottier, 1997). Values range from 0 to 90°, where lower values (0 - 45°) represent surface scattering, intermediate values (45°) represent volume scattering, and high values (> 45°) represent double bounce scattering (Cloude & Pottier, 1997).

2.2.5.3. Polarimetric Signatures

All polarimetric information of backscattered waves, including: power, ellipticity (χ) and orientation angle (ψ) can also be displayed on three dimensional plots to help interpret the dominant scattering mechanisms observed over specific targets (van Zyl et al., 1987). Plots can be constructed that represent backscattered power on the z-axis for waves that have the same or orthogonal polarizations as the incident wave, with values typically normalized to one. If the scattering matrix is considered, HH and VV are represented on co-polarized plots at 0/180° and 90°, respectively. Conversely HV and VH are represented on cross-polarized plots at 0/180° and 90°, respectively (van Zyl et al., 1987). This is because the orientation angle of the plot always represents the incident wave, where the power on the z-axis represents the backscattered wave.

Polarimetric plots also display pedestal height (linear power), which represents the amount of depolarization in the backscattered wave. Values range from 0 indicating little depolarization (noise) and or the presence of a single scattering mechanism, to one

indicating increasing noise and or multiple/dissimilar scatterers (van Zyl et al., 1987). Studies have shown that pedestal height can be sensitive to increases in surface roughness and vegetation density (Evans et al., 1988; van Zyl, 1989; Farr & van Zyl, 1992; McNairn et al., 2002).

2.3. Literature Review of Applications Pertinent to this Research

While the previous sections have summarized some of the theory of radar remote sensing and radar polarimetry, this section summarizes the applications literature, with a focus on studies that could be related to the SCAT substrate, geomorphologic, water and vegetation classes considered here. Specifically, this section highlights studies that have shown potential for substrate and wetland detection/mapping based mostly on the sensitivity of microwaves to surface roughness and volumetric moisture content, respectively. Examples from the literature of herbaceous vegetation detection/mapping are also provided where applicable. A short summary of the potential for using optical imagery is also provided, with a focus on studies that have been conducted in the Arctic.

2.3.1. Substrate Detection and Mapping on the Basis of Sensitivity to Surface Roughness

The potential for radar mapping of substrates on the basis of differences in surface roughness was well demonstrated in the late 1970s and 80s in Death Valley California (Evans et al., 1986). This area was primarily used as a test site as it was extremely dry, which reduced the impact of moisture on microwave-surface interactions (Henderson & Lewis, 1996). Differences in backscatter could then be largely attributed to differences in roughness. Much of this early work focused on visual enhancements of images, for

identification of geological units based on existing maps (Daily et al., 1979). For example, Sabins (1984) was able to discriminate three units of surface textures using SEASAT (L-HH) imagery. Class divisions were based primarily on particle size differences (> 5.7 cm, < 1.0 cm and between 1-5.7 cm), which corresponded to high, low and intermediate intensity values in the image, respectively. Similar results were also found, using airborne X- and L-band data (Sabins, 1984). Evans et al. (1986) could also interpret three classes of gravel, which were also based on differences in particle size.

While theory would suggest that shallow incidence angle imagery would be more sensitive to surface roughness variations (Peake & Oliver, 1971), some authors have found better results with steep incidence angles. Dong and Leblon (2004) for example, found Radarsat-1 (C-HH) imagery acquired at 23° better for characterizing rock textures, compared to imagery acquired at shallow incidence angles (45 to 49°). These findings are also in agreement with Singhroy and Saint Jean (1999) who suggested geomorphic and structural features are best characterized using steep incidence angles around 20 to 27° (Singhroy & Saint-Jean, 1999).

In contrast, Paradella et al. (2009) found shallow incidence angle standard mode (nominal resolution of 12.5 m, nominal incidence angle of 20°, nominal coverage of 100 km^2, available in one of HH, VV, HH+HV or VV+VH polarization combinations) Radarsat-2 imagery had a stronger relationship with RMS height of rocks than both steep incidence angle standard mode imagery and higher resolution fine mode (nominal resolution of 8 m, nominal incidence angle of 40°, nominal coverage of 50 km^2, available in one of HH, VV, HH+HV or VV+VH polarization combinations). These results are consistent with a number of articles that assessed roughness differences between

agricultural fields (Baghdadi et al., 2002; Baghdadi et al., 2008a; Baghdadi et al., 2008b; Ziribi & Deschambre, 2002; Rahman et al., 2008). Baghdadi et al. (2002) for example, found Radarsat-1 imagery acquired at 39° and 47° produced a higher classification accuracy (85%) for three classes of surface texture (rough, intermediate and smooth) compared to ERS-1 (European Remote Sensing Satellite, nominal spatial resolution of 25 m, nominal incidence angle of 23°, nominal coverage of 100 km^2, available in C-band VV) imagery acquired at 23°. It should also be noted that some have found better results using multiple incidence angles (Grunsky, 2002).

A number of articles have also suggested that HH is the best single polarization for detecting differences in roughness. Holah et al. (2005) found HH intensity was the most sensitive to RMS surface height over agricultural fields, through an analysis of fully polarimetric ASAR data. The second best polarization was HV, and VV did not show a strong correlation with RMS surface height at any incidence angle (20-43°). Dong and Leblon (2004) also found HH better for discriminating rock types by grain size compared to HV. They attributed this to the latter polarization typically being described as predominated by sub-surface volume scattering, as opposed to roughness (Blanchard & Rouse, 1980; Fung & Eom, 1981).

Since wavelength has a significant impact on the perceived roughness of the surface being imaged, the determination of an appropriate wavelength (band) must be related to the expected size of the objects of interest in the study area. Mackenzie and Pingrose (1986) for example, found that for a SEASAT image acquired at 24°, only rock fragments with a magnitude equal to or greater than that of the wavelength of the SAR showed considerable backscatter. Dong and Leblon (2004) also found L-band imagery

preferable to C-band for surface roughness characterization using SIR-C and SIR-L data.

There are relatively few examples in the literature of surficial geology/substrate mapping in Arctic environments. One example is Engeset and Weydahl (1998) who mapped glacial moraine material ranging in size from 5 to 30 cm in diameter, using ERS-1 imagery. They found variations of less than 4 dB over these areas, with typically higher backscatter over moraine material compared to smoother surroundings. Li et al. (1999) were also able to generally distinguish between substrates based on differences in roughness using steep angle ERS-1 imagery over Alaska.

2.3.2. Wetland Detection and Mapping on the Basis of Sensitivity to Roughness/Moisture

This section focuses on examples from the literature for shorter vegetation communities, though it should be noted that there are also a number of other examples available for forested wetlands and swamps (Kasischke & Bourgeau-Chavez, 1997; Henderson & Lewis, 2008).

Potential for wetland detection and mapping with radar has been observed in the literature, and in some cases classification accuracies greater than 90% have been achieved, as suggested in a review by Kasischke et al. (1997). In a more recent review by Henderson and Lewis (2008), the authors state that while general wetland detection is possible in most cases, confusion arises when attempts are made to distinguish among wetland types (Henderson & Lewis, 2008). Arzandeh and Wang (2002), for example found an accuracy of 88% for a binary wetland, non-wetland classification using texture measures generated from Radarsat-1 imagery, but acceptable accuracies could not be achieved for wetland type.

As with substrate mapping, optimal incidence angle also seems to be a function of the study area, sensor type, and study objectives. Where some studies found steep incidence angles best for wetland detection (Brown, et al., 1996), others found better results with shallow angles. A review by Ramsey (1998) for example, indicated shallower angles are preferable for detection of herbaceous wetlands. Based on this, it is important to consider whether differences in moisture or vegetation density and structure are desirable to detect. In theory, steeper incidence angle radar should penetrate farther into the canopy, and therefore be more sensitive to inundated areas and variations in surface moisture, while shallower angles provide greater interaction with vegetation canopies (Ramsey, 1998).

Some authors found that multiple incidence angles improved overall land cover classification accuracy (Hess et al., 1990; Kandus et al., 2001). Toyra et al. (2001) and Toyra and Pietroniro (2005) found sedges, flooded grasses and dead flooded willows were better detected using steep incidence angle Radarsat-1 Standard Mode images, but that shallow angles were also necessary to define the land water interface. However, Henderson and Lewis (2008) conclude that the use of multiple incidence angles does not always improve results. They state that this only provides additional information for surfaces that are close to specular reflectors, because a change in incidence angle does not significantly alter backscatter coefficients over rough surfaces due to dominant volume/diffuse scattering.

The use of multiple polarizations can increase classification accuracy and in some cases results were better than using multi-temporal data (Henderson & Lewis, 2008). In fact, too many images from different dates have shown potential for decreased

classification accuracy (Wang et al., 1998). Baghdadi et al. (2001) for example, found multiple date acquisitions did not increase the mapping accuracy of non-forested peat bog, open water, marsh, forest, clearings, and forested peat bog in Ontario with polarimetric airborne C-band imagery. They also found HV was the best single polarization overall, being required to separate forests, non-forested bogs, and forested bogs, but that HH was best for separating marshes from other classes.

In many cases, HH polarization has been described as optimal for wetland detection with single polarizations (Hess et al., 1990; Kasischke & Bourgeau-Chavez, 1997; Ramsey, 1998; Bourgeau-Chavez et al., 2001). In a review by Schmullius and Evans (1997) of SIR-C/X-SAR imagery, L-HH, C-VV, C-HV, and all X band polarizations were listed as useful data sources for herbaceous wetlands. In general, the optimal polarization also seems to be a function of the study area, sensor type, and study objectives. When only single polarizations are available it has been necessary to combine multiple date acquisitions to achieve adequate classification accuracy (Bourgeau-Chavez et al., 2005; Kasischke & Bourgeau-Chavez, 1997). Multiple band combinations also seem to increase overall classification accuracy. Borgeau-Chavez et al. (2001) found it necessary to combine L- and C-band imagery to map all wetland classes in a study area in Virginia. Simard et al. (2002) found C-VV could be used to distinguish grass swamps and Borgeau-Chavez et al. (2001) found herbaceous vegetation was best discriminated using L-HV imagery.

There are also few examples in the current literature related to wetland mapping in Arctic environments using SAR. Most have involved only ERS-1 or Radarsat-1 Standard Mode imagery (Henderson & Lewis, 2008). Morrissey et al. (1994) found a

strong correlation between image intensity and water table height using ERS-1 imagery acquired near Barrow, Alaska, including: intermediate backscatter coefficients for standing water, high values for flooded herbaceous vegetation and low values for dry areas. In a later article, Morrissey et al. (1996) used 24 ERS-1 images from the North Slope of Alaska to discriminate wetlands from non-wetlands. They found better results when temperatures were at or near freezing, because intensity remained relatively constant over wetlands but changed over non-wetlands.

Durden et al. (1996) expanded on this using polarimetric C and L-band AIRSAR imagery over Alaska combined with neural networks and image statistical analysis. They found similar classification accuracies (78 to 81%) for multiple polarizations (i.e., HH, HV and VV backscatter coefficients) and non-polarimetric (C-HH, L-HH and C-VV channels alone) imagery in classification of fens, water, bogs and forests, but using L-HH imagery alone, forests, water and fens could be accurately mapped. No L-band polarization combination could separate forests and bogs however, and in general C-band imagery alone produced lower classification accuracies. This is in contrast to Morrissey et al. (1994), who could identify fens with C-band imagery (Durden et al., 1996).

2.3.3. Land Cover Detection and Mapping in Arctic Environments

There are relatively few examples from the literature which have focused on SAR for general detection and or mapping of land cover types specific to Arctic environments. Instead, a number have focused on the use of optical imagery for habitat modelling, including: LANDSAT (Gratto-Trevor, 1996), SPOT and IKONOS (Ashenhurst & Hannon, 2007). Morrison (1997) used LANDSAT imagery to classify Prince Charles

Island, Northwest Territories with acceptable accuracies (> 85%) for: rock, gravel, mudflats, tundra vegetation, sparsely vegetated tundra, saturated marsh, salt marsh, and grassland.

For these studies, the extent to which results could be extrapolated through broad scale mapping remains varied. Success seems dependent on available data, as well as differences in phenology, moisture and substrate type (Morrison, 1997). Gratto-Trevor (1996) for example, extrapolated shorebird breeding habitat classification results from a previous study for Fish Island and the Taglu region to the entire outer Mackenzie River Delta, Northwest Territories, Canada. The authors suggested that classification accuracy was higher for areas that contained similar land cover types to the area used for training whereas proximity to the training area was less important.

Hall-Atkinson and Smith (2001) is the only known radar mapping analyses performed in the study region for classification of vegetation types specific to the Arctic. They show the potential to use interferometric ERS-1 and 2 winter imagery to improve class discrimination in the outer Mackenzie Delta. Observed interferometric coherence (measuring how well two waves are correlated (Woodhouse, 2006)], ranked from lowest to highest as: water, frozen channels, frozen lakes, spruce, and stands of willow-alder (Hall-Atkinson & Smith, 2001). This information was used to separate classes that were indistinct in amplitude imagery (i.e., willow-alder stands). They suggest coherence is high over willow-alder stands because backscatter is mainly from rigid branches, whereas less coherence was observed over spruce trees, which was attributed to the presence of needles (Hall-Atkinson & Smith, 2001).

2.3.4. Improved Detection/Mapping Through Combined Radar and Optical Data

The following section provides a short summary of a number of studies that have shown improved land cover detection and or classification through the combined use of radar and optical data. This is pertinent to this research as it was one of the objectives to combine SPOT-4 and optimal Radarsat-2 parameters in a simple Maximum Likelihood Classifier.

For substrate mapping, Dong and Leblon (2004) found better classification accuracy of various rock units differentiated by grain size, when they combined the spectral information from LANDSAT imagery with texture measures derived from dual polarized (HH and HV) L and C-band data. Texture measures were used specifically because they performed better than backscatter coefficients. Souza-Filho et al. (2002) also observed high classification accuracy for combined LANDSAT and Radarsat-1 imagery over northern Brazil. Using a Red Green Blue/Intensity Hue Saturation (RGB/IHS) transformation, they were able to visually differentiate 19 land covers, including: sand flats, mudflats, barrier beach ridges, sand ridges, marshes, and various mangrove stands. A number of other studies have also shown improved visual discrimination of substrates through optical and radar fusion (Sabins, 1984; Madhavan et al., 1999; Ricchetti, 2001; Teruiya et al., 2008).

Similar results have been observed for wetland detection and mapping. Toyra et al. (2001) found significantly higher accuracies with SPOT and Radarsat-1 standard mode imagery combined for mapping non-flooded, flooded and open water areas in Saskatchewan, Canada. These results were consistent with Toyra and Pietroniro (2005). Souza-Filho et al. (2009), also combined LANDSAT and Radarsat-1 imagery for

environmental sensitivity index mapping in Brazil. Using a combination of principal components and IHS transformations, they showed potential to identify a number of classes, including marsh.

2.3.5. Summary

A number of similar conclusions can be made regarding both wetlands and substrate mapping using SAR. HH has been identified as the best single polarization in most cases. Optimal incidence angle seems highly dependent on the study area and goals of the analysis. Multiple polarizations and bands seem to produce higher classification accuracies in most cases, and the fusion of optical and SAR data generally leads to improved detection and or mapping.

In the current literature there are few examples of SAR imagery being used to detect or map land covers specifically found in Arctic environments. Those that do exist suggest changes in moisture conditions may significantly alter results. Potential for differentiating shrubs from surrounding land covers has also been observed with coherence imaging (Hall-Atkinson & Smith, 2001).

3.0. Methods

3.1. Study Areas

The two study areas selected for this research are located along the Tuktoyaktuk coastland in the southern Beaufort Sea, Northwest Territories, Canada (Figure 6). Shorelines here are mostly composed of Quaternary aged sediments, including: mud, glacial diamict, gravel, sand and clay; that are typically ice-bonded and unconsolidated, making them highly susceptible to thermal and mechanical erosion (Rampton, 1982; Rampton, 1988). Regional coastline retreat averages about 1-2 m/year (Solomon, 2005), while rates of about 20 m/year have also been observed in some areas, mostly due to episodic storm surges (Harper, 1990; Solomon, 2005; Lantuit & Pollard, 2008). Surges destabilize sediments by increasing thaw rates due to prolonged contact with seawater, and can also decrease the amount of energy dissipated along nearshore bars, which intensifies wave action (Harper et al., 1978; Kobayashi & Atkan, 1986; Dallimore et al., 1996).

Erosional features present along these shorelines include inundated low lying tundra, ice rich and ice poor cliffs, typically about 10 m high, but up to 30 m in some areas (Solomon, 2005). Along these shorelines block failure, shallow sloughing, basal wave-cut and gullying are common (Harper, 1990; Solomon, 2005). Harper et al. (1990) also state that these and other erosional features make up 60% of the shoreline from Demarcation Point to Baillie Island (2077 km). Though accretional features make up the other 40%, it is estimated that overall 80% of shorelines are erosional because a number of deltas are eroding. Other common accretional features include spits and barrier islands. The inland portion of the region also contains a number of drained lake

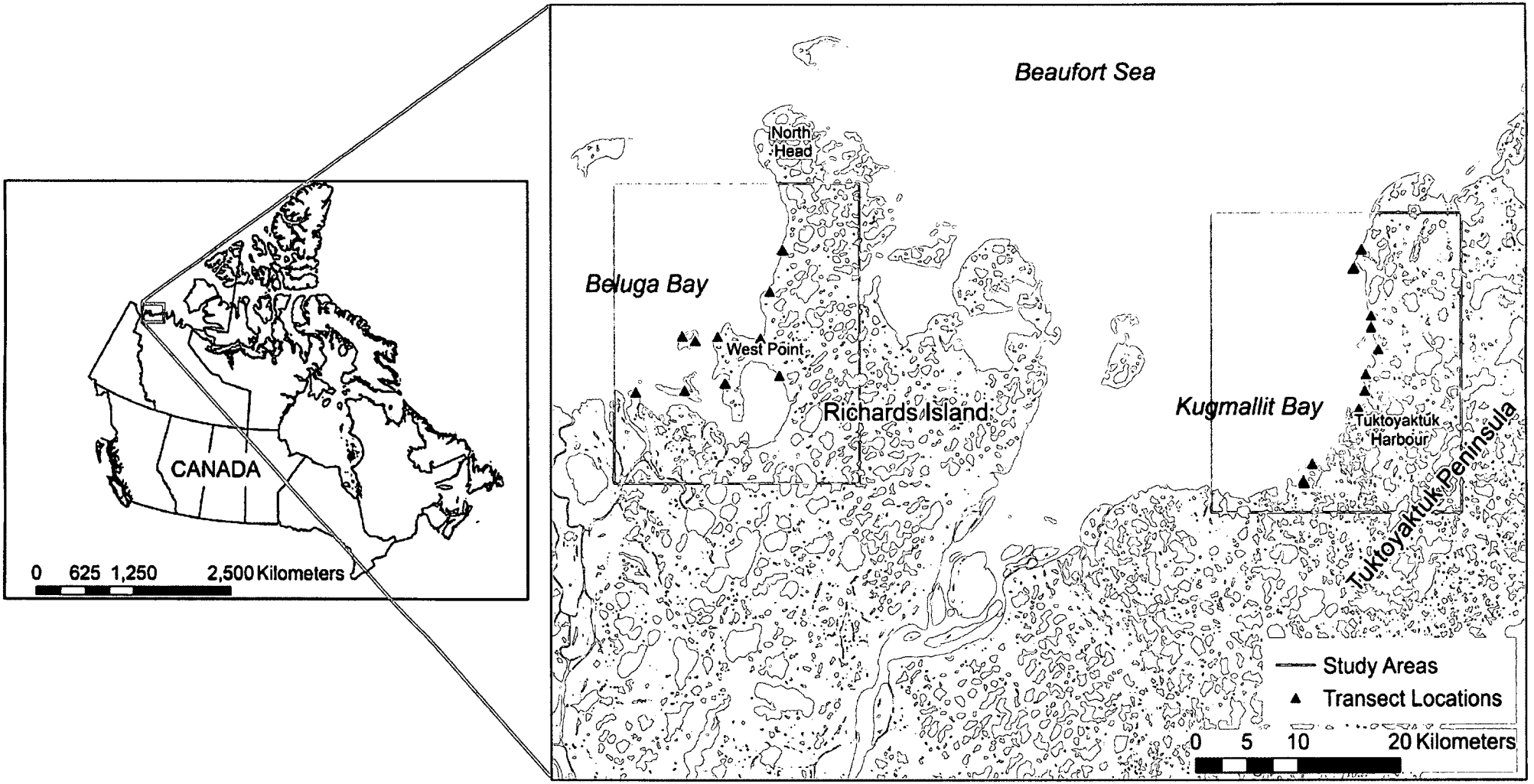

Figure 6: Map of the two study areas, including the West Point of Richards Island (west) and Tuktoyaktuk Harbour on the Tuktoyaktuk Peninsula (east). Location of transects where field data was collected are represented by black triangles.

basins as well as shallow lakes (Harper, 1990; Solomon, 2005).

The first study area (25 km^2) is centred on the West Point of Richards Island, hereafter called WP. In the southern portion of WP, islands about 1-2 m above sea level are common. These are mostly composed of peat and mud, and fronted by thin peat beaches, with high centre polygons in the backshore. Extensive mudflats are also located west of Richards Island, where the largest is approximately 12 km long and 3 km wide (Hequette & Barnes, 1990). These features are composed mainly of fine silt, sand and organic matter. The majority of shorelines along Richards Island are also composed of cliffs, fronted by thin sand or mixed sediment beaches. Many marshes have also developed along beaches behind the extensive mudflat (Rampton, 1988; Rampton, 1987a).

The second study area (25 km^2) is centred on Tuktoyaktuk Harbour, hereafter called TH. This site may be differentiated from the first by a lack of extensive mudflats and low tundra islands, as well as the presence of a number of anthropogenic features, including houses and roads. Spits and barrier islands are also more common here than in the WP study area, although the majority of shorelines are also composed of thin beaches at the base of tundra cliffs. Additionally, sediments north of the harbour are mostly sand, while those to the south typically contain pebble as well (Hequette & Barnes, 1990). Extensive inundated tundra is common and typically found in sheltered areas (Harper, 1985; Rampton, 1987b).

These study areas were selected because of the high number of different shoreline types present. This increased the number that could be assessed, making results more widely applicable. Both study areas also contain multiple occurences of certain

shorelines, which allows assessment of the repeatability of results.

3.2. Helicopter Videography and Field Data

In the summer of 2010 oblique high definition helicopter videography was acquired by the author along the shorelines of both study areas using a hand-held video camera through an open window in a Bell 206 helicopter. This was conducted to provide reference information for this research, but was also part of the eSPACE pre-SCAT project objective to improve on currently available maps of the area, and to develop improved methods for airborne-based shoreline assessment. Audio commentaries based on a continuous interpretation of the shoreline type and character, were recorded simultaneously.

Flight altitude and speed were consistent with conventional shoreline sensitivity mapping, at approximately 100 m above ground/water and 150 to 185 km/h. A handheld Global Positioning System (GPS) unit was also used to track helicopter flight paths to subsequently associate video segments with precise ground locations. All videos were recorded on July 20th or July 21st, 2010 to coincide approximately with the summer growing season and Radarsat-2 acquisitions. Prior to fieldwork, training with Environment Canada's Environmental Emergencies Branch and Dr. Ed Owens, an expert in shoreline segmentation, was completed by the author.

Quantitative and qualitative field data were recorded for a number of shoreline types between July 22nd and July 26th, 2010 to characterize the complexity, variability and density of surface features in order to develop an understanding of radar-surface interactions, and subsequently the intensity and polarimetric behaviour observed for each shoreline type. Transects were placed at locations noted by black triangles in Figure 6.

These were selected preceding field work to maximize the number of land cover types visited, while minimizing helicopter time.

Transects were also oriented perpendicular to the shore to characterize the transitions from the water's edge to upland areas. This is because many areas progressed from un-vegetated beaches and flats to drier upland tundra. Over homogeneous land covers, or where succession from one land cover type to another occurred over hundreds of metres, transect orientation was selected to be representative of typical conditions observed in the field. In total 13 transects per study area, for a total of 286 quadrats were completed. Nearly all land cover classes present in both study areas were sampled at least once.

Transect length was 51 m from the land-water interface and one GPS point was recorded at the beginning and end of each transect. A $1m^2$ quadrat was placed across the measuring tape at 5 m intervals (i.e., 0 - 1 m, 5 - 6 m, 10 - 11 m... 50 - 51 m). Within this 1 m^2 area the percent cover, average and maximum height of vegetation and substrates were estimated visually and classified on site (Table 2). The ranges used for classifying percent cover were taken from the commonly used Braun-Blanquet sampling strategy, as it was not expected that percent cover could be estimated to any greater precision (Mueller-Dombois & Ellenberg, 1974). As such, there may be some error in the assigned class when percent cover was close to two class boundaries.

The ranges used for classifying height were arbitrarily selected, but also allowed for quick visual assessments in the field (Table 2). Six categories were also used to record vegetation type: 1) shrubs, 2) grasses, sedges, horsetails and 3) other herbs, and surficial materials: 1) sand, 2) mixed sediment and 3) woody debris (Table 2). Grasses and sedges

Table 2: Criteria and classes used to record estimates for percent cover, average and maximum height for vegetation and substrates within quadrats.

Percent Cover		Average and Maximum Height	
Criteria (%)	**Class**	**Criteria (cm)**	**Class**
<2	1	<10	1
2 to 10	2	10 to 25	2
11 to 25	3	26 to 50	3
26 to 50	4	51 to 1	4
51 to 75	5	>1	5
76 to 100	6		

were discriminated from other herbs as these species are dominant in wetlands and marshes, respectively (Owens , 2010). Despite this initial distinction, these classes could not subsequently be identified in helicopter videography or other ancillary data and so were merged to form the Herb Dominant Tundra class (described subsequently). A photograph of every quadrat along all transects was also taken, which included the metre sticks for scale (Figure 7).

3.3. Land Cover Classes

Table 3 provides a brief description of the land cover classes used in this study and includes a number that have been adapted from the primary shoreline types utilized in pre-spill databases by Environment Canada's Environmental Emergencies Branch. Some classes have also been added (identified with an asterisk), including a number in the backshore where marine processes are not active. These were differentiated to potentially aid in the determination of accessibility and potential staging areas for cleanup, as well as to expand the applicability of results beyond that of oil spill response planning. Backshore classes may also provide an indication of the shoreline type present.

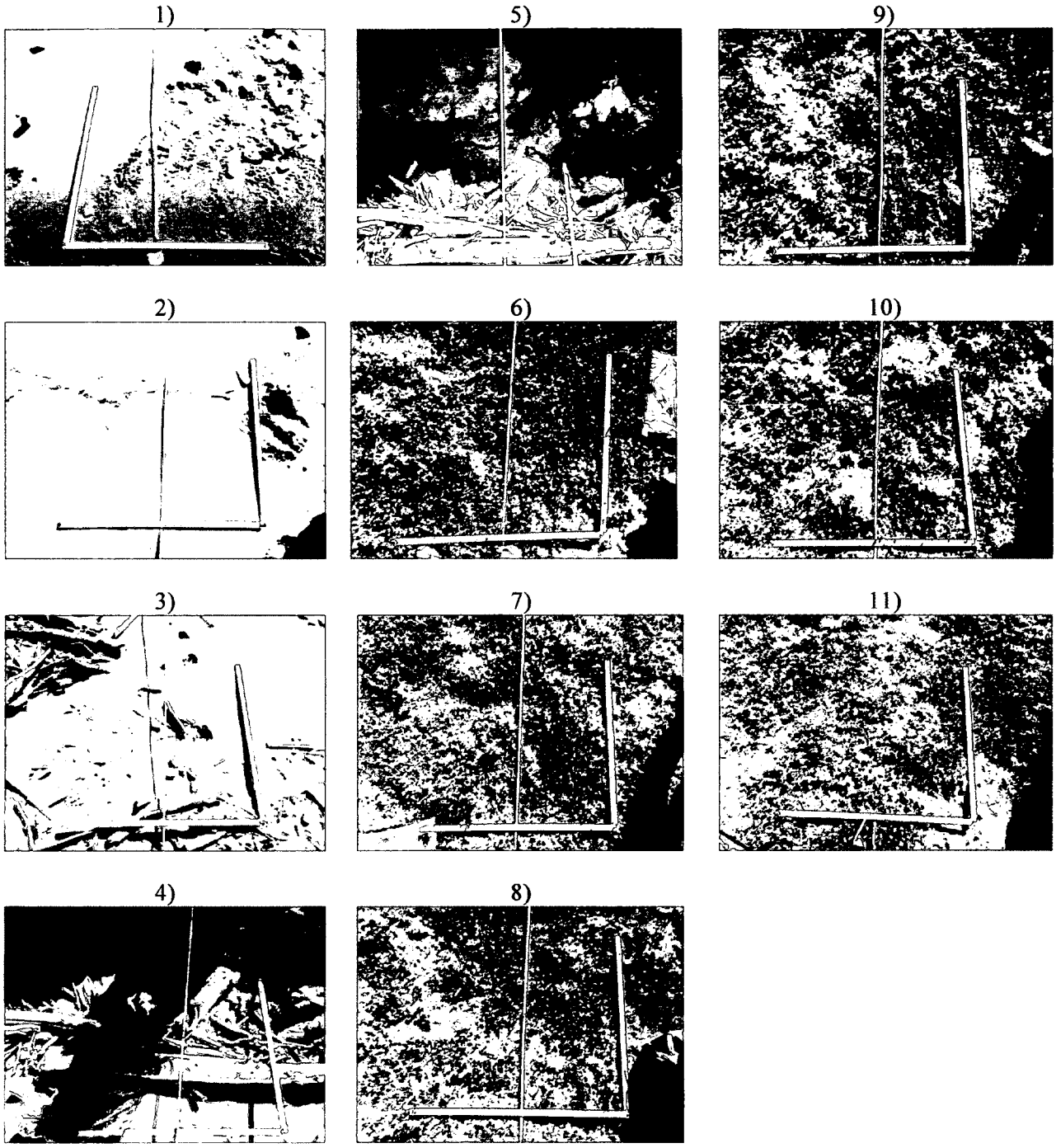

Figure 7: Photos of 11 quadrats from a transect in the TH study area, showing the transition from a sand beach (Photos 1 to 3) to a log line at the base of a micro-cliff (Photos 4 and 5), to low herbs in the backshore (Photos 6-11). Numbers mark quadrat order from the beginning (Photo 1) to end (Photo 11), with each quadrat being 5 m apart.

Table 3: Land cover classes considered in this analysis. Those marked with an asterisk (*) have not been considered previously for sensitivity mapping in Canada.

Class	Description
Anthropogenic	All structures composed of man-made materials impermeable to oil
Smooth/Un-Vegetated Mudflat	Predominantly silt and clay sediments < 0.0625 mm in diameter
Rough/Vegetated Mudflat	Mudflat that is roughened by caribou tracks and or a sparse vegetation cover
Peat Shoreline	Dominant substrate type is peat
Sand Beaches/Flats	Dominant grain size: 0.0625 mm to 2.0 mm, and up to 10% other sediment
Mixed Sediment Beaches/Flats	Sand mixed with any combination of : granule (2.0 to 4.0 mm), pebble (4.0 to 64.0 mm), cobble (64.0 to 256.0 mm)
Riprap	Human made rock feature placed along shorelines to prevent erosion Typically composed of boulders with dominant grain size: 256 to 400 mm
***Wood/Substrate Mix**	Sand or mixed sediment beach or flat littered with some woody debris (up to 50% coverage)
***Woody Debris**	Dominant substrate type is woody debris (> 50% coverage) Typically found in bays or along beaches
Marsh	Dominant vegetation cover is glasswort or sedge (coverage is sparse > 15% of land) Salt or brackish water covers these areas at least once a month, during high tide
Wetland	Does not contain significant amount of sedges or rushes, and is dominated by grasses
Inundated Low Lying Tundra (ILLT)	Mostly vegetated tundra that is at or near the water surface Flooded during storm surges/spring high tide and can be permanently submerged in some areas
***Low Centre Tundra Polygons**	An area with actively growing ice wedges forming polygonal features in the landscape Polygon centres are below margins and in the summer interstitial water is present above ice wedges
***High Centre Tundra Polygons**	An area with inactive ice wedges, which form polygonal features in the landscape Polygon centres are above margins and in the summer there is little to no interstitial water
Eroding Tundra	Mostly composed of retrogressive thaw slumps, though areas often contain mudflows, and surface wash
***Herb Dominant Tundra**	Upland tundra composed mostly of low lying herbaceous vegetation and shrubs
***Shrub Dominant Tundra**	Upland tundra composed dominantly by tall shrubs (> ~0.25 m)
Water	Any water surface such as the ocean, lakes, or ponds

As an example, inundated low lying tundra, which is a backshore class, is generally fronted by a peat beach (Owens, 2010). The added classes also generally showed a unique response in available Radarsat-2 imagery. Descriptions of shoreline types and snap shots from helicopter videography are provided in Appendix 1. While dominant in both study areas, ice rich and ice poor tundra cliffs were not considered in this study. The radar look direction of available imagery was not towards cliff faces, and so these features could not be discerned.

3.4. Radarsat-2 Image Processing and Analysis

The following describes the Radarsat-2 imagery acquired for this research, all pre-processing applied, and the image analyses conducted.

3.4.1. Image Acquisitions

Fully polarimetric Fine Quad Radarsat-2 imagery was provided for this research by the National Wildlife Research Centre of the Canadian Wildlife Service, Environment Canada. Radarsat-2 was launched on December 14th, 2007. It is capable of acquiring fully polarimetric imagery, can acquire images in an ascending (78°, approximately east) or descending (282°, approximately west) look direction, and can also acquire single polarizations at higher spatial resolutions, such as at 3 m in Ultra-Fine mode (MDA, 2011). Fine Quad imagery was used in this analysis to assess the benefit of having all four polarizations and the inter-channel phase information. This beam mode specifically, was also the highest spatial resolution available (nominal pixel size of 8 m). Acquiring all four polarizations also allowed for the determination of the best single polarization or

combination of polarizations for future acquisitions at higher resolutions. This partially addresses objective one, to determine optimal acquisition parameters.

In total, three images representing shallow (FQ 31 and 27), medium (FQ 21 and 20) and steep (FQ 3 and 4) incidence angles and covering a 25 km^2 area, were acquired over each study area (Table 4). It should also be noted that these images were all acquired in the same look direction (descending) to reduce additional geometric factors, besides incidence angle, which could affect scattering behaviour. To address objective four, which was to assess the repeatability of results, both sets of images also had approximately equal incidence angles (Table 4).

Table 4: Radarsat-2 image acquisitions over the TH and WP study areas, each covering approximately 25 km^2.

Study Area	Beam Mode	Incidence Angle (°)	Acquisition Date (UTC)	Time (UTC)	Tide Height (m above average sea level)
TH	FQ 31	48.4-49.5 (shallow)	2010-08-19	15:06	0.5
	FQ 21	40.2-41.6 (medium)	2010-08-15	15:23	0.6
	FQ 3	20.9-22.9 (steep)	2010-08-17	15:56	0.6
WP	FQ 27	45.3-46.6 (shallow)	2010-08-22	15:19	0.3
	FQ 20	39.3-40.8 (medium)	2010-08-25	15:31	0.3
	FQ 4	22.3-24.2 (steep)	2010-07-31	16:00	0.3

Due to the high demand for Radarsat-2 imagery within the vicinity of the study areas and the requirement to submit acquisition requests months in advance, it was not possible to plan around tidal elevations or weather conditions. Imagery taken at low tide would have exposed the greatest amount of shoreline, while images acquired under comparable weather conditions would have made for a more objective comparison between study areas and incidence angles. Instead, varying moisture levels must be

considered. Based on Fisheries and Oceans Canada (Table 2) gauges, while tidal heights were consistent between acquisitions (OFC, 2010); "drizzle" was noted for a short time prior to the acquisition of the medium angle image over the TH study area and medium and shallow angle images over the WP study area (EC, 2010). It should be noted that this information was also obtained from a weather station at Tuktoyaktuk, (~58 km from the WP), and it was not known whether this precipitation was widespread or localized.

3.4.2. Radarsat-2 Image Processing and Calibration

The following describes all calibration and processing applied to Radarsat-2 imagery prior to analyses, using PolsarPro version 4.2. All outputs were then imported into PCI Geomatica for slant to ground range conversions, and georeferencing. Polarimetric Signatures were generated in the Polarimetric Workstation as part of a separate analysis on slant range imagery (CCRS, 2011b). PolsarPro was selected for this processing as it is freely available and widely used (McNairn et al., 2009; Goodenough et al., 2011; Yonezawa et al., 2012).

Raw image files were calibrated to sigma nought (σ°) or radar backscatter in the form of the complex 2x2 scattering matrix [S], when first imported into PolsarPro. Sigma nought or the normalized backscatter coefficient is used to represent the energy returned from a distributed target, as a ratio of the power of the incident wave to the power recorded by the sensor for a given area on the ground (Henderson & Lewis, 1996). All scattering matrices were then converted to: 1) the symmetrized Covariance (C3), and 2) the symmetrized Coherency (T3) matrices, which were subsequently filtered with the Enhanced Lee speckle filter, using a 7x7 window (Lopez-Martinez et al., 2005).

To determine the optimal window filter size shallow, medium and steep angle imagery acquired over the TH study area were all filtered using 5x5, 7x7, and 9x9 window sizes. HH, HV and VV backscatter coefficients were then extracted, converted to dB and all three polarizations for each image were used as inputs for nine separability tests based on the Bhattacharyya Distance (BD). Since training data were normally distributed for all three polarizations, this provided a fast and quantitative way to assess the potential for class discrimination. It provides a measurement of the statistical separation between samples of land cover classes based on the distance between means, weighted by covariance (Bhattacharyya, 1943). BD values range from 0.0 to 2.0, where for the purpose of this research, values equal to or greater than 1.7 were considered indicative of significant separability, values between 1.5 and 1.7 were considered indicative of moderate separability, but reduced expected classification accuracy, and values less than 1.5 were considered indicative of poor separability and expected classification accuracy (Richards, 1994; Lillesand et al., 2004).

Following speckle filtering, the following parameters were generated from 1) C3 matrices: backscatter coefficients (dB), Freeman-Durden decomposition parameters, and 2) from T3 matrices: Cloude-Pottier decomposition parameters. These were generated from slant range images, as is commonly the practice in radar remote sensing, to preserve phase information (Jiao et al., 2011). Slant to ground range conversions and georeferencing were then applied to all parameters using PCI Geomatica Version 10.3. 1.5 m resolution digital ortho photos acquired in 2004 (provided by the Northwest Territories Centre for Geomatics) were used as a reference for the latter, for which models included a minimum of 20 ground control points (GCPs) used as inputs to second

order polynomial transformations.

These are relatively simple models that use a least squares approach to determine the best mathematical fit based on x and y coordinates only. As such, scale changes across the image, rotations, as well as translations can be modeled. This approach was selected over ortho-rectification, because the terrain was essentially flat. A second order, as opposed to a first order transformation was also selected, as this achieved an acceptable RMSE accuracy level of less than one pixel (8 m), as validated using ten independent check points not used in the transformation. Higher order polynomials (i.e., third through fifth), were therefore deemed unnecessary, as these can also introduce errors in areas without GCPs (PCI Geomatica, 2003).

The ortho photos were also referenced extensively, in addition to helicopter videography and ground transects, for generating training sites (sample size ranged from 127 to 1960 pixels, with each pixel covering 8 m^2). These training data were used as inputs for all analyses, including the generation of global statistics (see Appendix 2 for example of training site generation). Larger sample sizes were used for classes with higher perceived variance, and larger coverage in each scene. In some cases, the number of available pixels to sample was limited, as was observed for thin shoreline classes like Riprap. Despite this, all samples (except Freeman-Durden Decomposition parameters) showed normal distributions, indicating that class variability was well represented.

Following generation of training data for each class, multiple Student t-tests of difference of means ($p = 0.05$) were run to assess the consistency of values between study areas at like incidence angles, as well as the consistency between angles for the same study area (i.e., for all parameters except Freeman-Durden decomposition outputs). In

most cases significant differences were observed between training data, which may be attributable to large sample sizes. Such testing was not pursued further because spatial autocorrelation could also be high, since vector polygons were used to generate this training data. As an alternative, to evaluate in detail the consistency between sites for each class, box and whisker plots were visually assessed, and the percent of values within the overlap region produced by $\bar{x} \pm 2s$ for sample distributions was calculated.

3.5. Polarimetric Signatures to Determine Dominant Scattering Mechanism and Within-Class Variability

Polarimetric signatures were generated from the imagery to determine the dominant scattering mechanism, and the variability observed between classes. To generate these signatures, non-georeferenced imagery in the form of the 2x2 complex scattering matrix were used as inputs to the Polarimetric Work Station version 5.4 (CCRS, 2011b). This type of input is a requirement of the software in order to completely preserve phase information. Numerous plots were generated for each land cover type across each image, in order to determine a representative response.

3.6. Separabililty Analyses to Determine Optimal Polarization and Incidence Angle

Separability analyses (BD) were then performed on backscatter coefficients and Cloude-Pottier decomposition parameters. The first set of tests was used to determine the optimal polarizations (HH, HV or VV) and incidence angles for discriminating classes. Analyses performed on Cloude-Pottier decomposition parameters were used to determine the optimal parameters and incidence angles for class discrimination. Again, distributions for Freeman-Durden decomposition parameters were not normally distributed in all

cases, but were mostly bimodal or highly skewed when a given scattering mechanism contributed little to total power (Figure 8). Thus, no Freeman-Durden decomposition parameters were used in separability analyses.

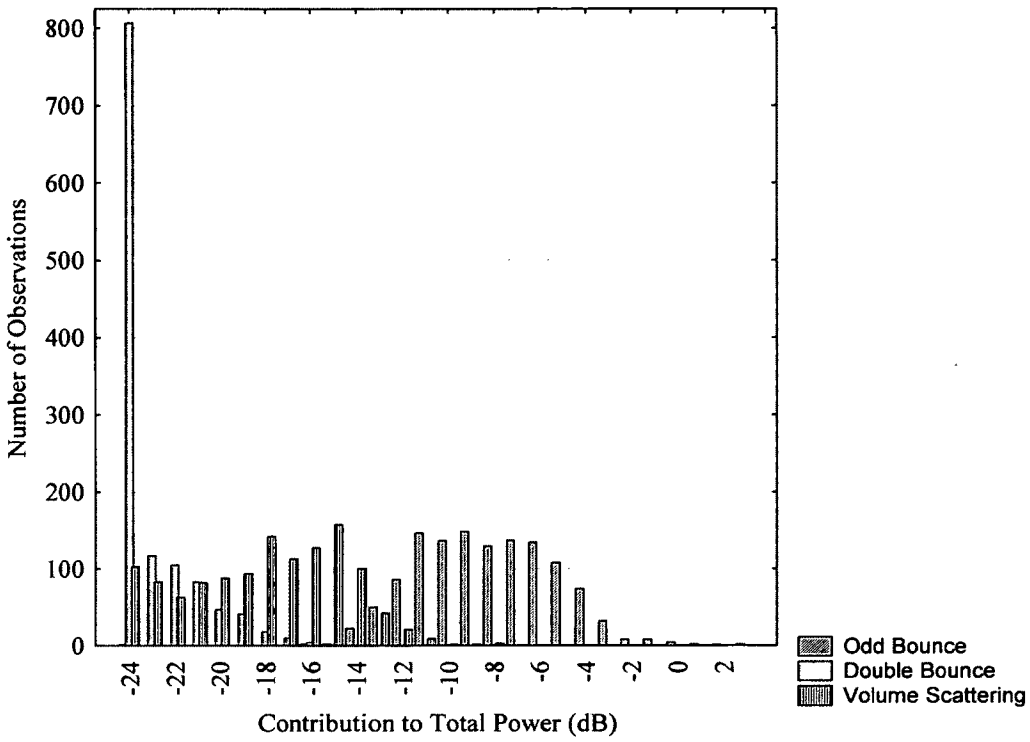

Figure 8: Histograms generated from training data for Sand (TH study area at steep anlges)for the three Freeman-Durden decomposition parameters.

3.7. Assessing Potential for Classification of Vegetation and Shoreline Substrate Classes

3.7.1. Segmentation of Entropy-Alpha and Entropy-Anisotropy Feature Space

Cloude and Pottier (1997) introduced a classification scheme based on the entropy-alpha feature space. This unsupervised method groups pixels into one of nine zones, based on target scattering behaviour (Figure 9). This classifier was applied to all

images, to identify scattering mechanisms, as well as to assess the potential for accurate classification. The latter was primarily evaluated using visual analyses and confusion matrices, based on the training data described previously. Note that low (< 0.5), medium (0.5 to 0.9), and high (> 0.9) entropy values are taken from Cloude and Pottier (1997).

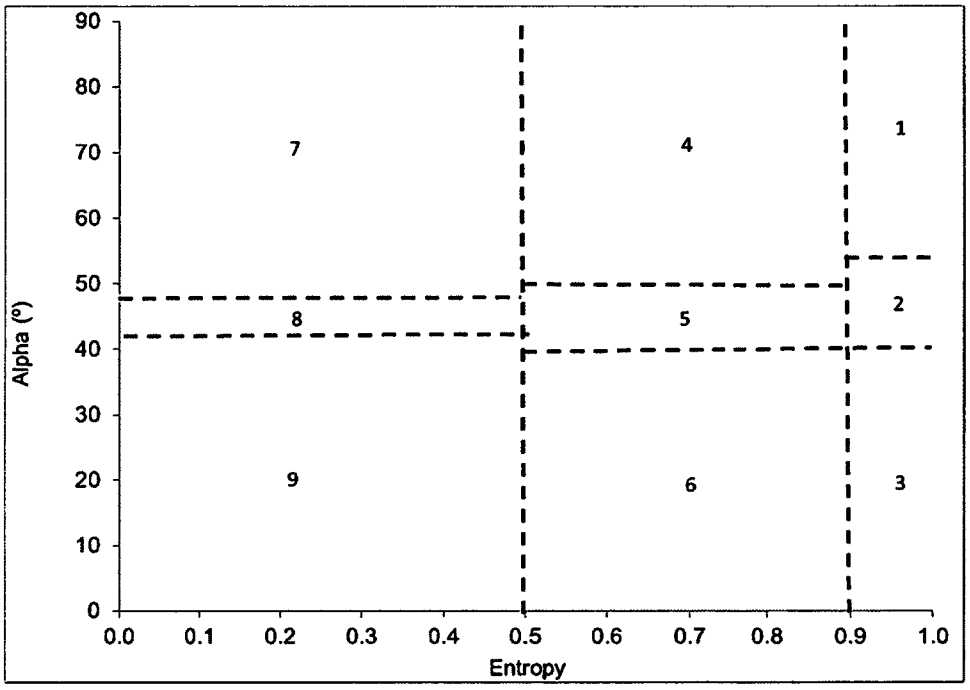

Figure 9: Schematic of the nine zones proposed by Cloude and Pottier (1997) for classification of pixels using the entropy-alpha feature space. Not shown on this graph are the curves representing the feasible range of values in the entropy-alpha feature space. For more information refer to Cloude and Pottier (1997).

Anisotropy can also be used in combination with entropy for a segmentation based on the entropy-anisotropy feature space. When used in combination with entropy, more information can be obtained about the surface scattering properties. As an example, when anisotropy values are low and entropy values are high the scattering process is random, whereas for the opposite case, there are two dominant scattering mechanisms (Cloude & Pottier, 1997). For further details refer to Ferro-Famil et al. (2002 & 2003).

3.7.2. *Unsupervised Wishart-Entropy/Alpha and Wishart-Entropy/Anisotropy/Alpha Classifiers*

The Wishart-entropy/alpha and Wishart-entropy/anisotropy/alpha unsupervised classifiers are commonly used to classify polarimetric imagery. Unsupervised classifiers automatically group pixels into statistically separable clusters based on input parameters. The analyst then determines what individual clusters of pixels represent on the ground, and assigns them to a land cover class. These classifiers produce 8 or 16 clusters based on an initial segmentation of: 1) the entropy, and alpha feature space, or 2) the entropy, alpha, and anisotropy feature space, respectively, as well as a minimum distance classifier, based on the Wishart distance applied to all elements of the symmetrized T matrix. For details refer to Lee and Pottier (2009).

The unsupervised Wishart-entropy/alpha and Wishart-entropy/anisotropy/alpha classifiers were applied to T3 matrix images acquired at shallow, medium and steep angles. All six images were visually assessed to determine the potential for accurate classification, while confusion matrices based on the training data described previously, were produced to show which classes were confused. Selection of independent training data for validation of these classifiers was unnecessary, since none of the training data described previously was used as model inputs.

3.7.3. *Supervised Maximum Likelihood Classification using Optimal Radar Parameters and Pan Sharpened SPOT-4 Imgery*

Based on the results of the previous analyses, the potential for using optimal radar parameters (based on visual and separability analyses) alone and in combination with, pan sharpened Satellite Pour l'Observation de la Terre (SPOT) 4 imagery was

investigated. For brevity, this analysis was applied only to imagery acquired over the TH study area (including a SPOT-4 image acquired on September 4th, 2006), as the focus was to exemplify how these data could be combined to assess the potential for accurate classification. Future work will assess whether results are comparable over the WP study area, and whether results can be spatially extendable, such as through using the statistics of training data collected over the TH study area to classify imagery acquired over the WP study area and vice versa. It should be noted that independent training and validation data were used for this analysis.

Despite the two data sets being acquired 4 years apart, it is not anticipated that significant changes in shoreline type, as well as the type of vegetation present, have occurred. It is possible that this, as well as slight differences in moisture conditions had some impact on model outputs and classification accuracy, though this could not be quantified at this time.

SPOT-4 was launched on March 24th, 1998 and acquires multi-spectral bands, including: green (0.50-0.59 μm), red (0.61-0.68 μm), near infrared (0.79-0.89 μm), and mid-infrared (1.58-1.75 μm) channels at a spatial resolution of 20 m, as well as a panchromatic channel (0.61-0.68 μm) at a spatial resolution of 10 m. Through panchromatic sharpening the spatial resolution of the multi spectral channels is improved by combining spectral information from these, with spatial information from the panchromatic band (Lillesand et al., 2004).

Two different algorithms (Intensity-Hue-Saturation and Simple Mean) in Arc Map version 10 were tested to determine which provided the best class separability (BD) and which maintained the spectral signature of the original data (assessed visually using

histograms). This analysis showed that the Simple Mean method was superior, and so it was selected for further testing. For algorithm details refer to ESRI (2010). Prior to pan sharpening, co-registration between spectral and panchromatic channels was also assessed using 10 check points, which showed x and y average RMSE of less than one pixel (10 m). Following pan sharpening, the image was georefenced to the 2004 ortho photos using the same procedure applied to the radar data.

Optimal Radarsat-2 parameters were then resampled from 8 to 10 m, and imported into the same file as the SPOT-4 pan sharpened image. Classification potential was assessed through generation of confusion matrices using independent validation sites. The Maximum Likelihood Classifier is one of the most commonly used techniques for land cover classification in remote sensing applications. It bases categorization of pixels on both variance within the class and covariance between classes, and determines for each pixel, the class that it has the highest probability of belonging to (Lillesand et al., 2004). Supervised classification methods also involve the user deriving a representative sample from a given scene to represent each land cover class.

Since there were a limited number of available sites for training and validation, some pixels initially used to generate global statistics, and for separability analyses (i.e., the training data described previously) were instead used for validation. Again, the number of pixels available for this was limited for some of the thinner shorelines. This is especially true in this case, because it was also necessary to maintain spatial independence between training and validation sites.

4.0. Results

4.1. Ground Data Collected During the 2010 Field Campaign

Table 5 and Table 6 show quadrats for each transect, classified by the dominant land cover types, with colours used to represent different surface materials and numbers used to represent percent cover classes from Table 2 (see Appendix 3 for maps of transect locations). This includes only those land covers representing greater than 2% of the total area within each quadrat (classes 2 to 6 from Table 2). Analysis of percent cover data showed that some classes like ILLT and Herb Dominant Tundra can be predominately composed of the same species (i.e., grasses). It is anticipated then, that some confusion may be observed between these classes, thus requiring additional data such as contextual information to discriminate them. As an example, ILLT and Herb Dominant Tundra may be distinguished by the fact that standing water is found interspersed among the former and not the latter.

Table 5 and Table 6 also show that some classes are more uniform than others across transects. Sand Beach for example, showed little diversity in terms of the surficial materials present. In contrast, Eroding Tundra, Herb Dominant Tundra and ILLT, showed greater diversity, as grasses, herbs and sometimes standing water, mud and or bare soil were found along transects. Un-vegetated beaches and flats also tended to progress to vegetated areas, as exemplified by transects 3 – 5 and 8 – 10 in Table 5, and by transects 5 – 6 and 10 – 13 in Table 6. This progression, also tended to be quicker (over fewer quadrats) in the WP study area, as beaches also tended to be thinner. This was also observed in helicopter videography.

Table 5: Classification of the transects used during the 2010 field campaign for the TH study area by percent cover class, showing for each quadrat the dominant land cover types.Colours indicate the surface material and numbers indicate the percent cover class for that material.

Transect Number	Description	Quadrat Number 1	2	3	4	5	6	7	8	9	10	11
1	Sand beach/flat	6	6	6	6	6	6	6	6	6	6	6
2	Mudflat, mixed sediment	6	6	6	6	6	5 4	6	6	5	6	6
3	Sand beach, herbs	6	6	6	5							
4	Sand beach, grass	6	6	6	5	4 5	4 4	5	5	4 4	6	6
5	Sand beach, shrubs	6	6	6	6	6	6	6	6	5	5	5
6	Sand flat	6	6	6	6	6	6	6	6	6	6	6
7	ILLT	6	5	6	6	6	6	5	6	5	5	5
8	Peat mat, Tundra Polygons	6	6	6	5 4	5	6	2 2 3 2	4 3	2 5	3 3	6
9	Mixed sediment, shrubs	6	6	5 4	5	6	6	6	6	6	6	6
10	Mixed sediment, shrubs	6	6	5 4	6	6	6	3 3	6	5	6	
11	Eroding Tundra	5	4	6	6	3 3	3	4	3	4	5	
12	Herb Dominant Tundra	4 4	6	5 4	6	4 5	4 4	5 4 3 3	2 3	2 5	3 5	
13	Shrub Dominant Tundra	5	6	6	6	6	6	6	6	6	6	6

Legend

Bare Soil		Woody Debris	
Mud		Grass, Sedge, Horsetail	
Peat		Other Herbs	
Sand		Shrubs	
Mixed Sediment		Water	

Table 6: Classification of the transects used during the 2010 field campaign for the WP study area by percent cover class, showing for each quadrat the dominant land cover types.Colours indicate the surface material and numbers indicate the percent cover class for that material.

Transect Number	Description	Quadrat Number 1	2	3	4	5	6	7	8	9	10	11
1	Marsh, sand beach								5	6	5	6
2	Cliff top, shrubs	6	5	5	5						5	3 4
3	Herb Dominant Tundra	4 3 5	3	5	5	5	4 4	2 5	3 5	5 4	5	5 5
4	Mudflat	6	6	6	6	6	6	6	6	6	6	6
5	Mudflat, herbs	5 3	5 3	6	6	5 3	5 3	6	6	5	5	5
6	Mixed sediment, grass	5 3	5 3	6	5 4	5						
7	Eroding Tundra	6	6	6	6	6	6	4	6	6	4 3	3 3
8	Wetland	6	5	5	6	6	6	6	6	6	6	6
9	Peat, ILLT	6	6	4	4	5 4	5 4	5 4	5 4	5 4	5 4	5 4
10	Sand beach, herbs	6	6	6	6	6	3	4	4	3		
11	Mixed sediment, herbs	5 4	5 4	6	6		3	4	4	4	2	
12	Peat, mudflat	6	6	6	5	5	5 4	6	5 3 3	4 3	4 3	4 3
13	Mudflat	6	6	6	6	6	6	5 3	5 3	5 3	6	5 3

Legend

Bare Soil		Woody Debris	
Mud		Grass, Horsetail	
Peat		Other Herbs	
Sand		Shrubs	
Mixed Sediment		Water	

4.2. Test to Determine Optimal Speckle Filter Window Size

The separability analysis to determine optimum speckle filter window size indicated that at steep incidence angles optimal classification potential was with a 7x7 window (Table 7). Most classes showed increases in separability when window size was increased from 5x5 to 7x7, although separability between Sand and other thinner shoreline classes tended to decrease. As an example, the BD between Mixed Sediment and Smooth/Un-Vegetated Mudflat was 1.85, 1.90, and 0.86 for the 5x5, 7x7 and 9x9 window sizes, respectively, for the steep angle image over the TH study area (Figure 10). For shallow and medium incidence angles, separability generally increased with window size from 5x5, to 7x7, to 9x9 pixels. There is potential that even larger window sizes could achieve higher separabilities, however the goal of this analysis was to select a window size that could be applied to all images, and to some shoreline classes that were relatively thin (< 50 m), so the 7x7 filter (covering an area of 56 m^2) was selected.

Table 7: Average Separability (BD) for all classes in the TH study area for shallow, medium and steep angles, using various window sizes in the Enhanced Lee filter to determine optimal processing technique.

Filter Size (Number of Pixels)	Incidence Angle		
	Shallow	Medium	Steep
5x5	1.27	1.26	1.19
7x7	1.43	1.37	1.28
9x9	1.48	1.44	1.24

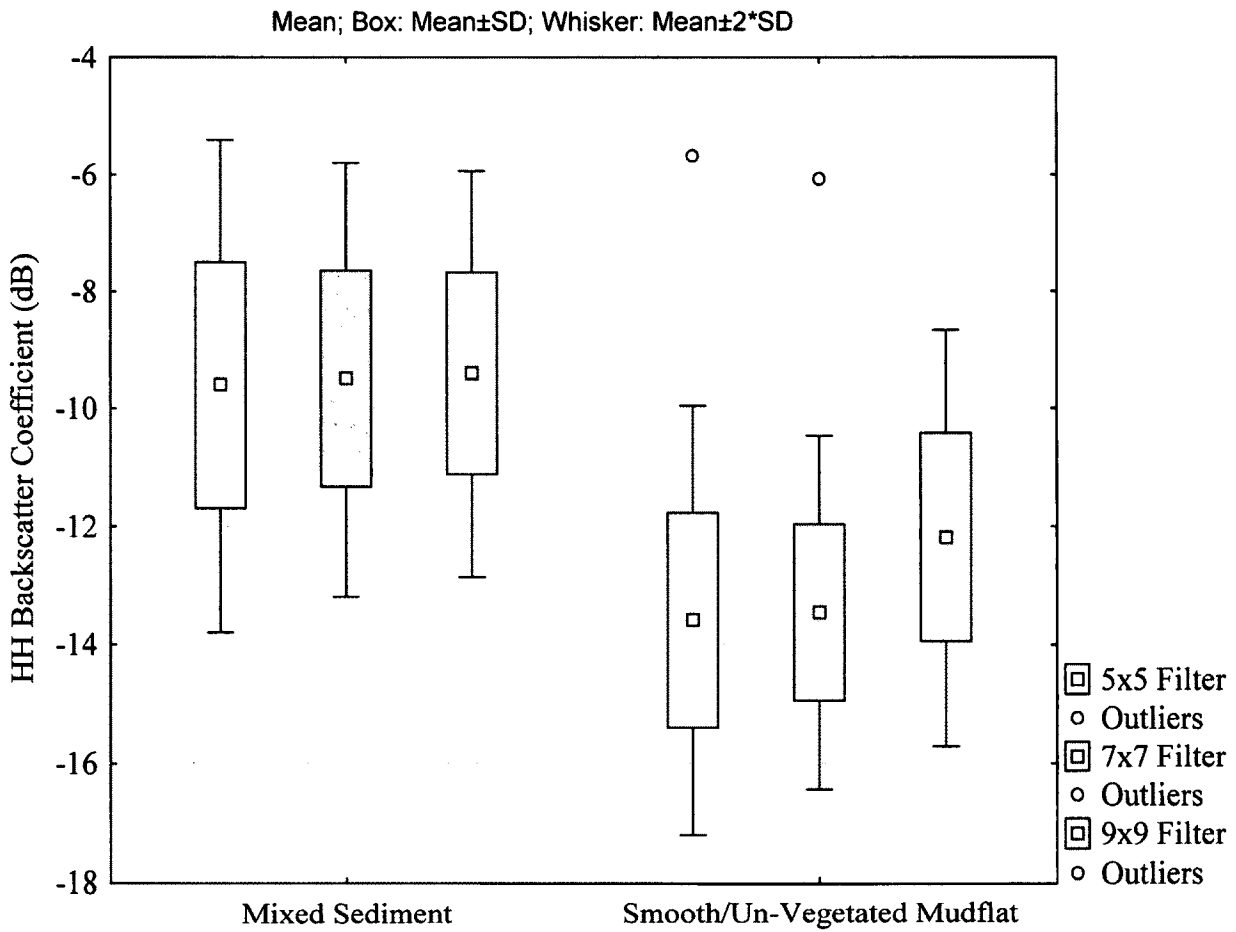

Figure 10: Box and whisker plots to show the distribution of training data for shallow angle HH for Mixed Sediment and Smooth/Un-Vegetated Mudflat from the TH study area. Samples are from Lee filtered images using 5x5 (red), 7x7 (green) and 9x9 (blue) window sizes. Box and whisker extents are represented by mean and standard deviation values because distributions were approximately normal. Outliers (values beyond whiskers), represent data that do not follow the same distribution as all other values, and are also infrequent observations.

4.3. Backscatter Characteristics of Arctic Land Cover Types

4.3.1. Sample Statistics,General Observations, and Trends

HH, HV and VV mean and standard deviation based on dB value distributions are provided in Table 8, Table 9, and Table 10. As mentioned previously, values are based on normally distributed training data as visually assessed using histograms. A number of trends can be identified; including that backscatter is lower over smooth surfaces and higher over rough surfaces. This was also more apparent at shallow incidence angles. As an example, average HH backscatter for Sand, Peat, Mixed Sediment and Riprap in the TH study area were: -21.53, -19.60, -13.50 and -12.45 dB, respectively. A large difference in image intensity was not observed between all classes however, nor was a substantial gradient from smooth to intermediate, to rough classes consistently apparent. Instead, backscatter showed potential for distinguishing between relatively smooth and rough surfaces. It should also be noted that both Anthropogenic and Wetland had the highest backscatter of all classes at all incidence angles.

HH and VV values tended to be comparable for a given class. This was especially the case at steep incidence angles for classes with smoother surfaces, including: Water, Smooth/Un-Vegetated Mudflat, Rough/Vegetated Mudflat, Peat and Sand. An analysis of correlation coefficients (Appendix 4) showed that, for these classes, the two co-polarizations provided redundant information ($r > 0.88$). As such, there may be no benefit in acquiring both at steep angles, especially in targeted acquisitions for these land cover types. Classes with rougher surfaces, including: Anthropogenic, Mixed Sediment, Riprap, Wood/Substrate Mix, and Woody Debris, typically showed lower correlations ($r_{HH/VV} <$

Table 8: Mean ($\bar{x}$) and standard deviation (s, based on dB distribution) of the backscattering coefficient (σ°) for HH polarization at all angles and both study areas. Sample size = # pixels in this and all subsequent tables.

Class	Study Area	Sample Size	Shallow		Medium		Steep	
			$\bar{x}$	s	$\bar{x}$	s	$\bar{x}$	s
Anthropogenic	TH	662	-5.41	3.18	-4.74	3.89	-3.54	3.89
	WP				N/A			
Water	TH	1960	-26.98	1.39	-23.76	1.23	-7.72	1.42
	WP	1056	-27.49	1.42	-25.33	1.16	-11.05	1.30
Smooth/Un-vegetated Mudflat	TH	268	-23.85	1.57	-21.46	1.45	-13.19	1.49
	WP	1050	-22.60	1.65	-20.08	1.89	-11.76	2.06
Rough/Vegetated Mudflat	TH				N/A			
	WP	937	-13.67	1.61	-10.89	1.89	-6.13	1.68
Peat	TH	127	-19.60	2.92	-15.94	3.15	-9.12	1.29
	WP	171	-14.99	2.72	-13.30	2.09	-7.84	1.66
Sand	TH	834	-21.53	2.13	-18.11	2.39	-12.16	2.01
	WP	1233	-20.62	3.46	-19.13	3.81	-9.64	2.94
Mixed Sediment	TH	760	-13.50	1.91	-11.91	1.80	-9.09	1.85
	WP	688	-13.59	1.71	-12.38	1.66	-9.52	1.71
Riprap	TH	140	-12.45	1.56	-11.42	2.37	-8.23	1.56
	WP				N/A			
Wood/ Substrate Mix	TH	662	-17.40	2.01	-14.95	1.94	-10.52	1.78
	WP	428	-11.78	2.79	-11.14	2.97	-9.58	2.40
Woody Debris	TH	799	-12.27	1.78	-8.98	2.02	-8.75	1.38
	WP	724	-6.99	1.71	-5.36	1.73	-6.13	1.45
Marsh	TH	249	-16.00	1.83	-13.50	1.53	-9.43	2.13
	WP	923	-13.89	2.17	-12.80	2.38	-9.04	1.51
Wetland	TH	474	-10.54	1.49	-7.76	1.55	-4.18	1.76
	WP	201	-10.70	1.90	-10.11	2.01	-8.66	1.96
ILLT	TH	705	-13.97	1.62	-11.53	1.84	-8.98	1.57
	WP	725	-12.81	1.30	-11.80	1.09	-9.46	1.40
High Centre Polygons	TH				N/A			
	WP	779	-11.82	1.14	-11.00	1.07	-8.83	1.15
Low Centre Polygons	TH	813	-14.06	1.53	-12.43	1.39	-8.62	1.36
	WP	681	-13.79	1.56	-13.21	1.40	-9.98	1.54
Eroding Tundra	TH	489	-12.18	1.47	-9.81	1.90	-8.26	2.56
	WP	477	-11.11	2.21	-9.75	2.37	-8.57	2.51
Herb Dominant Tundra	TH	806	-15.16	1.52	-13.71	1.17	-11.37	1.52
	WP	989	-14.41	1.46	-13.02	1.61	-11.42	1.89
Shrub Dominant Tundra	TH	942	-12.30	1.17	-11.23	1.13	-10.62	1.45
	WP	818	-10.44	1.48	-9.98	1.48	-9.56	1.26

Table 9: Mean ($\bar{x}$) and standard deviation (s, based on dB distribution) of the backscattering coefficient (σ°) for HV polarization at all angles and both study areas.

Class	Study Area	Sample Size	Shallow		Medium		Steep	
			$\bar{x}$	s	$\bar{x}$	s	$\bar{x}$	s
Anthropogenic	TH	662	-14.73	4.11	-12.91	4.43	-12.15	4.44
	WP		N/A					
Water	TH	1960	-33.30	1.07	-33.49	1.23	-30.75	1.22
	WP	1056	-34.35	1.12	-34.30	1.20	-33.74	1.21
Smooth/Un-vegetated Mudflat	TH	268	-32.43	1.45	-32.44	1.55	-31.71	1.72
	WP	1050	-30.99	1.55	-29.98	1.61	-29.20	2.27
Rough/Vegetated Mudflat	TH		N/A					
	WP	937	-22.70	1.83	-21.02	1.92	-20.51	2.54
Peat	TH	127	-29.20	2.42	-26.25	2.71	-25.12	2.07
	WP	171	-23.74	2.76	-21.65	2.38	-19.18	2.49
Sand	TH	834	-30.65	1.79	-29.02	2.42	-25.51	3.40
	WP	1233	-29.67	2.81	-28.79	3.34	-25.28	3.54
Mixed Sediment	TH	760	-21.06	2.78	-20.15	2.30	-19.23	3.43
	WP	688	-22.51	1.67	-21.04	2.08	-19.70	1.67
Riprap	TH	140	-21.78	1.97	-20.37	2.40	-18.96	2.07
	WP		N/A					
Wood / Substrate Mix	TH	662	-26.96	2.36	-25.08	2.43	-23.95	2.65
	WP	428	-22.18	2.74	-20.97	3.02	-21.06	2.80
Woody Debris	TH	799	-23.59	1.61	-20.72	1.68	-19.20	1.60
	WP	724	-17.28	1.53	-15.43	1.33	-16.96	1.69
Marsh	TH	249	-24.39	1.74	-21.12	2.09	-20.01	2.60
	WP	923	-21.74	2.42	-20.66	2.86	-20.23	3.38
Wetland	TH	474	-21.56	1.65	-19.34	1.58	-15.37	1.30
	WP	201	-21.14	1.89	-20.04	1.95	-19.66	2.39
ILLT	TH	705	-21.74	1.66	-19.89	1.66	-18.49	1.72
	WP	725	-20.01	1.05	-18.86	1.21	-17.57	1.33
High Centre Polygons	TH		N/A					
	WP	779	-19.74	1.18	-19.19	1.31	-17.42	1.24
Low Centre Polygons	TH	813	-21.94	1.81	-20.86	1.37	-18.55	1.61
	WP	681	-21.38	1.68	-20.40	1.65	-19.39	1.53
Eroding Tundra	TH	489	-18.00	1.98	-16.67	1.75	-16.66	1.98
	WP	477	-17.82	1.87	-16.83	1.78	-17.92	2.40
Herb Dominant Tundra	TH	806	-22.11	1.34	-20.57	1.47	-19.59	1.69
	WP	989	-20.70	1.54	-18.99	2.06	-19.79	1.55
Shrub Dominant Tundra	TH	942	-17.19	1.21	-16.58	1.32	-16.72	1.60
	WP	818	-15.27	1.07	-14.86	1.39	-15.83	1.38

Table 10: Mean ($\bar{x}$) and standard deviation (s, based on dB distribution) of the backscattering coefficient (σ°) for VV polarization at all angles and both study areas.

Class	Study Area	Sample Size	Shallow		Medium		Steep	
			$\bar{x}$	s	$\bar{x}$	s	$\bar{x}$	s
Anthropogenic	TH	662	-7.04	3.58	-6.08	3.91	-3.81	3.72
	WP				N/A			
Water	TH	1960	-22.21	1.32	-19.65	1.28	-7.11	1.36
	WP	1056	-24.16	1.26	-22.19	1.25	-10.14	1.23
Smooth/Un-vegetated Mudflat	TH	268	-19.27	1.90	-17.45	1.67	-11.94	1.63
	WP	1050	-17.55	1.80	-16.06	1.76	-10.60	1.88
Rough/Vegetated Mudflat	TH				N/A			
	WP	937	-10.97	1.53	-8.90	1.58	-5.14	1.66
Peat	TH	127	-17.71	2.49	-14.52	2.24	-8.46	1.19
	WP	171	-13.40	1.84	-12.10	1.51	-7.30	1.65
Sand	TH	834	-20.37	1.76	-17.75	2.16	-11.85	1.90
	WP	1233	-18.51	3.02	-17.52	3.34	-8.87	2.73
Mixed Sediment	TH	760	-13.10	1.84	-11.57	1.66	-8.82	1.78
	WP	688	-13.24	1.49	-11.95	1.54	-9.29	1.66
Riprap	TH	140	-12.85	2.09	-11.51	2.35	-8.28	1.19
	WP				N/A			
Wood/ Substrate Mix	TH	662	-17.38	1.95	-15.08	1.75	-10.16	1.73
	WP	428	-13.20	2.40	-12.26	2.69	-9.78	2.53
Woody Debris	TH	799	-14.71	1.37	-11.64	1.60	-10.13	1.40
	WP	724	-9.50	1.40	-7.77	1.50	-8.30	1.20
Marsh	TH	249	-16.22	1.40	-13.53	1.20	-9.36	1.86
	WP	923	-15.17	1.53	-13.61	1.59	-8.92	1.57
Wetland	TH	474	-10.57	1.26	-8.72	1.26	-11.09	1.91
	WP	201	-13.94	1.52	-13.60	1.74	-10.20	1.56
ILLT	TH	705	-14.93	1.95	-13.23	1.60	-10.26	1.49
	WP	725	-14.31	1.21	-13.38	1.29	-10.25	1.11
High Centre Polygons	TH				N/A			
	WP	779	-13.43	1.27	-12.84	1.27	-10.39	1.29
Low Centre Polygons	TH	813	-14.79	1.70	-13.48	1.84	-9.09	1.74
	WP	681	-14.62	1.63	-14.24	1.34	-10.30	1.28
Eroding Tundra	TH	489	-11.46	1.90	-9.98	1.73	-8.68	2.21
	WP	477	-12.20	1.91	-10.92	2.37	-8.79	2.37
Herb Dominant Tundra	TH	806	-15.52	1.46	-13.92	1.09	-11.46	1.40
	WP	989	-14.46	1.62	-13.39	1.60	-11.82	1.86
Shrub Dominant Tundra	TH	942	-11.44	1.20	-10.60	1.14	-10.37	1.31
	WP	818	-10.20	1.26	-9.68	1.30	-9.45	1.37

0.85). This was also true for all vegetated classes, with the exception of Eroding Tundra in the WP study area ($r_{HH/VV} = 0.88$). As with substrates, however, HH and VV were still generally more correlated than HH and HV, and VV and HV, which were not well correlated for any class at any angle.

4.3.2. Backscatter Consistency Between Study Areas and Incidence Angles

Box and whisker plots used to visually assess the consistency of training data between study areas are provided in Appendix 5, while the percent of values within the overlap region produced by $\bar{x} \pm 2s$ for sample distributions is provided in Table 11. All values greater than 80% were considered to be indicative of a high degree of consistency, and are bolded and italicized. Samples of a class from the two sites that had less than 80% of the pixels in the distribution overlap region were considered to be inconsistent between sites. The classes which showed inconsistencies for all or most incidence angles, across all polarizations, included: Water, Peat, Wood/Substrate Mix, Woody Debris, Wetland and ILLT, with Woody Debris class showing the least consistency. Based on these results, it is anticipated that these classes would be more susceptible to classification error through broad scale mapping.

Average backscatter coefficients were also generally consistent between shallow and medium angles. This is based on a similar assessment of box and whisker plots as well as a calculation of percent of values within the $\bar{x} \pm 2s$ overlap region for sample distributions. These values are provided in Table 12 with exceptions bolded and italicized. This generally included the same classes identified previously (i.e., Water, Peat, Wood/Substrate Mix, Woody Debris, Wetland and ILLT). These results show that

Table 11: Percent of backscatter coefficients within the overlap region produced by the $\bar{x} \pm 2s$ for sample distributions to show the consistency of backscatter between study areas at like polarizations and incidence angles. Values less than 80% are bolded and italicized.

Class	Sample Size	HH			HV			VV		
		Shallow	Medium	Steep	Shallow	Medium	Steep	Shallow	Medium	Steep
Water	3016	92.94	***72.51***	***29.64***	83.32	89.09	***30.87***	***66.41***	***47.48***	***33.22***
Smooth/Un-Vegetated Mudflat	1336	88.62	83.00	82.63	84.45	***63.66***	***73.75***	83.00	85.81	85.05
Peat	298	***60.07***	***77.18***	87.92	***48.99***	***51.34***	***27.52***	***46.98***	***70.81***	84.90
Sand	2067	84.66	81.86	81.18	87.37	90.32	96.81	***78.76***	85.73	75.33
Mixed Sediment	1448	94.06	93.30	94.68	83.49	93.44	81.01	92.40	94.75	93.23
Wood/Substrate Mix	1090	***46.18***	***75.62***	91.17	***56.03***	***70.84***	82.43	***57.31***	81.23	90.62
Woody Debris	1523	***14.25***	***46.16***	***53.25***	***0.00***	***2.04***	***67.63***	***1.38***	***27.25***	***64.28***
Marsh	1172	***77.39***	82.42	92.41	***66.30***	88.23	87.37	86.77	88.74	95.22
Wetland	675	93.01	***74.55***	***29.32***	95.83	93.15	***40.48***	***31.10***	***7.59***	86.76
ILLT	1430	***68.11***	***72.10***	***77.69***	***56.01***	***68.88***	***71.89***	***68.88***	***74.97***	***74.97***
Low Centre Polygons	1494	94.04	90.96	80.99	93.17	92.17	91.37	94.04	87.48	86.95
Eroding Tundra	966	86.75	91.20	96.17	96.07	95.13	87.47	95.13	89.44	95.76
Herb Dominant Tundra	1795	91.31	87.52	90.97	82.73	83.12	95.26	87.91	87.86	89.42
Shrub Dominant Tundra	1760	***71.88***	83.69	85.23	***59.83***	***75.06***	88.41	82.39	87.90	88.13

Table 12: Percent of values within the $\bar{x} \pm 2s$ overlap region for sample distributions extracted from different incidence angles. S = shallow, M = medium, and T = steep. All values less than 80% are bolded and italicized.

Class	Study Area	Sample Size	HH		HV		VV	
			S vs. M	S vs. T	S vs. M	S vs. T	S vs. M	S vs. T
Anthropogenic	TH	662	94.71	92.52	93.20	93.20	94.64	87.31
	WP				N/A			
Water	TH	1960	***28.70***	***0.00***	93.57	***43.57***	***49.62***	***0.00***
	WP	1056	***63.26***	***0.00***	96.12	91.10	***65.20***	***0.00***
Smooth/Un-vegetated Mudflat	TH	268	***62.31***	***0.00***	95.52	92.72	80.04	***0.00***
	WP	1050	***70.19***	***0.00***	88.38	85.10	86.38	***1.19***
Rough/Vegetated Mudflat	TH				N/A			
	WP	937	***65.74***	***0.00***	83.40	82.71	***71.50***	***2.03***
Peat	TH	127	***79.13***	***0.00***	***75.59***	***50.39***	***70.47***	***0.00***
	WP	171	86.84	***5.56***	84.50	***51.75***	86.26	***4.97***
Sand	TH	834	***69.54***	***0.00***	88.13	***69.36***	***75.66***	***0.00***
	WP	1233	94.32	***4.14***	93.84	***71.37***	95.34	***5.76***
Mixed Sediment	TH	760	84.54	***36.71***	91.38	90.92	84.21	***38.29***
	WP	688	86.85	***33.65***	86.56	***59.01***	85.61	***29.72***
Riprap	TH	140	87.50	***21.07***	92.14	***66.79***	92.14	***17.50***
	WP				N/A			
Wood/Substrate Mix	TH	662	***74.77***	***3.17***	86.71	***77.27***	***74.17***	***0.38***
	WP	428	93.18	83.06	93.29	91.76	93.65	***72.47***
Woody Debris	TH	799	***58.01***	***36.42***	***59.51***	***18.77***	***46.81***	***6.26***
	WP	724	81.28	88.60	***76.17***	94.27	***77.69***	80.87
Marsh	TH	249	***64.26***	***3.41***	***66.47***	***53.21***	***48.19***	***0.00***
	WP	923	91.22	***20.15***	94.10	90.90	81.31	***0.00***
Wetland	TH	474	***60.21***	***1.58***	***73.58***	***0.00***	***69.05***	86.53
	WP	201	93.43	85.86	90.15	89.39	93.43	***37.12***
ILLT	TH	705	***77.23***	***12.55***	80.14	***49.57***	81.13	***15.32***
	WP	725	84.14	***29.52***	80.83	***48.28***	88.14	***4.28***
High Centre Polygons	TH				N/A			
	WP	779	86.46	***27.15***	91.66	***51.93***	91.08	***34.98***
Low Centre Polygons	TH	813	***78.84***	***1.29***	87.64	***47.42***	86.10	***7.87***
	WP	681	91.85	***30.76***	88.55	***75.18***	92.07	***11.97***
Eroding Tundra	TH	489	***72.70***	***68.20***	87.32	88.34	86.30	***76.18***
	WP	477	89.62	81.66	89.20	92.14	89.73	***63.84***
Herb Dominant Tundra	TH	806	***76.18***	***27.11***	81.20	***60.67***	***72.08***	***17.31***
	WP	989	84.83	***59.50***	83.92	90.19	88.52	***70.27***
Shrub Dominant Tundra	TH	942	83.81	***77.44***	92.30	90.82	87.53	86.15
	WP	818	93.95	88.14	89.85	88.51	92.54	90.89

at relatively shallow angles a difference of 6-8° in incidence angle may not significantly alter backscattering behaviour. Multi-angle acquisitions may therefore be considered redundant. In contrast, backscatter coefficients between shallow and steep angles were generally inconsistent, except for classes with rougher surfaces, including Shrub Dominant Tundra. Anthropogenic also showed consistent backscattering behaviour at all angles and it should be noted that some polarizations showed more consistency than others, including HV for Smooth/Un-Vegetated Mudflat.

4.3.3. Assessment of Backscatter coefficients for Individual Classes and Potential for Feature Detection and Discrimination with Colour Composites

Based on a visual analysis of backscatter coefficients (using linear power values, with HH in red, HV in green, and VV in blue), there was overall better contrast between classes at shallow and medium angles. Despite this, some classes were easier to detect in steep angle imagery. The following section summarizes the potential observed for visual feature detection and discrimination, as well as a characterization of the contribution to total power from HH, HV and VV. Note that images provided in the following section show examples for shallow and steep angles only, since in most cases shallow and medium angle images were similar.

Anthropogenic

Overall, the total power observed over Anthropogenic was high relative to other classes, with HH contributing the most, followed closely by VV. As mentioned previously, changes in backscatter coefficients with incidence angle were small, indicating some consistency between incidence angles (Table 8, Table 9, and Table 10).

Figure 11 (a - c) shows that anthropogenic features appeared generally similar in all colour composites, as mostly magenta [red (HH) and blue (VV) contributions nearly equal], to red, as well as white [red (HH), green (HV) and blue (VV) contributions nearly equal] and green (> HV) in some low density areas, or where features were oriented close to parallel to radar line of sight.

Water and Substrates

On average VV contributed the most to total power for classes with relatively smooth surfaces, including: Water, Smooth/Un-Vegetated Mudflat, Rough/Vegetated Mudflats, Peat and Sand. This was observed at all angles and generally made features appear blue in colour composites. For these classes, the difference between HH and VV contributions also decreased with steeper incidence angles (e.g. for Smooth/Un-Vegetated Mudflat in the WP study area, VV was 5.05, 4.02 and 1.16 dB higher than HH at shallow, medium and steep angles, respectively). Rough/Vegetated Mudflat, Peat and Sand also had slightly higher HH contributions as a percentage of total power compared to Water and Smooth/Un-Vegetated Mudflat. The rank of these classes from lowest to highest backscatter (i.e., Water, Smooth/Un-Vegetated Mudflat, Sand, Peat, and Rough/Vegetated Mudflat), again seemed related to increasing surface roughness.

At shallow and medium angles it was difficult to distinguish Water, Smooth/Un-Vegetated Mudflats and Sand, as these classes all appeared relatively dark. It is of interest to note that those areas most confused with water were generally interpreted as wetter, and based on the fact that they were typically located near the land-water interface, they could have also been flooded during acquisitions. This is apparent in Figure 11 (d - f), which shows a relatively wet sand beach at the time helicopter videography was acquired.

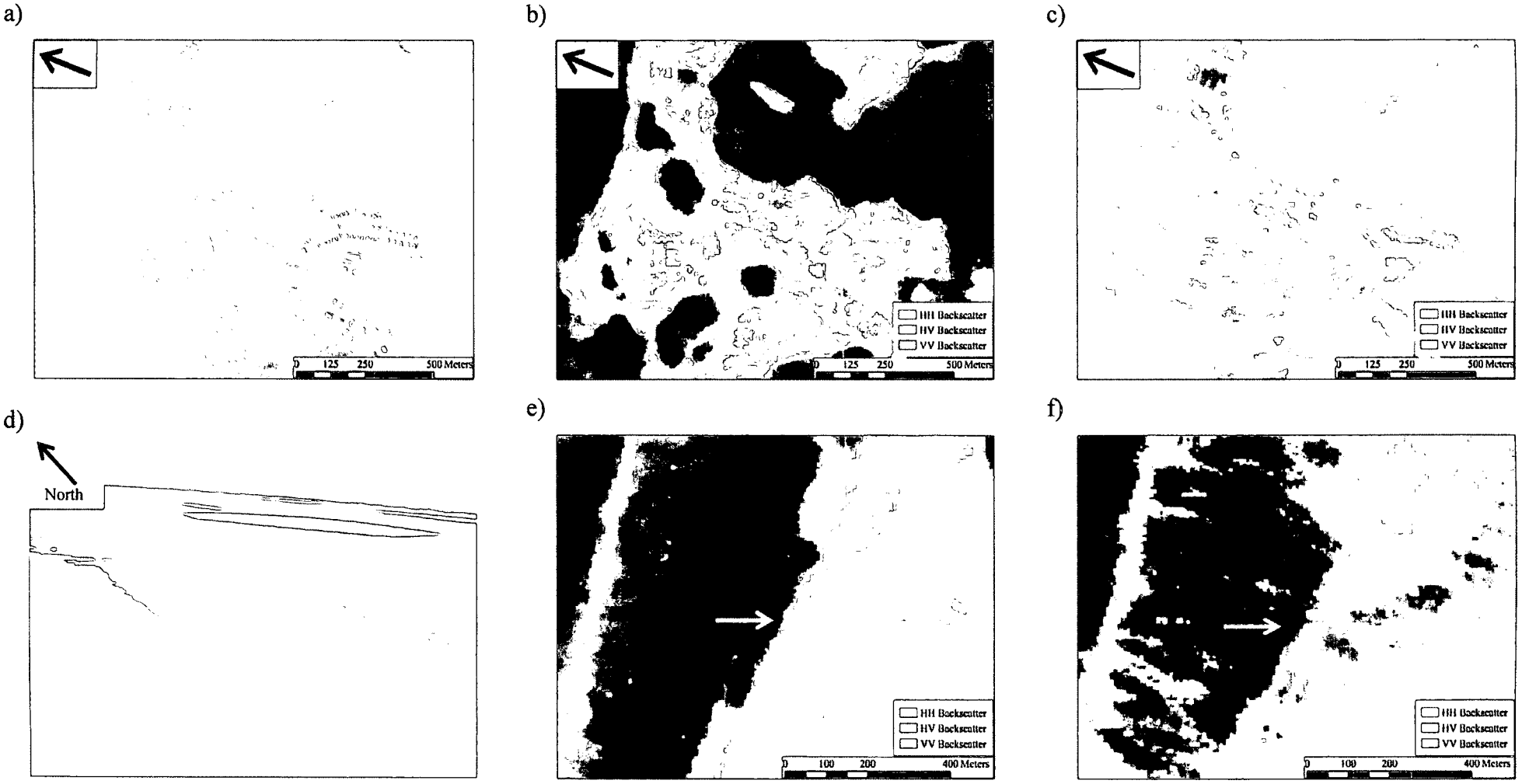

Figure 11: Segment of 2004 ortho photos of anthropogenic features from the TH study area (a), and colour composites of the same area at shallow (b), and steep (c) angles. Arrows show the look direction, with red and green circles indicating features oriented more perpendicular, and parallel, respectively. (d) shows a snapshot from 2010 helicopter videography of a sand beach, and colour composites at shallow (e) and steep (f) angles over the same area.

At steep angles the total power over Water was significantly higher than these classes making it easier to distinguish them, as the latter remained dark, while the former appeared bright purple to magenta [red (HH) and blue (VV) combined in different proportions]. This was especially true for the most saturated mudflats, which could not be distinguished from Water at shallow and medium angles [Figure 12 (a – c)].

Peat, Rough/Vegetated Mudflat, Mixed Sediment, Riprap, Wood/Substrate Mix and Woody Debris generally had higher intensity values than Water Smooth/Un-Vegetated Mudflat and Sand (5 – 10 dB on average, with larger differences observed at shallow angles) and so these groups could generally be distinguished from each other. Contributions from HH and VV were also more consistent for these classes, and again this was especially true at shallow angles. Based on this, a number of classes showed potential for detection. As an example, Rough/Vegetated Mudflats showed high visual contrast with Water and Smooth/Un-Vegetated Mudflat. This class was brighter, and also purple in colour at shallow and medium angles, and pink [red (HH), green (HV) and blue (VV) nearly equal, with slightly more red] at steep angles [Figure 12 (d – f)].

Mixed Sediment was also generally brighter and more textured than Water, Smooth/Un-Vegetated Mudflat, and Sand, as is apparent in Figure 13 (a – c). Despite this, it was also difficult to distinguish from Riprap and Wood/Substrate Mix; as all these features were all bright and pink to white in colour. Figure 13 (d – f) for example, shows an area of Wood/Substrate Mix which is indistinguishable from Mixed Sediment in Figure 13 (a – c). Woody Debris, however, could be distinguished from a number of these classes including Wood/Substrate Mix, as in most cases, this class was brighter and generally contained more white pixels, as is apparent in Figure 14 (a – c). It should also

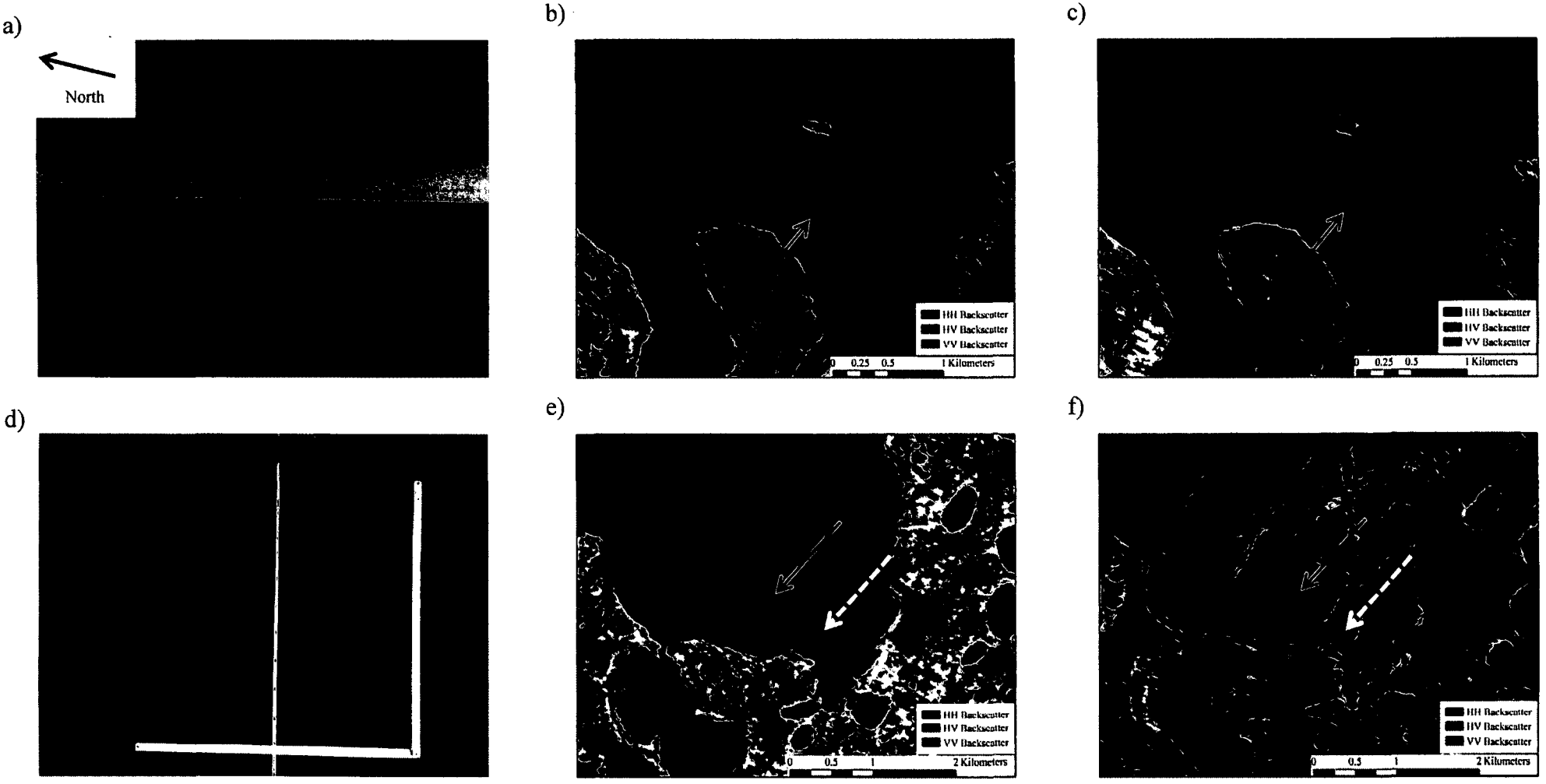

Figure 12: Snapshot from helicopter videography of a saturated mudflat (a) at the red arrow, which is indistinguishable in shallow (b) colour composites, but can be identified at steep angles (c). (d) shows a ground photo of Rough/Vegetated Mudflat with caribou tracks. Shallow (e) and steep (f) colour composites show the difference between this class (white arrows) and Smooth/Un-Vegetated Mudflat class (red arrows).

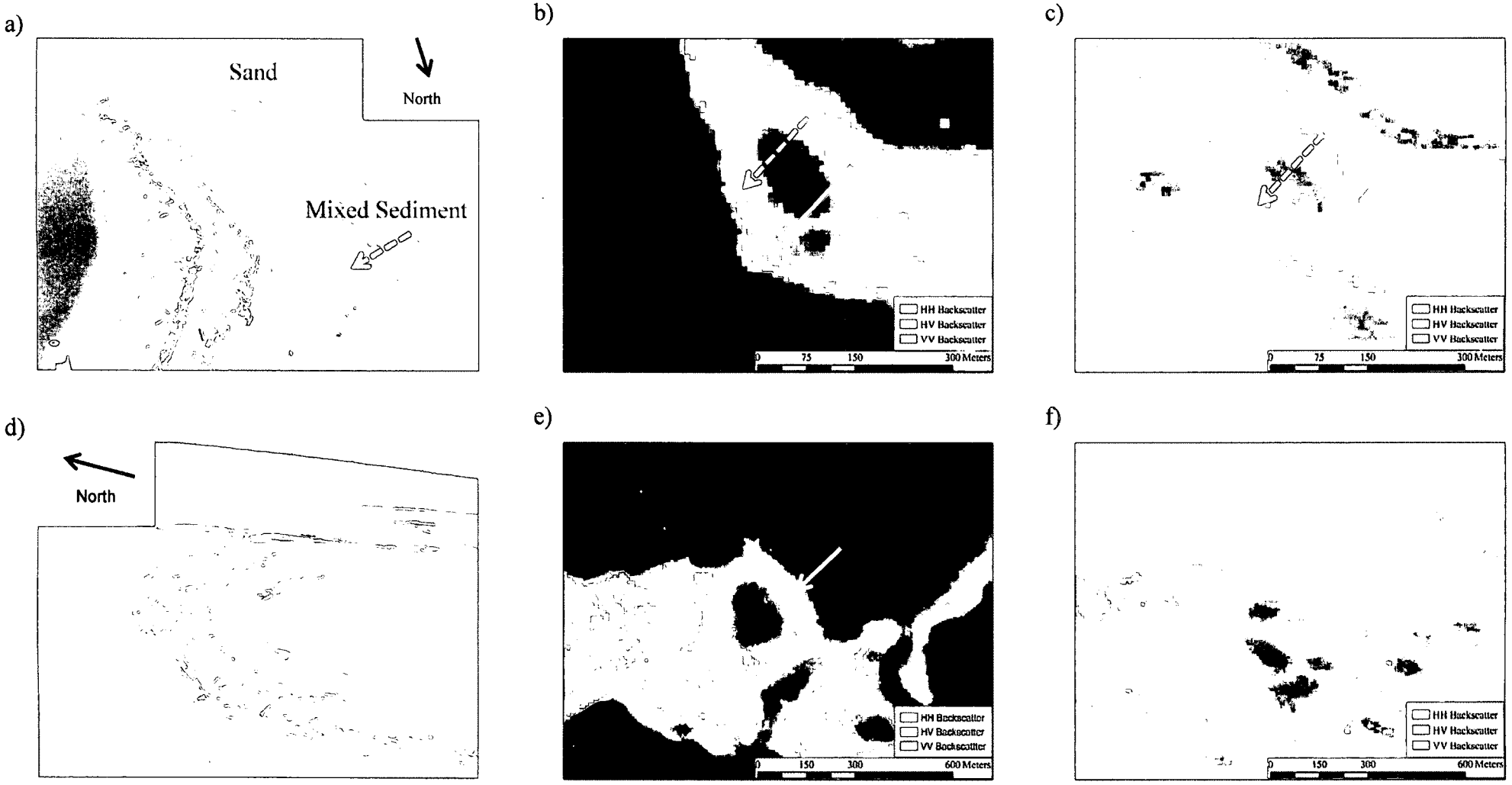

Figure 13: Snapshot from 2010 helicopter videography (a) of an area containing Sand (red arrow) and Mixed Sediment (white arrow) to show contrast between them at shallow (b) and steep angles (c). (d) also shows a snapshot from 2010 helicopter videography of Wood/Substrate Mix, as well as colour composites at shallow (e) and steep (f) angles of the same area.

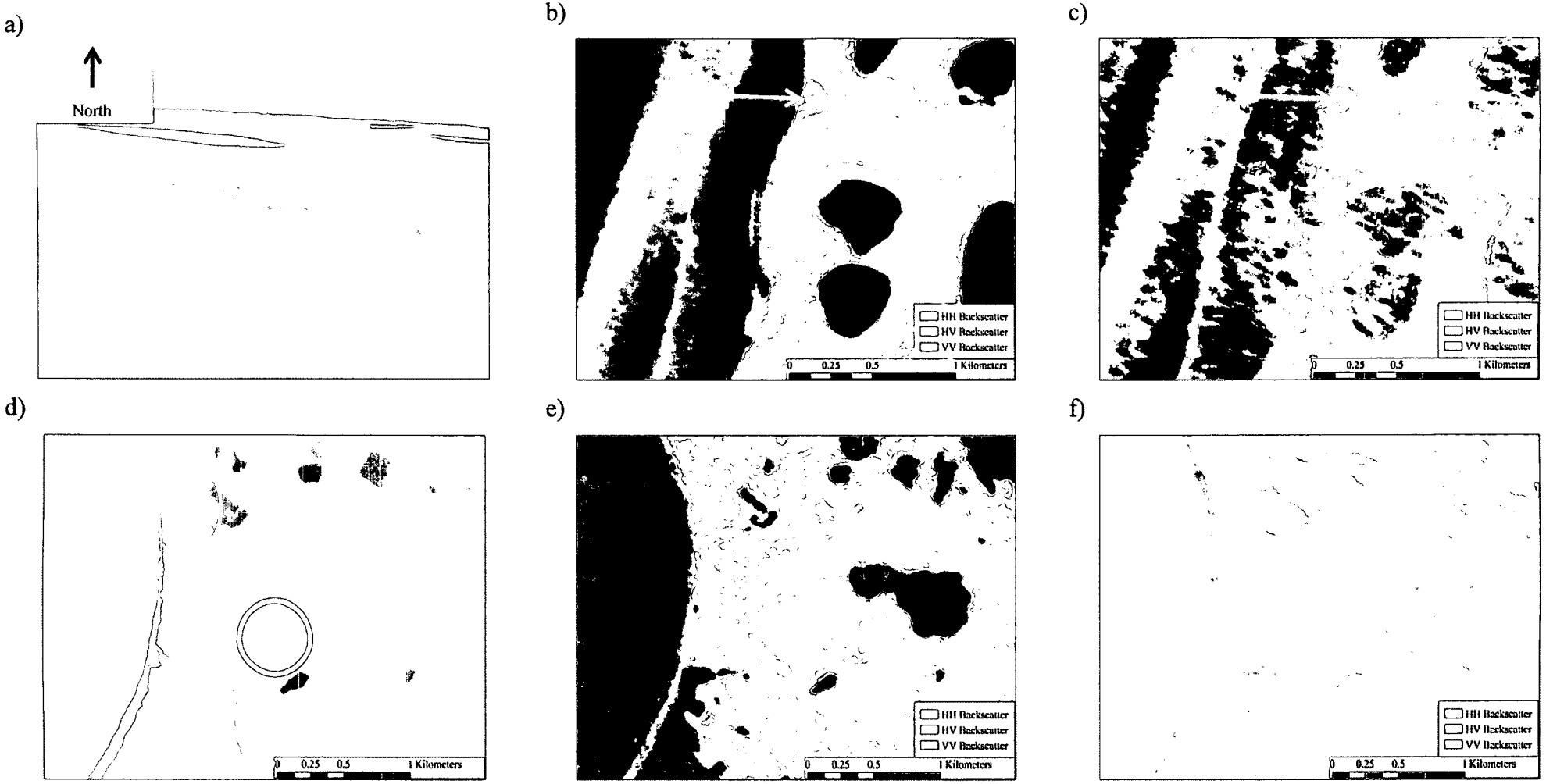

Figure 14: Snapshot from 2010 helicopter videography (a) of Woody Debris, as well as colour composites of the same area at shallow (b) and steep angles (c). d) shows a snapshot from helicoter videography with circles indicating a number of classes, including Shrub Dominant Tundra = red, Herb Dominant Tundra = yellow, ILLT = blue, and Low Centre Polygons = orange. e) and f) are radar colour composites of the area at shallow and steep angles, respectively.

be noted that both Wood/Substrate Mix and Woody Debris were easier to detect in the WP study area, as they were generally brighter than in the TH study area.

Vegetated Classes

Many of the vegetated classes appeared relatively similar in colour composites, including: Wetland (WP study area only), Marsh, ILLT, Low Centre Polygons, High Centre Polygons, and in some cases Herb Dominant Tundra [Figure 14 (d – f)]. These classes generally contained mixed pixels, and in some cases appeared similar to Mixed Sediment, and other substrates with rougher surfaces. All vegetated classes showed similar HH and VV contributions to total power with the exception of the Wetland class in the TH study area, which showed higher average HH backscatter (3.24 dB) than average VV at shallow angles. As was observed with substrate classes, however, the difference between HH and VV also tended to decrease with steeper incidence angles.

Eroding Tundra and Shrub Dominant Tundra could generally be distinguished from other classes, though not from one another, and this was especially true at shallow angles. This is due to Wetland (WP study area only), Marsh, ILLT, Low Centre Polygons, High Centre Polygons, and in some cases Herb Dominant Tundra being dominantly pink, purple and green in colour composites while Eroding Tundra and Shrub Dominant Tundra were mostly green to white, indicating a dominant contribution from HV to total power in most cases, and in other cases an equal contribution from all polarizations. This can be observed in Figure 14 (d – f). At steep angles it was more difficult to discern these classes, as most features tended to appear green, though Eroding Tundra and Shrub Dominant Tundra generally remained brighter. Significant potential was also observed for distinguishing between vegetated features and substrates with

smoother surfaces and Water. For example, this made it possible to identify marshes in the WP study area along the west side of Richards Island [Figure 15 (a-c)].

Wetland in the TH study area was distinct from other vegetated classes in that it was the only class to appear yellow at steep angles, in colour composites [nearly equal red (HH) and green (HV)] [Figure 15 (d – f)]. At shallow angles this wetland was coloured similarly to Marsh, ILLT, Low Centre Polygons, and High Centre Polygons, being mostly pink and purple. It should also be noted that this wetland was visually distinct from the Wetland in the WP study area.

4.4. Polarimetric Signatures of Arctic Land Cover Types

4.4.1. Sample Statistics, General Observations and Trends

Co-polarized polarimetric signatures showed potential for general feature detection and discrimination. This includes the ability to distinguish between rough and smooth surfaces, as well as to detect wetlands and anthropogenic features. Despite this, signatures were also highly variable, especially for features with rougher surfaces. This was especially the case for vegetated land covers, which also showed less contrast between classes.

Pedestal height was useful for differentiating classes (Appendix 6). Values generally increased with surface roughness, and this was more apparent at shallow angles. As an example, the co-polarized pedestal heights for Smooth/Un-Vegetated Mudflat, Sand, Mixed Sediment and Riprap in the TH study area were 0.14, 0.20, 0.23, and 0.26, respectively. Pedestal height was generally lower at steep compared to shallow angles, indicating that at steep angles a greater proportion of the backscattered signal was

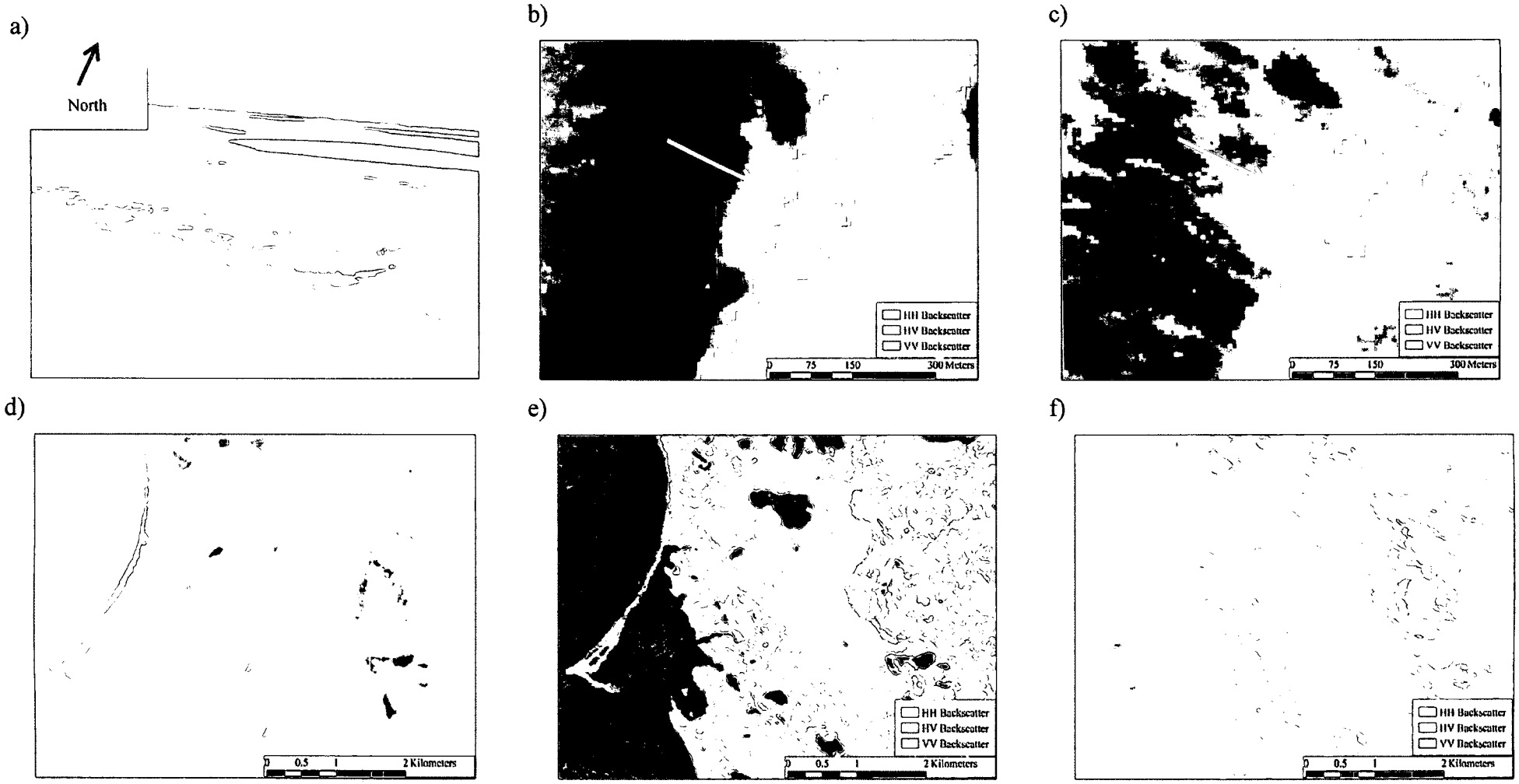

Figure 15: Snapshot from 2010 helicopter videography of a Marsh in the TH study area (a), and colour composites at shallow (b) and steep (b) angles of the same area. d) also shows a segment of 2004 ortho photos, including the Wetland class in the TH study area, with shallow (e) and steep (f) composites of the same area.

polarized. Values were also generally larger for vegetated surfaces compared to substrates.

Pedestal height is considered further in Section 4.4.3, as it can be useful in determining the dominant scattering mechanism. The following section summarizes results obtained from the polarimetric plot analysis and presents only shallow and steep signatures for select classes, as signatures from medium angle imagery were generally similar to shallow. Note that there are no signatures for Peat since it was generally too thin (< 4 pixels wide) and could not be reliably sampled using unfiltered, slant range imagery.

4.4.2. Consistency of Signatures Between Study Areas and Incidence Angles

Polarimetric signatures for each class were generally comparable between study areas for like-incidence angles except for Water and Wetland, for which responses were consistently different. In most cases interpretations for shallow and medium angle images were also similar for the same study area, except again for Water and Wood/Substrate Mix from the TH study area, and Water and Marsh from the WP study area. This is consistent with results observed for backscatter coefficients, indicating that a difference in incidence angle of 6-8° may not affect dominant scattering behaviour. In contrast, signatures generated at steep angles were generally distinct from shallow and medium, although for Mixed Sediment, Woody Debris, and ILLT, signatures were similar at all angles.

4.4.3. Assessment of Signatures for Individual Classes to Determine Scattering Mechanisms and Potential for Feature Detection and Discrimination

Overall, greater contrast between signatures was observed at shallow angles, whereas scattering behaviour was more comparable across land cover classes at steep incidence angles (Figure 16 and Figure 17). For brevity, the following section summarizes results for co-polarized signatures only.

Anthropogenic

Signatures generated for the Anthropogenic class were visually distinct from all classes, except for Wetland in the TH study area (Figure 18). At shallow and medium angles, co-polarized signatures for this class were also similar to theoretical responses produced for dihedral, or corner reflectors at similar incidence angles (45°). This includes a peak contribution from linear HH and two valleys at about 62 and 118° orientation angles, as well as a relatively high pedestal height at around 0.4 (van Zyl et al., 1987). At steep angles however, signatures generated for Anthropogenic showed less prominent double bounce, and were often indicative of volume and or multiple scattering. This interpretation is based on the fact that peak contributions were observed at HH as well as VV, and pedestal heights were also relatively high (van Zyl et al., 1987).

Water and Substrates

Signatures for classes with relatively smooth surfaces, including: Water, Smooth/Un-Vegetated Mudflat, Rough/Vegetated Mudflat and Sand could all be interpreted similarly (Figure 16). All showed a maximal response in linear VV return with relatively low pedestal heights, as well as a high VV to HH ratio at shallow angles,

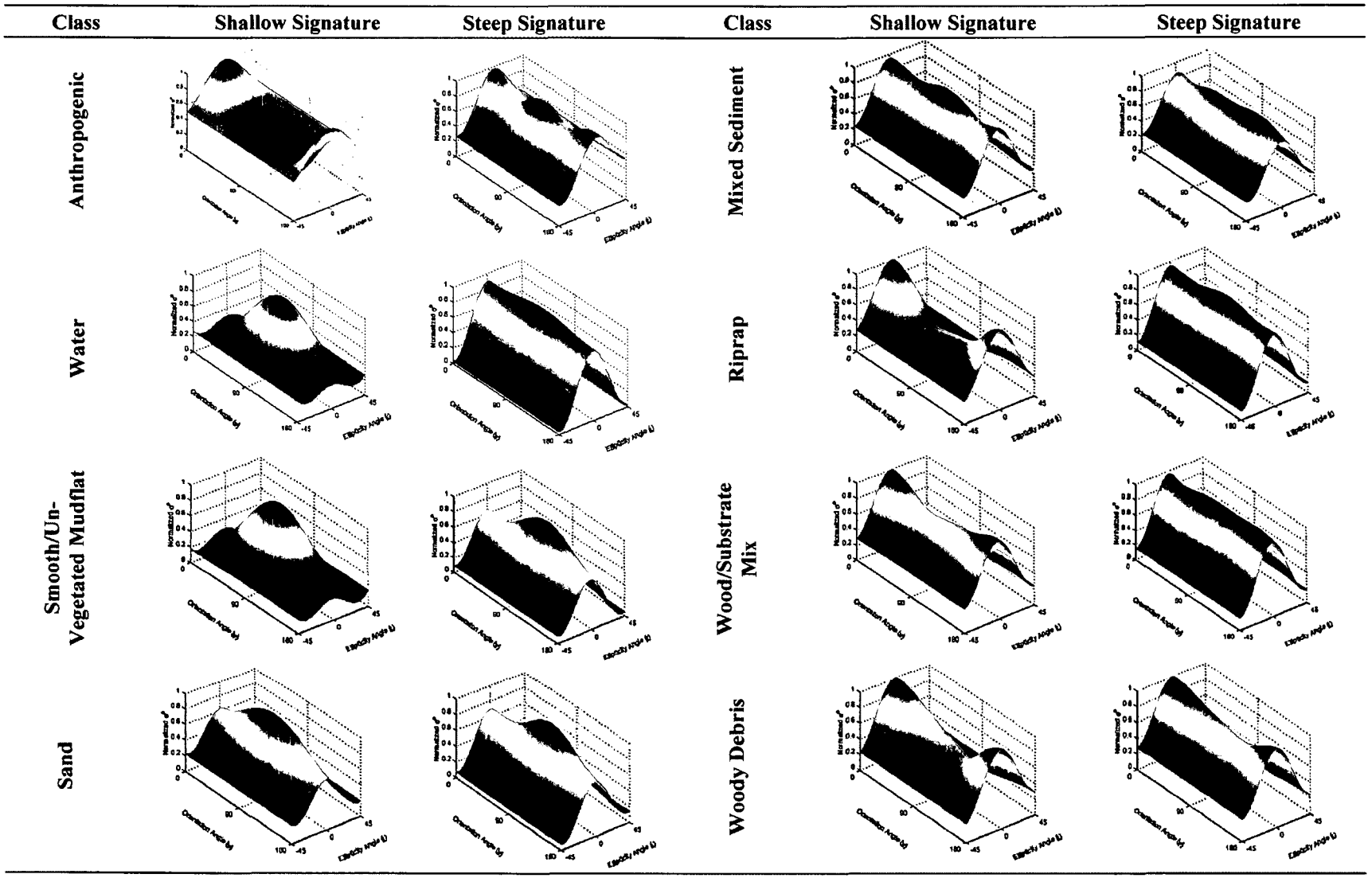

Figure 16: Co-polarized polarimetric signatures generated from shallow and steep angle imagery for Water and substrate classes in the TH study area. Signatures for Rough/Vegetated Mudflat are not shown because they were similar to Sand.

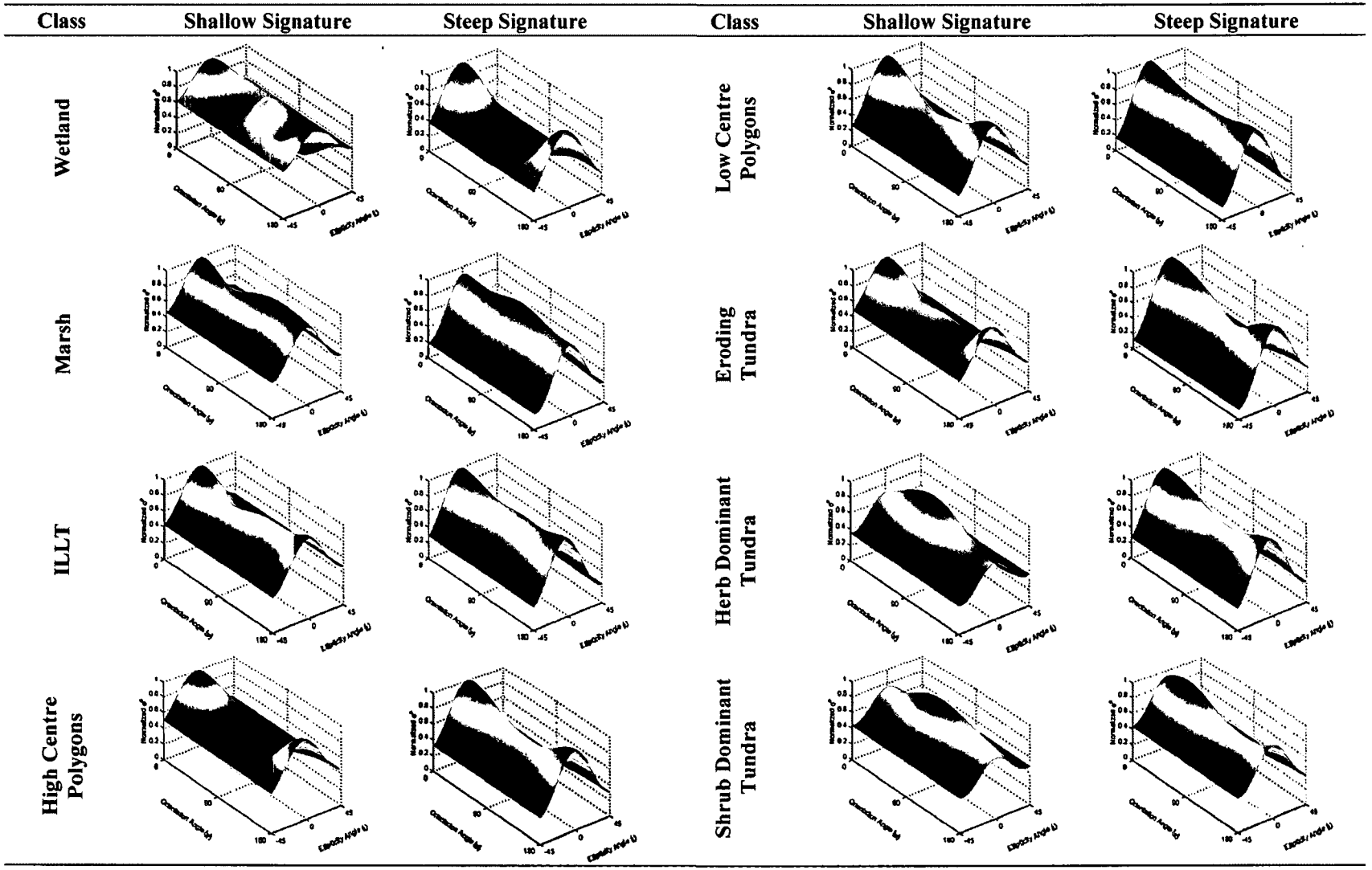

Figure 17: Co-polarized polarimetric signatures generated from shallow and steep angle imagery for vegetated classes in the TH study area, with the exception of the High Centre Polygons class from the WP study area.

a)

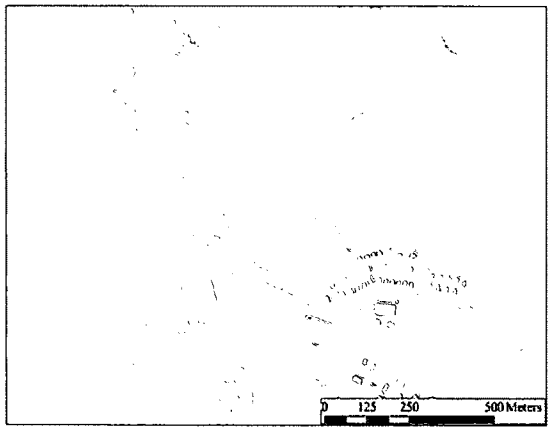

b)

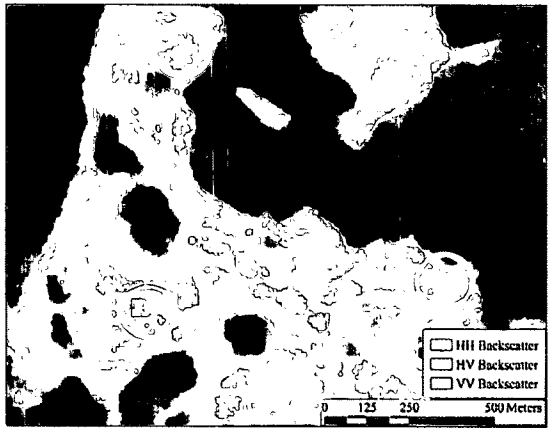

c)

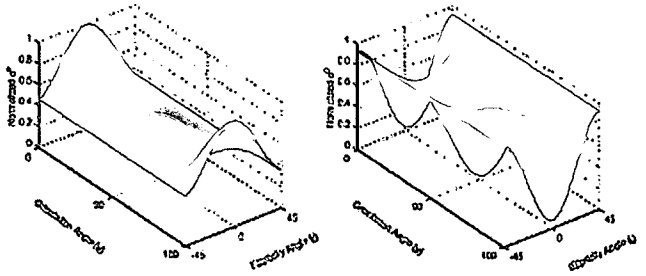

d)

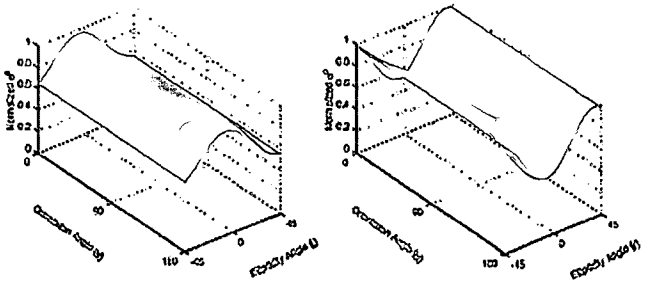

e)

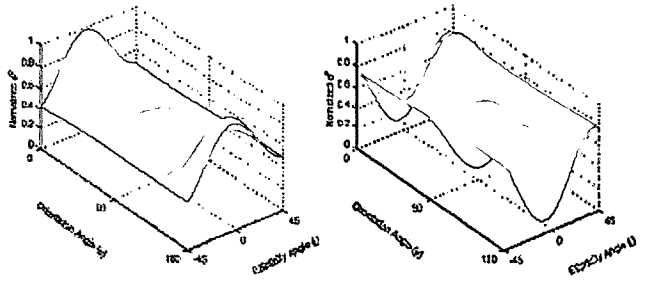

Figure 18: Co and cross-polarized polarimetric signatures over various anthropogenic features to show unique responses compared to all classes except Wetland in the TH study area. a) and b) show a portion of ortho photos and of shallow angle imagery from the TH study area, where samples were taken. c), d) and e) show co-polarized (left) and cross-polarized (right) signatures for the same areas indicated on the maps by red, green and blue circles, respectively.

which decreased as incidence angles steepened, as HH contributions increased. This behaviour is typical of surface scatterers, with the shape of shallow incidence angle plots also indicative of some element of Bragg scattering at shallow angles (van Zyl et al., 1987; Dobson & Ulaby, 1998). It should also be noted that at steep angles, Water also appeared similar to plots generated from theoretical models of a perfectly smooth dielectric surface (van Zyl et al., 1987).

With signatures, potential was observed to discriminate Rough/Vegetated Mudflat and Sand, from Water and Smooth/Un-Vegetated Mudflat at shallow angles. This is because plots for the former showed less prominent peaks in linear VV and therefore a lower VV to HH ratio. This is again consistent with observations made of backscatter coefficients, as these classes showed a higher contribution of HH to total power. There was also greater contrast observed between Water and Smooth/Un-Vegetated Mudflat at steep angles, as the peak in VV remained more prominent in the latter (Figure 16).

Signatures for Mixed Sediment were unique from Water and those substrates mentioned previously. Like all classes with rougher surfaces however, signatures also tended to be more variable. Generally, responses were indicative of dominant volume and or multiple scattering with near equal intensity contributions from all polarizations, as well as higher pedestal heights. Riprap also had a higher pedestal height compared to features with smoother surfaces; however the shape of plots at shallow angles was more indicative of dominant double bounce scattering (van Zyl et al., 1987). The responses for Riprap were also similar to Wood/Substrate Mix and Woody Debris. It is of interest to note that at shallow angles, the signature for Wood/Substrate Mix appeared to be a mixture of the signature generated for Sand and Woody Debris. This may be expected as

this land cover contains mixed pixels, comprised of both substrate types.

Vegetated Classes

Signatures generated for Marsh, ILLT, Low Centre Polygons and Eroding Tundra were highly variable with no potential to differentiate between them. Generally, signatures were indicative of dominant volume and or multiple scattering with near equal contributions at all polarizations, and relatively high pedestal heights (typically ~ 0.4). At shallow angles, signatures for Eroding Tundra were visually distinct from these classes, which was largely due to the higher pedestal heights (Figure 17). Signatures for High Centre Polygons (only in WP study area) were also distinct from these classes, especially because responses were more stable compared to other vegetated classes. For this class, a maximal response at HH with relatively little VV return was also observed, as well as a high pedestal height, indicating dominant double bounce scattering (van Zyl et al., 1987).

The responses observed for Wetland were also very distinct between study areas. Despite this, characteristics about cross-polarized plots may be useful for detecting these classes. Wetlands for both study areas, as well as Anthropogenic, were the only classes to show peaks outside 0° and 45/-45° orientation angle in cross-polarized plots. Shrub Dominant and Herb could be distinguished from those classes mentioned previously, including Wetland. Signatures for both, were indicative of rough surface scattering and while the shape of plots were similar, potential was observed for using pedestal height to differentiate these land covers (van Zyl et al., 1987). Values for Shrub Dominant Tundra specifically, were generally higher than Herb Dominant Tundra (Figure 17).

4.5. Freeman-Durden Decomposition Characteristics of Arctic Land Cover Types

4.5.1. Sample Statistics,General Observations, and Trends

Odd bounce, double bounce and volume scattering mean and standard deviation based on dB value distributions are provided in Table 13, Table 14 and Table 15. As mentioned previously, training data were not typically normally distributed, as visually assessed using histograms.

A number of trends from these data can be identified however, including that the total power observed over smooth surfaces is generally lower than over rough surfaces, and as with backscatter coefficients, this was more apparent at shallow compared to steep angles. As an example, for Smooth/Un-Vegetated Mudflat, Sand, and Mixed Sediment, average odd bounce contributions were: -19.17, -20.06, and -13.77, respectively. Similarly to backscatter coefficients, these differences showed potential to discriminate generally between rough and smooth surfaces. Odd bounce scattering also tended to be the dominant scattering mechanism for Water and substrates, while vegetated areas tended to be dominated by volume scattering (dominant scattering mechanisms for classes are bolded and italicized in Table 13, Table 14 and Table 15).

4.5.2. Consistency of Contributions to Total Power Between Study Areas and Incidence Angles for Odd Bounce, Double Bounce and Volume Scattering

Box and whisker plots were primarily used to visually assess the consistency of training data from Freeman-Durden decomposition parameters between study areas. These are provided in Appendix 7 using quartiles for box and whisker extents. Again, this is because data were not normally distributed, but often bimodal or highly skewed when a

Table 13: Mean ($\bar{x}$) and standard deviation (s), based on the dB distributions of the odd bounce contribution to total power at all angles for both study areas. Values bolded and italicized represent the dominant scattering mechanism for a given class at that angle.

Class	Study Area	Sample Size	Shallow		Medium		Steep	
			$\bar{x}$	s	$\bar{x}$	s	$\bar{x}$	s
Anthropogenic	**TH**	662	***-9.92***	10.32	***-11.00***	10.14	***-5.94***	6.92
	WP				N/A			
Water	**TH**	1960	***-23.43***	3.56	***-19.29***	1.58	***-4.52***	1.41
	WP	1056	-25.45	3.61	***-21.95***	1.69	***-7.70***	1.28
Smooth/Un-vegetated Mudflat	**TH**	268	***-19.17***	2.06	***-16.79***	1.66	***-9.85***	1.65
	WP	1050	***-17.62***	2.75	***-15.62***	2.16	***-8.47***	2.01
Rough/Vegetated Mudflat	**TH**				N/A			
	WP	937	***-10.65***	2.94	***-8.00***	2.08	***-3.09***	1.87
Peat	**TH**	127	***-17.38***	3.53	***-13.57***	2.90	***-6.18***	1.33
	WP	171	***-13.31***	4.60	***-12.02***	4.86	***-5.66***	1.94
Sand	**TH**	834	***-20.06***	2.88	***-16.45***	2.65	***-9.82***	2.28
	WP	1233	***-18.45***	4.32	***-17.01***	4.37	***-6.66***	3.00
Mixed Sediment	**TH**	760	-13.77	6.10	-11.58	4.28	***-7.48***	3.70
	WP	688	***-12.86***	4.68	***-11.60***	3.87	***-8.01***	3.01
Riprap	**TH**	140	***-12.27***	5.06	***-11.12***	6.94	***-6.75***	1.82
	WP				N/A			
Wood and Substrate Mix	**TH**	662	***-16.60***	2.78	***-13.88***	2.17	***-8.09***	1.93
	WP	428	***-11.59***	5.78	***-10.94***	5.35	***-7.91***	3.57
Woody Debris	**TH**	799	***-12.22***	3.82	***-8.74***	4.42	***-8.41***	2.61
	WP	724	***-7.28***	6.64	***-5.67***	6.09	***-5.85***	2.08
Marsh	**TH**	249	-16.66	5.39	-14.82	5.82	***-7.93***	3.19
	WP	923	-16.93	8.45	-14.69	6.93	***-7.25***	2.61
Wetland	**TH**	474	-14.02	4.46	-12.33	5.22	-9.88	6.83
	WP	201	-15.37	7.75	-14.08	8.15	-8.13	2.79
ILLT	**TH**	705	-16.73	6.84	-14.52	6.98	***-8.99***	2.77
	WP	725	-16.71	9.38	-16.40	8.02	-10.36	4.04
High Centre Polygons	**TH**				N/A			
	WP	779	-17.88	8.59	-16.46	7.76	-10.19	4.97
Low Centre Polygons	**TH**	813	-16.22	6.74	-14.53	6.05	***-7.75***	2.25
	WP	681	-16.59	6.89	-16.72	6.96	***-9.28***	2.61
Eroding Tundra	**TH**	489	-15.65	8.74	-12.18	9.08	-8.12	6.10
	WP	477	-15.06	10.14	-12.79	9.61	***-7.84***	4.16
Herb Dominant Tundra	**TH**	806	-17.08	6.47	-15.42	6.00	-11.31	2.79
	WP	989	-17.64	8.54	-16.70	7.91	-11.50	4.18
Shrub Dominant Tundra	**TH**	942	-17.13	8.61	-15.26	8.50	-12.60	4.42
	WP	818	-17.46	9.80	-16.38	8.75	-11.99	5.97

Table 14: Mean ($\bar{x}$) and standard deviation (s), based on the dB distributions of the double bounce contribution to total power at all angles for both study areas. Values bolded and italicized represent the dominant scattering mechanism for a given class at that angle.

Class	Study Area	Sample Size	Shallow		Medium		Steep	
			$\bar{x}$	s	$\bar{x}$	s	$\bar{x}$	s
Anthropogenic	**TH**	662	-7.42	10.70	-6.59	10.92	-5.39	7.74
	WP				N/A			
Water	**TH**	1960	-31.08	0.77	-29.69	0.81	-20.25	0.18
	WP	1056	-32.56	1.73	-30.65	0.42	-23.43	0.21
Smooth/Un-vegetated Mudflat	**TH**	268	-30.64	1.27	-29.08	1.44	-20.28	0.02
	WP	1050	-30.13	2.89	-28.64	2.11	-23.11	0.64
Rough/Vegetated Mudflat	**TH**				N/A			
	WP	937	-23.46	5.75	-23.39	4.69	-20.74	2.56
Peat	**TH**	127	-26.41	3.31	-25.53	3.26	-20.03	0.62
	WP	171	-23.89	5.89	-23.80	4.75	-20.52	2.77
Sand	**TH**	834	-28.64	2.31	-26.46	2.69	-20.18	0.38
	WP	1233	-26.87	4.14	-26.36	3.21	-22.14	1.64
Mixed Sediment	**TH**	760	-23.01	5.21	-21.85	5.03	-19.72	1.01
	WP	688	-22.31	6.19	-22.67	5.00	-20.61	2.66
Riprap	**TH**	140	-20.16	6.09	-20.03	6.12	-18.26	2.05
	WP				N/A			
Wood and Substrate Mix	**TH**	662	-25.81	3.43	-24.35	3.54	-20.01	0.59
	WP	428	-20.92	6.47	-21.25	5.39	-21.00	2.38
Woody Debris	**TH**	799	-21.80	4.86	-19.75	5.26	-17.63	2.43
	WP	724	-19.55	8.13	-19.17	7.10	-18.92	3.52
Marsh	**TH**	249	-22.66	4.54	-19.89	5.48	-19.25	1.26
	WP	923	-20.45	7.27	-20.48	5.74	-20.45	2.59
Wetland	**TH**	474	***-10.25***	2.53	***-7.61***	3.22	-15.36	4.01
	WP	201	-13.25	8.22	-14.57	8.02	-18.83	3.31
ILLT	**TH**	705	-20.21	6.30	-17.22	6.97	-18.76	1.76
	WP	725	-21.45	7.49	-20.64	6.31	-19.48	3.23
High Centre Polygons	**TH**				N/A			
	WP	779	-15.45	8.67	-14.67	6.84	-17.86	4.07
Low Centre Polygons	**TH**	813	-20.17	5.79	-17.81	5.84	-18.87	1.62
	WP	681	-19.98	6.94	-20.14	6.19	-20.64	2.65
Eroding Tundra	**TH**	489	-20.90	6.61	-18.36	7.03	-18.35	2.26
	WP	477	-21.15	7.84	-20.31	6.68	-19.47	3.03
Herb Dominant Tundra	**TH**	806	-26.76	3.81	-26.01	3.53	-19.89	0.81
	WP	989	-24.49	6.25	-25.26	4.32	-21.67	2.07
Shrub Dominant Tundra	**TH**	942	-24.41	4.97	-22.73	5.25	-19.43	1.36
	WP	818	-24.80	5.77	-21.17	6.21	-20.02	3.17

Table 15: Mean ($\bar{x}$) and standard deviation (s), based on the dB distributions of the volume scattering contribution to total power at all angles for both study areas. Values bolded and italicized represent the dominant scattering mechanism for a given class at that angle.

Class	Study Area	Sample Size	Shallow		Medium		Steep	
			$\bar{x}$	s	$\bar{x}$	s	$\bar{x}$	s
Anthropogenic	**TH**	662	-5.68	4.10	-4.13	4.32	-3.55	4.31
	WP				N/A			
Water	**TH**	1960	-23.69	1.58	-24.45	1.24	-20.21	0.25
	WP	1056	***-24.98***	1.42	-25.27	1.20	-23.41	0.25
Smooth/Un-vegetated Mudflat	**TH**	268	-23.40	1.45	-23.41	1.55	-20.23	0.29
	WP	1050	-21.86	1.64	-20.91	1.64	-20.13	2.10
Rough/Vegetated Mudflat	**TH**				N/A			
	WP	937	-13.64	1.86	-11.98	1.92	-11.48	2.54
Peat	**TH**	127	-20.04	2.48	-17.22	2.71	-16.08	1.96
	WP	171	-14.53	2.87	-12.56	2.42	-10.15	2.49
Sand	**TH**	834	-21.60	1.80	-19.97	2.43	-16.33	2.90
	WP	1233	-20.62	2.80	-19.77	3.32	-16.23	3.45
Mixed Sediment	**TH**	760	***-12.03***	2.78	***-11.09***	2.32	-10.22	3.39
	WP	688	-13.48	1.67	-12.00	2.09	-10.66	1.68
Riprap	**TH**	140	-12.71	1.98	-11.28	6.94	-9.93	2.07
	WP				N/A			
Wood and Substrate Mix	**TH**	662	-17.92	2.37	-16.04	2.44	-14.92	2.60
	WP	428	-13.10	2.78	-11.90	3.04	-12.00	2.82
Woody Debris	**TH**	799	-14.52	1.64	-11.66	1.71	-10.16	1.61
	WP	724	-8.19	1.57	-6.33	1.39	-7.93	1.69
Marsh	**TH**	249	***-15.30***	1.79	***-12.11***	2.07	-10.96	2.52
	WP	923	***-12.55***	2.52	***-11.51***	2.93	-11.19	3.39
Wetland	**TH**	474	-12.53	1.65	-10.30	1.59	***-3.98***	2.25
	WP	201	***-11.90***	2.05	***-10.58***	2.28	-10.56	2.44
ILLT	**TH**	705	***-12.58***	1.73	***-10.73***	1.77	-9.42	1.75
	WP	725	***-10.91***	1.10	***-9.70***	1.24	***-8.49***	1.37
High Centre Polygons	**TH**				N/A			
	WP	779	***-10.56***	1.29	***-10.04***	1.39	***-8.27***	1.35
Low Centre Polygons	**TH**	813	***-12.84***	1.84	***-11.75***	1.41	-9.51	1.61
	WP	681	***-12.29***	1.70	***-11.35***	1.65	-10.35	1.54
Eroding Tundra	**TH**	489	***-8.90***	2.01	***-7.61***	1.77	***-7.76***	1.88
	WP	477	***-8.79***	1.86	***-7.77***	1.87	-8.87	2.41
Herb Dominant Tundra	**TH**	806	***-13.03***	1.38	***-11.54***	1.45	***-10.55***	1.69
	WP	989	***-11.63***	1.53	***-10.11***	1.94	***-10.74***	1.56
Shrub Dominant Tundra	**TH**	942	***-8.34***	1.05	***-7.64***	1.23	***-7.85***	1.47
	WP	818	***-6.48***	0.97	***-6.13***	1.18	***-6.84***	1.34

certain scattering mechanism contributed little to total power. The percent of pixels from training data that fell within the overlap region produced by the $\bar{x} \pm 2s$ for sample distributions are also provided to give some indication of how spatially extendable parameters would be with parametric classifiers (Table 16). Results overall show that these parameters may perform poorly as inputs to broad scale classifiers, as they are much less spatially extendable (i.e., compared to backscatter coefficients).

Of all three scattering mechanisms, double bounce contributions were the least consistent between study areas. All classes had less than 80% of training data within this overlap region, except for Wetland at shallow angles. This may be expected since it was one of the few classes to be dominated by double bounce scattering, resulting in normally distributed training data. Conversely, double bounce values for all other classes were typically low, and as a consequence also highly skewed. For odd bounce and volume scattering, values for classes such as: Smooth/Un-Vegetated Mudflat, Peat, Wetland, and ILLT were also generally inconsistent between study areas. These are some of the same classes that showed inconsistencies for backscatter coefficients, though as mentioned previously, a number of additional classes such as Shrub Dominant Tundra also had inconsistent values (Table 16). Volume scattering contributions were the most consistent between study areas, with very few exceptions identified in Table 16.

Contributions to total power from the three scattering mechanisms were generally comparable for shallow and medium angles (Table 17), though some exceptions for odd bounce scattering include: Water and Smooth/Un-Vegetated Mudflat from both study areas, as well as Peat and Sand from the TH study area. Double bounce contributions were consistent between shallow and medium angles in all cases except for Water from

Table 16: Percent of values within the overlap region produced by the $\bar{x} \pm 2s$ for sample distributions to show the consistency of values between study areas for like scattering mechanisms and incidence angles. All values less than 80% are bolded and italicized.

Class	Sample Size	Odd Bounce			Double Bounce			Volume Scattering		
		Shallow	Medium	Steep	Shallow	Medium	Steep	Shallow	Medium	Steep
Water	3016	81.37	99.20	87.14	***14.36***	***13.30***	***0.00***	98.64	96.02	***0.00***
Smooth/Un-Vegetated Mudflat	1336	***5.77***	***0.91***	***0.00***	***11.99***	***9.18***	***0.00***	96.28	88.92	***32.17***
Peat	298	***76.51***	***28.86***	***0.00***	***34.56***	***29.19***	***0.00***	***79.87***	***79.19***	***55.70***
Sand	2067	96.08	97.68	97.10	***61.59***	***63.09***	***9.72***	98.36	98.02	***73.29***
Mixed Sediment	1448	92.13	96.41	96.48	***63.74***	***62.15***	***24.52***	96.62	99.45	96.62
Wood/Substrate Mix	1090	92.73	97.61	96.41	***70.93***	***70.10***	***18.22***	89.51	92.46	93.65
Woody Debris	1523	91.14	95.80	98.36	***65.99***	***62.31***	***45.57***	***55.55***	***66.58***	97.64
Marsh	1172	***74.32***	81.74	98.72	***68.00***	***67.66***	***32.85***	84.81	96.42	97.53
Wetland	675	91.82	87.20	***52.23***	95.09	***77.83***	***18.60***	98.07	96.58	***34.23***
ILLT	1430	***69.16***	***68.18***	***94.13***	***57.27***	***54.34***	***36.92***	88.46	96.36	97.48
Low Centre Polygons	1494	81.39	***78.18***	97.66	***73.43***	***69.88***	***33.60***	98.13	99.26	97.66
Eroding Tundra	966	***66.32***	***70.64***	88.43	***49.05***	***55.01***	***32.38***	96.63	97.06	99.31
Herb Dominant Tundra	1795	***71.87***	***68.36***	92.76	***36.77***	***30.92***	***18.16***	97.77	97.88	99.16
Shrub Dominant Tundra	1760	***38.30***	***45.63***	**69.20**	***18.98***	***26.36***	***22.73***	82.95	97.78	98.41

Table 17: Percent of values within the overlap region produced by the $\bar{x} \pm 2s$ for sample distributions to show consistency between incidence angles. Note that S = shallow, M = medium, and T = steep. All values less than 80% are bolded and italicized.

Class	Study Area	Sample Size	Odd Bounce		Double Bounce		Volume Scattering	
			S vs. M	S vs. T	S vs. M	S vs. T	S vs. M	S vs. T
Anthropogenic	TH	662	100.00	83.91	100.00	85.73	93.20	93.73
	WP							
Water	TH	1960	***63.11***	***0.00***	88.95	***0.00***	89.97	***0.00***
	WP	1056	***73.15***	***0.00***	***53.79***	***0.00***	93.61	***52.51***
Smooth/Un-vegetated Mudflat	TH	268	***70.52***	***0.00***	89.93	***0.00***	95.52	***0.00***
	WP	1050	***76.14***	***0.00***	89.76	***0.38***	89.95	86.29
Rough/Vegetated Mudflat	TH				N/A			
	WP	937	87.35	***6.94***	99.79	***75.40***	83.88	83.03
Peat	TH	127	***78.74***	***0.00***	96.06	***0.00***	***77.56***	***51.18***
	WP	171	97.95	***70.18***	94.74	***36.55***	84.80	***54.97***
Sand	TH	834	***77.34***	***0.00***	88.67	***0.00***	88.31	***60.79***
	WP	1233	93.59	***4.91***	96.07	***56.73***	93.80	***70.79***
Mixed Sediment	TH	760	91.18	82.30	97.96	***56.97***	91.18	90.72
	WP	688	96.22	82.41	99.56	***78.27***	86.92	***59.74***
Riprap	TH	140	89.29	***55.00***	98.21	***66.79***	91.07	***67.14***
	WP				N/A			
Wood/Substrate Mix	TH	662	83.08	***1.28***	96.75	***1.66***	86.56	***76.96***
	WP	428	94.59	87.53	99.53	***74.94***	92.94	91.29
Woody Debris	TH	799	93.18	86.30	99.00	***73.34***	***60.89***	***19.96***
	WP	724	94.34	90.94	100.00	***74.59***	***77.56***	94.75
Marsh	TH	249	87.15	***43.78***	96.59	***62.65***	***66.27***	***50.20***
	WP	923	85.59	***49.57***	99.02	***72.48***	93.88	92.09
Wetland	TH	474	93.35	87.34	89.03	***25.63***	***72.26***	***0.00***
	WP	201	99.49	***62.88***	92.93	***67.93***	88.89	90.40
ILLT	TH	705	100.00	***59.36***	97.09	***65.39***	80.43	***53.83***
	WP	725	100.00	***72.90***	99.31	***70.21***	80.83	***53.66***
High Centre Polygons	TH				N/A			
	WP	779	100.00	***69.96***	87.68	80.36	92.49	***60.27***
Low Centre Polygons	TH	813	80.69	***46.86***	97.17	***69.86***	85.61	***48.15***
	WP	681	92.44	***61.67***	100.00	***75.99***	88.47	***75.99***
Eroding Tundra	TH	489	100.00	***76.28***	95.09	***61.66***	88.65	90.08
	WP	477	100.00	***72.75***	97.27	***61.64***	89.20	91.72
Herb Dominant Tundra	TH	806	80.77	***73.64***	93.55	***0.56***	80.77	***61.66***
	WP	989	100.00	***75.78***	91.20	***60.72***	84.98	90.70
Shrub Dominant Tundra	TH	942	99.95	***70.86***	88.27	***45.91***	90.07	89.86
	WP	818	99.76	***62.71***	85.82	***40.40***	92.18	88.94

the WP study area, while volume scattering values were inconsistent for the Woody Debris class for both study areas, and for Peat, Marsh and Wetland from the TH study area only.

Additionally, in most cases contributions from shallow and steep angles were significantly different with the exception of odd bounce contributions for a number of classes with rougher surfaces. This was observed for Anthropogenic, Rough/Vegetated Mudflat, Mixed Sediment, Wood/Substrate Mix, and Woody Debris, indicating relatively consistent scattering behaviour. Additionally, volume scattering contributions for Eroding Tundra, Herb Dominant Tundra and Shrub Dominant Tundra were also mostly consistent between shallow and steep angles. Double bounce contributions were only consistent for Anthropogenic and High Centre Polygons.

4.5.3. Assessment of Freeman-Durden Decomposition Parameters for Individual Classes and Potential for Feature Detection and Discrimination with Colour Composites

Based on a visual analysis of colour composites with double bounce as red, volume scattering as green, and odd bounce as blue [commonly used for visual interpretations (Lee et al., 2004; Choe et al., 2011; Smith & Buckley, 2011)], there was better contrast between classes overall at shallow and medium angles. As was observed with backscatter coefficients however, steep angle imagery was preferred to discriminate some class pairs. The following section summarizes the potential observed for visual feature detection and discrimination, as well as a description of the dominant scattering mechanism observed for each class. Because colour composites provided a similar amount of contrast as backscatter coefficients, they are only provided when

improvements or significant differences were observed.

Anthropogenic

On average double bounce and slightly more volume scattering, were the dominant contributors to total power for Anthropogenic and this was observed at all angles. Compared to other classes, power contributions from the three scattering mechanisms were also nearly equal at all angles (i.e., 15-19%, 29-31% and 48-57%, for odd bounce, double bounce and volume scattering, respectively), again indicating consistency in scattering behaviour. In colour composites, these features appeared as mostly magenta (near equal odd and double bounce) to red (> double bounce), and white (near equal contribution from all scattering mechanisms). Additionally, some areas also appeared green (> volume scattering), but this was mostly over low density regions or when features were oriented close to parallel to the radar line of sight.

Water and Substrates

Classes with smoother surfaces, including: Smooth/Un-Vegetated Mudflat, Rough/Vegetated Mudflat, Peat, and Sand showed dominant odd bounce scattering contributions at all angles. At shallow angles, volume scattering was the second largest contributor to total power, though this decreased as incidence angle steepened, and double bounce contributions for these classes were low at all angles. Consequently, features appeared mostly blue in colour composites. It should also be noted that some portions of Rough/Vegetated Mudflat and Peat appeared pink, indicating double bounce scattering was greater. This was particularly evident for Peat in the WP study area.

Unlike these classes, Water was dominated by both odd bounce and volume

scattering contributions at shallow angles, which made up 40 to 50% of the total observed power. This may be attributable to increased surface roughness as a result of wave action, leading to multiple scattering. As incidence angles steepened, odd bounce contributions to total power increased to 61 - 70% for medium angles, and 94 - 95% at steep angles. Total power also increased at steeper angles, making water appear brighter, and much like backscatter coefficients, also made it easier to distinguish this class from substrates with smoother surfaces. Again, this was especially evident for the most saturated mudflats, which could only be discerned at steep incidence angles.

For Mixed Sediment and Riprap, both odd bounce and volume scattering were important contributors to total power, while for Wood/Substrate Mix and Woody Debris odd bounce contributions were highest at all angles. As mentioned previously, for all these classes odd bounce contributions increasingly dominated total power as incidence angles steepened. These classes also generally showed higher mean and standard deviations, compared to substrates with smoother surfaces, and so generally appeared brighter, and also more textured. As such, these features could generally be distinguished from Water and substrates with smoother surfaces, though it was still difficult to differentiate among many of the substrates with rougher surfaces, including between Riprap and Mixed Sediment.

Vegetated Classes

As with colour composites of backscatter coefficients, many of the vegetated classes appeared relatively similar, including: Wetland (WP study area), Marsh, ILLT, Low Centre Polygons, and High Centre Polygons. These classes contained mixed pixels and in some cases also appeared similar to substrates with rougher surfaces such as

Mixed Sediment. On average, volume scattering was the dominant contributor to total power at shallow and medium angles, though in a number of areas, double bounce contributions were also high, as features appeared pink to red (> double bounce).

While volume scattering remained the dominant scattering mechanism in most cases at steep angles, odd bounce became dominant for some classes, including Marsh and Low Centre Polygons for both study areas. Relative to colour composites of backscatter coefficients, in some cases Freeman-Durden decompositions at shallow and medium angles provided greater visual contrast between Wetland (WP study area), Marsh, ILLT, Low Centre Polygons, and High Centre Polygons and Herb Dominant Tundra (Figure 19). While the former contained some pink to red colours, Herb Dominant Tundra was mostly green-blue. At steep angles however, these classes became more difficult to distinguish as they mostly appeared green. It was also easier to distinguish between Herb and Shrub Dominant Tundra at shallow compared to steep angles (Figure 19). This is due to shrubs appearing greener and brighter because of greater volume scattering and a higher total power.

At shallow and medium incidence angles Wetland in the TH study was the only class to be dominated by double bounce scattering (Figure 19) producing significant red to pink colours. In some areas magenta and yellow pixels are also present, indicating nearly equal odd and double bounce contributions. At steep incidence angles, volume scattering dominated, which made it more difficult to differentiate between Wetland and Shrub Dominant Tundra compared with using backscatter coefficients.

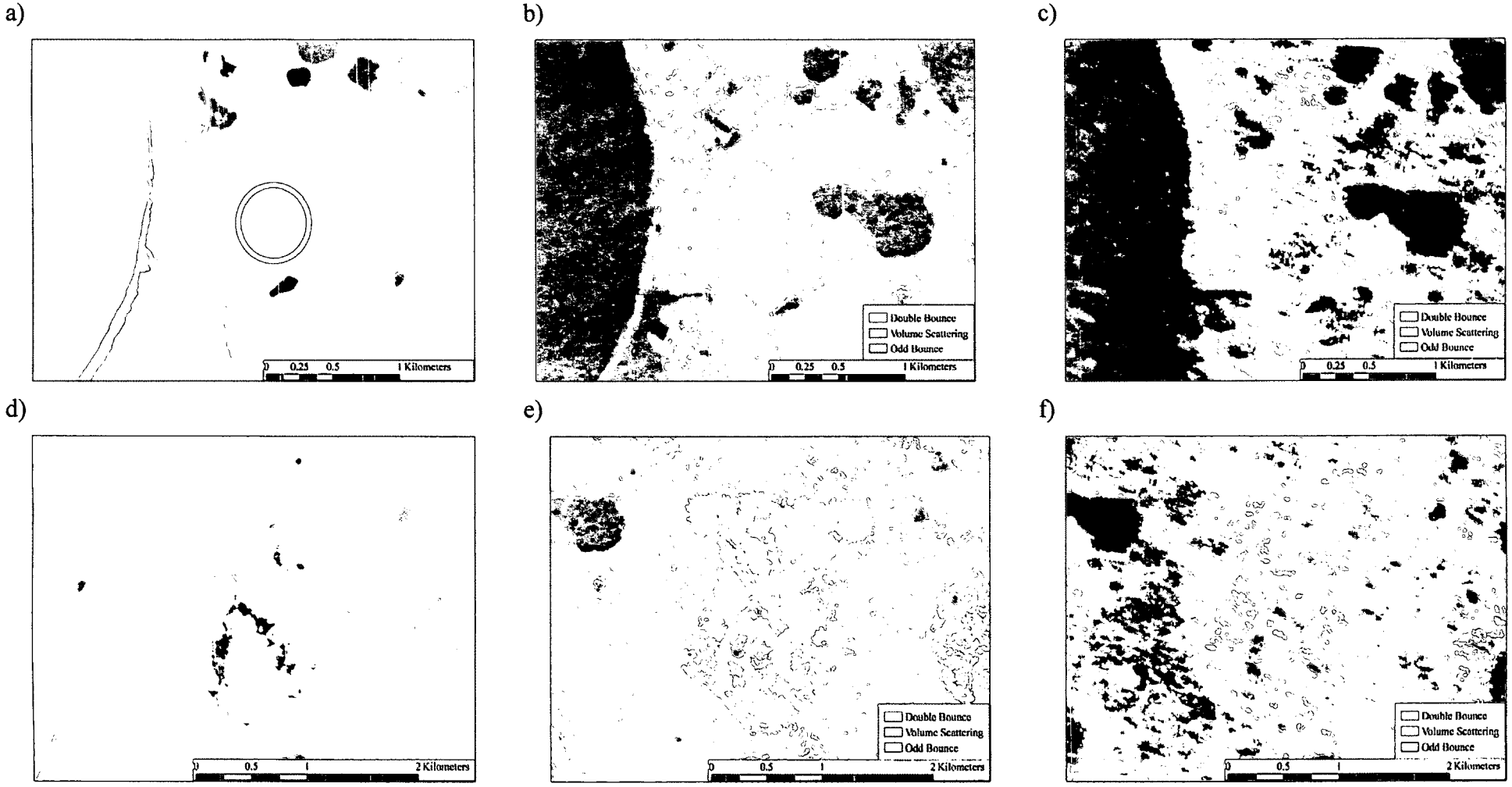

Figure 19: Segment of 2004 ortho photos with circles indicating where Shrub Dominant Tundra = red, Herb Dominant Tundra = yellow, ILLT = blue, and Low Centre Polygons = orange are present. b) and c) are colour composites of this area at shallow and steep angles. d) shows the Wetland from the TH study area, as well as colour composites of the same area at shallow (e) and steep angles (f).

4.6. Cloude-Pottier Decomposition (Entropy/Anisotropy/Alpha Parameters) Characteristics of Arctic Land Cover Types

4.6.1. Sample Statistics, General Observations and Trends

Entropy, anisotropy and alpha mean and standard deviation values are provided in Table 18, Table 19 and Table 20. All values are based on normally distributed training data as visually assessed using histograms.

4.6.2. Consistency of Entropy, Anisotropy, Alpha Between Study Areas and Incidence Angles

Similarly to backscatter coefficients, entropy, anisotropy and alpha values for each class were generally comparable between study areas at like incidence angles. This was visually assessed using box and whisker plots (Appendix 8), as well as the percent of pixels within the overlap region produced by the $\bar{x} \pm 2s$ for sample distributions (Table 21). Some classes identified as exceptions for backscatter coefficients were also identified for these parameters, including: Smooth/Un-Vegetated Mudflat, Peat and Wetland at medium and steep angles. Fewer classes were considered exceptions compared to backscatter coefficients and Freeman-Durden decomposition parameters however. This would indicate that the Cloude-Pottier parameters may be more appropriate as inputs to broad scale classifiers, but sample distributions also showed more overlap between classes (Appendix 8), indicating less potential for class discrimination.

Values were also generally comparable between shallow and medium angles for the same study area, though again exceptions included: Water and Smooth/Un-Vegetated Mudflat for entropy and alpha (Table 22). Comparing training data from shallow and

Table 18: Mean ($\bar{x}$) and standard deviation (s) of the entropy (H) parameter from the Cloude-Pottier Decomposition at all angles and both study areas.

Class	Study Area	Sample Size	Shallow		Medium		Steep	
			$\bar{x}$	s	$\bar{x}$	s	$\bar{x}$	s
Anthropogenic	TH	662	0.70	0.15	0.69	0.16	0.63	0.18
	WP				N/A			
Water	TH	1960	0.62	0.12	0.46	0.10	0.12	0.03
	WP	1056	0.70	0.09	0.55	0.10	0.13	0.04
Smooth/Un-vegetated Mudflat	TH	268	0.49	0.09	0.38	0.07	0.25	0.07
	WP	1050	0.51	0.11	0.45	0.11	0.23	0.07
Rough/Vegetated Mudflat	TH				N/A			
	WP	937	0.54	0.12	0.47	0.11	0.28	0.12
Peat	TH	127	0.59	0.13	0.53	0.13	0.26	0.08
	WP	171	0.58	0.15	0.61	0.14	0.43	0.14
Sand	TH	834	0.65	0.11	0.55	0.13	0.40	0.15
	WP	1233	0.64	0.12	0.60	0.13	0.27	0.11
Mixed Sediment	TH	760	0.70	0.13	0.68	0.12	0.51	0.20
	WP	688	0.66	0.12	0.65	0.13	0.55	0.13
Riprap	TH	140	0.61	0.16	0.63	0.16	0.53	0.14
	WP				N/A			
Wood/Substrate Mix	TH	662	0.64	0.10	0.59	0.10	0.38	0.12
	WP	428	0.64	0.17	0.64	0.15	0.49	0.16
Woody Debris	TH	799	0.61	0.13	0.58	0.13	0.62	0.11
	WP	724	0.62	0.11	0.62	0.11	0.56	0.10
Marsh	TH	249	0.75	0.10	0.77	0.10	0.57	0.17
	WP	923	0.79	0.09	0.75	0.11	0.46	0.17
Wetland	TH	474	0.72	0.09	0.69	0.09	0.59	0.16
	WP	201	0.72	0.12	0.73	0.14	0.57	0.13
ILLT	TH	705	0.80	0.07	0.79	0.09	0.65	0.12
	WP	725	0.83	0.08	0.82	0.07	0.73	0.08
High Centre Polygons	TH				N/A			
	WP	779	0.82	0.06	0.83	0.06	0.73	0.10
Low Centre Polygons	TH	813	0.80	0.08	0.79	0.07	0.59	0.10
	WP	681	0.82	0.06	0.82	0.06	0.62	0.11
Eroding Tundra	TH	489	0.82	0.07	0.80	0.09	0.70	0.16
	WP	477	0.82	0.07	0.81	0.08	0.63	0.13
Herb Dominant Tundra	TH	806	0.78	0.08	0.76	0.08	0.69	0.11
	WP	989	0.81	0.08	0.80	0.09	0.69	0.12
Shrub Dominant Tundra	TH	942	0.83	0.07	0.83	0.07	0.80	0.09
	WP	818	0.86	0.06	0.86	0.06	0.79	0.08

Table 19: Mean ($\bar{x}$) and standard deviation (s) of the anisotropy (A) parameter from the Cloude-Pottier Decomposition at all angles and both study areas.

Class	Study Area	Sample Size	Shallow		Medium		Steep	
			$\bar{x}$	s	$\bar{x}$	s	$\bar{x}$	s
Anthropogenic	TH	662	0.54	0.20	0.53	0.20	0.55	0.20
	WP				N/A			
Water	TH	1960	0.31	0.12	0.37	0.14	0.67	0.10
	WP	1056	0.36	0.13	0.35	0.13	0.68	0.10
Smooth/Un-vegetated Mudflat	TH	268	0.35	0.13	0.37	0.14	0.68	0.11
	WP	1050	0.38	0.14	0.36	0.14	0.54	0.14
Rough/Vegetated Mudflat	TH				N/A			
	WP	937	0.34	0.12	0.35	0.13	0.34	0.13
Peat	TH	127	0.45	0.13	0.43	0.14	0.44	0.16
	WP	171	0.41	0.15	0.38	0.14	0.37	0.14
Sand	TH	834	0.39	0.14	0.43	0.15	0.50	0.17
	WP	1233	0.44	0.14	0.44	0.14	0.47	0.15
Mixed Sediment	TH	760	0.35	0.14	0.35	0.14	0.38	0.15
	WP	688	0.38	0.14	0.36	0.14	0.34	0.14
Riprap	TH	140	0.44	0.18	0.47	0.18	0.38	0.16
	WP				N/A			
Wood/Substrate Mix	TH	662	0.39	0.14	0.39	0.14	0.43	0.15
	WP	428	0.45	0.17	0.41	0.15	0.39	0.16
Woody Debris	TH	799	0.42	0.15	0.40	0.16	0.39	0.16
	WP	724	0.34	0.14	0.32	0.12	0.34	0.13
Marsh	TH	249	0.40	0.13	0.40	0.14	0.37	0.14
	WP	923	0.38	0.14	0.38	0.14	0.39	0.16
Wetland	TH	474	0.63	0.13	0.62	0.13	0.33	0.13
	WP	201	0.49	0.14	0.44	0.15	0.40	0.16
ILLT	TH	705	0.36	0.14	0.37	0.15	0.34	0.13
	WP	725	0.31	0.13	0.32	0.12	0.32	0.13
High Centre Polygons	TH				N/A			
	WP	779	0.41	0.13	0.41	0.13	0.33	0.12
Low Centre Polygons	TH	813	0.39	0.14	0.41	0.14	0.33	0.12
	WP	681	0.37	0.13	0.36	0.14	0.33	0.13
Eroding Tundra	TH	489	0.33	0.12	0.33	0.13	0.30	0.13
	WP	477	0.31	0.12	0.31	0.12	0.34	0.13
Herb Dominant Tundra	TH	806	0.29	0.11	0.28	0.11	0.29	0.11
	WP	989	0.30	0.12	0.32	0.11	0.31	0.12
Shrub Dominant Tundra	TH	942	0.29	0.12	0.30	0.12	0.31	0.12
	WP	818	0.29	0.13	0.30	0.12	0.30	0.12

Table 20: Mean ($\bar{x}$) and standard deviation (s) of the alpha (α) parameter from the Cloude-Pottier Decomposition at all angles and both study areas.

Class	Study Area	Sample Size	Shallow		Medium		Steep	
			$\bar{x}$	s	$\bar{x}$	s	$\bar{x}$	s
Anthropogenic	TH	662	49.71	10.15	51.31	9.91	40.81	15.27
	WP				N/A			
Water	TH	1960	34.95	4.45	26.64	4.10	5.80	1.71
	WP	1056	37.49	5.43	27.98	4.76	6.22	1.86
Smooth/Un-vegetated Mudflat	TH	268	28.62	4.23	23.62	3.24	11.51	3.14
	WP	1050	31.99	4.97	26.61	4.97	11.57	2.87
Rough/Vegetated Mudflat	TH				N/A			
	WP	937	27.76	5.33	23.28	5.23	13.17	4.52
Peat	TH	127	30.46	6.95	27.75	5.76	10.49	3.32
	WP	171	30.30	7.10	29.94	7.53	18.44	6.15
Sand	TH	834	31.33	6.48	26.14	6.55	16.46	7.01
	WP	1233	33.50	6.48	30.66	6.75	12.55	4.51
Mixed Sediment	TH	760	34.39	7.23	32.45	6.71	22.57	10.06
	WP	688	31.56	6.55	30.04	6.95	24.27	6.40
Riprap	TH	140	33.11	9.27	34.81	8.44	22.61	6.89
	WP				N/A			
Wood/Substrate Mix	TH	662	29.13	6.28	26.38	6.07	15.86	5.33
	WP	428	32.93	7.79	31.83	7.16	21.62	8.11
Woody Debris	TH	799	31.14	5.87	29.31	6.17	28.80	5.73
	WP	724	30.80	5.46	30.51	5.52	26.43	4.73
Marsh	TH	249	38.46	6.48	40.15	6.32	25.46	8.65
	WP	923	42.40	6.33	39.41	7.27	21.04	7.98
Wetland	TH	474	50.96	4.90	51.97	5.14	42.65	4.02
	WP	201	47.17	6.22	46.00	4.85	26.91	6.72
ILLT	TH	705	42.17	6.01	41.87	6.61	30.38	6.29
	WP	725	43.51	6.04	43.21	5.32	34.48	5.47
High Centre Polygons	TH				N/A			
	WP	779	47.95	5.72	48.36	5.63	36.84	7.17
Low Centre Polygons	TH	813	41.78	6.55	42.05	6.01	25.97	5.66
	WP	681	42.22	5.36	43.32	5.50	27.74	6.34
Eroding Tundra	TH	489	42.75	5.75	40.87	6.26	33.67	10.61
	WP	477	41.94	5.58	41.44	6.33	28.21	7.45
Herb Dominant Tundra	TH	806	37.89	5.83	35.85	5.98	30.68	6.64
	WP	989	40.81	6.13	40.41	6.38	31.45	7.66
Shrub Dominant Tundra	TH	942	42.50	5.25	42.21	5.19	39.19	6.75
	WP	818	45.09	5.15	44.79	5.11	39.05	5.82

Table 21: Percent of Cloude-Pottier parameter values within the overlap region produced by the $\bar{x} \pm 2s$ for sample distributions to show the consistency between study areas for like scattering mechanisms and incidence angles. All values less than 80% are bolded and italicized.

Class	Sample Size	Entropy			Anisotropy			Alpha (°)		
		Shallow	Medium	Steep	Shallow	Medium	Steep	Shallow	Medium	Steep
Water	3016	85.97	86.31	94.26	94.03	93.67	94.56	93.24	93.97	94.89
Smooth/Un-Vegetated Mudflat	1336	90.74	***77.85***	93.78	94.69	95.98	***76.78***	84.45	***78.91***	94.84
Peat	298	93.29	90.27	***60.40***	92.28	92.62	90.27	94.63	87.25	***59.73***
Sand	2067	96.23	91.92	86.89	91.97	95.07	95.26	92.79	88.00	89.36
Mixed Sediment	1448	93.92	94.48	85.50	94.68	96.13	93.23	91.92	93.23	84.81
Wood/Substrate Mix	1090	89.97	90.80	85.92	93.19	94.02	94.20	91.26	86.84	87.49
Woody Debris	1523	92.78	93.83	89.76	91.40	87.52	90.09	94.68	94.16	90.22
Marsh	1172	94.88	93.94	89.16	94.03	94.62	93.43	91.38	93.86	94.45
Wetland	675	94.49	91.96	93.60	80.95	***73.51***	92.56	88.10	***77.08***	***18.01***
ILLT	1430	94.20	91.19	85.31	93.22	92.24	95.59	94.06	92.38	87.83
Low Centre Polygons	1494	92.10	92.77	94.44	94.71	92.44	93.98	92.84	93.44	94.31
Eroding Tundra	966	95.24	95.03	90.27	95.96	94.93	94.72	94.82	95.24	85.40
Herb Dominant Tundra	1795	93.20	91.75	94.71	96.49	93.31	94.82	90.70	86.91	93.48
Shrub Dominant Tundra	1760	92.22	93.41	95.51	95.74	96.25	96.08	91.02	91.25	94.38

Table 22: Percent of Cloude-Pottier parameter values within the overlap region produced by the $\bar{x} \pm 2s$ for sample distributions to show consistency between incidence angles. S = shallow, M = medium, and T = steep. All values less than 80% are bolded and italicized.

Class	Study Area	Sample Size	Entropy		Anisotropy		Alpha	
			S vs. M	S vs. T	S vs. M	S vs. T	S vs. M	S vs. T
Anthropogenic	TH	662	97.28	98.04	94.49	90.26	93.50	83.01
	WP				N/A			
Water	TH	1960	***59.13***	***0.00***	91.89	***11.02***	***40.18***	***0.00***
	WP	1056	***62.45***	***0.00***	95.74	***19.46***	***53.03***	***0.00***
Smooth/Un-vegetated Mudflat	TH	268	***74.81***	***10.07***	94.22	***18.10***	***74.81***	***0.00***
	WP	1050	90.10	***10.71***	95.62	***73.81***	***78.90***	***0.00***
Rough/Vegetated Mudflat	TH				N/A			
	WP	937	89.38	***36.82***	95.57	95.68	83.78	***14.99***
Peat	TH	127	90.55	***6.30***	96.46	***78.35***	90.94	***2.36***
	WP	171	95.91	***77.49***	93.86	92.69	94.44	***56.73***
Sand	TH	834	85.97	***46.04***	93.35	85.13	85.85	***36.45***
	WP	1233	94.08	***8.76***	95.54	94.24	91.97	***0.89***
Mixed Sediment	TH	760	95.46	***77.63***	95.99	94.34	93.55	***69.08***
	WP	688	94.55	82.78	95.20	93.39	93.90	**77.33**
Riprap	TH	140	94.64	90.36	96.79	91.79	93.21	***77.86***
	WP				N/A			
Wood/Substrate Mix	TH	662	92.15	***31.80***	95.85	93.66	92.45	***36.56***
	WP	428	93.88	84.94	93.41	93.53	94.71	***65.41***
Woody Debris	TH	799	95.12	93.74	95.12	94.74	93.93	92.99
	WP	724	95.99	90.19	93.92	95.44	94.96	85.29
Marsh	TH	249	94.78	***75.70***	95.18	95.58	94.98	***60.24***
	WP	923	93.07	***39.82***	95.67	94.37	92.42	***16.14***
Wetland	TH	474	92.41	***77.64***	88.82	***28.59***	93.57	***54.96***
	WP	201	94.70	82.07	91.67	88.64	91.92	***10.35***
ILLT	TH	705	94.61	***69.29***	95.89	95.74	94.33	***51.06***
	WP	725	93.24	***75.10***	95.24	95.93	94.34	***60.97***
High Centre Polygons	TH				N/A			
	WP	779	95.57	***79.27***	96.02	89.35	94.74	***61.42***
Low Centre Polygons	TH	813	95.57	***38.75***	93.91	91.57	94.46	***26.38***
	WP	681	95.37	***35.02***	95.59	92.51	94.20	***29.59***
Eroding Tundra	TH	489	92.33	***75.36***	95.81	96.11	92.74	***73.93***
	WP	477	95.70	***61.22***	96.65	94.86	93.82	***43.50***
Herb Dominant Tundra	TH	806	94.67	82.69	95.35	96.34	93.11	***77.42***
	WP	989	94.84	80.08	95.50	95.85	94.74	***72.55***
Shrub Dominant Tundra	TH	942	95.70	90.98	96.07	95.81	95.91	90.55
	WP	818	95.84	84.72	95.72	95.66	95.17	***78.61***

steep angle images, entropy and alpha also showed little consistency, with the exception of classes such as Anthropogenic, as well as Woody Debris and Shrub Dominant Tundra. Conversely, values for anisotropy were consistent between all incidence angles, with the exception of Water, Smooth/Un-Vegetated Mudflat and Wetland for the TH study area only.

4.6.3. Assessment of Entropy, Anisotropy and Alpha for Individual Classes and Potential for Feature Detection and Discrimination with Pseudocolour Images

Similar to backscatter coefficients and Freeman-Durden decomposition parameters, analysis of the potential to differentiate classes was completed for Cloude-Pottier decomposition parameters. As these results were less conclusive overall, pseudo colour images are provided in the following section at a regional level only, and parameters are assessed individually as opposed to by class. Overall pseudo colour images for steep angle imagery provided the best visual contrast between many of the classes and the least amount of confusion between land and water, which is the reverse of what was observed for backscatter coefficients and Freeman-Durden decomposition parameters.

Entropy

Entropy values were generally lower over features with smooth surfaces, including: Smooth/Un-Vegetated Mudflat, Rough/Vegetated Mudflat and Sand, and higher over features with rougher surfaces. At shallow and medium angles however, Water had higher entropy values than substrates with smoother surfaces. Vegetated classes also typically had higher entropy values than substrates, with Shrub Dominant

Tundra generally being the highest. Despite these distinctions, the entropy parameter showed significant confusion between land and water at shallow and medium angles, while even at steep angles only a few general land cover types could be identified (Figure 20 and Figure 21). This included Water and Shrub/Dominant Tundra, which had the lowest and highest entropy, respectively. Other classes showed intermediate entropy values and were not visually distinct from one another.

Entropy values also generally decreased as incidence angles steepened for both study areas. Only a few classes showed slight increases in entropy (< 0.03), between shallow and medium angles, or stayed about the same.

Anisotropy

The anisotropy parameter showed little potential to differentiate classes at any angle. Nearly all land cover classes had similar values, with the exception of Wetland (TH study area only) at shallow and medium angles, and Water and Smooth/Un-Vegetated Mudflat at steep angles (Figure 22), which showed relatively higher values, indicating the power contribution from the second scattering mechanism was much larger than the third. Since this parameter showed little potential for visual discrimination of the SCAT classes, only the example from the TH study area is provided (Figure 22).

Anisotropy values also tended to increase as incidence angles steepened for Water, and Smooth/Un-Vegetated Mudflat (e.g. 0.31 to 0.66 from shallow to steep angles, for Water in the TH study area). In contrast, Wetland anisotropy decreased as incidence angles steepened, particularly in the TH study area (i.e., 0.64 to 0.32 from shallow to steep angles). Most other classes showed differences of less than 0.05 across incidence angles. Some portions of Marsh, ILLT, and Low Centre Polygons had higher

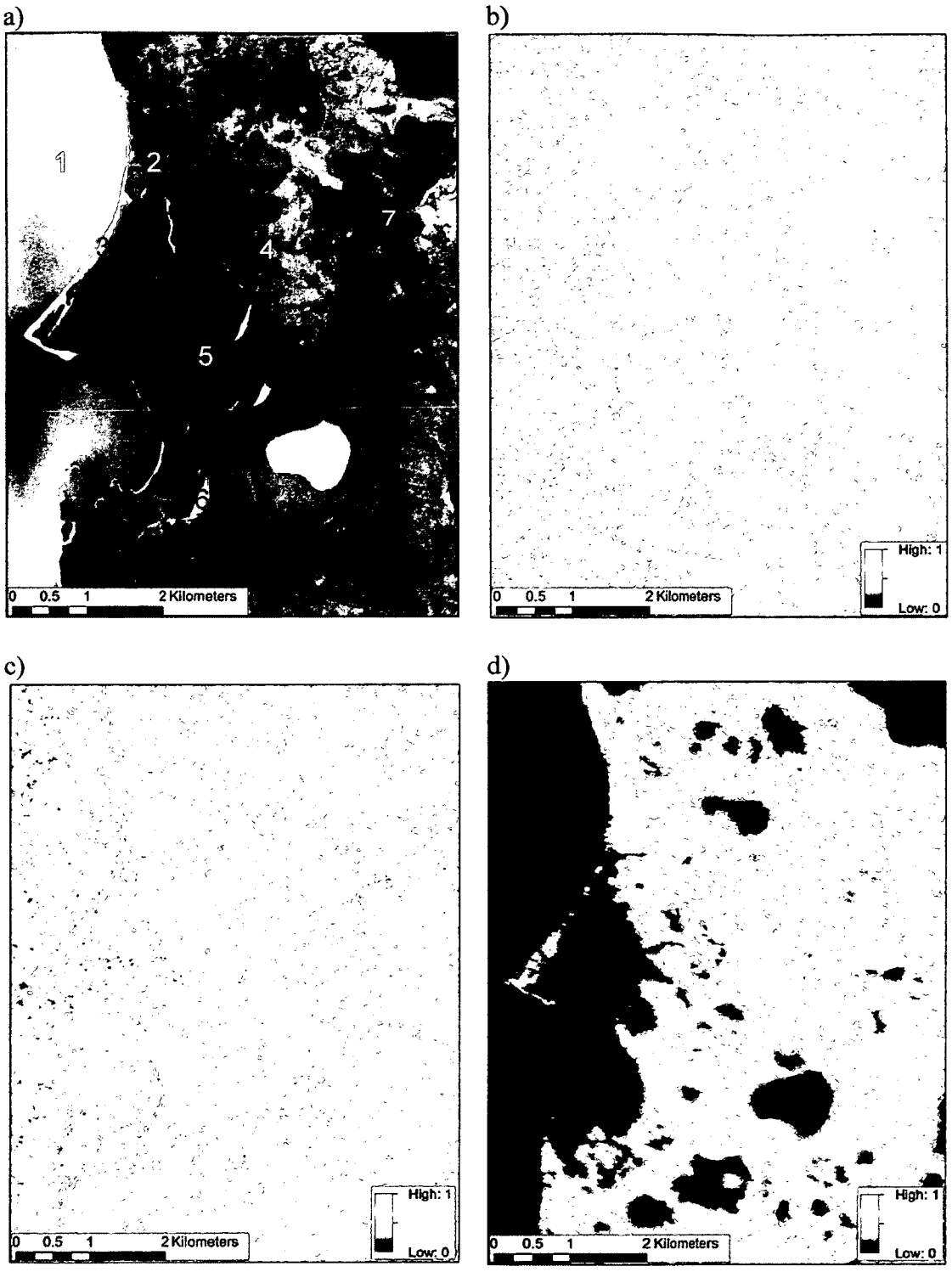

Figure 20: Ortho photo of TH study area (a), with numbers to represent areas where: Water (1), Shrub Dominant Tundra (2), Sand (3), Herb Dominant Tundra (4), ILLT (5), Woody Debris (6), and Wetland (7) are present. Cloude-Pottier entropy values for the same area are shown for shallow (b), medium (c) and steep angles (d).

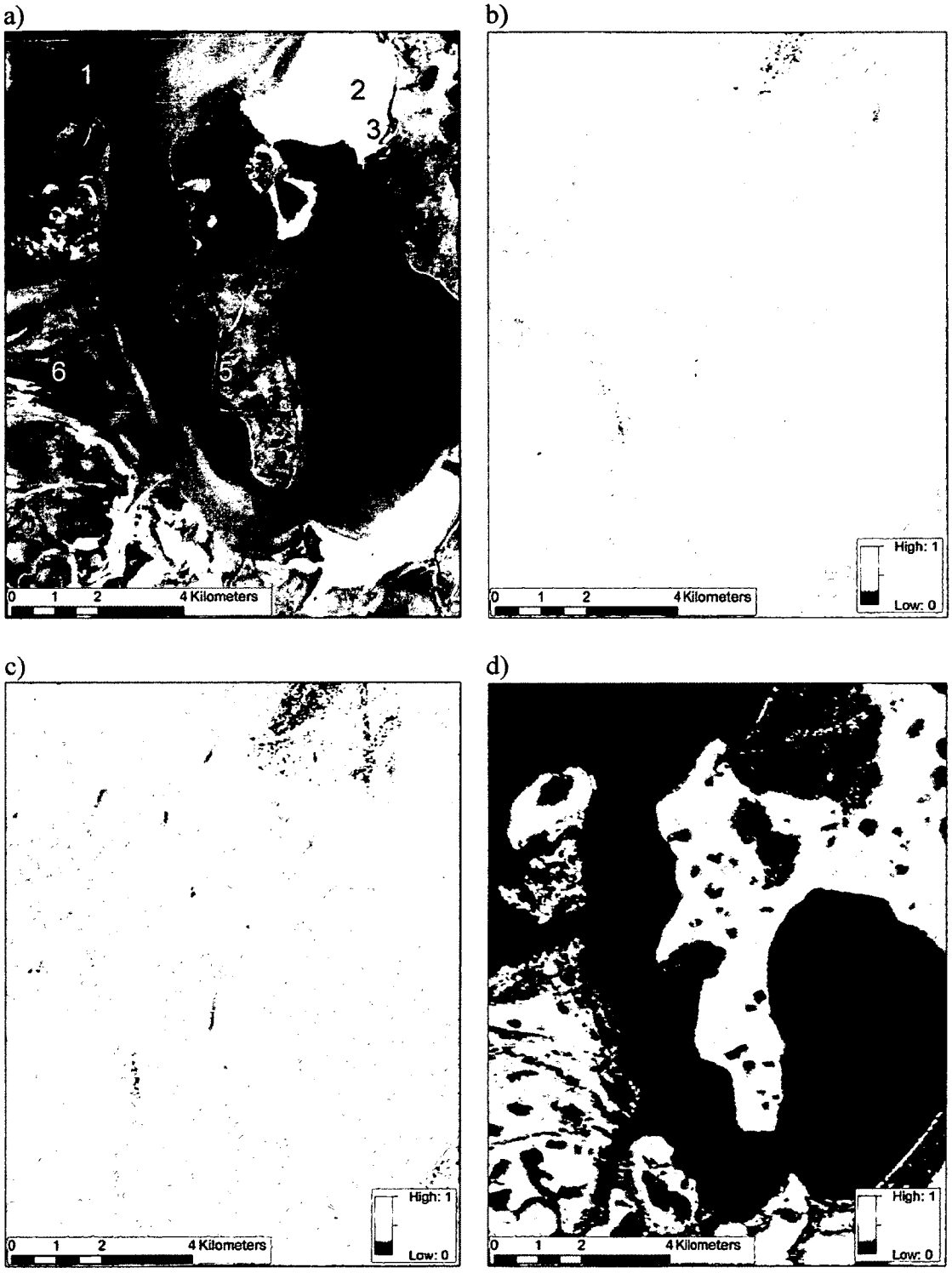

Figure 21: Ortho photo of WP study area (a), with numbers to represent areas where Water (1), Rough/Vegetated Mudflat (2) Smooth/Un-Vegetated Mudflat (3), Woody Debris (4), Shrub Dominant Tundra (5), and ILLT (6) are present. Cloude-Pottier entropy values for the same area are shown for shallow (b), medium (c) and steep angles (d).

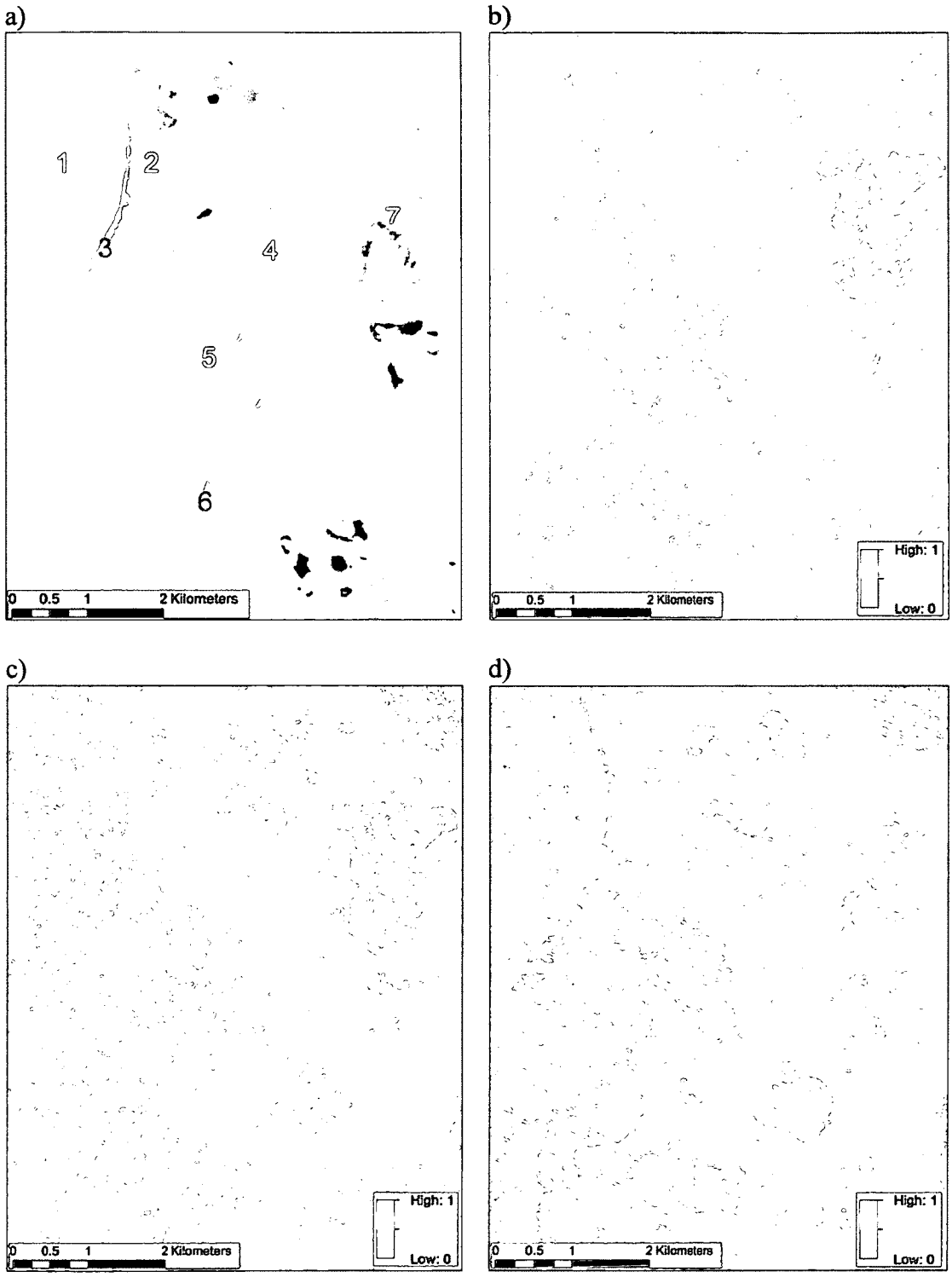

Figure 22: Ortho photo of TH study area (a), with numbers to represent areas where Water (1), Shrub Dominant Tundra (2), Sand (3), Herb Dominant Tundra (4), ILLT (5), Woody Debris (6), and Wetland (7) are present. Cloude-Pottier anisotropy values for the same area are shown for shallow (b), medium (c) and steep angles (d).

anisotropy values in the same areas where increased double bounce was observed in the Freeman-Durden decomposition.

Alpha

At shallow and medium angles, classes with smoother surfaces, including: Water, Smooth/Un-Vegetated Mudflat, Rough/Vegetated Mudflat, Peat, Sand, Wood/Substrate Mix, and Woody Debris, had average alpha values between 20 and 30°, indicating that surface scattering is dominant. Mixed Sediment and Riprap had values at around 30-35°, which could also indicate volume scattering contributions are slightly higher. Values for vegetated classes were typically between 35 and 50°, with Wetland (TH study area) being the highest at about 50°. This indicates that volume scattering contributions are highest for these classes, while values larger than 45° also indicate double bounce, as was observed for Wetland (TH study area) and Anthropogenic.

It was only possible to distinguish a few classes in pseudo colour images, including Wetland (yellow), and substrates with smoother surfaces (blue). Medium angle imagery also provided better contrast than shallow, while visual contrast between land and water was only observed with steep angle imagery (Figure 23). At steep angles most classes still appeared similarly, with the exception of Wetland and Shrub Dominant Tundra, which had slightly higher values. This also tended to be the case at shallow and medium angles. Alpha values also generally decreased as incidence angles steepened, especially for Water and substrates with smoother surfaces. Only the example from the TH study area is provided as both images appeared similar.

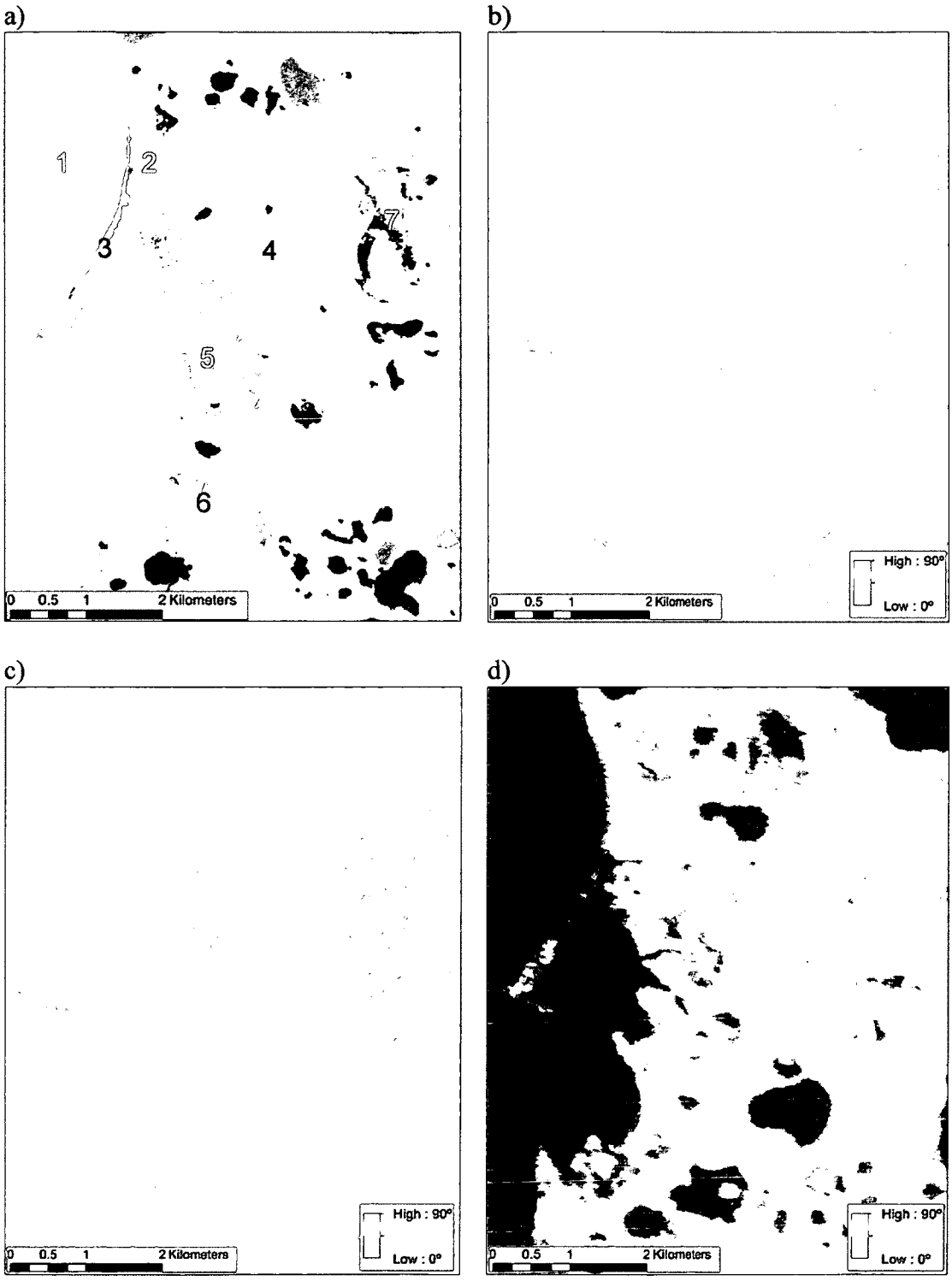

Figure 23: Ortho photo of TH study area (a), with numbers to represent areas where Water (1), Shrub Dominant Tundra (2), Sand (3), Herb Dominant Tundra (4), ILLT (5), Woody Debris (6), and Wetland (7) are present. Cloude-Pottier alpha values for the same area are shown for shallow (b), medium (c) and steep angles (d).

4.6.4. Assessment of the the Potential for Classification based on Feature-Space Segmentation using Entropy, Anisotropy and Alpha Parameters

Entropy-alpha (α) Feature Space

Anthropogenic

At shallow and medium angles, Anthropogenic was mostly classified as Zone 5: dominant dipole scattering; medium entropy, and Zone 4: dominant double bounce scattering; medium entropy (Figure 24). Like all other classes, distributions for shallow and medium angles were relatively similar, and at these angles there was less overlap between Anthropogenic and other classes compared to steep angles. Samples from steep angle imagery were also mostly in Zone 6: surface scattering; medium entropy (typically observed over rough surfaces), though a number of pixels still fell within Zones 4 and 5.

Water and Substrates

At shallow and medium angles Water fell between Zones 6 and 9: dominant surface scattering, with low entropy; whereas at steep angles the sample distribution falls only in Zone 9 (Figure 24). As with Anthropogenic, at all angles a number of pixels also fell outside Zones 6 and 9. All substrate classes showed distributions within Zones 6 and 9 at all angles (Figure 24 and Figure 25). This created a significant amount of overlap between classes, as well as with Water, and with Anthropogenic at steep angles. Compared to other classes, it is of interest to note that: Sand, Wood/Substrate Mix, Riprap, Mixed Sediment, and Woody Debris had similar distributions in all images, indicative of more consistent scattering behaviour regardless of incidence angle. Sample distributions for Woody Debris also showed less variability compared to other classes, as

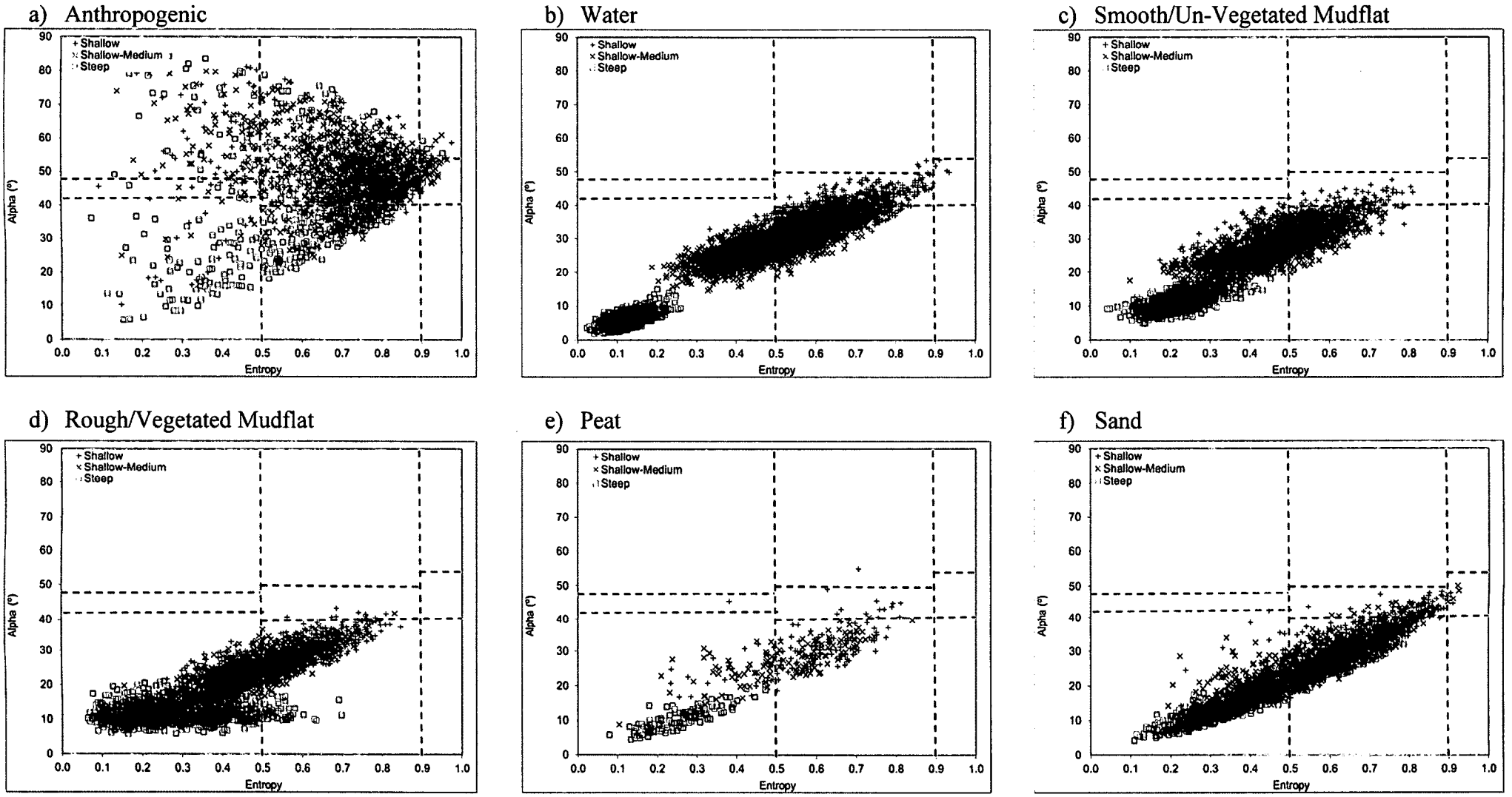

Figure 24: Scatter plots of various sample distributions in the entropy-alpha feature space.

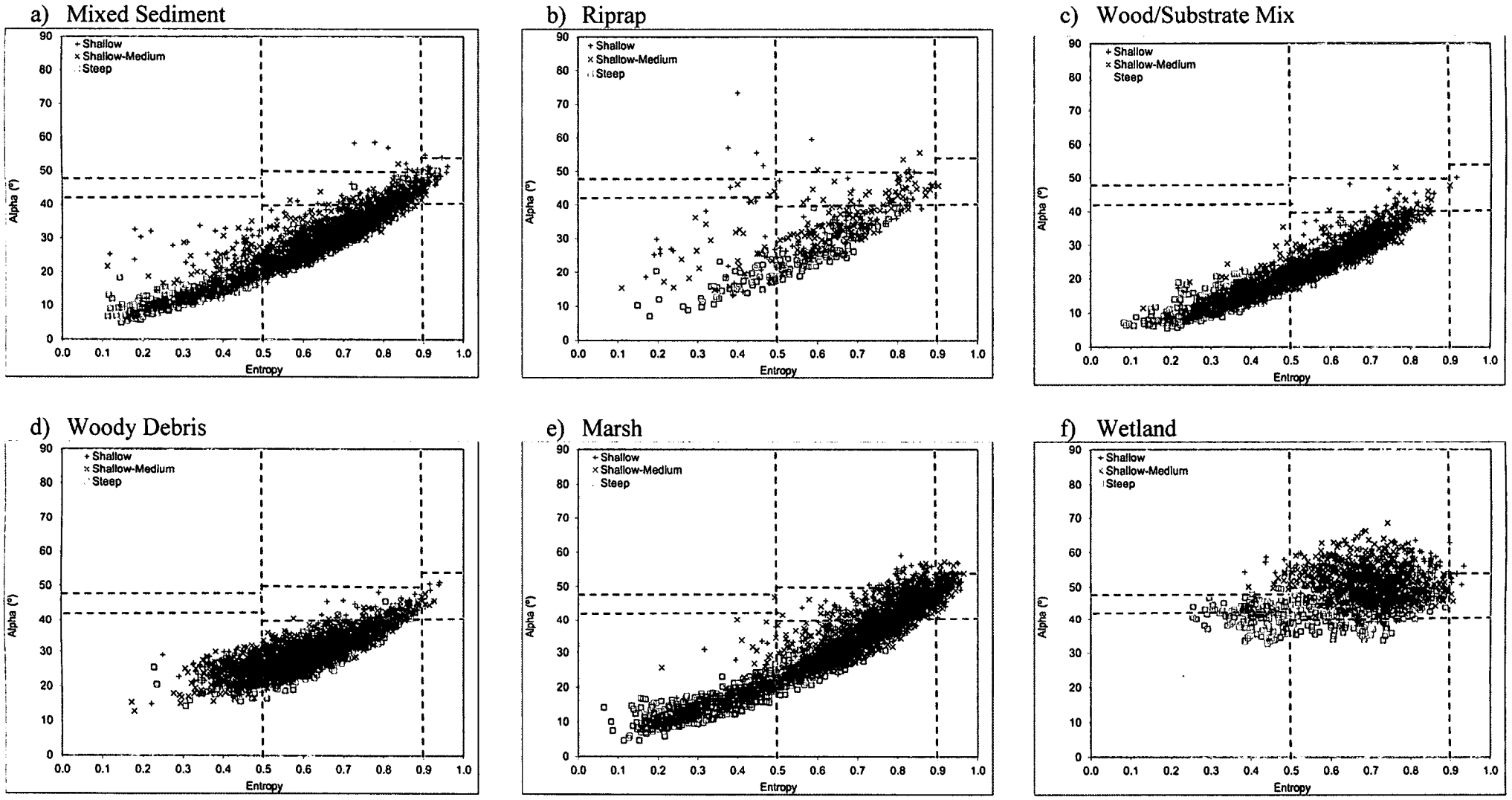

Figure 25: Scatter plots of various sample distributions in the entropy-alpha feature space.

distributions mostly fell within Zone 6 (Figure 25). Therefore, at steep angles there is some potential to distinguish this class from some substrates such as Smooth/Un-Vegetated Mudflat, Rough/Vegetated Mudflat, and Peat, since the distributions for these classes were mostly in Zone 9.

Vegetated Classes

At shallow and medium angles a number of vegetated classes may be distinguished from substrates, as distributions for Marsh, ILLT, Low Centre Polygons, High Centre Polygons, and Eroding Tundra were more centred on Zone 5 (Figure 25 and Figure 26). Despite this, a number of values for these classes also fell within Zone 6 (with most substrate samples), as well as within a number of other zones. With the exception of Marsh, which fell between Zones 6 and 9, distributions for these classes mostly fell in Zone 6 at steep angles. This created more confusion between vegetated classes and substrates.

Herb Dominant Tundra distributions were centred on Zone 6 at all angles, overlapping largely with substrates and some vegetated land covers like Shrub Dominant Tundra. Wetland (TH study area only) had a relatively unique distribution, relative to other vegetated class. At shallow and medium angles, distributions were centred on Zones 4 and 5, while at steep distributions were centred on Zones 5 and 8: dominant dipole scattering, with low entropy. The distributions between Wetland for the TH and WP study area were also only similar at shallow and medium angles.

This analysis shows that the combination of these parameters and this classification scheme are not well suited to the identification and differentiation of the majority of the classes of interest. Scatterplots are also consistent with observations made

a) ILLT

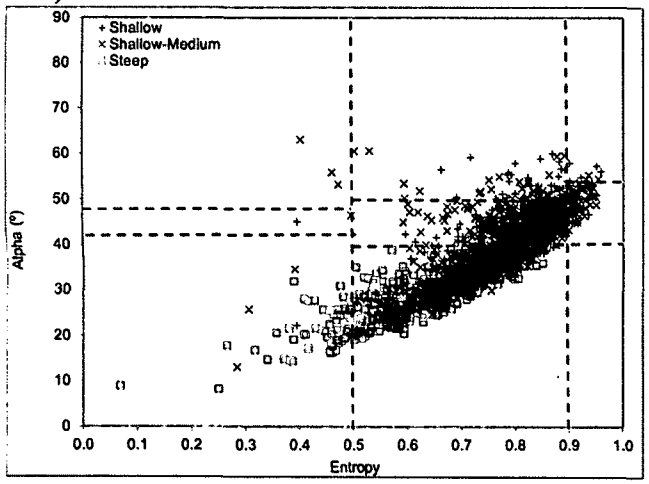

b) Low Centre Polygons

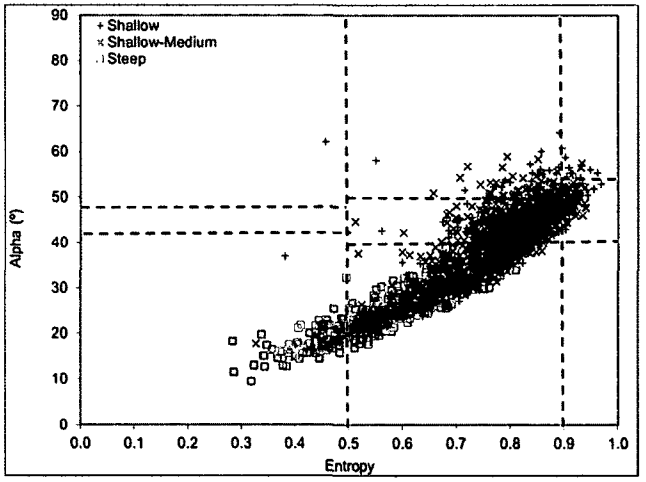

c) High Centre Polygons

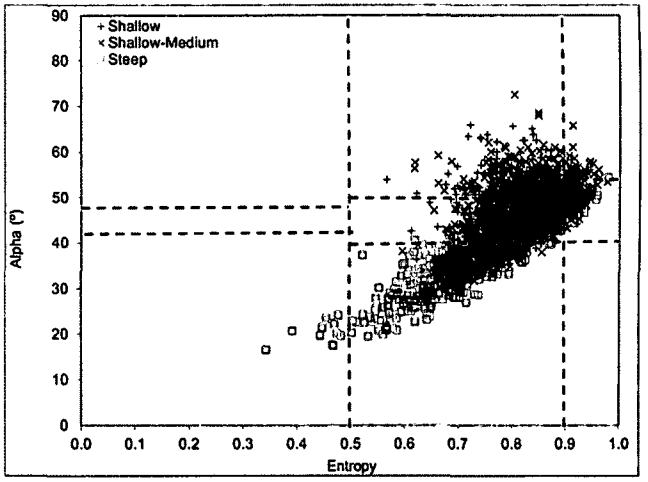

d) Eroding Tundra

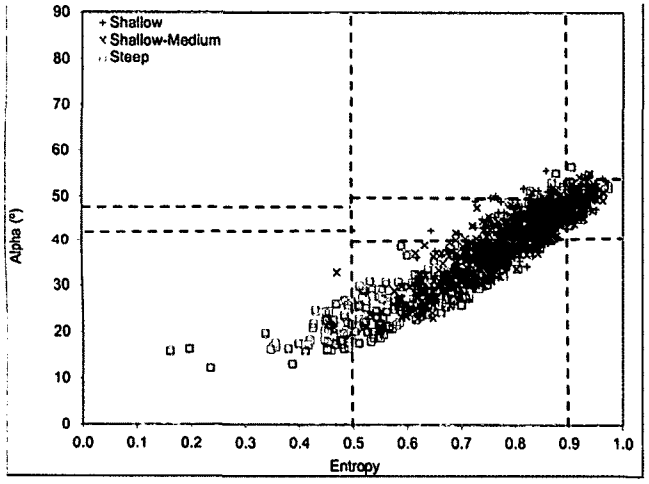

e) Herb Dominant Tundra

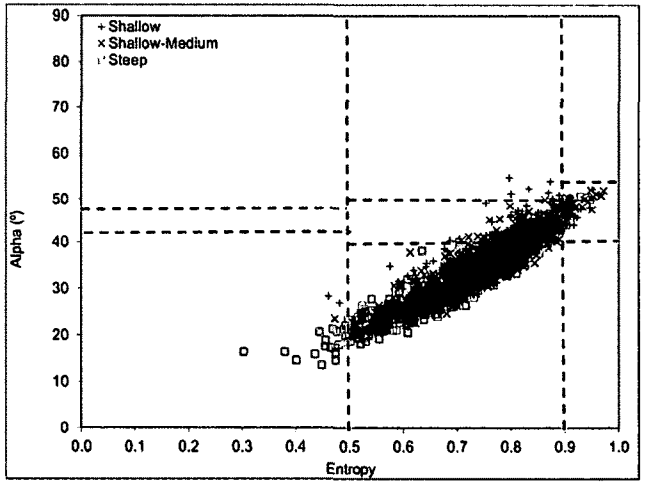

f) Shrub Dominant Tundra

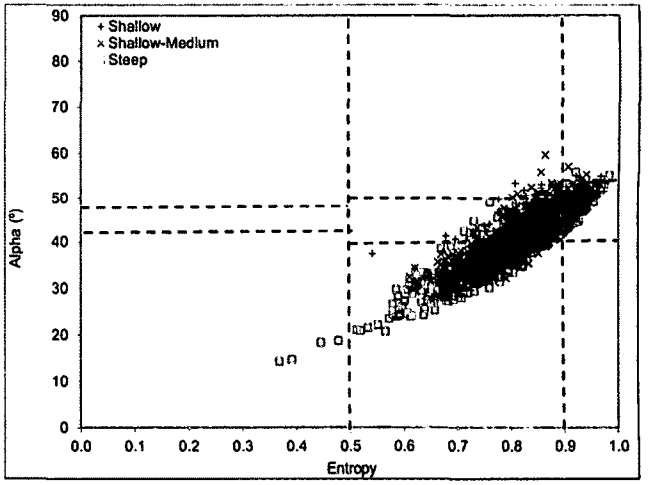

Figure 26: Scatter plots of various sample distributions in the entropy-alpha feature space.

of colour coded maps segmented using the zones described by Cloude and Pottier (Figure 27 and Figure 28). As mentioned previously, shallow angle imagery shows confusion amongst most classes, though there is some potential for detection of Wetland and Shrub Dominant Tundra, which improved at medium angles. As well, Smooth/Un-Vegetated Mudflat and Water were best distinguished at shallow angles. Steep angle images showed little diversity, as the majority of land covers are classified as Zone 6 and 9. As an example, the extensive mud tidal flat west of Richards Island is classified as Zone 9 with Water. There is however, better land-water discrimination at steep angles, and there is some potential for identification of Wetland and Shrub Dominant Tundra, though these classes could not be differentiated from one another.

Entropy-Anisotropy Feature Space

Using a similar classification scheme as described previously for the entropy-alpha feature space, a similar degree of confusion was also observed for classes with the entropy-anisotropy feature space; the results of which (i.e., scatter plots) are not presented for brevity. It is of interest to note however, that a number of classes showed potential for classification using this classification scheme, including Wetland at shallow and medium angles, as well as saturated mudflats and Rough/Vegetated Mudflat at steep angles (Appendix 9).

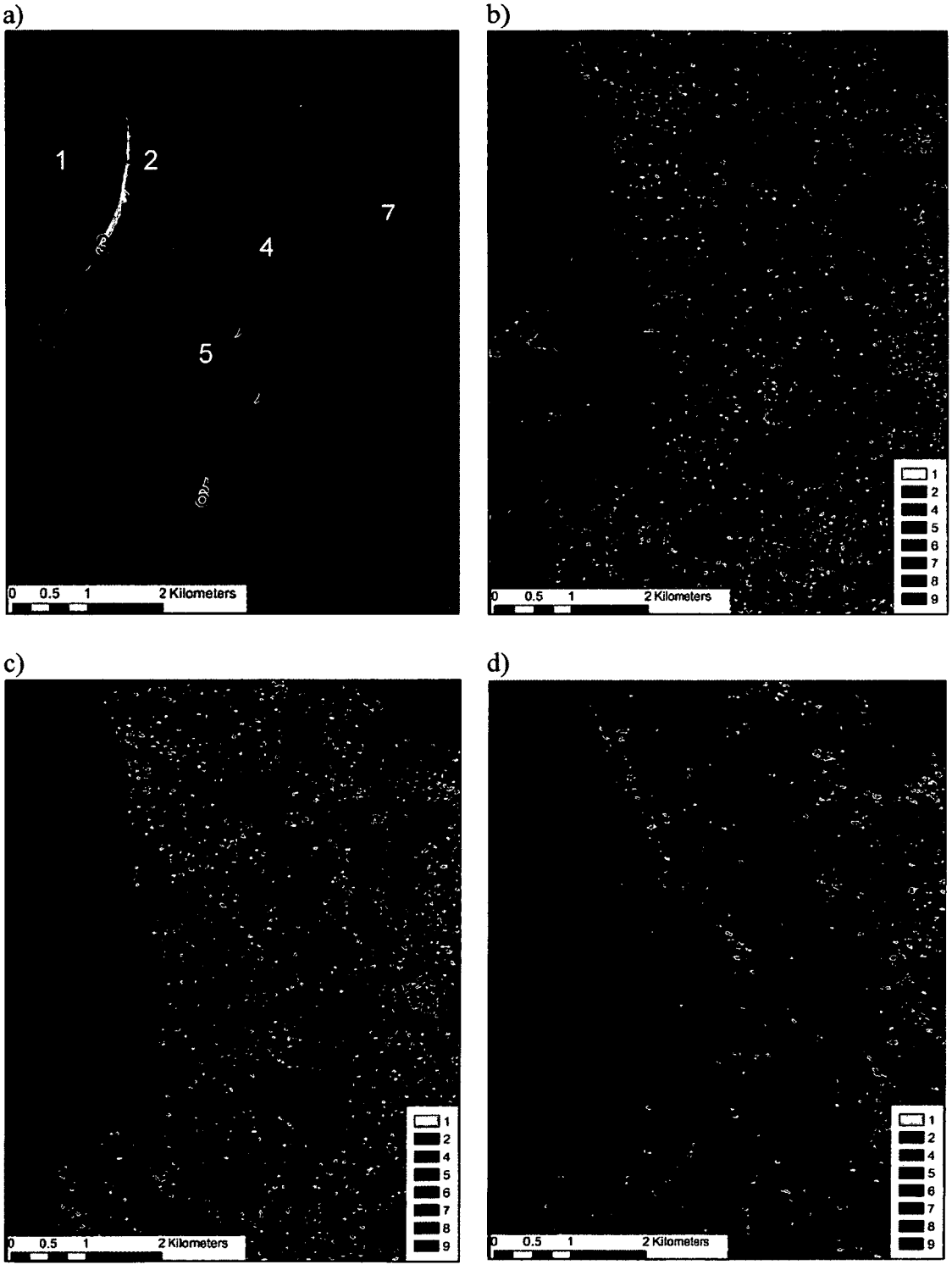

Figure 27: Ortho photo of TH study area (a), with numbers to represent areas where Water (1), Shrub Dominant Tundra (2), Sand (3), Herb Dominant Tundra (4), ILLT (5), Woody Debris (6), and Wetland (7) are present. Entropy-alpha segmentations [legend numbers represent the 9 zones defined by Cloude and Pottier, (1997)] for the same area show shallow (b), medium (c) and steep angles (d).

Figure 28: Ortho photo of WP study area (a), with numbers to represent areas where Water (1), Rough/Vegetated Mudflat (2) Smooth/Un-Vegetated Mudflat (3), Woody Debris (4), Shrub Dominant Tundra (5), and ILLT (6) are present. Entropy-alpha segmentations [legend numbers represent the 9 zones defined by Cloude and Pottier, (1997)] for the same area show shallow (b), medium (c) and steep angles (d).

4.7. Assessment of the Potential to Classify Arctic Land Covers Using the Unsupervised Wishart Classifier

Tests of both the Wishart-entropy/alpha and Wishart-entropy/anisotropy/alpha classifier were completed. Since the results of the latter were slightly better, these are primarily discussed subsequently (see Appendix 10 for confusion matrices). Potential for distinguishing either rough or smooth surfaces in general was observed, though neither classifier could differentiate among substrates and vegetated classes. This potential also tended to diminish as incidence angle steepened, though Wetland was also better differentiated from some other classes at steep angles. This indicates that a multi-angle approach may still be optimal. Figure 29 and Figure 30 show classifier results at a broad scale, while the following focuses on results applied to individual classes.

Anthropogenic

Anthropogenic showed confusion with Shrub Dominant Tundra and Wetland at shallow and medium angles, as well as with Wetland, and a number of other classes at steep angles. As with the Wishart-entropy/alpha classifier, confusion with other classes tended to increase as incidence angle steepened. Again this was due to a greater number of pixels being identified outside clusters 1 and 10, which the majority of pixels were identified as at shallow and medium angles.

Water and Substrates

The addition of the Anisotropy parameter did not significantly reduce confusion between Water and smoother substrates such as Smooth/Un-Vegetated Mudflat, Peat and Sand, and this confusion also tended to worsen as incidence angle steepened (Figure 31). This for example, was especially the case for the Smooth/Un-Vegetated Mudflat class.

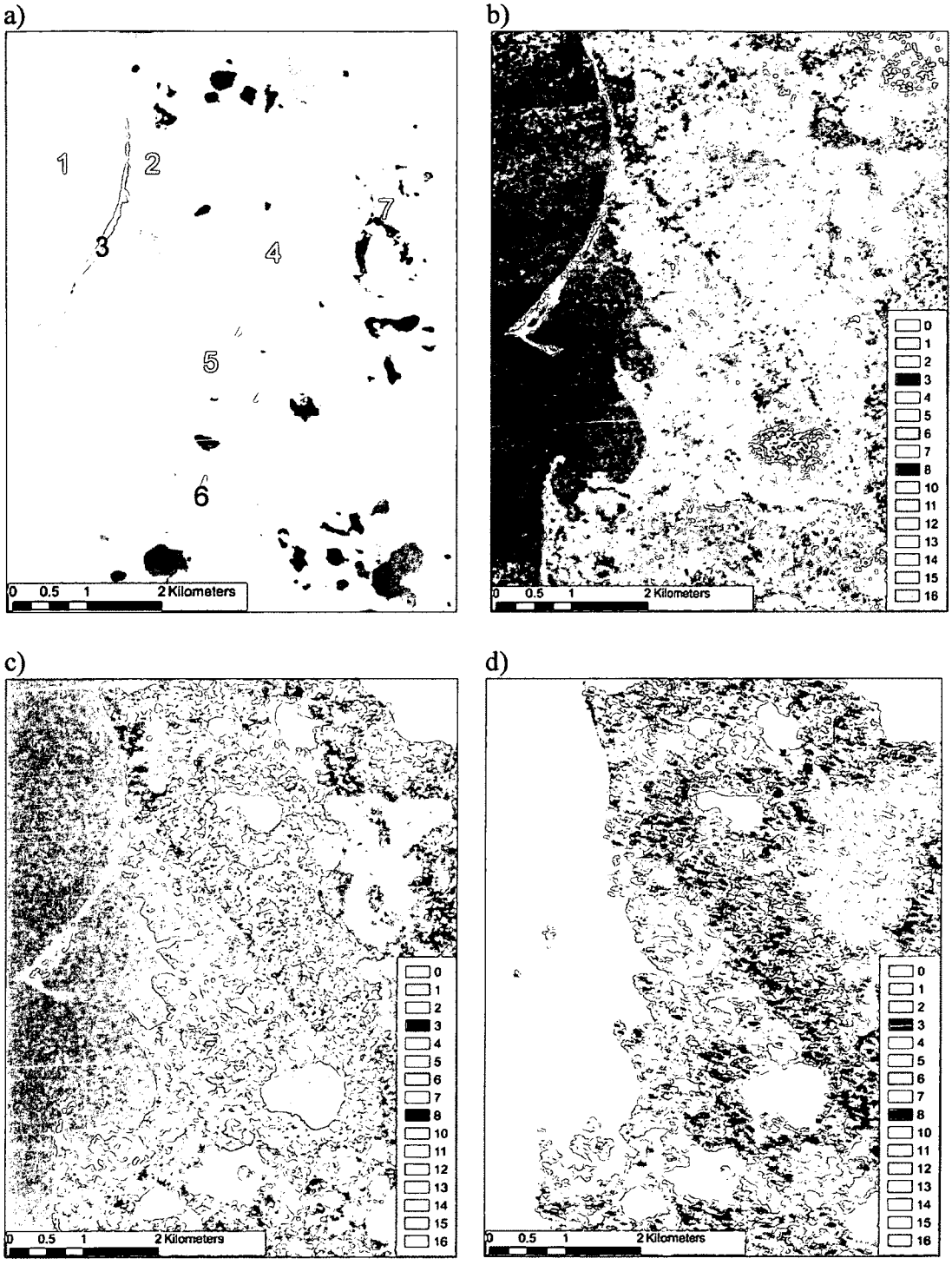

Figure 29: Ortho photo of TH study area (a), with numbers to represent areas where Water (1), Shrub Dominant Tundra (2), Sand (3), Herb Dominant Tundra (4), ILLT (5), Woody Debris (6), and Wetland (7) are present. These corresponded in some cases with the clusters of the unsupervised Wishart-entropy/anisotropy/alpha classifier applied to shallow (b), medium (c) and steep (d) angle imagery.

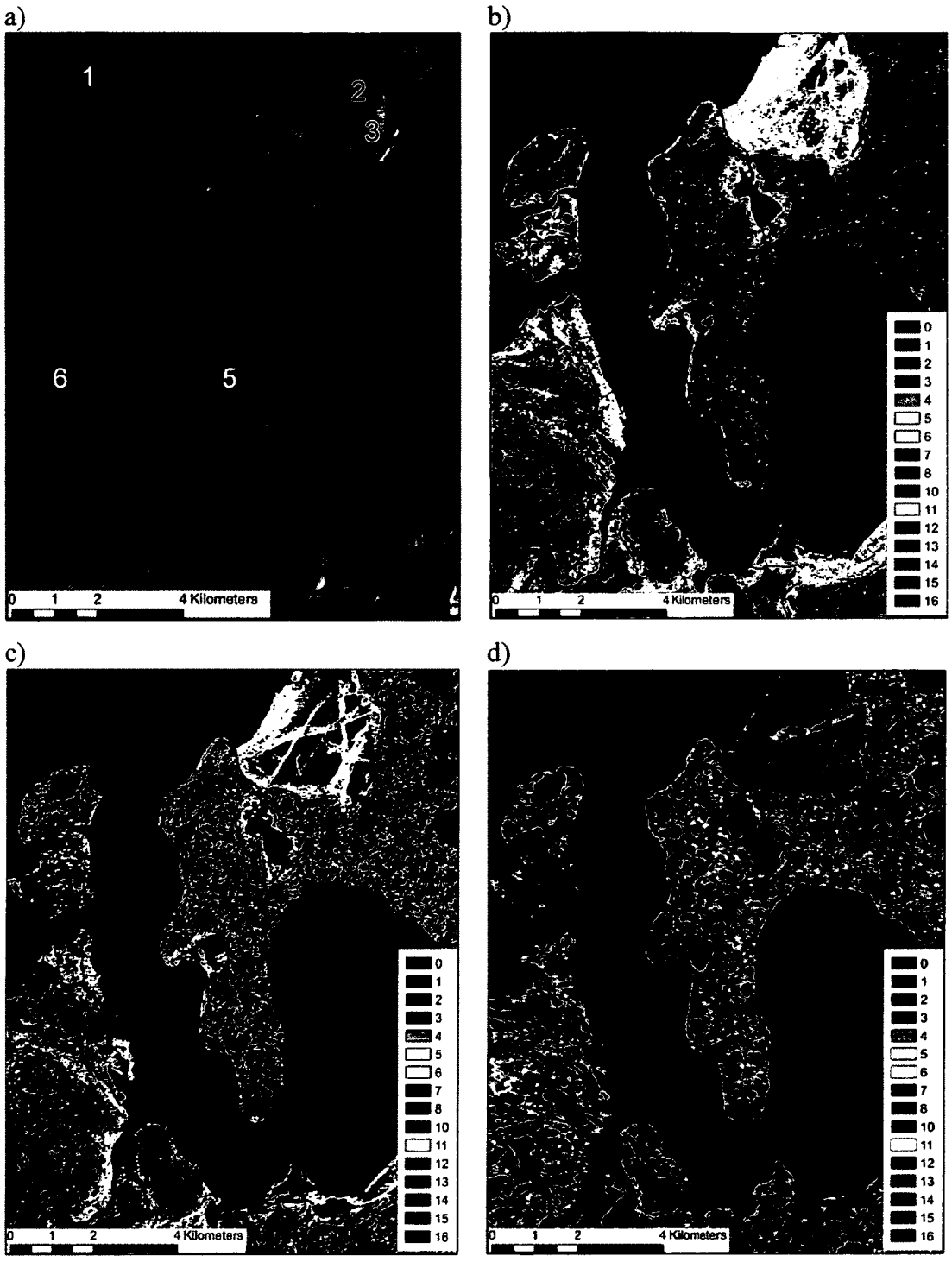

Figure 30: Ortho photo of WP study area (a), with numbers to represent areas where Water (1), Rough/Vegetated Mudflat (2) Smooth/Un-Vegetated Mudflat (3), Woody Debris (4), Shrub Dominant Tundra (5), and ILLT (6) are present. These corresponded in some cases with the clusters of the unsupervised Wishart-entropy/anisotropy/alpha classifier applied to shallow (b), medium (c) and steep (d) angle imagery.

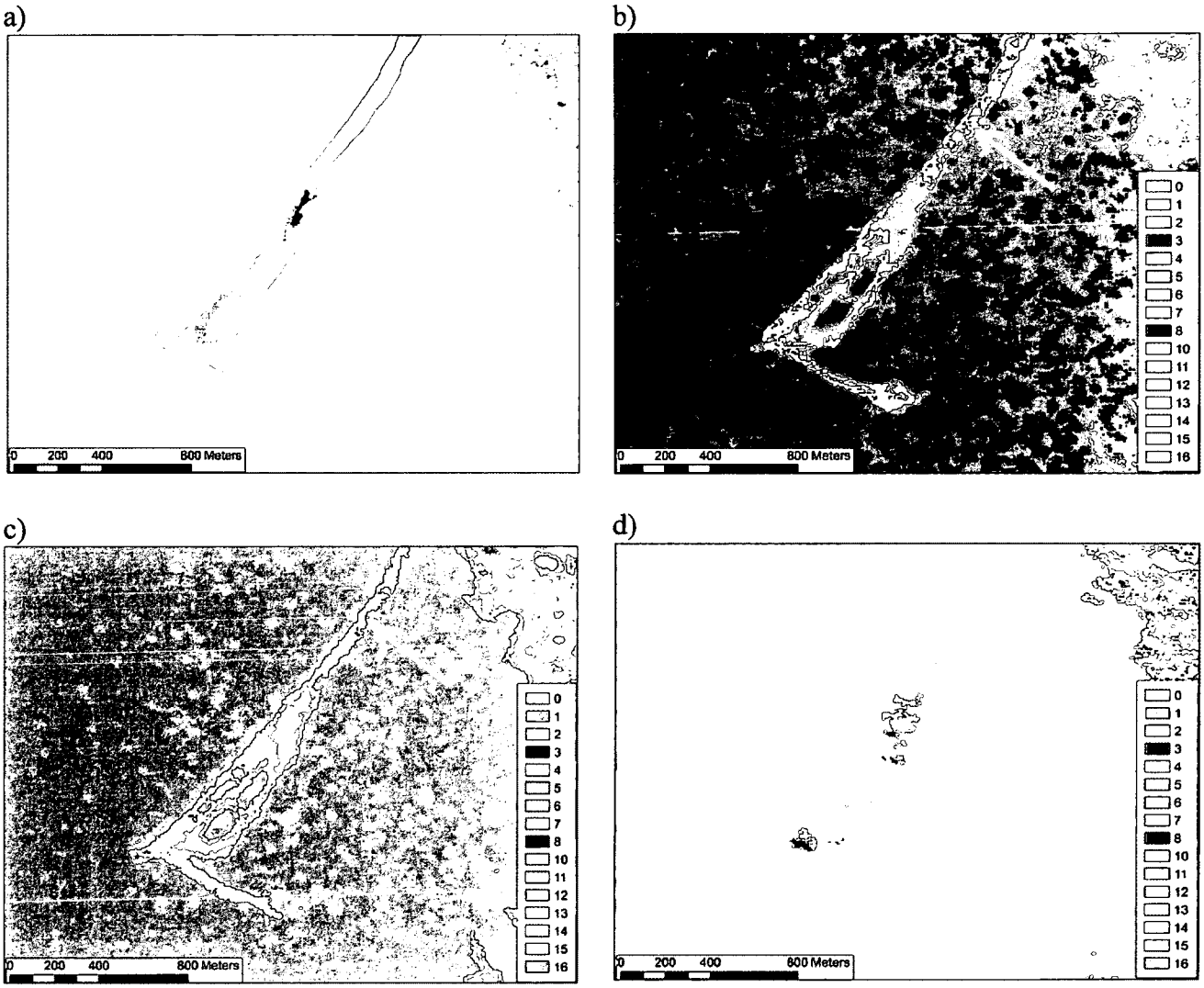

Figure 31: Portion of 2004 ortho photos of a sand spit in the TH study area (a), as well as unsupervised Wishart-entropy/anisotropy/alpha classifications of the same area from shallow (b), medium (c) and steep (d) incidence angle imagery. The red arrow shows a portion of the spit that is easily discerned from water (dark blue) in the shallow angle image, but becomes less visible at medium, and completely indiscernable at steep angles.

It should also be noted however, that the Rough/Vegetated Mudflat class could also be more easily differentiated from Water and Smooth/Un-Vegetated Mudflat at steep angles, indicating that a multi-angle approach may be required to distinguish all classes (Figure 30).

This observation is also consistent with the Wishart-entropy/alpha classifier, which also showed little potential was observed for distinguishing between substrates with smoother surfaces, including: Smooth/Un-Vegetated Mudflat, Peat and Sand. Generally however, these classes were identified as different clusters from substrates with rougher surfaces, including: Mixed Sediment, Riprap and Woody Debris, which also could not be distinguished from one another. Confusion between these groups of classes also tended to increase with steeper incidence angles. Rough/Vegetated Mudflat and Wood/Substrate Mix also tended to be identified in several of the same clusters for smooth and rough surface substrates. This may be expected since these classes have an intermediate surface roughness.

Vegetated Classes

Vegetated areas with relatively smooth surfaces such as Herb Dominant Tundra could generally be distinguished from classes like Shrub Dominant Tundra at shallow angles, though again this potential decreased as incidence angles steepened (Figure 29 and Figure 30). Marsh, ILLT, High Centre Polygons and Low Centre Polygons were generally confused, which was similarly observed with the Wishart-entropy/alpha classifier. The use of the anisotropy parameter did improve the ability to distinguish between Wetland and Shrub Dominant Tundra at shallow angles (Figure 32), though it also increased the confusion between Herb Dominant Tundra and portions of ILLT at

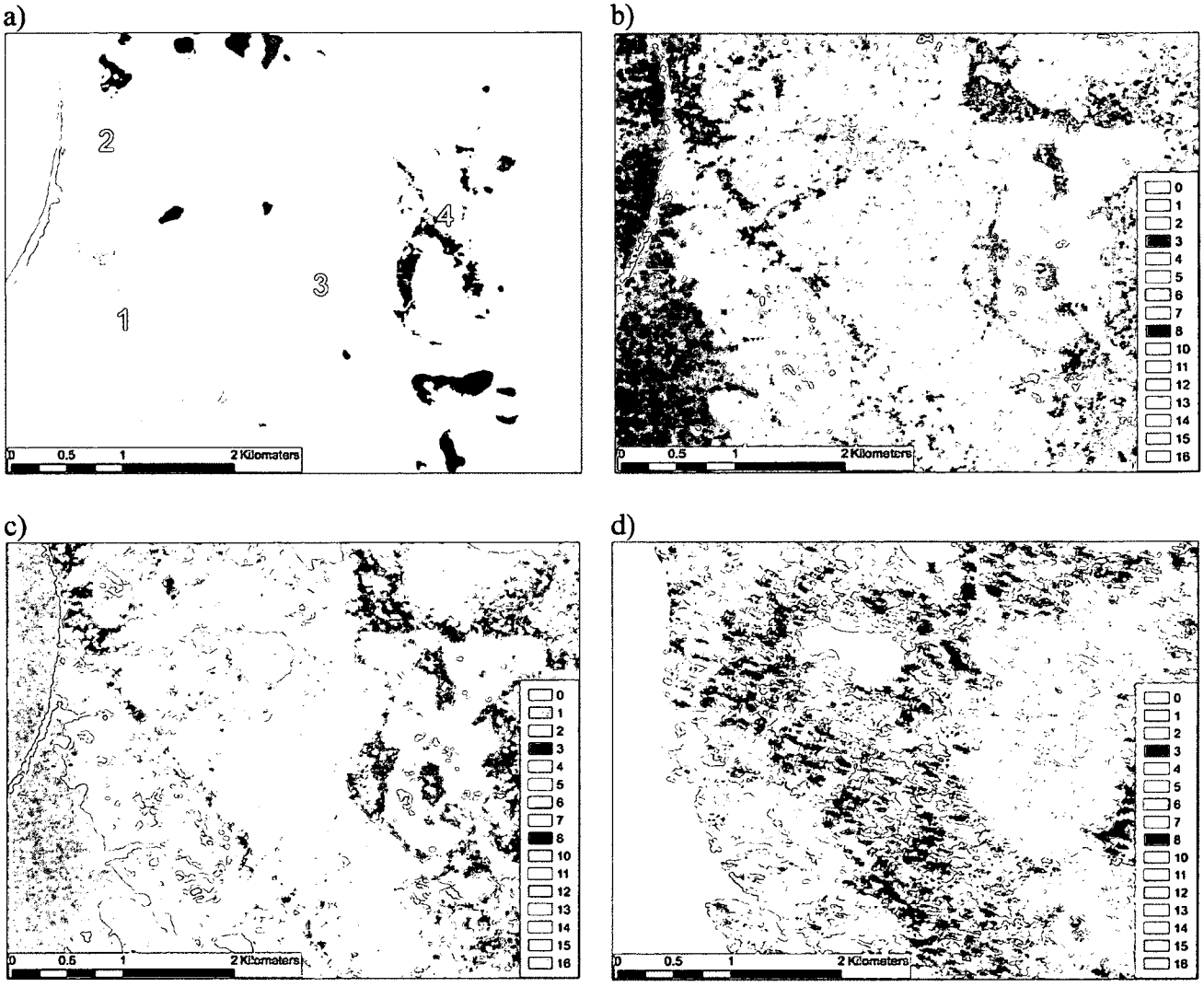

Figure 32: Ortho photo of TH study area (a), with numbers to represent areas where ILLT (1), Shrub Dominant Tundra (2), Herb Domiannt Tundra (3), and Wetland (4) are present. These corresponded in some cases with the clusters of the unsupervised Wishart-entropy/anisotropy/alpha classifier applied to shallow (b), medium (c) and steep (d) angle imagery.

shallow angles, which were better differentiated with the Wishart-entropy/alpha classifier.

4.8. Separability Analysis to Assess the Potential for Maximum Likelihood Classification

Separability analyses were performed on backscatter coefficients and Cloude-Pottier decomposition parameters. Freeman-Durden decomposition parameters were not included in this analysis because sample values were not normally distributed. The following focuses on assessing the optimal polarization, incidence angle, polarimetric parameter and multiple polarized image (HH, HV and VV backscatter coefficients), for classification of the SCAT land cover classes.

4.8.1. Backscatter coefficients

4.8.1.1. Optimal Single Polarization

Shallow HV provided the best average class separability, while HV was also the best single polarization at medium and steep angles (Table 23). For the TH study area the HH backscatter coefficient at shallow and medium angles provided similar results, whereas for the WP study area there was a substantial difference between average BD for HH and HV polarizations. At steep angles average separability for co-polarizations was about half of those for cross-polarizations, indicating that these polarizations alone show little potential as classifier inputs. As such, the highest separability achieved for any class pair was rarely HH or VV at steep angles (Appendix 11).

Overall, moderate to high classification potential (BD > 1.5) was observed for a

Table 23: Average separability (BD) for all single polarizations, co-pol and cross-pol combinations, the best polarimetric image (HH, HV and VV combined) for shallow, medium, steep, and all incidence angles combined.

Study Area	Variables	Incidence Angle			
		Shallow	Medium	Steep	All
TH	HH	1.10	1.02	0.55	1.38
	HV	1.13	1.05	0.98	1.38
	VV	0.96	0.88	0.42	1.27
	HH and VV	1.25	1.17	0.79	1.59
	HH and HV	1.35	1.28	1.18	1.65
	VV and HV	1.30	1.25	1.16	1.63
	HH, HV and VV	1.43	1.37	1.28	1.75
WP	HH	0.95	0.91	0.40	1.22
	HV	1.07	1.00	0.82	1.28
	VV	0.81	0.83	0.38	1.16
	HH and VV	1.25	1.16	0.68	1.52
	HH and HV	1.25	1.18	1.04	1.56
	VV and HV	1.25	1.24	1.08	1.58
	HH, HV and VV	1.39	1.36	1.18	1.71

number of classes (Table 24 and Table 25). Appendix 11 shows all configurations that resulted in BD values greater than 1.5.

Anthropogenic

In most cases shallow HH provided the highest separability between Anthropogenic and other classes. This was especially the case for vegetated classes, though steep VV also provided the highest separability between Wetland and Anthropogenic. Despite this, little potential was observed for using single polarizations to discriminate between Anthropogenic and most vegetated classes, as well as to discriminate between Anthropogenic and substrates with rougher surfaces, including: Mixed Sediment, Riprap, and Woody Debris. Conversely, high separabilities were

Table 24: Maximum separability (BD) achieved using a single polarization for classes in the TH study area.

	Anthropogenic	Water	Smooth/Un-Vegetated Mudflats	Peat	Sand	Mixed Sediment	Riprap	Wood/Substrate Mix	Woody Debris	Marsh	Wetland	ILLT	Low Centre Polygons	Eroding Tundra	Herb Dominant Tundra
Water	2.00														
Smooth/Un-Vegetated Mudflat	2.00	1.66													
Peat	1.86	1.50	1.53												
Sand	1.97	1.36	0.86	1.02											
Mixed Sediment	1.31	2.00	1.98	1.40	1.74										
Riprap	1.18	2.00	2.00	1.57	1.92	0.15									
Wood/Substrate Mix	1.81	1.95	1.64	0.42	0.81	0.96	1.29								
Woody Debris	1.19	2.00	2.00	1.50	1.89	0.48	0.49	1.36							
Marsh	1.70	2.00	1.98	1.09	1.61	0.70	0.89	0.69	1.05						
Wetland	0.91	2.00	2.00	1.97	1.99	1.23	1.04	1.84	1.44	1.80					
ILLT	1.45	2.00	2.00	1.68	1.93	0.29	0.54	1.23	0.39	0.53	1.46				
Low Centre Polygons	1.49	2.00	2.00	1.63	1.90	0.32	0.26	1.24	0.75	0.42	1.44	0.13			
Eroding Tundra	1.15	2.00	2.00	1.93	1.99	0.69	0.74	1.79	1.38	1.53	0.88	0.79	1.14		
Herb Dominant Tundra	1.65	2.00	2.00	1.72	1.96	0.59	1.09	1.28	1.25	0.54	1.82	0.50	0.75	1.19	
Shrub Dominant Tundra	1.26	2.00	2.00	1.99	2.00	1.02	1.38	1.96	1.86	1.91	1.72	1.47	1.47	0.31	1.70

Moderate Classification Potential: BD 1.5 - 1.7 ■ High Classification Potential: BD > 1.7 □

Table 25: Maximum separability (BD) achieved with a single polarization in the WP study area.

	Water	Smooth/Un-Vegetated Mudflat	Rough/Vegetated Mudflat	Peat	Sand	Mixed Sediment	Wood/Substrate Mix	Woody Debris	Marsh	Wetland	ILLT	High Centre Polygons	Low Centre Polygons	Eroding Tundra	Herb Dominant Tundra
Smooth/Un-Vegetated Mudflat	1.77														
Rough/Vegetated Mudflat	2.00	1.96													
Peat	2.00	1.78	0.82												
Sand	1.39	0.35	1.67	1.25											
Mixed Sediment	2.00	1.95	1.09	0.33	1.56										
Wood/Substrate Mix	1.99	1.84	1.06	0.48	1.33	0.28									
Woody Debris	2.00	2.00	1.73	1.78	1.97	1.76	1.31								
Marsh	2.00	1.83	1.34	0.24	1.44	0.37	0.23	1.70							
Wetland	2.00	1.99	1.43	0.84	1.73	0.54	0.18	1.61	0.57						
ILLT	2.00	2.00	1.59	1.08	1.93	0.81	0.88	1.81	0.72	0.51					
High Centre Polygons	2.00	2.00	1.56	1.08	1.93	0.84	0.96	1.68	0.78	0.59	0.18				
Low Centre Polygons	2.00	1.98	1.60	0.76	1.72	0.51	0.39	1.90	0.36	0.63	0.40	0.72			
Eroding Tundra	2.00	2.00	1.15	1.23	1.94	1.14	0.85	0.97	0.75	0.63	0.48	0.47	0.81		
Herb Dominant Tundra	2.00	1.99	1.69	1.15	1.82	0.48	0.35	1.86	0.65	0.87	0.54	0.83	0.34	0.60	
Shrub Dominant Tundra	2.00	2.00	1.93	1.86	2.00	1.94	1.69	1.26	1.69	1.74	1.84	1.73	0.93	0.80	1.79

Moderate Classification Potential: BD 1.5 - 1.7 ■ High Classification Potential: BD > 1.7 ■

achieved between Anthropogenic and Water, as well as between Anthropogenic and substrates with smoother surfaces (e.g. Sand).

Water and Substrates

High potential was shown to discriminate between Water and most other classes with rougher surfaces, such as Shrub Dominant Tundra. High separabilities were found between Water and Smooth/Un-Vegetated Mudflat and between Water and Peat in the TH study area. In most cases this was achieved using one of: shallow HH or HV, medium HH or HV, and steep HV. This shows that targeted acquisitions for discriminating between Water and some other class can be more flexible in terms of the polarization and incidence angle configuration. This could allow users planning single polarization acquisitions to optimize parameters for other classes, such as to increase the separability between Mixed Sediment and Sand.

High classification potential was observed using single polarizations to distinguish Smooth/Un-Vegetated Mudflat from all classes except Sand, which showed BD values of 0.86 and 0.35 for the TH and WP study areas, respectively. Additionally, only moderately high BD was observed between Smooth/Un-Vegetated Mudflat and Peat and between Smooth/Un-Vegetated Mudflat and Water for the TH study area. Other substrate classes showed less potential for accurate classification using single polarizations, as those with smoother surfaces were generally confused with each other and with Water, while those with rougher surfaces were generally confused with each other and some vegetated classes. It should also be noted that some classes showed better overall separability in one study area. This was the case for Woody Debris in the WP study area, while the reverse was true for Peat.

Vegetated Classes

Using single polarizations, most vegetation classes could only be distinguished from smoother classes such as Water, Smooth/Un-Vegetated Mudflat, and Sand. Again, not only were vegetation classes generally confused with rougher substrates, but they could not generally be distinguished from one another. One exception was Shrub Dominant Tundra which showed high separability with most classes. This was generally achieved with shallow and medium HV.

4.8.1.2. Optimal Dual Polarization

Some variability in the best dual polarization combination was observed between study areas. In the TH study area for example, shallow HH and HV was the best combination overall, whereas in the WP study area all polarization combinations at shallow angles provided the same average separability (Table 23). While HH and HV also provided the highest separability at medium and steep angles in the TH study area, VV and HV were best in the WP study area.

With two polarizations it is possible to generate scatter plots to visually convey class separability. To highlight some of the previous observations made of backscatter coefficients, Figure 33 shows improved sensitivity to differences in surface roughness at shallow compared to steep angles. While this example shows Sand versus Mixed Sediment only, a similar degree of separability was also observed for Smooth/Un-Vegetated Mudflat versus Rough/Vegetated Mudflat, as well as Shrub Dominant Tundra versus Herb Dominant Tundra. For all these classes, the optimal dual polarization combination at all

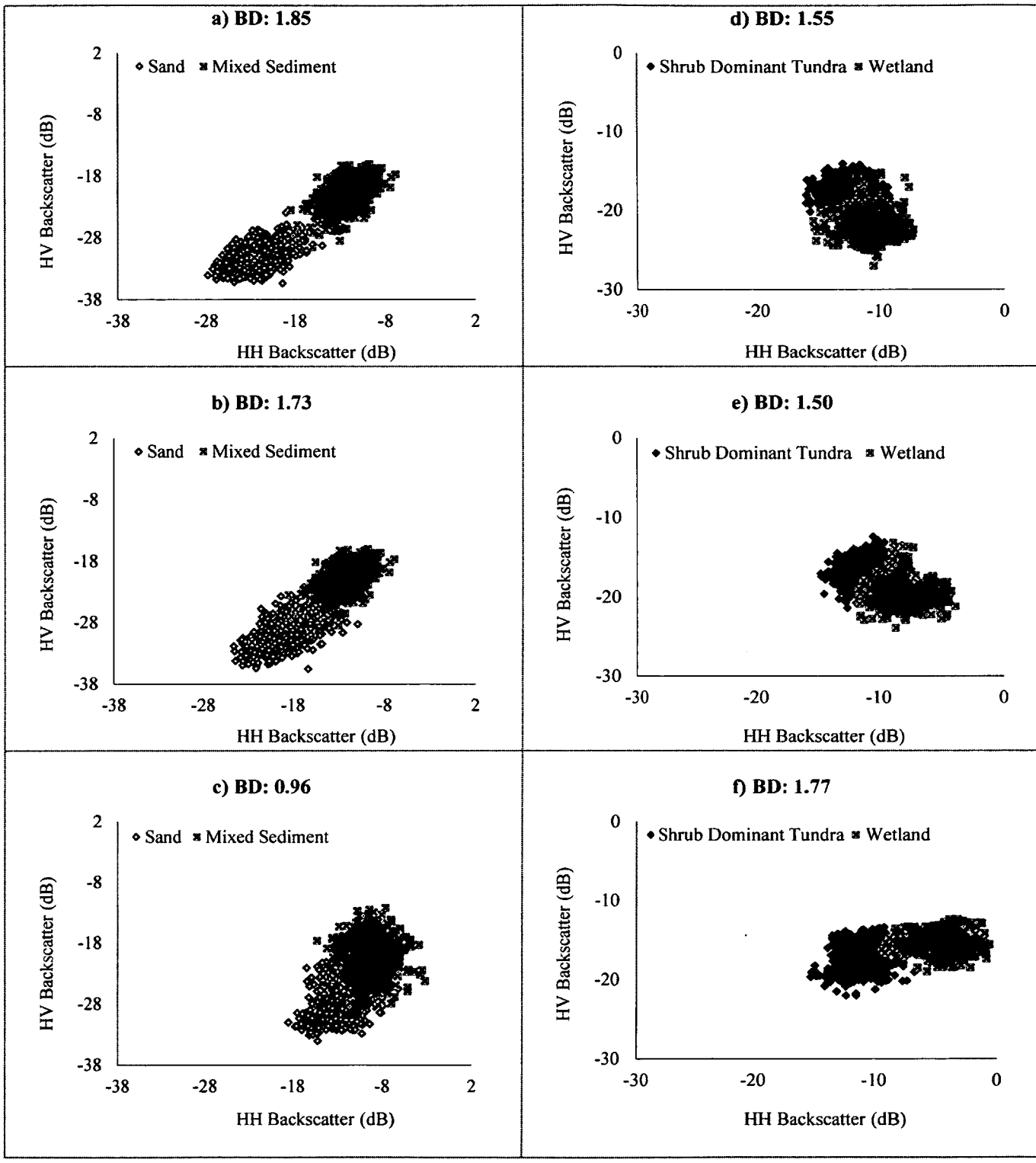

Figure 33: Scatter plots of training data for Sand versus Mixed Sediment and Shrub Dominant Tundra versus Wetland, for shallow (a, d), medium (b, e) and steep (c, f) angles.

angles was HH and HV. Figure 33 also shows improved sensitivity to moisture at steep compared to shallow angles. This was observed for Shrub Dominant Tundra versus Wetland, Anthropogenic versus Wetland, and Riprap versus Wetland. The optimal dual polarization combination for these classes was also HH and HV at all angles. Based on this, it is clear that there is some potential for accurate classification of a number of classes using only two polarizations, and that in most cases this is achieved with HH and HV polarizations.

4.8.1.3. Separability Analysis of Combined HH, VV, and HV Data

Compared to single, and dual polarization combinations, a greater number of class pairs showed acceptable separabilities (BD > 1.50) when all three polarizations were combined. Shallow angles showed the highest average separability for both study areas, followed closely by medium angles (Table 23), while some class pairs still showed better separability with steep angle imagery. Table 26 and Table 27 show the highest achieved separability regardless of incidence angle, while the images that achieved these presented in Appendix 12, along with all combinations that achieved a BD > 1.50.

Anthropogenic

In all cases, shallow angle imagery provided the highest separability between Anthropogenic and other classes. Use of all polarizations also resulted in improved separability (BD > 1.50) between Anthropogenic and a number of vegetated classes such as Wetland, ILLT, and Low Centre Polygons, for which poor separability (BD < 1.5) values were observed with any single polarization. As was the case for single polarizations, for which steep VV provided best separability between Anthropogenic and

Table 26: Maximum separability (BD Distance) for all combined HH, VV and HV images for classes in the TH study area.

	Anthropogenic	Water	Smooth/Un-Vegetated Mudflats	Peat	Sand	Mixed Sediment	Riprap	Wood/Substrate Mix	Woody Debris	Marsh	Wetland	ILLT	Low Centre Polygons	Eroding Tundra	Herb Dominant Tundra
Water	2.00														
Smooth/Un-Vegetated Mudflat	2.00	1.70													
Peat	1.92	1.68	1.81												
Sand	1.98	1.77	1.21	1.12											
Mixed Sediment	1.40	2.00	2.00	1.51	1.90										
Riprap	1.33	2.00	2.00	1.76	1.98	0.34									
Wood/Substrate Mix	1.86	1.97	1.86	0.57	0.91	1.14	1.50								
Woody Debris	1.51	2.00	2.00	1.76	1.98	0.94	0.68	1.56							
Marsh	1.78	2.00	2.00	1.18	1.76	0.84	1.17	0.78	1.13						
Wetland	1.64	2.00	2.00	2.00	2.00	1.85	1.84	1.98	1.85	1.88					
ILLT	1.56	2.00	2.00	1.76	1.95	0.65	0.69	1.33	0.71	0.68	1.67				
Low Centre Polygons	1.57	2.00	2.00	1.75	1.95	0.53	0.46	1.33	0.82	0.61	1.80	0.19			
Eroding Tundra	1.33	2.00	2.00	1.95	2.00	0.88	0.95	1.85	1.47	1.73	1.68	1.00	1.34		
Herb Dominant Tundra	1.74	2.00	2.00	1.78	1.97	0.78	1.16	1.30	1.29	0.59	1.94	0.55	0.80	1.56	
Shrub Dominant Tundra	1.57	2.00	2.00	1.99	2.00	1.09	1.43	1.97	1.93	1.98	1.81	1.60	1.61	0.41	1.84

Moderate Classification Potential: BD 1.5 - 1.7 ☐ High Classification Potential: BD > 1.7 ☐

Table 27: Maximum separability (BD Distance) for all combined HH, VV and HV images for classes in the WP study area.

	Water	Smooth/Un-Vegetated Mudflat	Rough/Vegetated Mudflat	Peat	Sand	Mixed Sediment	Wood/Substrate Mix	Woody Debris	Marsh	Wetland	ILLT	High Centre Polygons	Low Centre Polygons	Eroding Tundra	Herb Dominant Tundra
Smooth/Un-Vegetated Mudflat	1.84														
Rough/Vegetated Mudflat	2.00	1.98													
Peat	2.00	1.81	0.90												
Sand	1.67	0.83	1.73	1.41											
Mixed Sediment	2.00	1.99	1.20	0.44	1.66										
Wood/Substrate Mix	2.00	1.97	1.20	0.61	1.54	0.44									
Woody Debris	2.00	2.00	1.94	1.89	1.99	1.90	1.58								
Marsh	2.00	1.93	1.52	0.66	1.52	0.57	0.47	1.84							
Wetland	2.00	2.00	1.76	1.25	1.88	1.06	0.60	1.80	0.69						
ILLT	2.00	2.00	1.83	1.34	1.95	1.06	1.06	1.94	0.86	0.78					
High Centre Polygons	2.00	2.00	1.79	1.32	1.95	1.13	1.22	1.91	0.96	0.71	0.30				
Low Centre Polygons	2.00	2.00	1.77	0.94	1.80	0.68	0.69	1.97	0.56	0.78	0.54	0.81			
Eroding Tundra	2.00	2.00	1.68	1.31	1.95	1.24	0.96	1.06	0.93	1.03	0.73	0.77	0.98		
Herb Dominant Tundra	2.00	2.00	1.76	1.25	1.86	0.67	0.82	1.89	0.94	1.13	0.79	1.05	0.35	0.73	
Shrub Dominant Tundra	2.00	2.00	1.95	1.88	2.00	1.96	1.75	1.35	1.88	1.88	1.95	1.84	0.87	0.96	1.86

Moderate Classification Potential: BD 1.5 - 1.7 High Classification Potential: BD > 1.7

Wetland, steep HH, HV and VV also provided the best separability between these classes. Despite using all polarizations as inputs, acceptable separabilities could still not be achieved to differentiate Anthropogenic from Mixed Sediment, Riprap and Eroding Tundra (BD < 1.50).

Water and Susbtrates

With all polarizations as inputs, Water showed high separabilities with most class pairs, and this was typically achieved at all incidence angles. Separability with Sand however, was only moderate in the WP study area, and high in the TH study area. This was not achieved using any single polarization, and so it may be necessary to acquire multiple polarizations for accurate classification of these land cover types. Moderate separability was also observed between Water and both Smooth/Un-Vegetated Mudflat and Peat in the TH study area.

Substrates with smoother surfaces showed better separability with each other using all polarizations as inputs. As an example, Smooth/Un-Vegetated Mudflat showed acceptable separabilities with a number of additional classes, though no combination could provide moderate separability with Sand for either study area. Despite this increased separability using all polarizations, potential was only shown for general discrimination based on differences in surface roughness. Rougher substrates for example, also showed confusion with vegetated classes (e.g. Mixed Sediment versus ILLT, Eroding Tundra, Low Centre Polygons and Herb Dominant Tundra).

Vegetated Classes

Wetland in the TH study area was one of the few vegetated classes to show moderate to high separability with all other classes. Wetland from the WP study area however, showed low separabilities with most other vegetated classes, as well as with some substrates. Marsh, ILLT, Low Centre Polygons, High Centre Polygons, and Eroding Tundra, were also confused between each other and some substrates, while higher classification potential was observed for Shrub Dominant Tundra and Herb Dominant Tundra. As was observed with single polarizations, shallow angle imagery generally provided the highest separability between Shrub Dominant Tundra and other classes.

4.8.2. Cloude-Pottier Decomposition Parameters

Unlike backscatter coefficients, the Cloude-Pottier decomposition parameters entropy, anisotropy and alpha derived from steep angle imagery provided the highest average separability, which is consistent with the previous interpretations using pseudo colour images. Overall separability was low for single parameters, and only slight improvements were observed when multiple parameters were combined. The two parameters which provided the best separability were also entropy and alpha. Even when all parameters were combined however, significantly less potential for accurate classification was observed, compared to backscatter coefficients (Table 28).

4.9. Maximum Likelihood Classification using the Optimal Radar Parameters and SPOT-4 Data

From the above visual and separability analyses, the MLC was implemented using

Table 28: Average separability (BD) for all single polarizations, co-pol and cross-pol combinations, the best polarimetric image (HH, HV and VV combined) for shallow, medium, steep, and all incidence angles combined.

Study Area	Variables	Incidence Angle			
		Shallow	Medium	Steep	All
TH	Entropy	0.38	0.49	0.68	0.99
	Anisotropy	0.21	0.17	0.32	0.58
	Alpha	0.46	0.61	0.82	1.14
	Entropy and Alpha	0.74	0.87	1.00	1.42
	Entropy and Anisotropy	0.55	0.62	0.77	1.22
	Alpha and Anisotropy	0.62	0.73	0.92	1.31
	Entropy, Anisotropy, Alpha	0.84	0.94	1.06	1.50
WP	Entropy	0.52	0.61	0.83	1.13
	Anisotropy	0.09	0.06	0.24	0.37
	Alpha	0.47	0.62	0.79	1.16
	Entropy and Alpha	0.75	0.82	0.91	1.39
	Entropy and Anisotropy	0.59	0.66	0.87	1.24
	Alpha and Anisotropy	0.55	0.67	0.85	1.27
	Entropy, Anisotropy, Alpha	0.80	0.86	0.96	1.45

the optimal backscatter coefficients only, which included: shallow HH, HV and VV polarizations. Little potential for accurate classification was demonstrated with these inputs alone (Figure 34), as the overall accuracy (number of pixels correctly classified/total number of pixels) was 52.9% (Table 29). Only Water, Wood Substrate Mix and Wetland showed some potential for accurate classification.

Classification of SPOT-4 data (Table 30) was significantly better, as there was greater consistency between class accuracies, and class spatial distributions resembled more closely what was observed in the field, and interpreted from the ortho photos (Figure 34). It is of interest to note that while Mixed Sediment could not be accurately classified using backscatter coefficients alone; there was increased confusion between Sand and Mixed Sediment using the SPOT-4 data alone. This is evident in Figure 34,

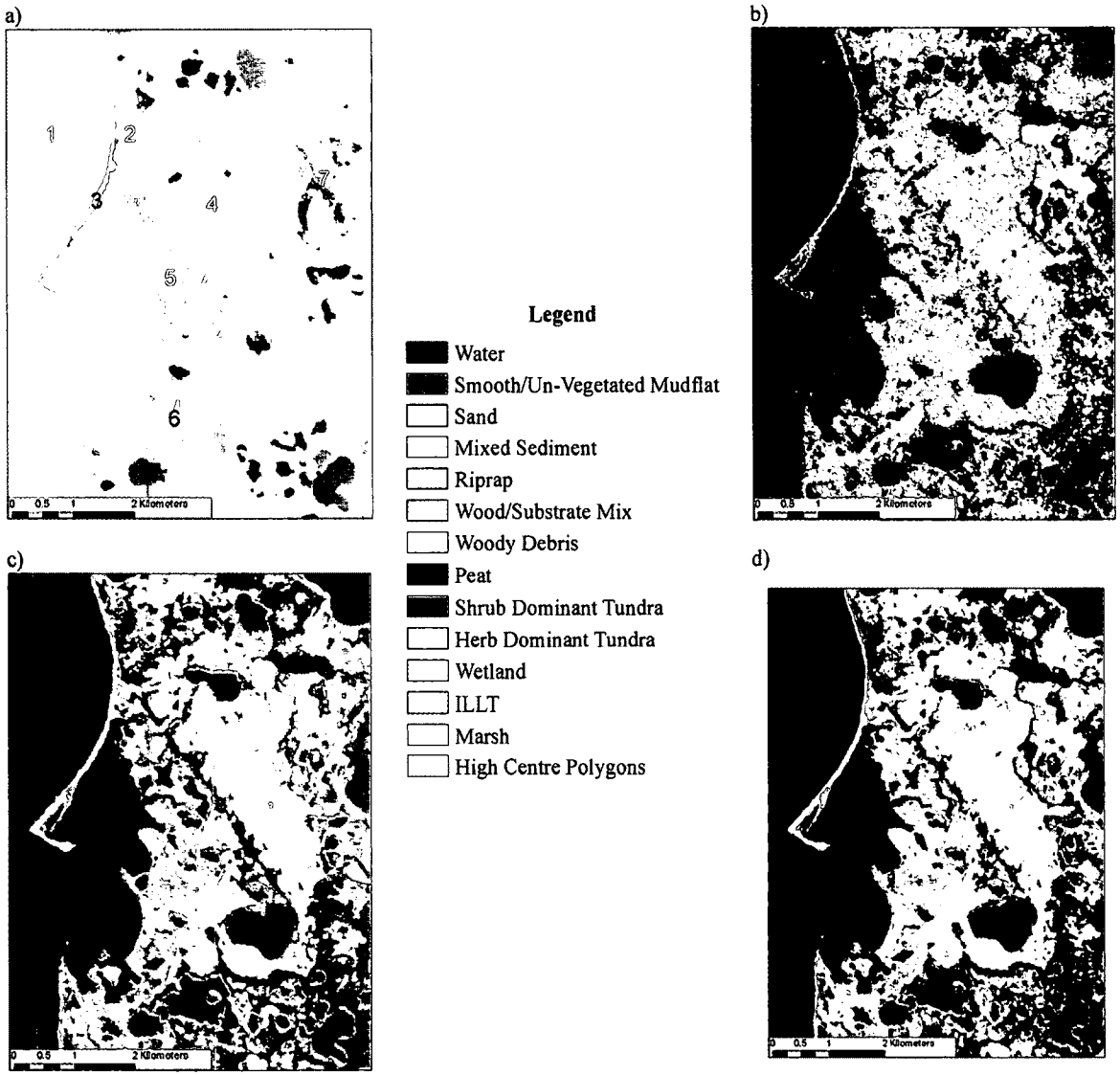

Figure 34: Ortho photo of TH study area (a), with numbers to represent areas whereWater (1), Shrub Dominant Tundra (2), Sand (3), Herb Dominant Tundra (4), ILLT (5), Woody Debris (6), and Wetland (7) are present. In some cases these correspond to the classes identified by the Maximum Likelihood using backscatter coefficients (b), SPOT-4 bands (c) and both combined (d).

Table 29: Confusion matrix showing classification accuracy of the TH study area when using the three shallow angle polarizations, plus steep HV as inputs to a Maximum Likelihood Classifier. Overall accuracy was 52.9%.

		Reference Data																
		Anthropogenic	Water	Smooth/Un-Vegetated Mudflats	Peat	Sand	Mixed Sediment	Riprap	Wood/Substrate Mix	Woody Debris	Marsh	Wetland	ILLT	Low Centre Polygons	Eroding Tundra	Herb Dominant Tundra	Shrub Dominant Tundra	Total	User's Accuracy (%)
Classification Data	Anthropogenic	**61**	0	0	1	0	1	1	0	0	0	7	0	1	0	9	7	88	69.3
	Water	0	**912**	12	3	17	0	0	0	0	0	0	0	0	0	0	0	944	96.6
	Smooth/Un-Vegetated Mudflat	0	232	**22**	0	8	0	0	1	0	0	0	0	0	0	0	0	263	8.4
	Peat	4	34	0	**3**	71	0	2	31	0	0	14	0	0	0	0	0	159	1.9
	Sand	2	16	0	5	**106**	0	2	30	0	0	0	0	0	0	0	0	161	65.8
	Mixed Sediment	3	0	0	0	1	**10**	0	0	0	0	61	5	11	1	15	10	117	8.6
	Riprap	3	0	0	0	0	21	**0**	2	12	0	31	16	10	0	2	1	98	0.0
	Wood/Substrate Mix	2	0	0	5	14	1	1	**89**	0	0	8	0	0	0	0	0	120	74.2
	Woody Debris	2	0	0	0	1	8	1	3	**85**	0	1	12	11	0	18	0	142	59.9
	Marsh	4	0	0	0	12	10	5	23	3	**0**	19	18	5	0	11	0	110	0.0
	Wetland	4	0	0	0	0	4	1	0	1	0	**113**	7	6	1	5	4	146	77.4
	ILLT	2	0	0	0	0	16	0	3	9	0	6	**71**	34	0	36	1	178	39.9
	Low Centre Polygons	2	0	0	0	0	26	4	1	29	0	4	49	**91**	0	47	4	257	35.4
	Eroding Tundra	10	0	0	0	0	10	0	0	1	0	23	10	32	**13**	30	64	193	6.7
	Herb Dominant Tundra	1	0	0	0	0	25	0	4	1	0	1	37	41	1	**105**	30	246	42.7
	Shrub Dominant Tundra	0	0	0	0	0	8	0	0	0	0	11	3	7	37	6	**131**	203	64.5
	Total	100	1194	34	17	230	140	17	187	141	0	299	228	249	53	284	252		
	Producer's Accuracy (%)	56.0	76.4	64.7	17.7	46.1	7.1	0.0	47.6	60.3	N/A	37.8	31.1	36.6	24.5	37.0	52.0		

Table 30: Confusion matrix showing classification accuracy of the TH study area when using SPOT-4 imagery as inputs to a Maximum Likelihood Classifier. Overall accuracy was 82.8%.

		Reference Data																	
		Anthropogenic	Water	Smooth/Un-Vegetated Mudflats	Peat	Sand	Mixed Sediment	Riprap	Wood/Substrate Mix	Woody Debris	Marsh	Wetland	ILLT	Low Centre Polygons	Eroding Tundra	Herb Dominant Tundra	Shrub Dominant Tundra	Total	User's Accuracy (%)
Classification Data	Anthropogenic	**56**	0	0	0	6	0	0	7	21	0	0	7	0	0	0	0	97	57.7
	Water	0	**1194**	0	0	0	0	0	0	0	0	0	0	0	0	0	0	1194	100.0
	Smooth/Un-Vegetated Mudflat	0	0	**32**	0	0	0	0	0	0	0	0	0	0	0	0	0	32	100.0
	Peat	0	0	0	**17**	3	0	5	0	0	0	0	0	0	0	0	0	25	68.0
	Sand	3	0	2	0	**108**	0	0	53	0	0	0	0	0	0	0	0	166	65.1
	Mixed Sediment	36	0	0	0	31	**131**	3	3	0	0	0	5	0	2	0	0	211	62.1
	Riprap	0	0	0	0	1	9	**9**	3	0	0	0	0	0	0	0	0	22	40.9
	Wood/Substrate Mix	0	0	0	0	80	0	0	**121**	0	0	0	0	0	0	0	0	201	60.2
	Woody Debris	1	0	0	0	0	0	0	0	**120**	0	0	0	0	0	0	0	121	99.2
	Marsh	4	0	0	0	1	0	0	0	0	**0**	25	7	0	4	7	0	48	0.0
	Wetland	0	0	0	0	0	0	0	0	0	0	**175**	0	5	6	0	4	190	92.1
	ILLT	0	0	0	0	0	0	0	0	0	0	0	**171**	7	19	30	0	227	75.3
	Low Centre Polygons	0	0	0	0	0	0	0	0	0	0	46	3	**222**	14	6	1	292	76.0
	Eroding Tundra	0	0	0	0	0	0	0	0	0	0	0	13	6	**1**	0	0	20	5.0
	Herb Dominant Tundra	0	0	0	0	0	0	0	0	0	0	0	10	9	0	**222**	1	242	91.7
	Shrub Dominant Tundra	0	0	0	0	0	0	0	0	0	0	53	12	0	7	19	**246**	337	73.0
	Total	100	1194	34	17	230	140	17	187	141	0	299	228	249	53	284	252		
	Producer's Accuracy (%)	56.0	100.0	94.1	100.0	47.0	93.6	52.9	64.7	85.1	N/A	58.5	75.0	89.2	1.9	78.2	97.6		

where a significant portion of the sand spit (3) is classified as Mixed Sediment.Additionally, the coastline produced from the radar classification more closely resembles the shoreline that is visible in 2004 ortho photos (Figure 34).

Combining the shallow angle backscatter coefficients for all polarizations with the SPOT-4 data (Table 31) showed only a small increase in average accuracy. Certain classes improved significantly, including Sand versus Mixed Sediment, as the majority of the sand spit in Figure 34 is correctly classified. It is also of interest to note that approximately the same extent is classified as Wetland in all three classifications. For most classes acceptable accuracies were observed by combining the shallow angle radar and SPOT-4 data, though it is also anticipated that increased accuracy could be achieved through class merging. This wasbeyond the scope of this thesis, which focussed on the analysis of backscatter characteristics and mechanisms of the SCAT land cover classes, as well as to determine parameters with strong potential for classification. Future work will assess additional radar parameters such as the Radar Vegetation Index, pedestal height, intensity ratios etc., as well as vegetation and soil indices derived from SPOT-4 data, to determine if improved classification accuracy can be achieved.

Table 31: Confusion matrix showing classification accuracy of the TH study area when using the three shallow angle polarizations and the SPOT-4 data as inputs into Maximum Likelihood. Overall accuracy is 86.1%.

		Reference Data																
		Anthropogenic	Water	Smooth/Un-Vegetated Mudflats	Peat	Sand	Mixed Sediment	Riprap	Wood/Substrate Mix	Woody Debris	Marsh	Wetland	ILLT	Low Centre Polygons	Eroding Tundra	Herb Dominant Tundra	Shrub Dominant Tundra	Total	User's Accuracy (%)
Classified Data	Anthropogenic	**73**	0	0	0	0	1	0	2	37	0	0	0	0	0	0	0	113	64.6
	Water	0	**1194**	0	1	0	0	0	0	0	0	0	0	0	0	0	0	1195	99.9
	Smooth/Un-Vegetated Mudflat	0	0	**31**	0	0	0	0	0	0	0	0	0	0	0	0	0	31	100.0
	Peat	0	0	0	**16**	4	0	8	2	0	0	0	0	0	0	0	0	30	53.3
	Sand	8	0	3	0	**196**	0	0	38	0	0	0	0	0	0	0	0	245	80.0
	Mixed Sediment	16	0	0	0	3	**132**	6	1	0	0	7	4	0	9	0	0	178	74.2
	Riprap	0	0	0	0	1	4	**3**	2	0	0	0	0	0	0	0	0	10	30.0
	Wood/Substrate Mix	2	0	0	0	25	3	0	**140**	0	0	0	0	0	0	0	0	170	82.4
	Woody Debris	0	0	0	0	0	0	0	2	**104**	0	0	0	0	0	0	0	106	98.1
	Marsh	1	0	0	0	1	0	0	0	0	**0**	9	3	1	0	14	0	29	0.0
	Wetland	0	0	0	0	0	0	0	0	0	0	**185**	0	1	4	0	0	190	97.4
	ILLT	0	0	0	0	0	0	0	0	0	0	2	**189**	18	0	20	2	231	81.8
	Low Centre Polygons	0	0	0	0	0	0	0	0	0	0	87	12	**223**	15	21	10	368	60.6
	Eroding Tundra	0	0	0	0	0	0	0	0	0	0	0	9	0	**2**	0	0	11	18.2
	Herb Dominant Tundra	0	0	0	0	0	0	0	0	0	0	0	11	5	0	**223**	1	240	92.9
	Shrub Dominant Tundra	0	0	0	0	0	0	0	0	0	0	9	0	1	23	6	**239**	278	86.0
	Total	100	1194	34	17	230	140	17	187	141	0	299	228	249	53	284	252		
	Producer's Accuracy (%)	73.0	100.0	91.2	94.1	85.2	94.3	17.7	74.9	73.8	N/A	61.9	83.0	89.6	3.8	78.5	94.8		

5.0. Discussion

Since there are very few known Arctic studies, such as this thesis, results regarding scattering behaviour and factors affecting it are compared to previous research in other applications such as agriculture and geology, as well as coastal studies in non-arctic regions, where appropriate.

5.1. Backscatter Characteristics of Arctic Land Cover Types

5.1.1. Sample Statistics,General Observations, and Trends

The increase in sensitivity to surface roughness observed at shallow angles is consistent with studies that have characterized the surface roughness of agricultural fields (Ziribi & Deschambre, 2002; Baghdadi et al., 2008a; Baghdadi et al., 2008b; Rahman et al., 2008), and distinguishing geological units by grain size (Paradella et al., 2009). As mentioned previously however, for the latter application there are also a number of studies that showed improved results at steep angles, specifically in the 22-27° range (Derion et al., 1997; Singhroy & Saint-Jean, 1999; Dong & Leblon, 2004). While this may be true for specific study areas and applications, better discrimination of a number of classes inlcuding Sand and Mixed Sediment, was observed in this analysis at shallow angles.

At steep incidence angles, HH and VV provided redundant information, especially for classes with smoother surfaces including: Water, Smooth/Un-Vegetated Mudflat, Rough/Vegetated Mudflat, Peat and Sand ($r_{HH\text{-}VV} > 0.85$). Thus, for these classes, there may be no benefit in acquiring more than one co-polarization at steep

angles, including possibly at higher spatial resolutions (e.g. 3 m Ultra-Fine and 1 m Spotlight mode Radarsat-2 imagery). These results are consistent with Sokol et al. (2004), who found HH and VV to be highly correlated (r = 0.99) at steep angles for bare agricultural fields.

5.1.2. Backscatter Consistency Between Study Areas and Incidence Angles

Inconsistencies in training data between study areas were observed for: Water, Peat, Wood/Substrate Mix, Woody Debris, Wetland and ILLT. For the Water class, this may be attributable to varying weather conditions at the time of acquisitions, since the scattering behaviour observed over water is highly dependent on surface roughness. Water has a high dielectric constant, which prevents much penetration, resulting in high surface scattering (Woodhouse, 2006). Higher wind speeds and greater wave action in one of the study areas may have produced increased surface roughness and backscatter (i.e., in the TH study area, since backscatter coefficients over Water were higher here). It is also of interest to note that VV was the most inconsistent between study areas of all polarizations, which is not surprising since it has been described as more sensitive to surface waves (Ulaby et al., 1986).

For all other classes differences in training data between study areas may be attributable to differences in moisture, roughness, or the size, orientation, and density of objects at the surface. Compared to Sand and Mixed Sediment for example, Peat, Wood/Substrate Mix and Woody Debris are made up of more water-absorptive materials, and since some precipitation was recorded prior to the acquisition of some images, this could partially explain observed differences. For the Peat class, higher backscatter

coefficients in the WP study area may also be attributable to the presence of low cliffs (< 1 m above average sea level), with steep faces (> 40°). These are adjacent to most of the peat shorelines in this area (Rampton, 1987a), which produced double bounce in some areas (as interpreted from Freeman-Durden decomposition parameters), which generally results in increased backscatter. These types of variations specifically, may contribute to classification errors when training data from one area is used to classify another.

Overall, results also indicated that a difference in incidence angle of 6 to 8° may not significantly affect the scattering behaviour observed for most classes. Classes that did show significant differences between shallow and medium angles, also showed inconsistencies between study areas, so their differences may also be attributable to additional factors, such as differences moisture. In contrast, backscatter consistency was observed at all angles for some classes which generally tended to have rougher surfaces (e.g., Shrub Dominant Tundra). This is sensible, since scattering from these surfaces is typically less dependent on incidence angle as it is more diffuse (Fung & Ulaby, 1983).

These results are consistent with Henderson and Lewis (2008), who suggested in a review of several studies, that the use of multiple incidence angles did not always improve classification results for rougher surfaces, as this only provided additional information for specular reflectors. Further work is needed to qualify this statement however, as in this study some dependency upon polarization was also observed for surface scatterers such as Smooth/Un-Vegetated Mudflat, since HV was nearly equal at all angles, whereas HH and VV showed incidence angle backscatter dependence.

Based on the above, for a number of the SCAT classes, there may be no benefit in acquiring multiple incidence angles for use as classifier inputs. This information is

important, as it may be helpful in cases where certain incidence angles are not available over a given region for the required acquisition period. This is a situation that commonly occurs when another user (perhaps with higher priority) selects a conflicting configuration over an adjacent site.

5.1.3. Assessment of Backscatter coefficients for Individual Classes and Potential for Feature Detection and Discrimination with Colour Composites

The better overall contrast in colour composites (with double bounce as red, volume scattering as green, and odd bounce as blue) between classes at shallow compared to steep angles may be explained by a number of factors. First, others have found that shallow angle provided better land-water discrimination, which they attributed to steep angle imagery being more sensitive to Bragg scattering as a result of surface waves (Toyra et al., 2001; Toyra & Pietroniro, 2005). Additionally, it is possible that differences in surface roughness are more important for distinguishing those classes for which shallow angle radar is more sensitive.

Anthropogenic

High backscatter coefficients observed over anthropogenic features can be attributed in some cases to objects acting as corner reflectors, resulting in waves being mostly directed back in the direction of the sensor. This explains why the orientation of features is of importance and could explain why lower backscatter was observed over buildings oriented closer to parallel to the radar line of sight. Metallic objects, which are likely present in these areas, are also good conductors. This prevents penetration and or absorption of incident waves, resulting in little energy being lost through surface

interaction (Woodhouse, 2006). Additionally, backscatter contributions can be from multiple sources, including double bounce from the sides of buildings, and single bounce interactions from roofs (Dong et al., 1997; Cloude & Pottier, 1997).

Water and Substrates

Over smooth surfaces, HH and VV contributions are near-equal at steep angles, while VV increasingly dominates, as angles become shallower (Dobson & Ulaby, 1998). This behaviour similarly observed in this study for a number of classes, including: Water, Smooth/Un-Vegetated Mudflat, Rough/Vegetated Mudflat, Peat and Sand. As such, it is likely that relative to the C-band wavelength these features were smooth, which explains why lower backscatter coefficients were typically observed for these classes (Peake & Oliver, 1971). This interpretation is also be consistent with results of the Freeman-Durden decomposition, which showed predominant odd bounce scattering over these classes, which is typically of smooth surfaces (Freeman & Durden, 1998).

In the case of dry sand, there is also some potential that low backscatter coefficients are also a result of significant signal attenuation. This is due to the ability of microwaves to penetrate dry sand, which decreases the amount of energy returned in the direction of the sensor. This may also explain why more volume scattering was observed over this class compared to others like Smooth/Un-Vegetated Mudflat. Some authors have also observed significant attenuation over wet sand (Williams & Greely, 2001; Williams & Greeley, 2004), while others have also observed higher VV return over sand compared to HH and HV (Hugenholtz & van der Sanden, 2001), as was the case in this study.

At steep angles the backscatter coefficients observed over Water increased

substantially, whereas values remained relatively low for other features with smooth surfaces (i.e., Smooth/Un-Vegetated Mudflat, Rough/Vegetated Mudflat, Peat and Sand). It is possible that this is due to greater sensitivity to Bragg scattering as a result of surface waves at these angles (Thompson et al., 1998; Pietroniro et al., 2005; Toyra et al, 2005). Since this has been shown to result in greater confusion between land and water, shallow angle imagery has been recommended for shoreline mapping. Toyra et al. (2001) for example, found greater contrast between land and water using Radarsat-1 standard mode imagery acquired at 47° compared to 24°. In this research however, some classes were better distinguished from Water at steep angles, including substrates with smoother surfaces, especially the most saturated and smooth mudflats. This is likely a product of specular reflection still being dominant over these surfaces, which are not periodically rough like surface waves on water. Baghdadi et al. (2004) also found mudflats were better distinguished from water at steep compared to shallow angles.

The increased backscatter observed over Peat, Rough/Vegetated Mudflat, Mixed Sediment, Riprap, Wood/Substrate Mix and Woody Debris (i.e., compared to Water, Smooth/Un-Vegetated Mudflat, Rough/Vegetated Mudflat, Peat and Sand), may be attributable to increased surface roughness. Not only were larger differences in backscatter observed at shallow compared to steep angles, the former of which are more sensitive to the effects of roughness, but there was also less of a difference between HH and VV contributions, which has been attributable to scattering from rough surfaces (Dobson & Ulaby, 1998).

It is important to note that a significant potential source of confusion between some substrate classes could be moisture content, which has been shown to reduce the

effects of roughness on backscatter (Jackson & O'Neill, 1985). This could explain why beaches located near the land-water interface that appeared saturated in helicopter videography were generally the most confused with Water. It could also explain why there was less contrast between classes in the WP study area at shallow and medium angles, since some precipitation was recorded prior to these acquisitions.

Overall, given the factors and interpretations described above, potential for reliable discrimination of individual substrate classes was very limited using backscatter coefficients alone, but strong potential was observed for distinguishing generally between rough and smooth substrate types.

Vegetated Classes

A number of vegetated classes appeared similar in colour composites, including: Wetland (WP study area only), Marsh, ILLT, Low Centre Polygons, High Centre Polygons, and in some cases Herb Dominant Tundra. This may be due to similarities in the density of vegetation, as well as the species present, which included mostly low lying herbs and grasses. As such, it is expected that contextual information may also be useful in discriminating these classes. For example, Marsh typically represented thin, linear features, located at the land-water interface along sand beaches.

The potential observed to discriminate between the classes listed above and Shrub Dominant Tundra may be attributable to increased volume and or multiple scattering. This interpretation is based on the higher contribution from HV, which is representative of increased wave depolarization, as a result of volume scattering and or multiple bounce interactions (Fung & Ulaby, 1983). The greater ability to distinguish between Shrub Dominant Tundra and those vegetated classes mentioned previously at shallow compared

to steep angles, may therefore be due to the longer path length incident microwaves are required to travel through the canopy, resulting in greater canopy interaction (Woodhouse, 2006).

Improved canopy penetration, and as a result, reduced canopy interaction at steep angles has been well demonstrated in agricultural applications. Bush and Ulaby (1978) showed that incidence angles should be less than 20° for characterisation of soil in crop covered areas. While the results of this research are consistent with these and other examples (Ulaby & Batlivala, 1976), it should also be noted that some authors have observed better characterization of crop canopies at steep angles. Jiao et al. (2011) for example, found steep angle (25°) Radarsat-2 imagery was more correlated to crop LAI than imagery acquired at 40°. While under some circumstances this may be true, better discrimination of these vegetation types was observed at shallow angles in this study.

Conversely, Wetland (TH study area) was better differentiated from other classes at steep angles, which is probably due to the greater sensitivity to moisture compared to shallow angles. This is consistent with results in other wetland studies (Brown et al., 1996), and is also consistent with a number of agricultural studies on soil moisture (Ulaby & Batlivala, 1976; Daughtry et al., 1991), which have generally shown improved results at steep compared to shallow angles. Some authors have also found good results at shallow angles, though this may be attributed to both longer wavelength SARs being used (e.g. L-band compared to C-band), which results in greater canopy penetration and interaction at the soil level, or in some cases may be because vegetation cover was sparse (Henderson & Lewis, 1996).

5.2. Polarimetric Signatures of Arctic Land Cover Types

5.2.1. Sample Statistics,General Observations, and Trends

Substantial variability in scattering behaviour was observed with polarimetric signatures for the majority of land cover classes. This includes substantial intra-class variability, which resulted in visually distinct responses depending on the site and sample size used to generate plots. This may be a product of image speckle as plots were generated from unfiltered, slant range imagery as required by the software (CCRS, 2011b). For this reason, the average response had to be determined through a comparison of several plots for the same land cover class to determine the typical scattering behaviour. Despite this, some potential was observed to discriminate generally between rough and smooth substrates, to identify anthropogenic features and to a lesser extent, to distinguish between some vegetated classes.

Co-polarized signatures were more useful overall than cross-polarized signatures, which has also been previously observed. Singhroy and Molch (2004) for example, found this to be the case for discrimination of various surficial materials, including: alluvium, marine sediments, and till, using fully polarimetric C-band airborne radar imagery over Ottawa, Canada. As mentioned previously however, in this analysis cross-polarized plots were also useful for identification of Anthropogenic and Wetland classes.

Increasing pedestal height with surface roughness, as observed in this analysis, has also been observed by some authors. Zebker and van Zyl (1991) found an increase in pedestal height with roughness from playas (RMS surface height ~1 cm), to alluvial surfaces (RMS surface height ~2.5 cm), to lava flows (RMS surface height ~4 cm) using airborne C-band imagery acquired at a 43° incidence angle. Similar observations were

made by Zebker et al. (1987) over lava fields in Idaho. Since an increase in pedestal height represents an increase in the amount of depolarized energy in the backscattered signal, it can be inferred that a class such as Mixed Sediment causes more wave depolarization compared to Sand, due to its greater surface roughness. Other authors that showed an increase in pedestal with roughness include van Zyl et al. (1989) and Ray et al. (1992), while McNairn et al. (2002) also showed pedestal height was sensitive to volume and or multiple scattering.

5.2.2. Consistency of Signatures Between Study Areas and Incidence Angles

Water and Wetland showed inconsistent scattering behaviour between study areas. Water specifically, showed an increased pedestal height in the WP study area at shallow angles which, similarly to the backscatter analysis, may be a result of increased surface roughness due to wind. Scattering behaviour for Wood/Substrate Mix and Woody Debris on the other hand, were consistent between study areas. In contrast to the observations made of backscatter coefficients, this indicates that while the observed signal power may vary, there is potential that microwave-surface interactions are still similar for these classes. For example, for the ILLT class scattering behaviour was highly variable for all images as well as for polarimetric signatures, even though the average signature looked relatively similar between study areas.

5.2.3 Assessment of Signatures for Individual Classes to Determine Scattering Mechanisms and Potential for Feature Detection and Discrimination

As with colour composites of backscatter coefficients, polarimetric signatures

generated at shallow angles showed more contrast between classes than those generated with steep angle imagery.

Anthropogenic

At shallow and medium angles, the co-polarized signatures generated for Anthropogenic were similar to theoretical responses produced for dihedral corner reflectors (van Zyl et al., 1987). van Zyl et al. (1987) also had similar responses over urban areas in San Francisco, using imagery acquired at a 45° incidence angle. The pedestal height they observed was also closer to the values observed in this analysis (~0.6), than that which was modelled for a perfect dihedral corner reflector at ~0.4. As shown in Appendix 6, pedestal height was useful for distinguishing this class from a number of others, because it was typically much higher. Based on this, it is anticipated that this parameter, when generated globally from shallow or medium angle imagery, could be a useful input for classification. At steep incidence angles however, pedestal heights for Anthropogenic were similar to other classes like Mixed Sediment.

The dominant double bounce scattering observed at shallow angles is commonly explained by incident waves striking the ground then the sides of houses, before being returned in the direction of the sensor, or vice versa (Henderson & Lewis, 1996). At steep angles, signatures were consistent with multiple and or volume scattering with peak contributions in HH and VV polarizations, as well as relatively high pedestal heights (van Zyl et al., 1987; Evans et al., 1988). This may be a product of the combined double bounce from the sides of buildings, as well as surface scattering from roofs.

Dong et al. (1997) showed similar responses to those of this analysis for urban areas in Australia using NASA/JPL AirSAR imagery acquired at 25 (near range) to 65°

(far range). They suggested that for houses oriented perpendicular to the radar line of sight, and when incidence angles were about 30° (or about the same degree as roofs are sloped from the horizontal) this produces a strong single bounce return as local incidence angles are effectively 0°. While the authors suggested that this made surface scattering the dominant scattering mechanism at steep angles, the shape of signatures and the higher pedestal height, are also consistent with multiple and or volume scattering (van Zyl et al., 1987).

Water and Substrates

Signatures produced for Water, Smooth/Un-Vegetated Mudflat, Rough/Vegetated Mudflat, and Sand were also similar to theoretical models of rough surface scatterers produced by van Zyl et al. (1987), particularly at shallow angles. At steep angles plots for Water could be interpreted as scattering from smooth, dielectric surfaces, since they showed near equal HH and VV contributions, and low pedestal heights (van Zyl et al., 1987). Signatures for these classes were also similar to those produced by Zebker and van Zyl (1991) over ocean waves, and playas, representing smooth surfaces. This was especially the case for signatures of this research produced from medium angle imagery, which were more comparable to the incidence angles used by the authors (~44°). Zebker and van Zyl also attributed the higher VV to HH component to possible rough surface scattering, as well as some potential Bragg scattering.

Hugenholtz and van der Sanden (2001) generated plots for a number of substrate types in the Bay of Fundy, Canada using airborne imagery acquired at shallow angles (60-67°). Their responses for water, mud, silty sand and gravel were similar to those generated in this analysis for Water, Smooth/Un-Vegetated Mudflat, Rough/Vegetated

Mudflat, and Sand, which they also interpreted as rough surface scatterers. Additionally, it was observed that the HH contribution tended to increase with roughness and or grain size, as it did in this analysis. Hugenholtz and van der Sanden (2001) also generated plots over bedrock, which were similar to that observed for Riprap, indicating dominant double bounce scattering, as was interpreted in this analysis (c.f. van Zyl et al., 1987).

Zebker and van Zyl (1991) also generated signatures over alluvial surfaces and lava flows that were similar to that observed in this analysis for Mixed Sediment. These surfaces had RMS surface heights between 2.5 and 4 cm, which are comparable to the dominant grain size of material observed in the Mixed Sediment class (i.e., pebbles: 0.4 to 6.4 cm in diameter). The ability to distinguish a number of different sediment types was also observed by Singhroy and Molch (2004) using shallow angle imagery (72°). They largely attributed differences in signatures to the effect of sediment texture on microwave-surface interactions.

While there are no known examples in the literature of polarimetric signatures generated for Woody Debris, it would be consistent with interpretations made for Anthropogenic to suggest that the dominant scattering mechanism observed over this class was also double bounce (van Zyl et al., 1987). As mentioned previously, it is also of interest to note that the response observed over Wood/Substrate Mix appeared to be a mixture of the response for Sand and for Woody Debris, which again may be expected since this class is a mixture of both land cover types.

Vegetated Classes

Responses for Marsh, ILLT, Low Centre Polygons and Eroding Tundra, while highly variable, could be interpreted similarly to the polarimetric signatures generated for

salt marsh/sand, and salt marsh/mud classes by Hugenholtz and van der Sanden (2001). Dominant multiple and or volume scattering from these classes may be expected due to the complex nature of objects at the surface, including: vertical vegetation, smooth water surfaces, exposed soil and or mud, all of which could have contributed to a mixture of scattering mechanisms. Despite this, some potential was observed for distinguishing Eroding Tundra from these classes due to a higher pedestal height.

This may be a product of differences in the vegetation present. Evans et al. (1988) for example, showed that pedestal height was sensitive to vegetation density, with NASA/JPL airborne SAR data acquired over Wind River Basin area, Wyoming. McNairn et al. (2002) showed similar results, with an increase in pedestal height with surface roughness, especially over vegetated areas. Differences between Eroding Tundra and other vegetated classes may also be due to differences in moisture as well as surface roughness, since this was often observed in the field. The response for Low Centre Polygons was indicative of dominant double bounce scattering. This is consistent with field observations of this class, which included elevated tundra, adjacent to low lying standing water. It is believed that scattering from the water to this blunt edge (and vice versa), resulted in double bounce scattering.

Double bounce was also observed over Wetland. Plots for this class were similar to those Li et al. (2011) generated over paddy rice fields during the growing season in southern China, using Radarsat-2 imagery acquired at 40°. The authors similarly interpreted that the shape of plots was indicative of dominant double bounce, since they were similar to theoretical models for dihedral reflectors (van Zyl et al., 1987). This was anticipated since rice plants represent vertical objects standing above water, where double

bounce contributions are believed to be from the water surface to the standing vegetation (or vice versa), then back in the direction of the sensor (Li et al., 2011). The authors also similarly observed two peaks in cross-polarized plots, corresponding to transmitted waves at 62 and 118° orientation angles in the linear polarization. As such, it may be expected that some standing water was present in the Wetland in the TH study area. This would also explain why signatures were comparable for Wetland in the WP study area, since standing water was also observed there.

5.3. Freeman-Durden Decomposition Characteristics of Arctic Land Cover Types

5.3.1. Sample Statistics,General Observations, and Trends

While training data for backscatter coefficients and Cloude-Pottier decomposition parameters were normally distributed in all cases, the same training data produced highly skewed and bimodal distributions for Freeman-Durden decomposition parameters. While Trudel et al. (2009) observed similar results over wet and dry snow using C and L-band airborne polarimetric data acquired at a 55°, there are few other examples available from the literature. This observation is important for future work, since these data may not be appropriate as inputs in parametric classifiers. Despite this, better visual contrast than colour composites of backscatter coefficients was observed between some classes, including: Wetland and Herb Dominant Tundra, and ILLT and Herb Dominant Tundra, and so it still may be beneficial to explore non-parametric classification methods to utilize these data.

In most cases, the scattering mechanism identified using polarimetric signatures was consistent with the dominant scattering mechanism derived from Freeman-Durden

decomposition parameters. This included dominant odd bounce scattering over most substrates and Water at all angles. Conversely, volume scattering was generally dominant over vegetated areas at shallow and medium angles, while some classes also showed dominant odd bounce at steep angles.

5.3.2. Consistency of Contribution to Total Power Between Study Areas and Incidence Angles for Odd Bounce, Double Bounce and Volume Scattering

Division of total power values into respective contributions from odd bounce, double bounce and volume scattering, resulted in less consistency between study areas for a given parameter compared to backscatter coefficients. This could be due to parameters being more sensitive to moisture, or differences in the density and orientation of objects at the surface, which may be expected since reflection symmetry is assumed (Freeman & Durden, 1998; Lee et al., 2004). For this reason, parameters are roll variant, meaning that different results may be achieved due to changes in the objects' geometry, with the respect to the radar line of sight (Lee et al., 2004).

This is a well-known limitation of the Freeman-Durden decomposition in urban areas, where the orientation of buildings largely affects whether dominant double bounce (typically observed with objects oriented close to perpendicular to the radar line of sight) or volume scattering (typically observed with objects oriented closer to parallel to the radar line of sight) is observed (Yamaguchi et al., 2005). This would also explain why values for a given class were still generally consistent between shallow and medium angles for the same study area, as the object orientation and look direction of the radar would remain constant, with the exception of the slight change in incidence angle. Based

on this, it may be reasonable to expect that these parameters would not perform well as inputs to broad scale classifiers.

5.3.3. Assessment of Freeman-Durden Decomposition Parameters for Individual Classes and Potential for Feature Detection and Discrimination with Colour Composites

As with backscatter coefficients and polarimetric signatures, more visual contrast between classes was observed at shallow angles than at steep.

Anthropogenic

The predominance of volume scattering over anthropogenic features may again be a product of their orientation with respect to the radar line of sight. Similar to backscatter coefficients, it was observed that when objects were oriented approximately perpendicular to the radar line of sight, greater double bounce was observed compared to when objects were oriented closer to parallel. This has been known to cause buildings to be identified as dominant volume scatterers, which can result in confusion between vegetation and urban areas (Yamaguchi et al., 2005; Yamaguchi et al., 2011).

Water and Substrates

For Water, volume scattering contributions were high at shallow angles. Polarimetric signatures for this class at shallow angles also indicated some element of Bragg scattering, which shows that the water was likely roughened by wave action. It should be noted that the odd bounce element of the Freeman-Durden decomposition is also modelled after a "first order" Bragg surface scatterer, which shows that the ocean

surface in this case could have been more randomly rough, as opposed to periodically rough (Freeman & Durden, 1998).

Odd bounce scattering contributions were dominant over substrates with smoother surfaces, including: Smooth/Un-Vegetated Mudflat, Rough/Vegetated Mudflat, Peat, and Sand, which is consistent with interpretations of backscatter coefficients and polarimetric signatures. Additionally, as incidence angle increased, odd bounce contributions increasingly dominated contributions to total power. Choe et al. (2011) also observed dominant odd bounce contributions over mud and sand flats using C-band Radarsat-2 data acquired around 36°, as well as with L-band ALOS data acquired around 23°. Dominant odd bounce was also observed over Wood/Substrate Mix and Woody Debris. For Woody Debris, this may be because logs were much larger than the wavelength of incident microwaves. Surface roughness would therefore be at a scale too large to be detected by this C-band radar (Peake & Oliver, 1971).

The increased double bounce observed over Peat in the WP study area, may be from incident waves striking the smooth water or peat and mud adjacent to elevated tundra areas, which in some areas produced a highly geometric shape in the form of micro-cliffs. For Mixed Sediment and Riprap both volume and odd bounce scattering were important contributors to total power. Since this is indicative of higher HV returns, there must be more wave depolarization occurring over these features compared to substrates with smoother surfaces (Lee et al., 2004).

Vegetated Classes

Most vegetated classes showed dominant volume scattering at steep angles and so were generally more difficult to differentiate. At shallow and medium angles however,

there was more visual contrast between a number of classes, which is consistent with observations of backscatter coefficients. Herb Dominant Tundra, for example, appeared blue-green in colour indicating that both volume and odd bounce contributions were high. This is consistent with observations by Lee et al. (2004), who found some vegetation showed dominant odd bounce scattering in their E-SAR imagery acquired over Oberpfaffenhofen, Germany, and their AIRSAR imagery acquired over San Francisco, California. They attributed this to the model for the volume scattering component being based on thin, cylindrical objects, distributed at random. While this may appropriately characterize coniferous species, it may not be appropriate for classifying the low lying herbaceous species present in these Arctic areas (Lee et al., 2004). Despite this, the higher odd bounce component improved the visual discrimination between Herb Dominant Tundra and a number of other classes, including: Wetland, Marsh, ILLT, Low Centre Polygons, and High Centre Polygons.

It was also observed for these classes, and especially for Wetland in the TH study area, that double bounce scattering was dominant in some areas. In the case of Wetland and Marsh, this could be attributed to some areas being composed of standing water with vertically oriented vegetation. This is a commonly used explanation for double bounce interactions that are typical of wetlands. Brisco et al. (2011) for example, observed an increase in the double bounce contribution for wetland vegetation found in standing water, compared to wetland vegetation found without standing water using airborne C-band data. Standing vertical vegetation could have also been present in some areas for ILLT, Low Centre Polygons and High Centre Polygons, but, as mentioned previously, it was observed in the field that these classes had a strong geometric shape including micro-

cliffs. In the case of tundra polygons for example, this is a product of ice wedge development (Rampton, 1988). As such, there is some potential that double bounce scattering was due to incident waves striking these flat, low-lying areas, then the margins of upland tundra, before being returned in the direction of the sensor.

5.4. Cloude-Pottier Decomposition (Entropy/Anisotropy/Alpha Parameters) Characteristics of Arctic Land Cover Types

5.4.1. Sample Statistics,General Observations, and Trends

The results of the Cloude-Pottier decomposition were less conclusive than those described previously for backscatter coefficients, polarimetric signatures and Freeman-Durden decomposition parameters. Pseudo colour images specifically were more difficult to interpret, due to a higher noise level, and overall there was less visual contrast between land cover types, including generally between land and water.

5.4.2. Consistency of Values Between Study Areas and Incidence Angles

As mentioned previously, Cloude-Pottier decomposition parameters showed greater consistency between study areas compared to backscatter coefficients and Freeman-Durden decomposition parameters, though less potential was observed for these data as classifier inputs because substantial overlap was observed between training data for a number of SCAT classes. This is likely to cause greater confusion between classes, compared to backscatter coefficients.

For a given study area, comparable Anisotropy values were observed at all angles, indicating that the relative contribution of the second and third scattering mechanism may

be less sensitive to differences in incidence angle and or moisture. Classes that proved exceptions to this included: Water, Smooth/Un-Vegetated Mudflat and Wetland (TH study area only). Conversely, values for entropy and alpha were significantly different between shallow and steep angles, indicating that both the degree of wave depolarization and or the number of scattering mechanisms, respectively, may be more sensitive to incidence angle, and moisture. Classes where entropy and alpha were consistent between shallow and steep angles were also generally those with rougher surfaces, including Shrub Dominant Tundra, and this is consistent with the backscatter coefficients.

Entropy

Unlike backscatter coefficients, polarimetric signatures and Freeman-Durden decomposition parameters, better overall visual contrast between classes was observed at steep compared to shallow angles. Unfortunately, there are no known articles in the literature for comparing decomposition parameters for different incidence angles, as well as for applying this decomposition method to many of the land cover types considered in this analysis.

At shallow and medium angles Water had higher entropy values than substrates with smooth surfaces, including: Smooth/Un-Vegetated Mudflat, Rough/Vegetated Mudflat and Sand. This indicates that greater signal depolarization and or potentially more than one scattering mechanism, was observed, which may be a result of wind induced surface roughness (Cloude & Pottier, 1997). As incidence angles steepened entropy values decreased substantially for Water and most other classes, with the exception of those with rougher surfaces like Shrub Dominant Tundra, for which entropy values remained relatively constant.

This indicates that for most of the classes considered here, less wave depolarization and or fewer scattering mechanisms are observed at steep compared to shallow angles (Cloude & Pottier, 1997). For vegetated classes this may be due to decreased path length, resulting in less canopy interaction, which can cause wave depolarization, volume and or multiple scattering (Woodhouse, 2006). Additionally, the greater sensitivity to roughness at shallow angles, resulting in greater wave depolarization and higher cross-pol backscatter, has also been attributed to increasing entropy with incidence angle (Hajnsek et al., 2003). Low entropy values over bare substrates, and increasing values with vegetation size have similarly been observed in the literature (Garestier et al., 2006).

Anisotropy

The little overall diversity in the Anisotropy parameter amongst classes indicates that there was a degree of consistency in the normalized difference between the magnitude of the second and third scattering mechanism. Some exceptions include: Wetland, ILLT at shallow and medium angles, and Water at steep angles, which all had relatively high anisotropy values. Little diversity in observed anisotropy has also been observed by others in the literature. Corcoran et al. (2011) for example, found this to be true for wetlands mapping using steep angle (28°) Radarsat-2 quad pol imagery acquired over Minnesota. The authors also observed high anisotropy values over water, which is consistent with this analysis.

Alpha

As with entropy and anisotropy, there was relatively little diversity in alpha values between most classes, with greater confusion generally observed at shallow and medium angles. In most cases, alpha increased with incidence angle, which is consistent with Hajnsek et al. (2003), who used laboratory measurements as well as L-band SAR data over bare soil. It is of interest to note that in general, the same scattering mechanisms inferred from alpha values were also identified using polarimetric signatures and Freeman-Durden decomposition parameters.

5.5. Assessment of the the Potential for Classification based on Feature-Space Segmentation using Entropy, Anisotropy and Alpha Parameters

Entropy (H) / alpha (α) Feature Space

A well-known limitation of the entropy-alpha segmentation, is that the physical boundaries proposed by Cloude and Pottier (1997) do not always coincide with the natural breaks of input data (Lee et al., 1999). This has been observed in this analysis as the majority of distributions generated from training data fell within multiple zones. As described by Cloude and Pottier (1997), selection of these boundaries was somewhat arbitrary, and at the time they were proposed it was also anticipated that a number of data and sensor parameters such as measurement noise floor would have an impact on their definition. These zones are still commonly used however, as they cannot be defined by the user in most of the currently available software (i.e., PolsarPro version 4.2.). The degree of overlap observed in this analysis however, was severe and so little improvement in results was anticipated even if natural breaks or new boundary definitions were used.

Entropy (H) / Anisotropy (A) Feature Space

Similar results were also observed with a similar segmentation of the entropy/anisotropy feature space. While some authors have shown potential for discrimination of surface roughness conditions (Cloude et al., 1999), it is clear from this analysis that backscatter coefficients provide more information, and more specifically, it does not appear that this or the entropy/alpha segmentation provide much, if any, additional information.

5.6. Assessment of the Potential to Classify Arctic Land Covers Using the Unsupervised Wishart Classifier

Improved classification results were observed with the Wishart-entropy/alpha and Wishart-entropy/anisotropy/alpha classifiers compared to the feature space segmentation. Potential was observed for classification of a number of general land cover types, which seemed primarily based on differences in surface roughness. Classifications also showed potential for generating water masks, though as incidence angle decreased, confusion between land and water increased, especially for substrates with smoother surfaces like Smooth/Un-Vegetated Mudflat and Sand. The opposite was observed with backscatter coefficients, where smoother substrates showed better contrast with water at steep angles, and so it is clear that there is some benefit in using all T3 matrix elements and not just backscatter coefficients. This is consistent with observations made by Lee et al. (1999) using L-band AIRSAR data acquired over San Francisco, California.

It should be noted again that a slight improvement in results was observed with the inclusion of the anisotropy parameter (i.e., in distinguishing Wetland and Shrub Dominant Tundra at shallow angles), though overall results were relatively consistent,

indicating that the majority of useful information lies in entropy and alpha parameters. As an example, there was still confusion observed between Water and substrates with smoother surfaces at steep angles.

5.7. Separability Analysis and Maximum Likelihood Classifications

Backscatter coefficients were superior to Cloude-Pottier decomposition parameters in terms of class separability. In fact, shallow angle HV alone performed better (BD = 1.13 and 1.07 for the TH and WP study areas, respectively) than all three Cloude-Pottier parameters combined at steep angles (BD = 1.06 and 0.96, for the TH and WP study areas, respectively). Results of the separability analysis were also consistent with visual interpretations of the data for both backscatter coefficients and Cloude-Pottier decomposition parameters.

Results of the separability analysis to determine the optimal single polarization were generally consistent with the literature. As an example, overall shallow HV provided the best separability between Water and most other classes, while in most cases, acceptable separability levels could be achieved using any polarization at shallow angles. This observation is consistent with Baghdadi et al. (2007) who assessed the impact of incidence angle and polarization on coastline mapping using C-band ASAR imagery acquired over Gabon in Central Africa, observing that angles larger than 30° are optimal for this application and that at these angles high separability could be achieved using any polarization. They also found that at steep angles HV provided substantially better results than HH and VV. This is consistent with observations made in this analysis, which showed that steep HH and VV were rarely better than steep HV for class discrimination.

Other authors have similarly observed improved land-water discrimination at shallow compared to steep angles (Toyra et al., 2001; Toyra & Pietroniro, 2005).

As described in the review section (2.3) a number of studies have shown that HH is the best polarization for detecting differences in roughness (Dong & Leblon, 2004; Holah et al., 2005). In this study, this was true for some cases, particularly in the TH study area, however shallow HV provided the highest separability between most class pairs that differed in roughness (e.g., Sand and Mixed Sediment in the WP study area). Since this polarization has been attributed to dominant sub-surface volume scattering, it is possible that differences in roughness as well as volume and or multiple scattering proportions are important for class discrimination (Blanchard & Rouse, 1980; Fung & Eom, 1981). This interpretation is consistent with results of the Freeman-Durden decomposition, which showed volume scattering contributions from Mixed Sediment were higher than for Sand.

In a number of cases steep angle (especially HV), provided optimal separability between Marsh, Wetland, ILLT, High Centre Polygons, and Low Centre Polygons, and a number of other mostly vegetated classes. This is relatively inconsistent with a number of observations in the literature, which have suggested that HH is optimal for wetland detection and or volumetric moisture characterization (Hess et al., 1990; Kasischke & Bourgeau-Chavez, 1997; Ramsey, 1998; Bourgeau-Chavez et al., 2001; Brisco et al., 2011).

This analysis has determined the polarization (HV) and incidence angle (shallow) which provided the greatest potential for accurate discrimination of the classes of interest. This is a significant contribution as it is often a difficult task to select optimal acquisition

parameters for specific applications and land cover types, such as those considered here, for which there is little information on in the current literature. However, overall, little classification potential was observed using just one polarization and incidence angle, as acceptable separabilities (BD > 1.5) were only achieved between some class pairs. The use of multiple polarized images (HH, HV and VV backscatter coefficients) improved class separability substantially, and this is also consistent with observations made by other authors (Henderson & Lewis 2008; Brisco et al., 2011).

5.8. Optimal Parameters in Maximum Likelihood Classification

Significantly improved classification results were observed using combined radar and optical data. As described in the introduction, this may be expected since both sources provide different, but complementary information. This has also been found in other studies (Toyra et al., 2001; Souza-Filho & Paradella, 2002; Dong & Leblon, 2004; Waske & Benediktsson, 2007).

6.0. Research Limitations and Recommendations

Image resolution with respect to shoreline width was a significant limitation in this analysis. This reduced the amount of available training and validation data, especially along beaches, which in some cases were less than 50 m wide. While fully polarimetric Radarsat-2 data are not currently available at higher spatial resolutions, it may be of value to assess the potential for using higher resolution single polarized data (i.e., ultra-fine Radarsat-2). While VV was useful in some cases for class discrimination, most of the time HH and HV were optimal. As such, it is recommended that ultra-fine imagery at

these polarizations be a focus. It should also be noted that speckle filtering probably resulted in a significant amount of class mixing in the case of small or narrow entities.

A number of classes showed inconsistencies between studies areas, which needs to be considered for future acquisitions. More specifically, users need to consider weather conditions during acquisitions as this may result in significantly different backscatter values, for certain classes. This is especially important with radar data due to its sensitivity to moisture. This along with image speckle, have been attributed to high image-to-image variability, even under constant acquisition parameters, which has the potential to decrease classification accuracy, especially in terms of extrapolating classifiers to other regions (Baghdadi et al., 2002; Lee & de Grandi, 1999).

It is recommended that future work focuses on assessing the potential of other classifiers developed specifically for polarimetric SAR data, including the unsupervised Wishart-Freeman-Durden decomposition (Lee et al., 2004), as well as the supervised Wishart classifier (Lee & Grunes, 1994). The former was not available at the time of writing this thesis (i.e., in PolsarPro version 4.2) and the latter is limited by the fact that the software used in this analysis also requires that classifications are applied to slant range imagery to preserve phase information. Since many of the shorelines in this area are thin, it would have been difficult to select training data without any earth surface reference, such as the 2004 ortho photos or the GPS field transect locations. As such, this method may only be reasonably applied to much larger and easily referenced features, such as the extensive mudflat west of Richards Island. Other non-parametric classifiers, such as Random Forests (Deschamps et al., 2012) have also been successfully applied to SAR data and should be explored further.

Additionally other parameters derived from optical and radar data, including pedestal height, also have the potential to improve classification accuracy and should be investigated further.

7.0. Conclusions

Overall, this research has shown that for the land cover types of the two arctic study areas, shallow incidence angle imagery is optimal, and that there is potential for using this imagery alone for general land-water discrimination, for discrimination of rough and smooth substrates, and for discrimination of wetlands. The following provides a summary of the major findings.

a) The effect of incidence angle on backscatter for a given land cover type can be significant when differences are larger than 15°, but generally not when differences are less than 6 to 8°.

b) The degree of spatial consistency of backscatter is dependent upon differences in moisture conditions, especially for materials that are absorptive and or subject to spatial or temporal changes in surface roughness, as was observed for Water.

c) Overall, Cloude-Pottier decomposition parameters were more spatially extendable, followed by backcatter values, then Freeman-Durden decomposition parameters.

d) For backscatter coefficients, shallow HV provided the best average class separability when only single polarizations were considered. Shallow angle images also provided the best average class separability when all polarizations (HH, HV and VV) were considered.

e) Conversely, Cloude-Pottier decomposition parameters showed signficiant noise, and greater confusion at shallow and medium angles, while parameters derived from steep angle images provided the best class separability. Even at steep angles though, separability values for Cloude-Pottier decomposition parameters were about the same as just one single polarization, indicating that no additional information to backscatter coefficients was provided.

f) Full use of the T3 matrix at shallow angles through the unsupervised Wishart-entropy/alpha and Wishart-entropy/anisotropy/alpha classifiers improved the discrimination between Water and a number of substrates with smoother surfaces which, when using backscatter coefficients alone was better at steep angles.

g) With shallow angle imagery, potential was observed for general land-water discrimination, as well as for discrimination of rough and smooth substrates, and for wetland detection.

h) Maximum Likelihood Classification of SPOT-4 data produced much higher accuracies than were achieved with the optimal radar data (shallow angle; all polarizations). However, some confusion (e.g., between Sand and Mixed Sediment) in the SPOT classification was improved by combining the SPOT and optimal radar data in classification, while the overall accuracy increased marginally.

These results will be used to inform the current literature, as well as future research conducted under the eSPACE project. More specifically, optimal acquisition parameters (incidence angle and polarization) have been defined, and will be considered for future acquisition planning, including the acquisition of higher resolution single and dual polarization Radarsat-2 imagery, over the same and new study areas. Similar processing techniques may also be applied to these data, including the use of a 7x7 window for speckle filtering. The use of backscatter coefficients specifically, as well as the fusion of radar and optical data, are also anticipated to be a major focus of future analyses, as this research has shown substantial potential for both.

References

Arzandeh, S., & Wang, J. (2002). Texture Evaluation of Radarsat Imagery for Wetland Mapping. *Canadian Journal of Remote Sensing*, 28 (5), 653-666.

Ashenhurst, A. R., & Hannon, S. J. (2007). Effects of Seismic Lines on the Abundance of Breeding Birds in the Kendall Island Bird Sanctuary, Northwest Territories, Canada. *Arctic*, 61 (2), 190–198.

Atlas, R. M. (1981). Microbial Degradation of Petroleum Hydrocarbon: an Environmental Perspective. *Microbiology*, 45 (1), 180-200.

Baghdadi, N., Bernier, M., Gauthier, R., & Neeson, I. (2001). Evaluation of C-band SAR Data for Wetlands Mapping. *International Journal of Remote Sensing*, 22 (1), 71-88.

Baghdadi, N., Cerdan, O., Ziribi, M., Auzet, V., Darboux, F., El Hajj, M., & Kheir, R. B. (2008 b). Operational Performance of Current Synthetic Aperture Radar Sensors in Mapping Soil Surface Characteristics in Agricultural Environments: Application to Hydrological and Erosion Modelling. *Hydrological Processes*, 22 (1), 9-20.

Baghdadi, N., Gratiot, N., Lefebvre, J. P., Oliverod, C., & Bourguignon, A. (2004). Coastline and Mudbank monitoring in French Guiana: Contributions of Radar and Optical Satellite Imagery. Canadian Journal of Remote Sensing, 30 (2), 109-122.

Baghdadi, N., King, C., Bourguignon, A., & Remond, A. (2002). Potential of ERS and Radarsat Data for Surface Roughness Monitoring over Bare Agricultural Fields: Application to Catchments in Northern France. *International Journal of Remote Sensing*, 23 (17), 3427-3442.

Baghdadi, N., Pedreros, R., Lenotre, N., Dewez, T., & Paganini, M. (2007). Impact of Polarization and Incidence of the ASAR Sensor on Coastline Mapping: Example of Gabon. *International Journal of Remote Sensing*, 28 (17), 3841-3849.

Baghdadi, N., Ziribi, M., Loumagne, C., Ansart, P., & Anguela, T. P. (2008 a). Analysis of TerraSAR-X Data and Their Sensitivity to Soil Surface Parameters over Bare Agricultural Fields. *Remote Sensing of Environment*, 112 (12), 4370-4379.

Bhattacharyya, A. (1943). On a Measure of Divergence Between Two Statistical Populations Defined by their Probability Distributions. *Bulletin of the Calcutta Mathematical Society*, 35, 99-109.

Billings, W. D., & Mooney, H. A. (1968). The Ecology of Arctic and Alpine Plants. *Biological Reviews of the Cambridge Philosophical Society*, 43 (4), 481-529.

Blanchard, A. J., & Rouse, J. W. (1980). Depolarization of Electromagnetic Waves Scattered from an Inhomogeneous Half Space Bounded by a Rough Surface. *Radio Science*, 15 (4), 773-779.

Bliss, L. C., Courtin, G. M., Pattie, d. L., Whitfield, D. W., & Widden, P. (1973). Arctic Tundra Ecosystems. *Annual Review of Ecology and Systematics*, (4), 359-399.

Born, M., & Wolf, E. (1999). Principles of Optics: Electromagnetic Theory of Propagation, Interference (7). Cambridge, UK: Cambridge University Press.

Bourgeau-Chavez, L. L., Kasischke, E. S., Brunzell, S. M., Mud, J. P., Smith, K. B., & Frick, A. L. (2001). Analysis of Space-Borne SAR Data for Wetland Mapping in Virginia Riparian Ecosystems. *International Journal of Remote Sensing*, 22 (18), 3665-3687.

Bourgeau-Chavez, L. L., Smith, K. B., Brunzell, S. M., Richardson, C. J., Romanowicz, E. A., & Kasischke, E. S. (2005). Remote Monitoring of Regional Scale Inundation Patterns and Hydroperiod in the Greater Everglades Using Synthetic Aperture Radar. *Wetlands*, 25 (1), 176-191.

Brisco, B., Kapfer, M., Hirose, T., Tedford, B., & Liu, J. (2011). Evaluation of C-band Polarization Diversity and Polarimetry for Wetland Mapping. *Canadian Journal of Remote Sensing*, 37(1), 82-92.

Brown, R., Brisco, B., D'Iorio, M., Prevost, C., Ryerson, R., & Singhroy, V. (1996). Radarsat Applications: Review of GlobeSAR Program. *Canadian Journal of Remote Sensing*, 22 (4), 404-419.

Bush, T. F., & Ulaby, F. T. (1978). An Evaluation of Radar as a Crop Classifier. *Remote Sensing of Environment*, 7 (1), 15-36.

Cameron, W. L. (1996). Simulated Polarimetric Signatures of Primitive Geometrical Shapes. *IEEE Transactions on Geoscience and Remote Sensing*, 34 (3), 793–803.

Carnaghan, M., & Goody, A. (2006). Canadian Arctic Sovereignty. Retrieved 2011, from Department of National Defence, Political and Social Affairs Division: http://www.parl.gc.ca/Content/LOP/researchpublications/prb0561-e.htm

Canadian Centre for Remote Sensing (CCRS). (2011a). Radar Polarimetry Tutorial. Retrieved 2011, from Canada Centre for Remote Sensing: http://www.ccrs.nrcan.gc.ca/resource/tutor/polarim/pdf/polarim_e.pdf

Canadian Centre for Remote Sensing (CCRS). (2011b). Polarimetric Work Station. The Canadian Centre for Remote Sensing.

Choe, B. H., Kim, D., Hwang, J., Oh, Y., & Moon, W. M. (2011). Oyster Reef Signature in Tidal Flats Detected by Multi-Frequency Polarimetric SAR Data. Geoscience and Remote Sensing Symposium (IGARSS) (pp. 3775-3778). Vancouver: IEEE International.

Cloude, S. R. (1985). Target Matrix Decomposition Theorems in Radar Scattering. *Electronic Letters*, 21 (1), 22-24.

Cloude, S. R., & Pottier, E. (1996). A Review of Target Decomposition Theorems in Radar Polarimetry. *IEEE Transactions on Geoscience and Remote Sensing*, 34 (2), 498-518.

Cloude, S. R., & Pottier, E. (1997). An Entropy Based Classification Scheme for Land Applications of Polarimetric SAR. *IEEE Transactions on Geoscience and Remote Sensing*, 35 (1), 68-78.

Cloude, S. R., Papathanassiou, K., & Hajnsek, I. (1999). An Eigenvector Method for the Extraction of Surface Parameters in Polarimetric SAR. SAR Workshop: CEOS Committee on Earth Observation Satellites; Working Group on Calibration and Validation. 450, pp. 693-698. Toulouse, France: European Space Agency.

Corcoran, J., Knight, J., Brisco, B., Kaya, S., Cull, A., & Murnagan, K. (2011). The Integration of Optical, Topographic, and Radar Data for Wetland Mapping in Northern Minnesota. *Canadian Journal of Remote Sensing*, 37 (5), 564-582.

Daily, M., Farr, T., Elachi, C., & Schaber, G. (1979). Geologic Interpretation from Composited Radar and Landsat Imagery. *Photogrammetric Engineering and Remote Sensing*, 45 (197), 1109-1116.

Dallimore, S. R., Wolfe, S. A., & Solomon, S. S. (1996). Influence of Ground Ice and Permafrost on Coastal Evolution, Richards Island, Beaufort Sea Coast, N.W.T. *Canadian Journal of Earth Sciences*, 33 (5), 664-675.

Daughtry, C. S., Ranson, K. T., & Biehl, L. L. (1991). C-Band Backscattering from Corn Canopies. *International Journal of Remote Sensing*, 12 (5), 1097-1109.

Derion, J. P., Company, A., & Simonin, A. (1997). An Empirical Model for Interpreting the Relationship between Backscattering and Arid Land Surface Roughness as Seen with the SAR. *IEEE Transactions on Geoscience and Remote Sensing*, 35 (1), 86-92.

Deschamps, B., McNairn, H., Shang, J., & Jiao, X. (2012). Towards Operational Radar-Only Crop Type Classification: Comparison of Traditional Decision Tree with a Random Forest Classifier. *Canadian Journal of Remote Sensing*, 38 (1), 60-68.

DF Dickens and Associates (2004). Advancing Oil Spill Response in Ice-Covered Waters. Cordova, Alaska: Prince William Sound Oil Spill Recovery Institute.

Dobson, M. C., & Ulaby, F. T. (1998). Mapping Soil Moisture Distribution with Imaging Radar. In F. M. Henderson, & A. J. Lewis, Principles and Applications of Imaging Radar, Manual of Remote Sensing (Vol. 2, pp. 407-433). New York: Wiley.

Dong, P., & Leblon, B. (2004). Rock Unit Discrimination on Landsat TM, SIR-C and Radarsat Images Using Spectral and Textural Information. *International Journal of Remote Sensing*, 25 (18), 3745-3768.

Dong, Y., Forster, B., & Ticehurst, C. (1997). Radar Backscatter Analysis for Urban Environments. *International Journal of Remote Sensing*, 18(6), 1351-1364.

Durden, S., Haddad, Z., Morrissey, L., & Livingston, G. (1996). Classification of Radar Imagery over Boreal Regions for Methane Exchange Studies. *International Journal of Remote Sensing*, 17 (6), 1267-1273.

Engeset, R. V., & Weydahl, D. J. (1998). Analysis of Glaciers and Geomorphology on Svalbard Using Multi-Temporal ERS-1 SAR Images. *IEEE Transactions on Geoscience and Remote Sensing*, 36 (6), 1879-1886.

Environment Canada (EC). (2010). National Climate Data and Information Archive. (Environment Canada) Retrieved August 2010, from http://www.climate.weatheroffice.gc.ca/advanceSearch/searchHistoricDataStations_e.html?searchType=stnProv&timeframe=1&lstProvince=NWT&StartYear=2010&EndYear=2011&optLimit=specDate&Month=8&Day=19&Year=2011&selRowPerPage=25&cmdProvSubmit=Search&startRow=51.

ESRI. (2010). ArcGIS10. Fundamentals of Panchromatic Sharpening.

Evans, D. L., Farr, T. G., Ford, J., Thompson, T., & Werner, C. (1986). Multi-Polarization Radar Images for Geological Mapping and Vegetation Discrimination. *IEEE Transactions on Geoscience and Remote Sensing*, GE-24 (2), 246-257.

Evans, D. L., Farr, T. G., van Zyl, J. J., & Zebker, H. (1988). Radar Polarimetry: Analysis Tools and Applications. *IEEE Transactions on Geoscience and Remote Sensing*, 26 (6), 774-789.

Ferro-Famil, L., Pottier, E., & Lee, J. S. (2002). Classification and Interpretation of Polarimetric SAR Data. International Geoscience and Remote Sensing Symposium (IGARSS). Toronto, Canada.

Ferro-Famil, L., Pottier, E., & Lee, J. S. (2003). Unsupervised Classification of Natural Scenes from Polarimetric Interferometric SAR Data. In C. H. Chen, Frontiers of Remote Sensing Information Processing. Toh Tuck, Singapore: World Scientific Publishing.

Fisheries and Oceans Canada (FOC). (2012). Tides, Currents and Water Levels. (Government of Canada) Retrieved September 2010, from http://www.waterlevels.gc.ca/eng/find/region/2.

Freeman, A., & Durden, S. L. (1998). A Three Component Scattering Model for Polarimetric SAR Data. *IEEE Transactions on Geoscience and Remote Sensing*, 36 (3), 963-973.

Fung, A. K., & Eom, H. J. (1981). Note on the Kirchoff Rough Surface Solution in Backscattering. *Radio Science*, 16 (3), 229-302.

Fung, A. K., & Ulaby, F. T. (1983). Matter-Energy Interaction in the Microwave Region. In R. N. Colwell, Manual of Remote Sensing (pp. 115-164). Bethesda, MD: American Society of Photogrammetry.

Garestier, F., Dubois-Fernandex, P., Dupuis, X., Paillou, P., & Hajnsek, I. (2006). PolInSAR Analysis of X-Band Data over Vegetated and Urban Areas. *IEEE Transactions on Geoscience and Remote Sensing*, 44 (2), 356-364.

Goodenough, G., Chen, H., Richardson, A., Cloude, S., Hong, W., & Li, Y. (2011). Mapping Fire Scars Using Radarsat-2 Polarimetric SAR Data. *Canadian Journal of Remote Sensing*, 37 (5), 500-509.

Gratto-Trevor, C. L. (1996). Use of Landsat TM Imagery in Determining Important Shorebird Habitat in the Outer Mackenzie Delta, Northwest Territories. *Arctic*, 49 (1), 11-22.

Grunsky, E. C. (2002). The Application of Principal Components Analysis to Multi-Beam Radarsat-1 Satellite Imagery: a Tool for Land Cover and Terrain Mapping. *Canadian Journal of Remote Sensing*, 28 (6), 758-769.

Hajnsek, I., Pottier, E., & Cloude, S. R. (2003). Inversion of Surface Parameters from Polarimetric SAR. *IEEE Transactions on Geoscience and Remote Sensing*, 41 (4), 727-744.

Hall-Atkinson, C., & Smith, L. C. (2001). Delineation of Delta Ecozones Using Interferometric SAR Phase Coherence, Mackenzie River Delta, N.W.T., Canada. *Remote Sensing of Environment*, 78 (3), 229-238.

Harper, J. (1990). Morphology of the Canadian Beaufort Sea Coast. *Marine Geology*, 91 (1-2), 75-91.

Harper, J. R. (1985). Beaufort Sea Physical Shore-Zone Analysis. Geological Survey of Canada (Open File).

Harper, J. R., Owens, E. H., & Wiseman, W. J. (1978). Arctic Beach Processes and the Thaw of Ice-Bonded Sediments in the Littoral Zone. Proceedings of the 3rd International Permafrost Conference, (pp. 195-199). Edmonton, Canada.

Henderson, F. M., & Lewis, A. (2008). Radar Detection of Wetland Ecosystems: a Review. *International Journal of Remote Sensing*, 29 (20), 5809-5835.

Henderson, F. M., & Lewis, A. J. (1996). Manual of Remote Sensing, Third Edition: Principles and Applications of Imaging Radar (Vol. 2). New York, NY: John Wiley & Sons.

Hequette, A., & Barnes, P. (1990). Coastal Retreat and Shoreface Profile Variations. *Marine Geology*, 91 (1-2), 113-132.

Hess, L., Melack, J., & Simonett, D. (1990). Radar Detection of Flooding Beneath the Forest Canopy: a Review. *International Journal of Remote Sensing*, 11 (7), 1313-1325.

Holah, N., Baghdadi, N., Ziribi, M., Bruand, A., & King, C. (2005). Potential of ASAR/ENVISAT for the Characterization of Soil Surface Parameters over Bare Agricultural Fields. *Remote Sensing of Environment*, 96 (1), 78-86.

Hugenholtz, C., & van der Sanden, J. (2001). Polarimetric SAR for Geomorphic Mapping in the Intertidal Zone, Minas Basin, Bay of Fundy, Nova Scotia. Natural Resources Canada, Canadian Centre for Remote Sensing (CCRS).

Huynen, J. (1965). Measurement of the Target Scattering Matrix. *IEEE Transactions on Geoscience and Remote Sensing*, 53 (8), 936-946.

Jackson, T. J., & O'Neill, P. E. (1985). Aircraft Scatterometer Observations of Soil Moisture on Rangeland Watersheds. *International Journal of Remote Sensing*, 6 (7), 1135-1152.

Jiao, X., McNairn, H., Shang, J., Pattey, E., Liu, J., & Champagne, C. (2011). The Sensitivity of RADARSAT-2 Polarimetric SAR Data to Corn and Soybean Leaf Area Index. *Canadian Journal of Remote Sensing*, 37 (1), 69-81.

Kandus, P., Karszenbaum, H., Pultz, T., Parmuchi, G., & Bava, J. (2001). Influence of Flood Conditions and Vegetation Status on the Radar Backscatter of Wetland Ecosystems. *Canadian Journal of Remote Sensing*, 27 (6), 651-662.

Kasischke, E., & Bourgeau-Chavez, L. (1997). Monitoring South Florida Wetlands Using ERS-1 SAR Imagery. *Photogrammetric Engineering and Remote Sensing*, 63 (3), 281-289.

Kasischke, E., Melack, J., & Dobson, M. (1997). The Use of Radars for Ecological Applications: a Review. *Remote Sensing of Environment*, 59 (2), 141–156.

Kennaugh, K. (1951). Effects of Type of Polarization on Echo Characteristics. The Ohio State University, Antenna Laboratory, Columbus, Ohio.

Kobayashi, N., & Atkan, D. (1986). Thermoerosion of Frozen Sediment under Wave Action. *ASCE Journal of Waterway, Port, Coastal and Ocean Division*, 112 (1), 140-158.

Laflamme, A., & Percy, R. (2003). Sensitivity Mapping - with Flare! An Internet Approach to Environmental Mapping. International Oil Spill Conference. Publication No. 14730B. Washington, United States: American Petroleum Institute.

Lamarche, A., Owens, E. H., Martin, V., & Laforest, S. (2003). Combining Pre-Spill Shoreline Segmentation Data and Shoreline Assessment Tools to Support Early Response Management and Planning, Technical Seminar. Proceedings of the Twenty-Sixth Arctic and Marine Oilspill Programme (AMOP) (pp. 219-231). Ottawa, Canada: Environment Canada.

Lamarche, A., Sergy, G. A., & Owens, E. H. (2007). Shoreline Cleanup and Assessment Technique (SCAT) Data Management Manual. Emergencies Science and Technology division, Science and Technology Branch. Ottawa, Canada: Environment Canada.

Lantuit, H., & Pollard, W. H. (2008). Fifty Years of Coastal Erosion and Retrogressive Thaw Slump Activity on Herschel Island, Southern Beaufort Sea, Yukon Territory, Canada. *Geomorphology*, 95 (1-2), 84-102.

Lee, J. S., & de Grandi, G. (1999). Polarimetric SAR Speckle Filtering and its Implication for Classification. *IEEE transactions on Geoscience and Remote Sensing*, 37 (5), 2363-2373.

Lee, J. S., & Grunes, M. R. (1994). Classification of Multi-Look Polarimetric SAR Data Based on Complex Wishart Distribution. *International Journal of Remote Sensing*, 15 (11), 2299-2311.

Lee, J. S., & Pottier, E. (2009). Polarimetric Radar Imaging: from Basics to Applications. Boca Raton, United States: Taylor & Francis Group.

Lee, J. S., & Pottier, E. (2009). PolSAR Terrain and Land-Use Classification. In Polarimetric Radar Imaging: from Basics to Applications (pp. 265-300). Boca Raton, United States: Taylor and Francis Group.

Lee, J. S., Grunes, M. E., Pottier, E., & Ferro-Famil, L. (2004). Unsupervised Terrain Classification Preserving Polarimetric Scattering Characteristics. *IEEE Transactions on Geoscience and Remote Sensing*, 42 (4), 722-731.

Lee, J. S., Grunes, M. R., Ainsworth, T. L., Du, L. J., Schuler, D. L., & Cloude, S. R. (1999). Unsupervised Classification Using Polarimetric Decomposition and the Complex Wishart Classifier. *IEEE Transactions on Geoscience and Remote Sensing*, 37 (5), 2249-2258.

Li, K., Zhang, F., Shao, Y., Cai, A., Yuan, J., & R., T. (2011). Polarization Signature Analysis of Paddy Rice in Southern China. *Canadian Journal of Remote Sensing*, 37 (1), 122-135.

Li, S., Guritz, R., Logan, T., Shingle, M., Groves, J., Olmsted, C., Carsey, F., Macmahon, J. (1999). Summer Environmental Mapping Potential of a Large-Scale ERS-1

SAR Mosaic of the State of Alaska. *International Journal of Remote Sensing*, 20 (2), 387-401.

Lillesand, T. M., Kiefer, R. W., & Chipman, J. W. (2004). Remote Sensing and Image Interpretation 5th Edition. New Jersey: Wiley and Sons.

Lopez-Martinez, C., Ferro-Famil, L., & Pottier, E. (2005). PolsarPRO Version 4.2. Tutorial. Do it Yourself: Speckle Filtering.

Mackenzie, J. S., & Ringrose, P. S. (1986). Use of SEASAT SAR Imagery for Geological Mapping in a Volcanic Terrain: Askja Caldera, Iceland. *International Journal of Remote Sensing*, 7 (2), 181-194.

Madhavan, B. B., Venkataraman, G., Mohan, B. K., & Shah, S. D. (1999). Airborne SAR and IRS-1A LISS II Data Interpretation of Coastal Geomorphology in Godavari Delta, India. *Geocarto International*, 14 (2), 52-61.

McNairn, H., Duguay, C., Brisco, B., & Pultz, T. J. (2002). The Effect of Soil and Crop Residue Characteristics on Polarimetric Radar Response. *Remote Sensing of Environment*, 80 (2), 308-320.

McNairn, H., Shang, J., Jiao, X., & Champagne, C. (2009). The Contribution of ALOS PALSAR Multi-Polarization and Polarimetric Data to Crop Classification. *IEEE Transactions on Geoscience and Remote Sensing*, 47 (12), 3981-3992.

MDA, M. D. (2011). Radarsat-2 Product Format Definition. Retrieved from http://gs.mdacorporation.com/includes/documents/RN-RP-51-2713%20RS-2%20Product%20Format%20Definition_1_10.pdf

Morrison, R. I. (1997). The Use of Remote Sensing to Evaluate Shorebird Habitats and Populations on Prince Charles Island, Foxe Basin, Canada. *Arctic*, 50 (1), 55–75.

Morrissey, L., Durden, S., Livingston, G., Stearn, J., & Guild, L. (1996). Differentiating Methane Source Areas in Arctic Environments with Multi-Temporal ERS-1 SAR Data. *IEEE Transaction of Geoscience and Remote Sensing*, 34 (3), 667-672.

Morrissey, L., Livingston, G., & Durden, S. (1994). Use of SAR in Regional Methane Exchange Studies. *International Journal of Remote Sensing*, 15 (6), 1337-1342.

Mueller-Dombois, D., & Ellenberg, H. (1974). Aims and Methods of Vegetation Ecology. New York, United States: Wiley.

Owens, E. (2010). Primary Shoreline Types of the Canadian North. Environment Canada, National Wildlife Research Centre.

Owens, E. H. (1983). The Application of Videotape Recording (VTR) Techniques for Coastal Studies. *Shore and Beach*, 51 (1), 29-33.

Owens, E. H., & Sergy, G. A. (1994). Field Guide to the Documentation and Description of Oiled Shorelines. Edmonton, AB: Environment Canada.

Owens, E. H., & Sergy, G. A. (2000). The SCAT Manual - a Field Guide to the Documentation and Description of Oiled Shorelines (Second Edition). Edmonton, AB: Environment Canada.

Owens, E. H., & Sergy, G. A. (2004). The Arctic SCAT Manual: a Field Guide to the Documentation and Description of Oiled Shorelines in Arctic Regions. Edmonton, AB: Environment Canada.

Paradella, W. R., Silva, A. Q., Knust, S. S., Rabelo, T. N., Santos, A. R., Renno, C. D., Rodrigues, T. G. (2009). Effect of Microtopography on Radarsat-1 and Palsar Backscattering from Rock Alteration Products in the Curaca Valley, Brazil. *Canadian Journal of Remote Sensing*, 35(2), 262-269.

PCI Geomatica (2003). PCI Geomatica OrthoEngine User Guide: Understanding the Polynomial Math Model.

Peake, W., & Oliver, T. (1971). The Response of Terrestrial Surface at Microwave Frequencies. Columbus, United States: Ohio State University Columbus Electroscience Lab, Defense Technical Information Center.

Percy, R. J., LeBlanc, S. R., & Owens, E. H. (1997). An Integrated Approach to Shoreline Mapping for Spill Response Planning in Canada. Proceedings of the International Oil Spill Conference. 4651, pp. 277-288. Washington, United States: American Petroleum Institute.

Pietroniro, A., Toyra, J., Leconte, R., & Kite, G. (2005). Remote Sensing of Surface Water and Soil Moisture. In c. R. Duguay, & A. Pietroniro, Remote Sensing in Northern Hydrology: Measuring Environmental Change (pp. 119-142). Washington, United States: American Geophysical Union.

Rahman, M. M., Moran, M. S., Thoma, D. P., Collins, C. D., Jackson, T., Orr, B. J., & Tischler, M. (2008). Mapping Surface Roughness and Soil Moisture Using Multi-Angle Radar Imagery Without Ancillary Data. *Remote Sensing of Environment*, 112 (2), 391-402.

Rampton. V. N. (1982). Quaternary Geology Yukon Plain, Yukon Territory-Northwest Territories, Canada. Geological Survey of Canada (GSC) Bulletin.

Rampton, V. N. (1987a). Surficial Geology of the Mackenzie Delta. In Geological Survey of Canada (GSC), Marine Science Atlas of the Beaufort Sea: Geology and Geophysics. Ottawa, Canada: Minister of Supply and Services Canada.

Rampton, V. N. (1987b). Surficial Geology of the Tuktoyaktuk Peninsula. In Geological Survey of Canada (GSC), Marine Science Atlas of the Beaufort Sea. Ottawa: Minister of Supply and Services Canada.

Rampton, V. N. (1988). Quaternary Geology of the Tuktoyaktuk Coastlands, Northwest Territories, Memoir 423. Geological Survey of Canada (GSC).

Ramsey, E. I. (1998). Radar Remote Sensing of Wetlands. In R. Lunetta, & C. Elvidge (Eds.), Remote Sensing Change Detection: Environmental Monitoring Methods and Applications (pp. 211-243). Chelsea, United States: Ann Arbor Press.

Ray, T. W., Farr, T. G., & van Zyl, J. J. (1992). Polarization Signatures for Abandoned Agricultural Fields in the Manix Basin Area of the Mojave Desert: Can Polariemtric SAR Detect Desertification? Proceedings of the International Geoscience and Remote Sensing Symposium (IGARSS) (pp. 947-949). Houston: Geoscience and Remote Sensing Society.

Ricchetti, E. (2001). Visible-infrared and Radar Imagery Fusion for Geological Application: a New Approach Using DEM and Sun-Illumination Model. *International Journal of Remote Sensing*, 22 (11), 2219-2230.

Richards, J. A. (1994). Remote Sensing Digital Image Analysis: an Introduction. New York, United States: Springer-Verlag.

Sabins, F. (1984). Geological Mapping of Death Valley from Thematic Mapper Thermal Infrared, and Radar Images. Proceedings Third Thematic Conference. Ann Arbor, United States: Environmental Research Institute of Michigan.

Schmullius, C., & Evans, D. (1997). Synthetic Aperture Radar (SAR) Frequency and Polarization Requirements for Applications in Ecology, Geology, Hydrology and Oceanography: a Tabular Status Quo after SIR-C/X-SAR. *International Journal of Remote Sensing*, 18 (13), 2713-2722.

Simard, J., Degrandi, G., Saatchi, S., & Mayaux, P. (2002). Mapping Tropical Coastal Vegetation Using JERS-1 and ERS-1 Radar Data with a Decision Tree Classifier. *International Journal of Remote Sensing*, 23 (7), 1461-1474.

Singhroy, V., & Molch, K. (2004). Geological Case Studies Related to Radarsat-2. *Canadian Journal of Remote Sensing*, 30 (6), 893-902.

Singhroy, V., & Saint-Jean, R. (1999). Effects of Relief on the Selection of Radarsat-1 Incidence Angle for Geological Applications. *Canadian Journal of Remote Sensing*, 25 (3), 211-217.

Sletten, M. A., & Mc Laughlin, D. J. (2005). Radar Polarimetry. In K. Chang (Ed.), Encyclopedia of RF and Microwave Engineering: Volume 3 (pp. 4080-4095). Hoboken, United States: John Wiley & Sons.

Smith, A. M., & Buckley, J. R. (2011). Investigating RADARSAT-2 as a Tool for Monitoring Grassland in Western Canada. *Canadian Journal of Remote Sensing*, 37 (1), 93-102.

Sokol, J., McNairn, H., & Pultz, T. J. (2004). Case Studies Demonstrating the Hydrological Applications of C-Band Multi-Polarized and Polarimetric SAR. *Canadian Journal of Remote Sensing*, 30 (3), 470-483.

Solomon, S. M. (2005). Spatial and Temporal Variability of Shoreline Change in the Beaufort-Mackenzie Region, Northwest Territories, Canada. *Geo-Marine Letters*, 25 (2-3), 127–137.

Souza-Filho, P. W., & Paradella, W. (2002). Recognition of the Main Geobotanical Features along the Bragança Mangrove Coast (Brazilian Amazon Region) from Landsat TM and RADARSAT-1 Data. *Wetlands Ecology and Management*, 10 (2), 123–132.

Souza-Filho, P. W., Goncalves, F. D., Rodrigues, S. W., Costa, F. R., & Miranda, F. P. (2009). Multi-Sensor Data Fusion for Geomorphological and Environmental Sensitivity Index Mapping in the Amazonian, Mangrove Coast, Brazil. *Journal of Coastal Research*, 56, 1592-1596.

Trillium Engineering and Hydrographs (THE) Inc. (1997). Tuktoyaktuk Erosion Control Using Monolithic Concrete Slabs. Tuktoyaktuk, NWT.

Teruiya, R. K., Paradella, W. R., Dos Santos, A. R., Dall'Agnol, R., & Veneziani, P. (2008). Integrating Airborne SAR, Landsat TM and Airborne Geophysics Data for Improving Geological Mapping in the Amazon Region: the Cigano Granite,

Carajas Province, Brazil. *International Journal of Remote Sensing*, 29 (13), 3957-3974.

Thompson, D. R., Elfouhaily, T. M., & Chapron, B. (1998). Polarization Ratio for Microwave Backscattering from the Ocean Surface at Low to Moderate Incidence Angles. *IEEE Transactions on Geoscience and Remote Sensing*, 3, 1671-1673.

Touzi, R., & Lopes, A. (1994). The Principle of Speckle Filtering in Polarimetric SAR Imagery. *IEEE Transactions on Geoscience and Remote Sensing*, 32 (5), 1110-1114.

Touzi, R., Boerner, W. M., Lee, J. S., & Lueneburg, E. (2004). A Review of Polarimetry in the Context of Synthetic Aperture Radar: Concepts and Information Extraction. *Canadian Journal of Remote Sensing*, 30 (3), 380-407.

Toyra, J., & Pietroniro, A. (2005). Towards Operational Monitoring of a Northern Wetland Using Geomatics-Based Techniques. *Remote Sensing of Environment*, 97 (2), 174-191.

Toyra, J., Pietroniro, A., & Martz, L. (2001). Multi-Sensor Hydrologic Assessment of Freshwater Wetland. *Remote Sensing of Environment*, 75 (2), 162-173.

Trevett, J. W. (1986). Imaging Radar for Resources Surveys. New York, United States: Chapman and Hall.

Trudel, M., Magagi, R., & Granberg, H. (2009). Application of Target Decomposition Theorems over Snow-Covered Forested Areas. *IEEE Transactions on Geoscience and Remote Sensing*, 47 (2), 508-512.

Ulaby, F. T., & Batlivala, P. P. (1976). Optimum Radar Parameters for Mapping Soil Moisture. *IEEE Transactions on Geoscience and Remote Sensing*, 14 (2), 81-93.

Ulaby, F. T., Held, D., Donson, M. C., McDonald, K. C., & Senior, T. B. (1987). Relating Polarization Phase Difference of SAR Signals to Scene Properties. *IEEE Transactions on Geoscience and Remote Sensing*, GE-25 (1), 83-92.

Ulaby, F. T., Moore, R. K., & Fung, A. K. (1986). Microwave Remote Sensing, Active and Passive. In Volume Scattering and Emission Theory- Advanced Systems and Applications (Vol. 3). Dedham, United States: Artech House, Inc.

van Zyl, J. J. (1989). Unsupervised Classification of Scattering Behaviour Using Radar Polarimetry Data. *IEEE Transactions on Geoscience and Remote Sensing*, 27 (1), 36-45.

van Zyl, J. J., Zebker, H. A., & Elachi, C. (1987). Imaging Radar Polarization Signatures: Theory and Observation. *Radio Science*, 22 (4), 529-543.

Wang, J., Shang, J., Brisco, B., & Brown, R. (1998). Evaluation of Multidate ERS-1 and Multispectral Landsat Imagery for Wetland Detection in Southern Ontario. *Canadian Journal of Remote Sensing*, 24 (1), 60-68.

Waske, B., & Benediktsson, J. A. (2007). Fusion of Support Vector Machines for Classification of Multisensor Data. *IEEE Transactions on Geoscience and Remote Sensing*, 45 (12), 3858-3866.

Weeks, R., Smith, M., Pak, K., & Gillespie, A. (1997). Inversion of SIR-C and AIRSAR Data for the Roughness of Geological Surfaces. Remote Sensing of Environment, 59 (2), 383-496.

Williams, K. K., & Greeley, R. (2004). Laboratory and Field Measurements of the Modification of Radar Backscatter by Sand. *Remote Sensing of Environment*, 89 (1), 29-40.

Williams, K. K., & Greely, R. (2001). Radar Attenuation by Sand: Laboratory Measurements of Radar Transmission. *IEEE Transactions on Geoscience and Remote Sensing*, 39 (11), 2521-2526.

Woodhouse, I. H. (2006). Introduction to Microwave Remote Sensing. Boca Raton, United States: Taylor and Francis Group.

Yamaguchi, Y., Moriyama, T., Ishido, M., & Tamada, H. (2005). Four-Component Scattering Model for Polarimetric SAR Image Decomposition. *IEEE Transactions on Geoscience and Remote Sensing*, 43 (8), 1699-1706.

Yamaguchi, Y., Sato, A., Boerner, W. M., Sato, R., & Yamada, H. (2011). Four-Component Scattering Power Decomposition with Rotation of Coherency Matrix. *IEEE Transactions on Geoscience and Remote Sensing*, 49 (6), 2251-2258.

Yonezawa, C., Negishi, M., Azuma, K., Watanabes, M., Ishitsuka, N., Ogawa, S., & Saito, G. (2012). Growth Monitoring and Classification of Rice Fields Using Multitemporal RADARSAT-2 Full-Polarimetric Data. *International Journal of Remote Sensing*, 33 (18), 5696-5711.

Zebker, H. A., & van Zyl, J. J. (1991). Imaging Radar Polarimetry: a Review. *Proceedings of the IEEE*, 79 (11), 1583-1606.

Zebker, H. A., van Zyl, J. J., & Held, D. N. (1987). Imaging Radar Polarimetry from Wave Synthesis. *Journal of Geophysical Research*, 92 (B1), 683-701.

Ziribi, M., & Deschambre, M. (2002). A New Empirical Model to Retrieve Soil Moisture and Roughness from C-Band Radar Data. *Remote Sensing of Environment*, 84 (1), 42-52.

Appendix 1.

Land cover class descriptions and snapshots from 2010 helicopter videography.

Anthropogenic

Anthropogenic features are located primarily in the Hamlet of Tuktoyaktuk and for the purpose of this research, included features such as docks, houses and other structures along the coast and in the backshore (Figure 35). These features are impermeable to oil and so are considered less sensitive compared to other shorelines (Owens, 2010). This class remains important for contingency planning however, as these features provide access and staging grounds, which are uncommon along Arctic shorelines.

Peat Shorelines

Two types of peat shorelines are present in the study areas, including peat slurries and peat mats. In the WP study area the latter are more common, and form mostly at the base of low peat scarps along the low islands in the southwest. Both types are present in the TH study area, though peat mats are also more common there. These are typically a brownish colour due to a significant mud component; where peat slurries are mostly black (Figure 35). In the region tundra cliffs are one of the greatest contributors of peat, and these shoreline types are typically less than 20 m wide (Owens, 1998).

Smooth/Un-Vegetated Mudflats

In the WP study area mud tidal flats are more numerous and extensive than those found in the TH study area. They are mostly composed of mud, with some

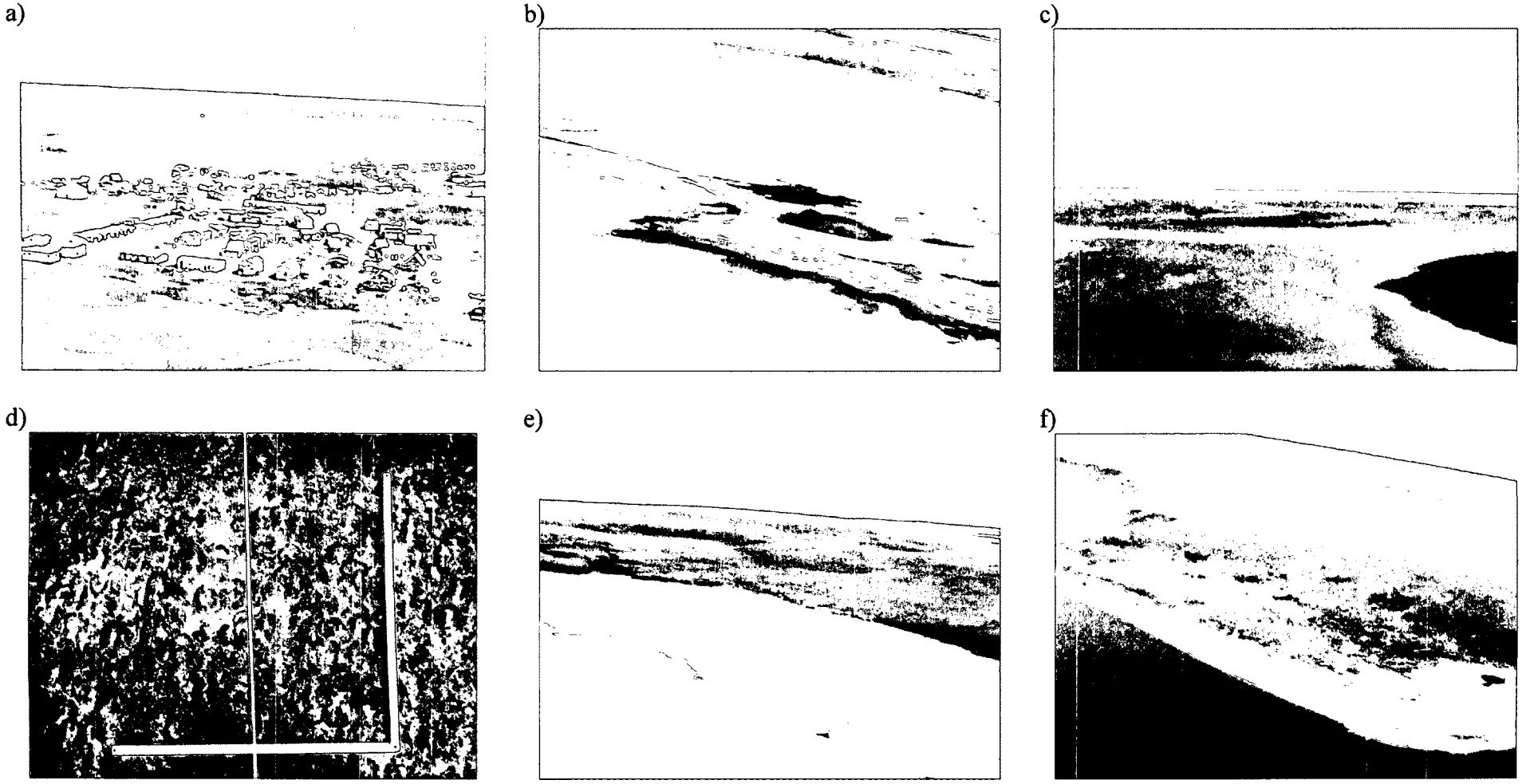

Figure 35: Snapshots from helicopter videography acquired in 2010, and one ground photo of the various land cover classes described, including of the Anthropogenic class (a), both types of peat shorelines, including a peat mat in the foreground and a peat slurry in the background (b), a Smooth/Un-Vegetated Mudflat (c), a ground photo of the Rough/Vegetated Mudflat (d), a sand beach representing the Sand class, and a Mixed Sediment beach (f).

sand, and peat in some areas and can be tens of kilometres wide. In the TH study area these features exist only in sheltered and isolated areas and typically contain more sand (Figure 35).

Rough/Vegetated Mudflats

In the WP study area mud tidal flats that were roughened by caribou tracks and or a sparse vegetation cover showed a unique signature in radar imagery compared to those that were smooth and un-vegetated (Figure 35). Where the former was bright and textured, the latter was darker and had a smooth image texture. For this reason, these classes were distinguished in this analysis.

Sand Beaches/Flats

For the purpose of shoreline sensitivity mapping it is desirable to map both beaches and flats. In the SCAT classification system these features are largely differentiated on the basis of local slope (beaches > 5 ° and flats < 5 °), which was not discernible with available Radarsat-2 imagery (Owens, 2010). The focus of this analysis was therefore to identify sandy material in general. This class (hereafter called Sand), also represents relatively narrow (typically < 50 m) shorelines, common in both study areas, especially along the base of cliffs and low sloping tundra. In the WP study area these features were predominately located on the west side of Richards Island (Figure 35), and in the TH study area, these features were mostly north of Tuktoyaktuk.

Mixed Sediment Beaches/Flats

For the same reasons provided above, no attempt was made to discern mixed sediment beaches and mixed sediment flats. In the WP study area, mixed sediment

beaches/flats (hereafter called Mixed Sediment) are mostly located within the bay south of West Point, whereas in the TH study area the majority of shorelines south of Tuktoyaktuk and within Tuktoyaktuk Harbour contain mixed sediment (Figure 35). In both study areas these shoreline types are also typically less than 50 m wide.

Riprap

Riprap is present in the Hamlet of Tuktoyaktuk on the western side of the spit adjacent to the entrance of Tuktoyaktuk Harbour (Figure 36). It was constructed in 1998 and is composed of limestone boulders 0.25 to 1 m in diameter, with boulder size generally decreasing landward (TEH, 1997). As this is a human-made feature this class is uncommon throughout the region, but is again sensitive to the effects of oil due to its high porosity (Owens, 2010).

Wood/Substrate Mix

The Wood/Substrate Mix class represents sand or mixed sediment beaches and or flats, where woody debris covers up to 50% of the area (Figure 36). In large part this class was distinguished from the Woody Debris class (described subsequently), and other substrates because of the unique signature observed in Radarsat-2 images. Wood/Substrate Mix is not currently a class used in shoreline sensitivity mapping; however the amount of debris present is typically noted on maps and atlases. In this research an attempt was made to assess the potential for discerning these features. There is at least some woody debris present along nearly every segment of shoreline in both study areas, with the exception of the bay south of West Point.

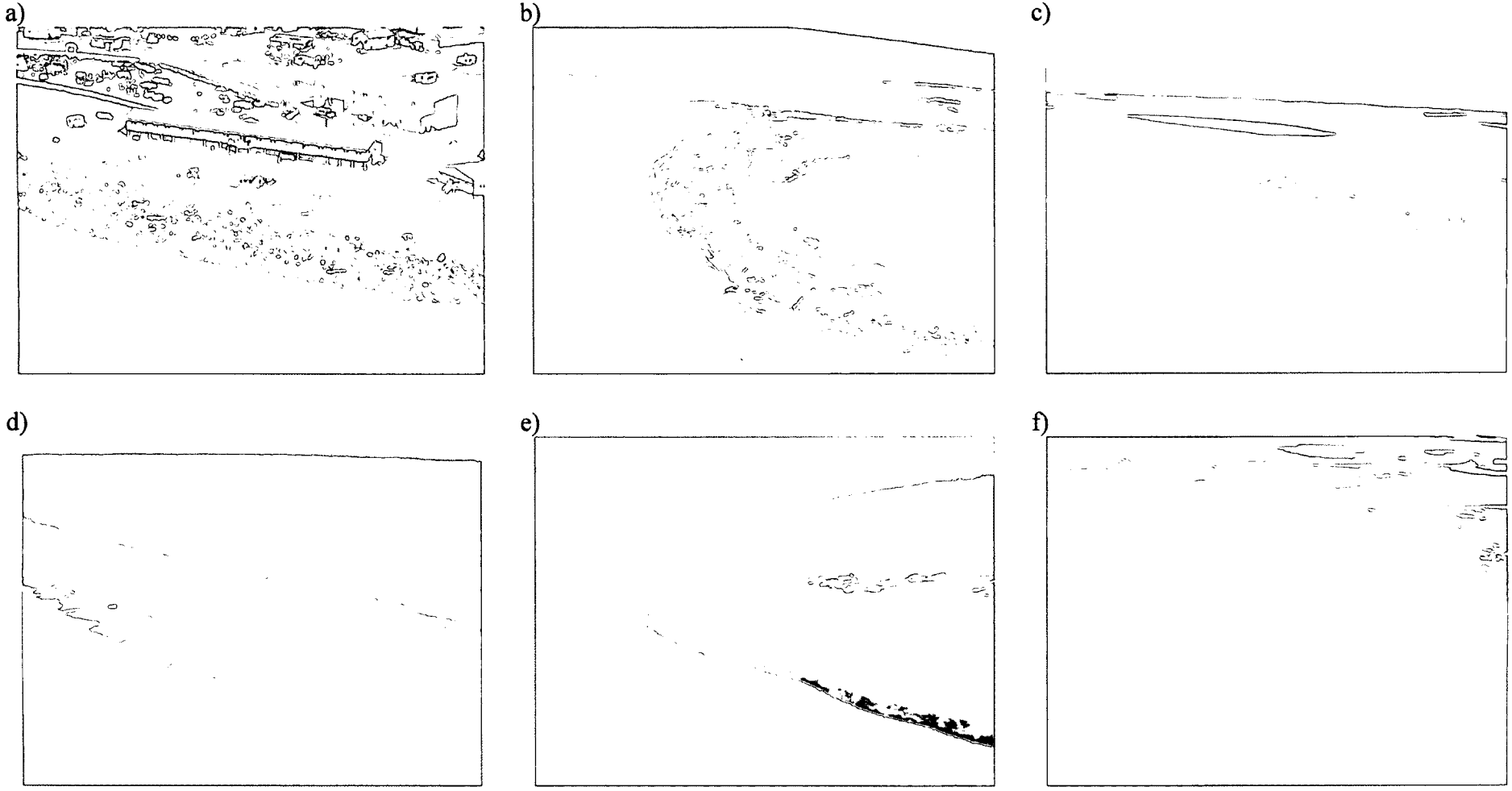

Figure 36: Snapshots from helicopter videography acquired in 2010 of the various land cover classes described, including of the Riprap class from the TH study area (a), the Wood/Substrate Mix class from the TH study area (b), the Woody Debris class from the WP study area (c), the Marsh class from the WP study area,the Wetland class from the WP study area, and the ILLT class from the TH study area (f).

Woody Debris

Woody Debris is the assigned class when it is the dominant substrate type (> 50% coverage). Woody Debris is found mostly in bays or sheltered areas, as well as in the form of "log lines" typically less than 10 m wide (Figure 36). This shoreline type is common throughout both study areas and while most of the woody debris that has accumulated in bays close to the coast was clearly visible in radar imagery such as the 8 m pixel imagery of this study, many smaller deposits and log lines found further inland were not, and so were excluded from this analysis.

Marsh

Salt marshes are not a common shoreline type in the Arctic though when present; occur as a wide meadow or narrow, fringing strips along beaches in the upper intertidal zone. The latter is the type most common along the outer Mackenzie Delta and Tuktoyaktuk Peninsula (Figure 36). These may also be considered low marshes, which are inundated under even moderate tidal elevations and are characterized by patchy vegetation, and low species diversity (dominantly glasswort or sedge), which also tend to be salt tolerant (halophytic). Marshes are common along the western side of Richards Island behind the extensive mud tidal flat. In the TH study area however, only one marsh was observed at Topkak Point (Howes et al., 1993).

Wetland

For the purpose of this analysis marshes and wetlands are differentiated on the basis of species composition (Owens, 2010). Where marshes typically contain glasswort and sedge species, wetlands are predominated by grasses. The subsurface of these

features contains organic materials, and forms vary from wide meadows to narrow fringes along beaches. Species tend to be salt tolerant though flooding typically only occurs during surges and spring high tides. Only a single wetland was observed in both study areas, though the wetland in the WP study area could also be considered ILLT, but it was saturated at the surface and so it was treated as a wetland (Figure 36). The wetland in the TH study area was identified using Radarsat-2 imagery and 2004 ortho photos, but was too far inland to be visible in helicopter videography.

Inundated Low Lying Tundra

Inundated Low Lying Tundra (hereafter ILLT) is relatively common throughout both study areas and while predominately composed of grass species, is differentiated from wetlands on the basis of its morphology, including greater species diversity, and in most cases the upper intertidal zone of this class is composed of a peat beach. In the TH study area specifically, the majority of ILLT is located in one vast segment of shoreline north of Tuktoyaktuk Harbour, in the sheltered inlet between Topkak and Beluga Point (Figure 36).

Low Centre Polygons

The Low Centre Polygon class represents both the actively growing ice wedges located in low lying troughs, as well as the higher tundra that form polygon shapes between them. "Low centre" refers to the centre of polygons, which are below their outside margins (Figure 37). In the summer, the tops of troughs are usually filled with water due to melting ice. Both high and low centre polygons are primarily a backshore class and so exist mostly beyond the extent of marine activity. These features are located

throughout Richards Island in the WP study area, and on the Tuktoyaktuk Peninsula in the TH study area.

High Centre Polygons

The High Centre Polygon class represent both the inactive ice wedges located in low lying troughs, as well as the higher tundra that form polygon shapes between them. "High centre" refers to the centre of polygons, which are above their outside margins (Figure 37). In comparison to low centre polygons, these features have little to no interstitial water. High centre polygons were only identified in the WP study area, in the backshore of the low lying islands to the southwest. For this analysis low and high centre polygons were initially discerned because it was believed that differences in their morphologies would impact backscatter.

Eroding Tundra

Eroding Tundra includes retrogressive thaw slumps and the features typically associated with them such as, mud flows (Owens, 2010). These features are considered part of the backshore, and so are not likely places where oil would become stranded in the event of a spill. Their location and extent however, is pertinent information for contingency planning and response efforts, since these are unstable places that in most cases cannot be used to access affected shorelines through the backshore. This shoreline type is relatively uncommon throughout both study areas and is only found where upland tundra is present (Figure 37). This is because they are largely associated with permafrost degradation and significant ground ice accumulation.

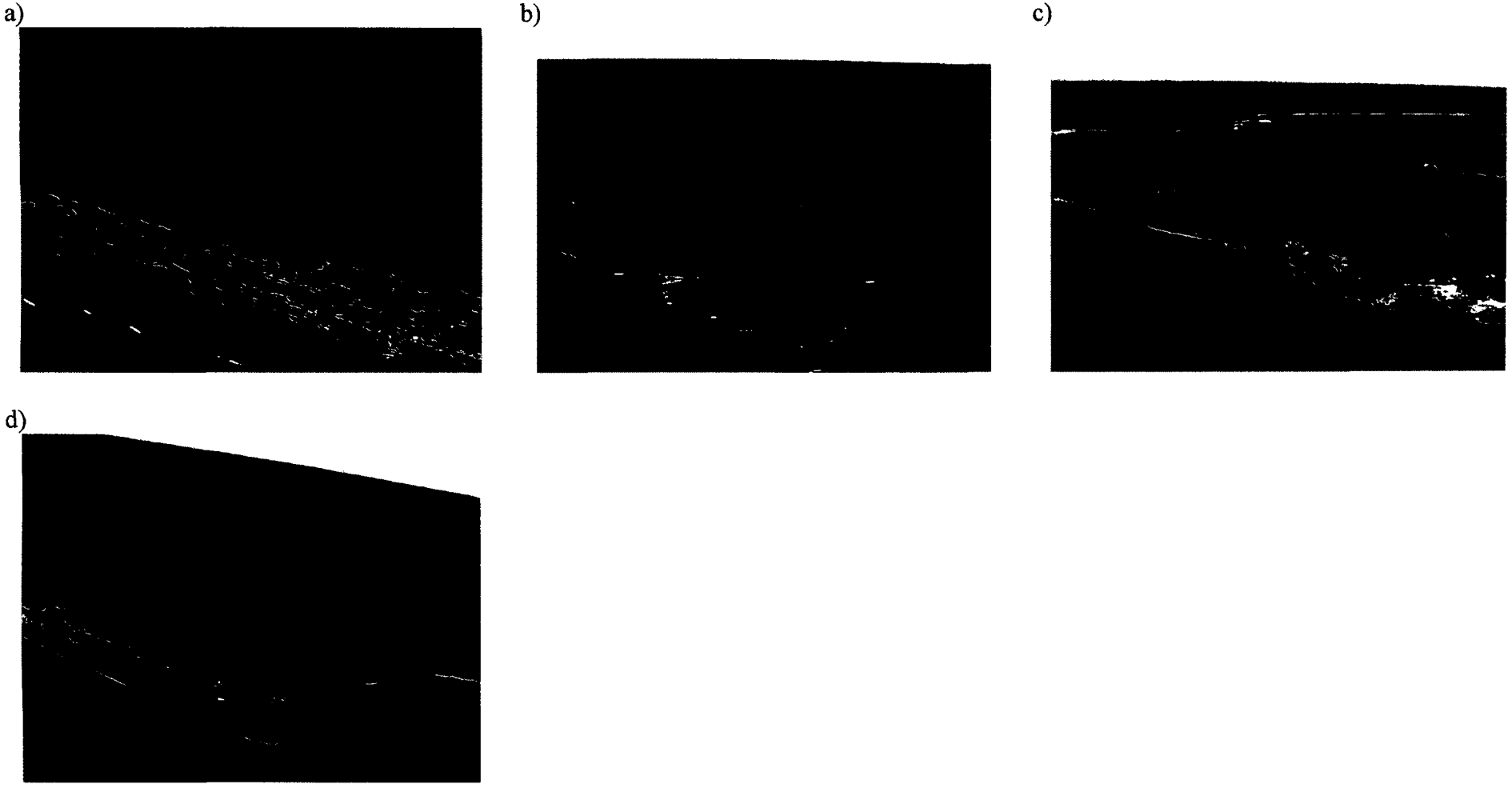

Figure 37: Snapshots from helicopter videography acquired in 2010 of the various land cover classes described, including of the Low Centre Polygon class from the TH study area (a), the High Centre Polygon class from the WP study area (b), the Eroding Tundra class from the TH study area (c) and both Herb and Shrub Dominant Tundra from the TH study area (d), using a red circle to indicate the latter.

Herb Dominant Tundra

Herb Dominant Tundra represents backshore tundra primarily vegetated with low lying herbaceous vegetation and shrubs (Figure 37). The majority of the backshore in both study areas can be represented by this class and in some cases this also includes sparsely vegetated areas, which appeared similar in radar intensity images. Species here include: shrubs, graminoids, bryophytes, lichens and herbaceous perennials (Billings & Mooney, 1968; Bliss, Courtin, Pattie, Whitfield, & Widden).

Shrub Dominant Tundra

Shrub Dominant Tundra represents backshore tundra primarily vegetated with shrubs taller than ~0.25 m (Figure 37). Much like the High and Low Centre Polygon classes this class was distinguished from Herb Dominant Tundra due to the unique response observed in radar imagery. Areas dominated by tall shrubs for example, were brighter compared to those dominated by low lying herbs and shrubs. It is anticipated that this information may be pertinent to oil spill contingency planning as well, since the presence of thick, tall shrubs may negatively impact access and the potential for staging areas in comparison to low herbs.

Appendix 2.

Example of training site generation using ortho photos and 2010 helicopter videography.

a)

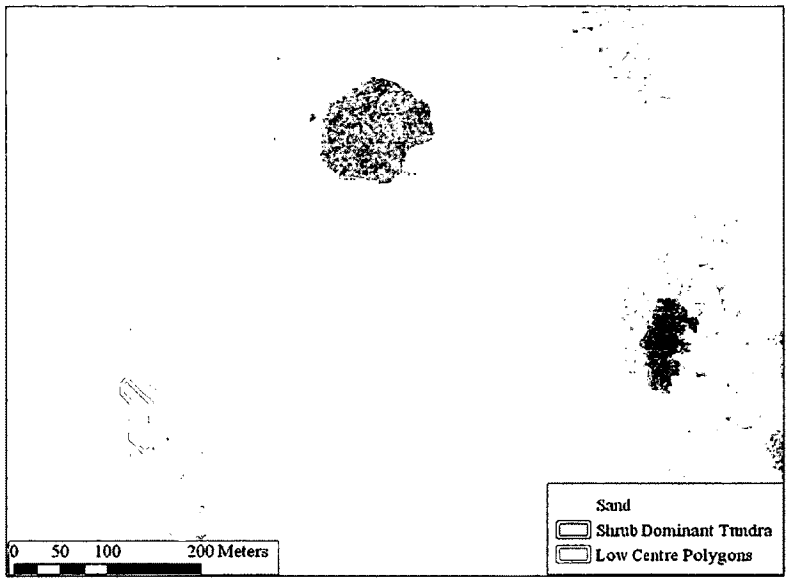

b)

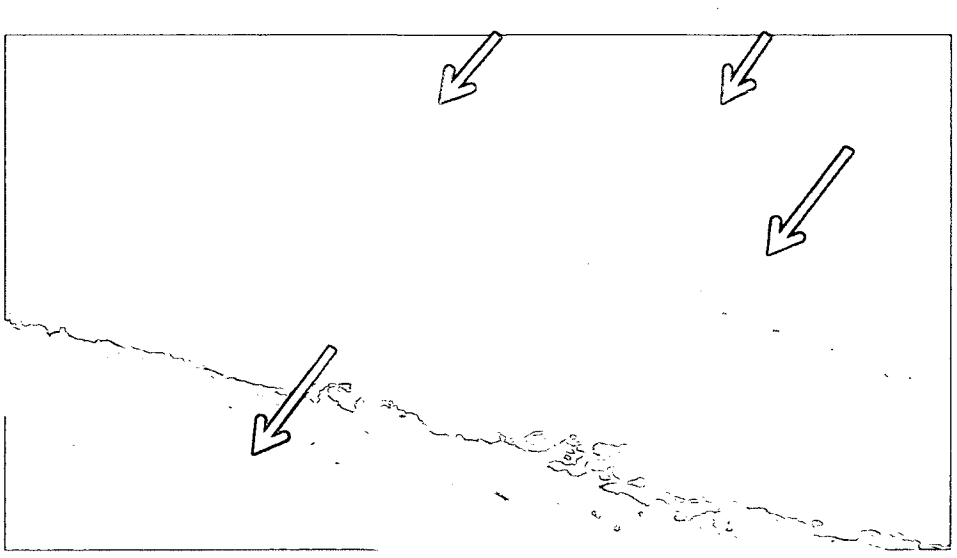

Figure 38: Example of training site generation based on visual analyses of ortho photos and 2010 helicopter videography. a) shows a portion of 2004 ortho photos, with a number of polygons to represent training sites for Sand (yellow), Shrub Dominant Tundra (green) and Low Centre Polygons (red), covering a total of 1350 m^2, 2650 m^2, and 4900 m^2, respectively. b) shows a snap shot from 2010 helicotper videpgraphy of the same area with arrows to represent the same areas where polygons for Sand (yellow), Shrub Dominant Tundra (green) and Low Centre Polygons (red) are drawn. This area specifically, was also ground truthed.

Appendix 3.

Maps of transect locations.

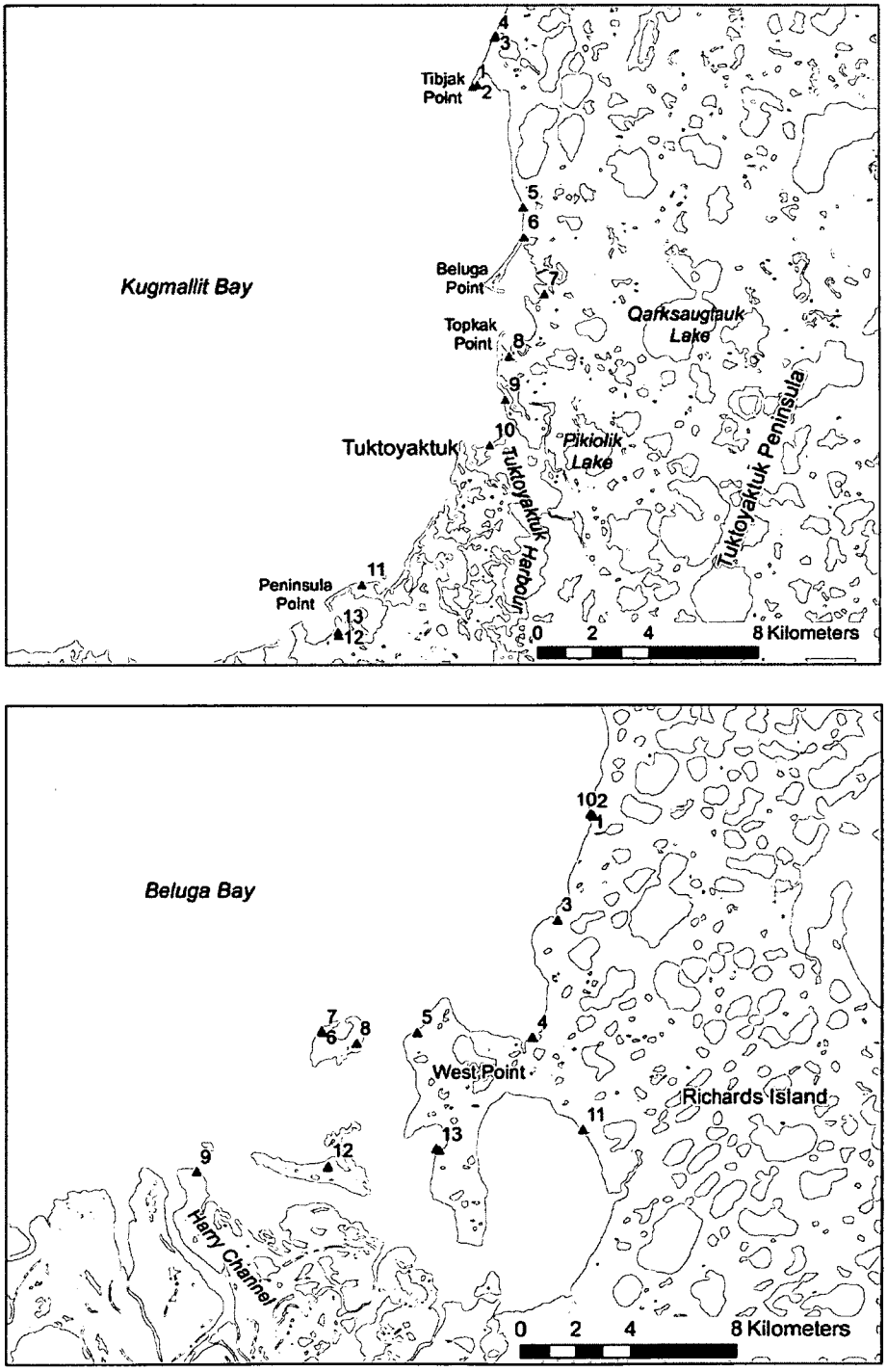

Figure 39: Maps of transect locations in the TH (top) and WP (bottom) study areas, identified with numbers as displayed in Table 5.

Appendix 4.

Backscatter coefficient (σ° dB) correlation (r) for all combinations of polarizations and incidence angles.

Anthropogenic, Water and Substrates Classes

Class	Parameters (σ°)	r Value (TH)			r Value (WP)		
		Shallow	Medium	Steep	Shallow	Medium	Steep
Anthropogenic	HH : VV	0.77	0.78	0.84		N/A	
	HH : HV	0.54	0.62	0.51			
	VV : HV	0.64	0.69	0.60			
Water	HH : VV	0.49	0.59	0.95	0.49	0.53	0.93
	HH : HV	0.18	0.01	0.06	0.12	0.17	0.14
	VV : HV	0.15	0.06	0.06	0.11	-0.06	0.17
Smooth/Un-vegetated Mudflat	HH : VV	0.70	0.79	0.89	0.72	0.76	0.92
	HH : HV	0.53	0.54	0.27	0.48	0.43	0.62
	VV : HV	0.49	0.54	0.32	0.45	0.43	0.57
Rough/Vegetated Mudflat	HH : VV				0.58	0.75	0.89
	HH : HV		N/A		0.42	0.50	0.13
	VV : HV				0.38	0.46	0.02
Peat	HH : VV	0.76	0.81	0.87	0.55	0.53	0.82
	HH : HV	0.68	0.63	-0.02	0.62	0.55	0.29
	VV : HV	0.55	0.53	-0.12	0.33	0.32	0.29
Sand	HH : VV	0.60	0.62	0.88	0.87	0.89	0.94
	HH : HV	0.53	0.60	0.39	0.81	0.83	0.64
	VV : HV	0.37	0.43	0.09	0.72	0.77	0.52
Mixed Sediment	HH : VV	0.64	0.56	0.82	0.59	0.66	0.74
	HH : HV	0.60	0.53	0.05	0.13	0.37	0.04
	VV : HV	0.52	0.40	0.00	0.06	0.21	-0.04
Riprap	HH : VV	0.24	0.53	0.71		N/A	
	HH : HV	0.13	0.15	0.24			
	VV : HV	0.50	0.21	0.18			
Wood and Substrate Mix	HH : VV	0.68	0.68	0.84	0.74	0.79	0.83
	HH : HV	0.59	0.65	0.31	0.35	0.58	0.22
	VV : HV	0.57	0.52	0.10	0.44	0.62	0.24
Woody Debris	HH : VV	0.54	0.68	0.48	0.72	0.65	0.64
	HH : HV	-0.29	-0.16	-0.14	0.08	0.04	0.15
	VV : HV	0.00	0.09	0.07	0.15	0.11	0.24

Vegetated Classes

Class	Parameters (σ^o)	r Value (TH)			r Value (WP)		
		Shallow	Medium	Steep	Shallow	Medium	Steep
Marsh	HH : VV	0.43	0.40	0.80	0.47	0.48	0.63
	HH : HV	0.39	0.37	0.21	0.68	0.73	0.29
	VV : HV	0.09	0.31	0.09	0.33	0.40	-0.15
Wetland	HH : VV	0.37	0.37	-0.20	0.61	0.41	0.65
	HH : HV	0.03	-0.02	-0.10	0.35	0.20	0.40
	VV : HV	0.01	-0.08	0.37	0.36	0.36	0.23
ILLT	HH : VV	0.45	0.51	0.46	0.29	0.26	0.48
	HH : HV	0.49	0.33	0.22	-0.13	0.14	0.19
	VV : HV	0.47	0.27	0.10	-0.07	0.24	0.07
High Centre Polygons	HH : VV				0.04	0.15	0.20
	HH : HV		N/A		0.12	0.05	0.07
	VV : HV				0.03	0.25	-0.02
Low Centre Polygons	HH : VV	0.39	0.50	0.63	0.55	0.46	0.65
	HH : HV	0.28	0.25	0.26	0.52	0.36	0.19
	VV : HV	0.42	0.40	0.31	0.59	0.27	0.13
Eroding Tundra	HH : VV	0.27	0.44	0.83	0.68	0.79	0.88
	HH : HV	0.15	0.00	0.06	0.61	0.66	0.58
	VV : HV	0.65	0.59	0.12	0.59	0.60	0.59
Herb Dominant Tundra	HH : VV	0.49	0.26	0.67	0.44	0.56	0.79
	HH : HV	0.36	0.21	0.43	0.45	0.46	0.38
	VV : HV	0.38	0.24	0.35	0.46	0.50	0.29
Shrub Dominant Tundra	HH : VV	0.18	0.22	0.56	0.25	0.34	0.35
	HH : HV	0.02	0.21	0.17	0.20	0.30	0.22
	VV : HV	0.15	0.14	0.12	0.26	0.22	0.14

Appendix 5.

Box and whisker plots to show the consistency of sample distributions between study areas and incidence angles for HH, HV and VV backscatter coefficients (dB).

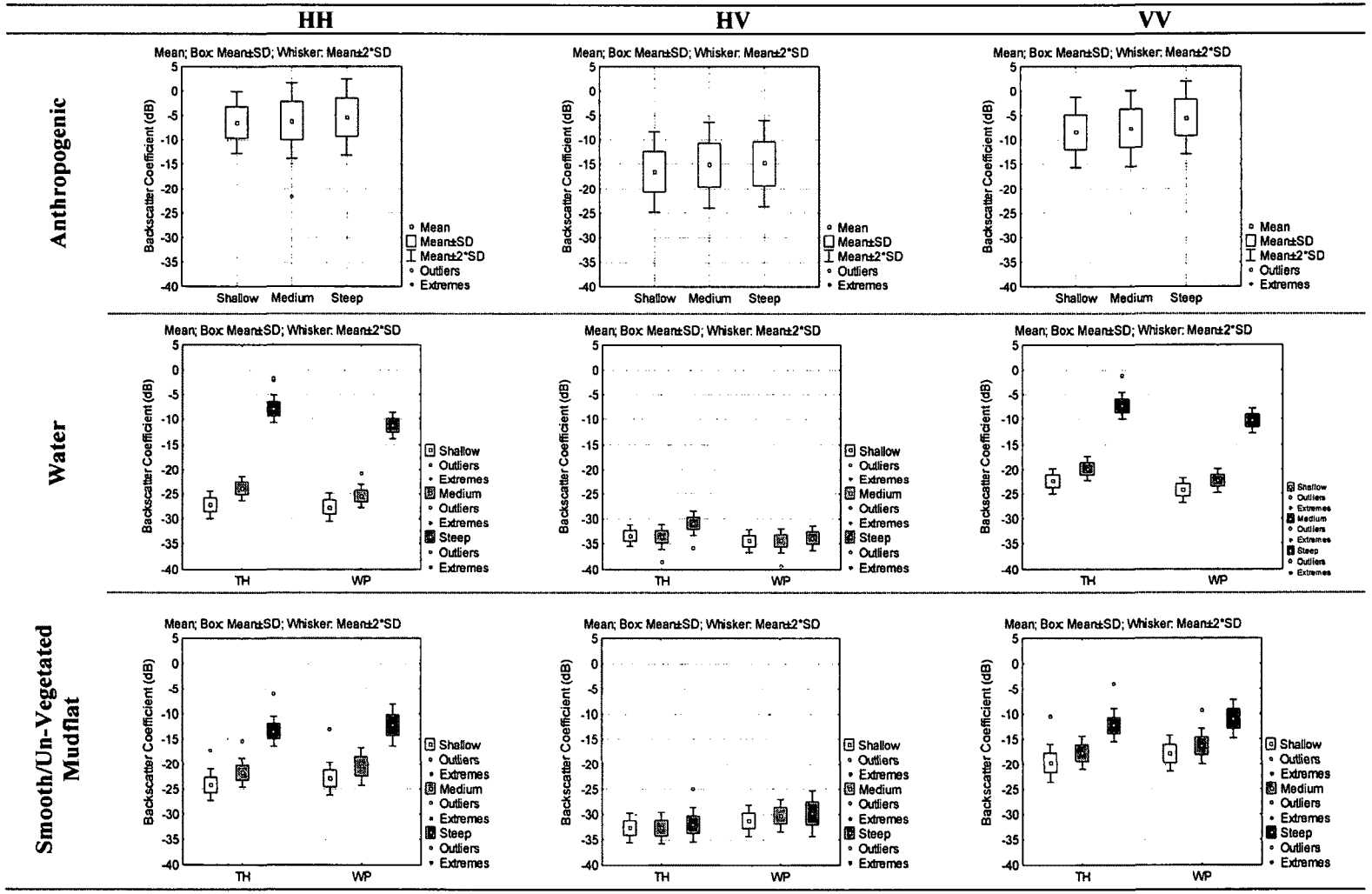

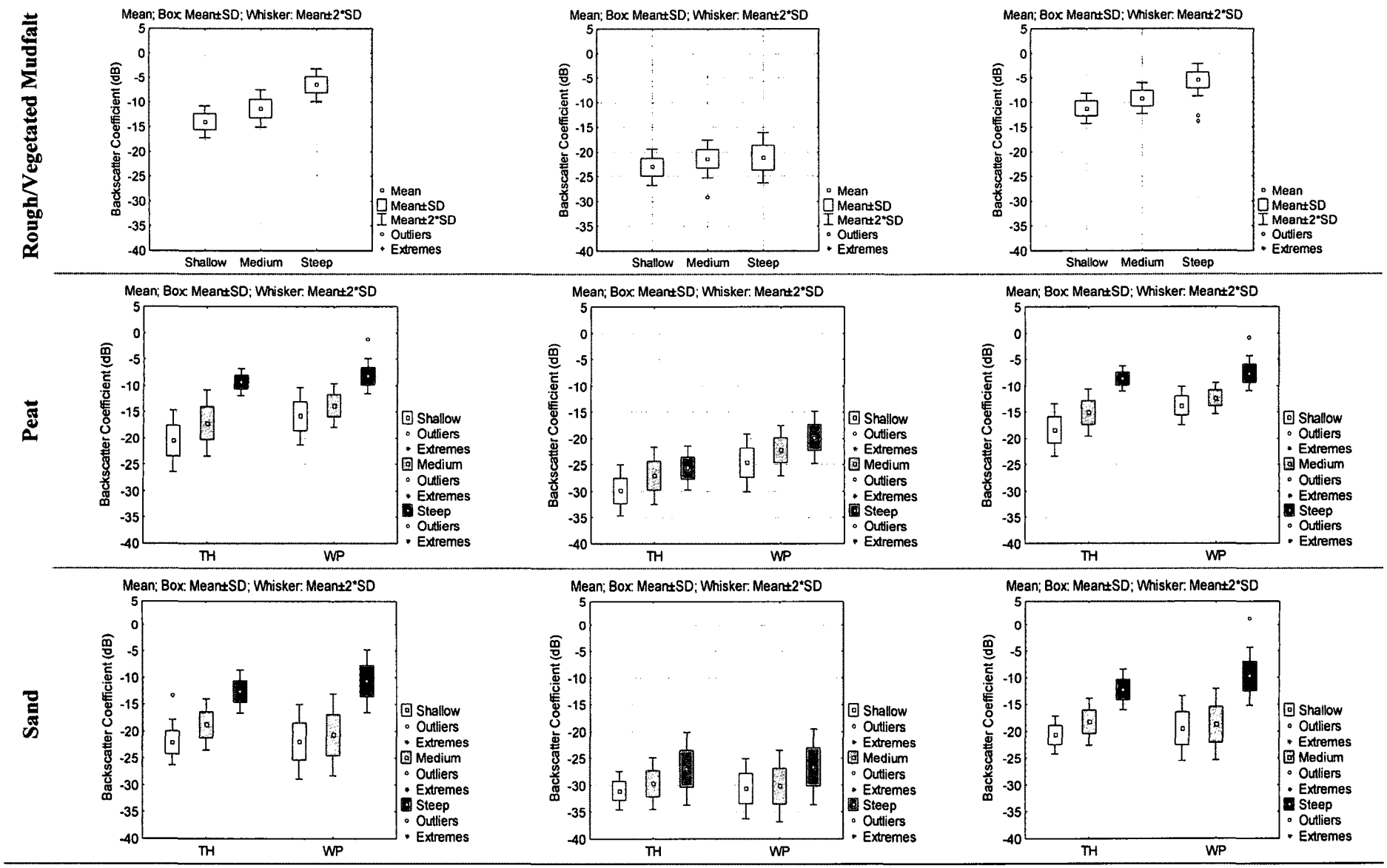
Rough/Vegetated Mudflat
Peat
Sand
Mean; Box: Mean±SD; Whisker: Mean±2*SD
Backscatter Coefficient (dB)
5
0
-5
-10
-15
-20
-25
-30
-35
-40
Shallow
Medium
Steep
TH
WP
Mean
Mean±SD
Mean±2*SD
Outliers
Extremes

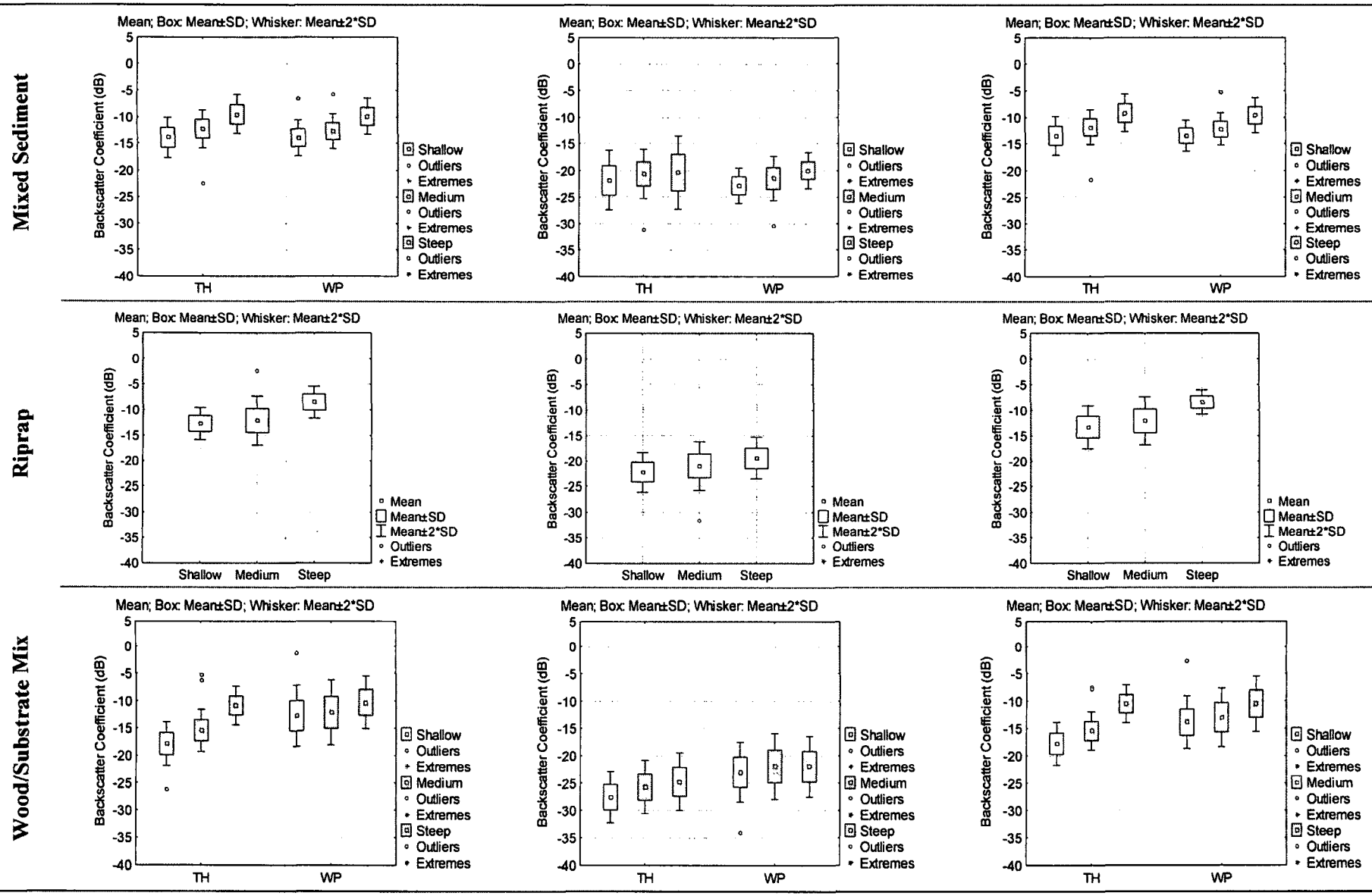
Mixed Sediment
Riprap
Wood/Substrate Mix
Mean; Box: Mean±SD; Whisker: Mean±2*SD
Backscatter Coefficient (dB)
5
0
-5
-10
-15
-20
-25
-30
-35
-40
TH
WP
Shallow
Outliers
Extremes
Medium
Steep
Mean
Mean±SD
Mean±2*SD
Shallow Medium Steep

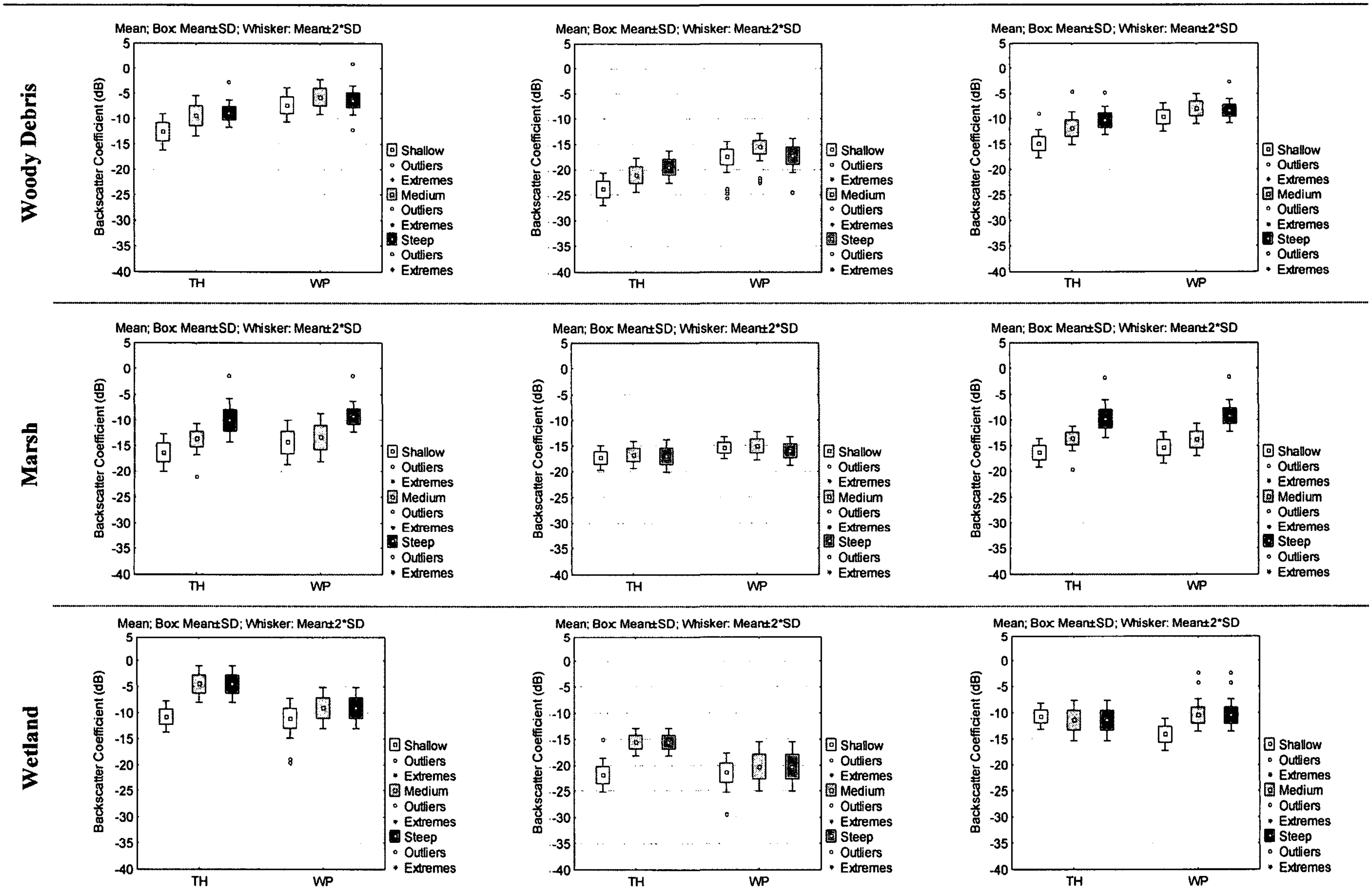
Woody Debris
Marsh
Wetland
Mean; Box: Mean±SD; Whisker: Mean±2*SD
Backscatter Coefficient (dB)
5
0
-5
-10
-15
-20
-25
-30
-35
-40
TH
WP
Shallow
Outliers
Extremes
Medium
Outliers
Extremes
Steep
Outliers
Extremes

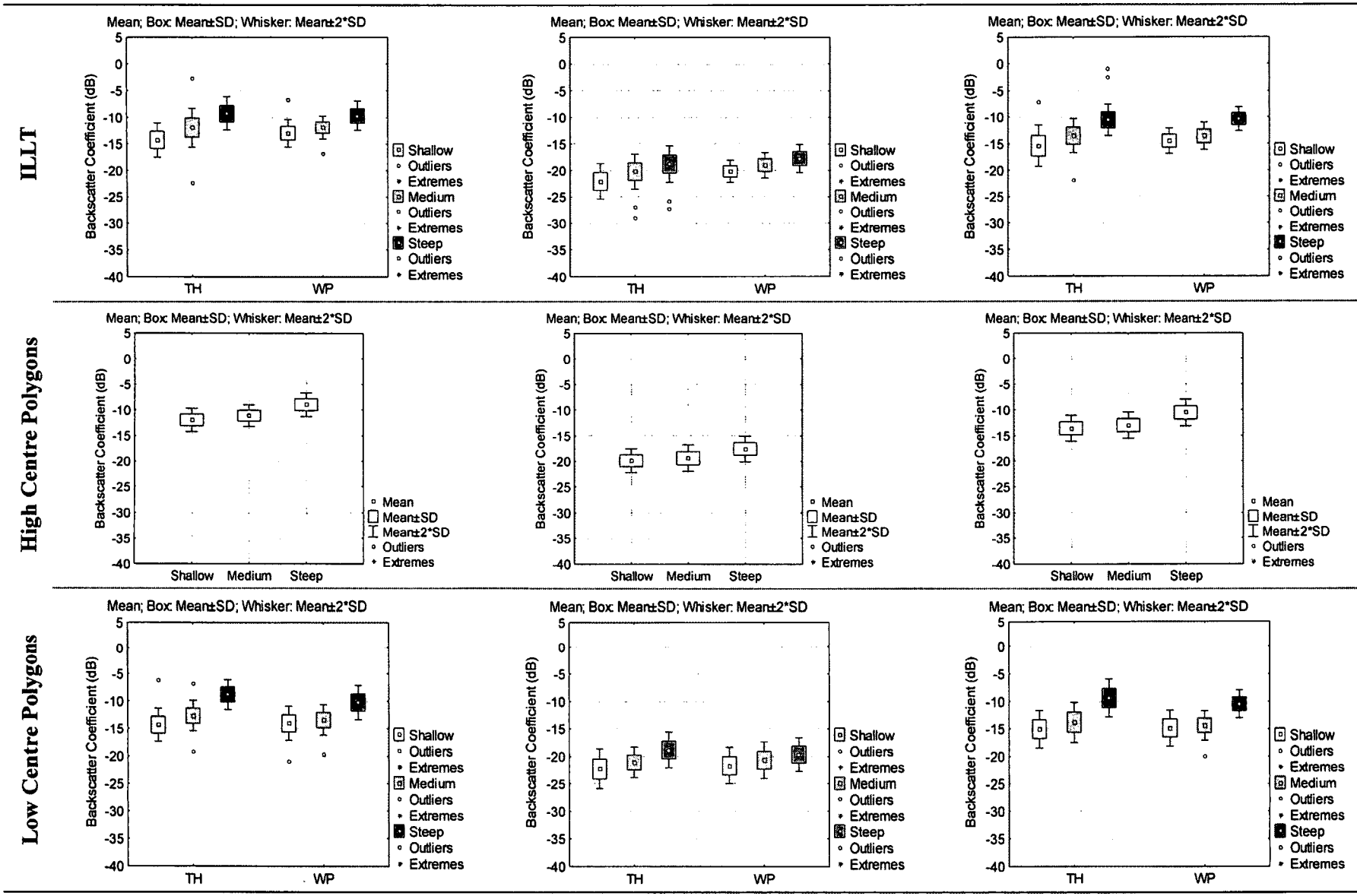
ILLT
High Centre Polygons
Low Centre Polygons
Mean; Box: Mean±SD; Whisker: Mean±2*SD
Backscatter Coefficient (dB)
5
0
-5
-10
-15
-20
-25
-30
-35
-40
TH
WP
Shallow
Outliers
Extremes
Medium
Outliers
Extremes
Steep
Outliers
Extremes
Mean
Mean±SD
Mean±2*SD
Outliers
Extremes
Shallow
Medium
Steep

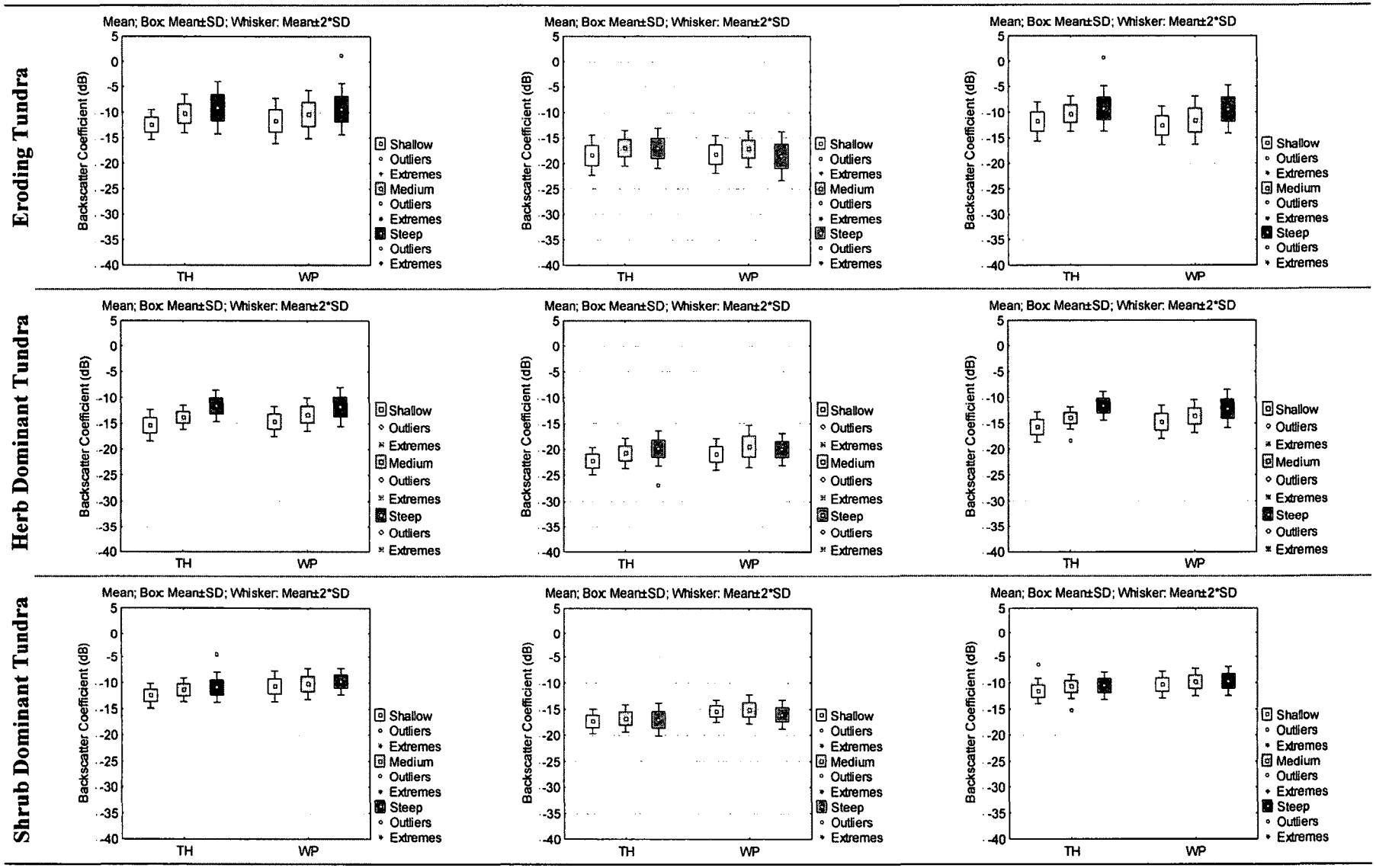
Eroding Tundra
Herb Dominant Tundra
Shrub Dominant Tundra
Mean; Box Mean±SD; Whisker: Mean±2*SD
Backscatter Coefficient (dB)
5
0
-5
-10
-15
-20
-25
-30
-35
-40
TH
WP
Shallow
Outliers
Extremes
Medium
Outliers
Extremes
Steep
Outliers
Extremes

Appendix 6.

Co and cross-polarized pedestal height based on averaged values from three plots, for all classes at all incidence angles.

Land Cover Class	Study Area	Shallow		Medium		Steep	
		Co	Cross	Co	Cross	Co	Cross
Anthropogenic	TH	0.59		0.20			
	WP						
Water	TH	0.19	0.24	0.10	0.10	0.02	0.00
	WP	0.34	0.31	0.13	0.11	0.01	0.01
Smooth/Un-Vegetated Mudflat	TH	0.14	0.12	0.08	0.07	0.06	0.02
	WP	0.08	0.07	0.09	0.09	0.05	0.02
Rough/Vegetated Mudflat	TH					0.09	0.08
	WP			N/A			
Sand	TH	0.20	0.16	0.08	0.03	0.07	0.02
	WP	0.14	0.13	0.08	0.11	0.06	0.02
Mixed Sediment	TH	0.23	0.12	0.23	0.12	0.23	0.15
	WP	0.14	0.07	0.16	0.09	0.10	0.05
Riprap	TH	0.26	0.15	0.30	0.17	0.10	0.03
	WP			N/A			
Wood/Substrate Mix	TH	0.24	0.13	0.27	0.14	0.14	0.06
	WP	0.21	0.08	0.18	0.08	0.05	0.02
Woody Debris	TH	0.19	0.11	0.17	0.08	0.20	0.11
	WP	0.16	0.11	0.09	0.06	0.12	0.10
Marsh	TH	0.40	0.24	0.35	0.20	0.18	0.10
	WP	0.38	0.20	0.25	0.13	0.08	0.04
Wetland	TH	0.37	0.12	0.28	0.10	0.16	0.17
	WP	0.30	0.23	0.34	0.23	0.18	0.10
ILLT	TH	0.36	0.21	0.32	0.22	0.24	0.13
	WP	0.35	0.26	0.38	0.32	0.35	0.26
High Centre Polygons	TH			N/A			
	WP	0.43	0.32	0.42	0.34	0.31	0.21
Low Centre Polygons	TH	0.27	0.15	0.31	0.19	0.16	0.09
	WP	0.47	0.24	0.43	0.25	0.18	0.09
Eroding Tundra	TH	0.33	0.18	0.30	0.17	0.16	0.04
	WP	0.30	0.29	0.42	0.26	0.13	0.04
Herb Dominant Tundra	TH	0.37	0.23	0.32	0.18	0.24	0.17
	WP	0.31	0.21	0.24	0.18	0.14	0.08
Shrub Dominant Tundra	TH	0.37	0.34	0.46	0.32	0.34	0.23
	WP	0.40	0.34	0.42	0.37	0.30	0.24

Appendix 7.

Box and whisker plots to show consistency of sample distributions between study areas and incidence angles for odd bounce, double bounce and volume scattering (dB) derived from the Freeman-Durden Decomposition.

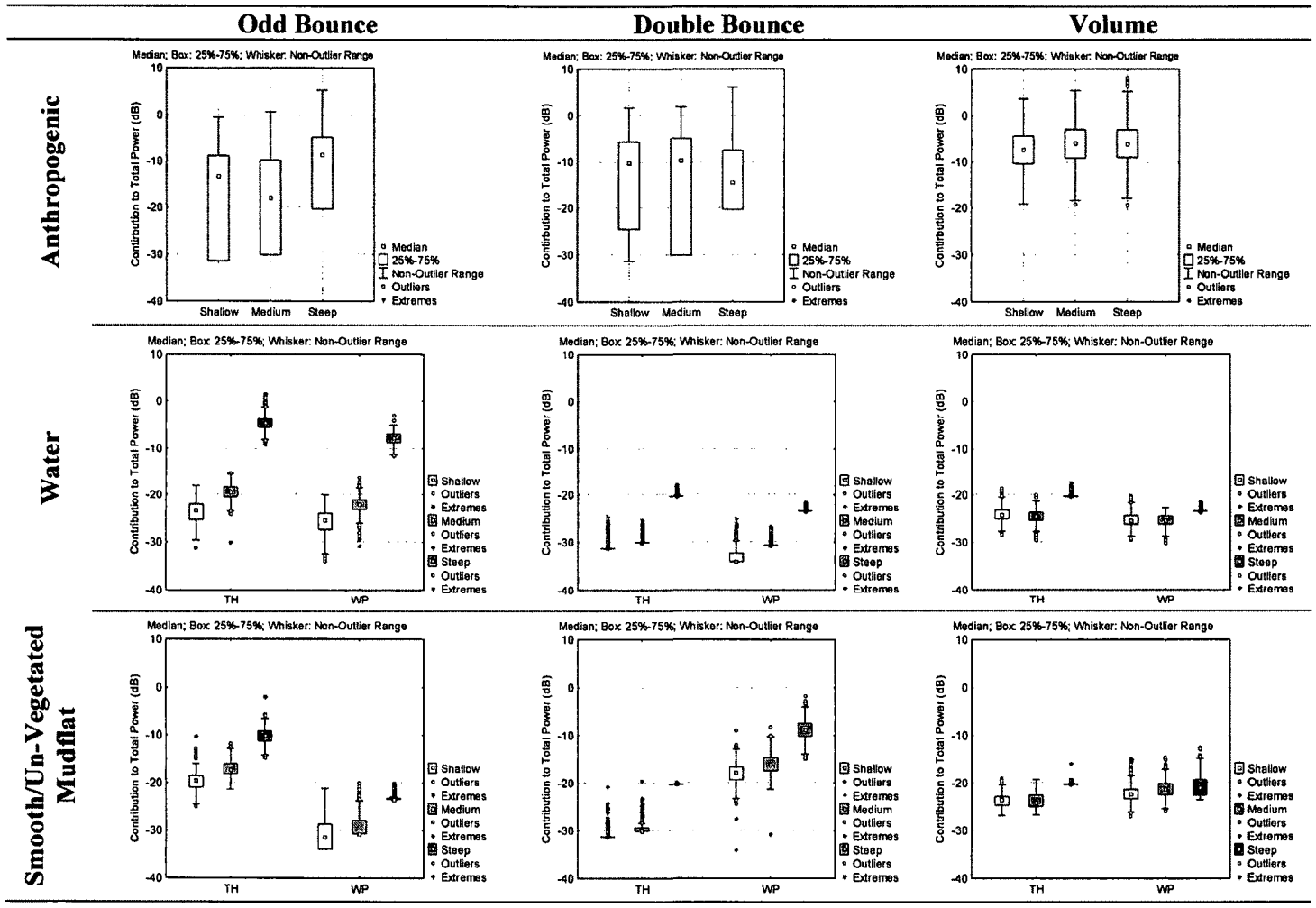

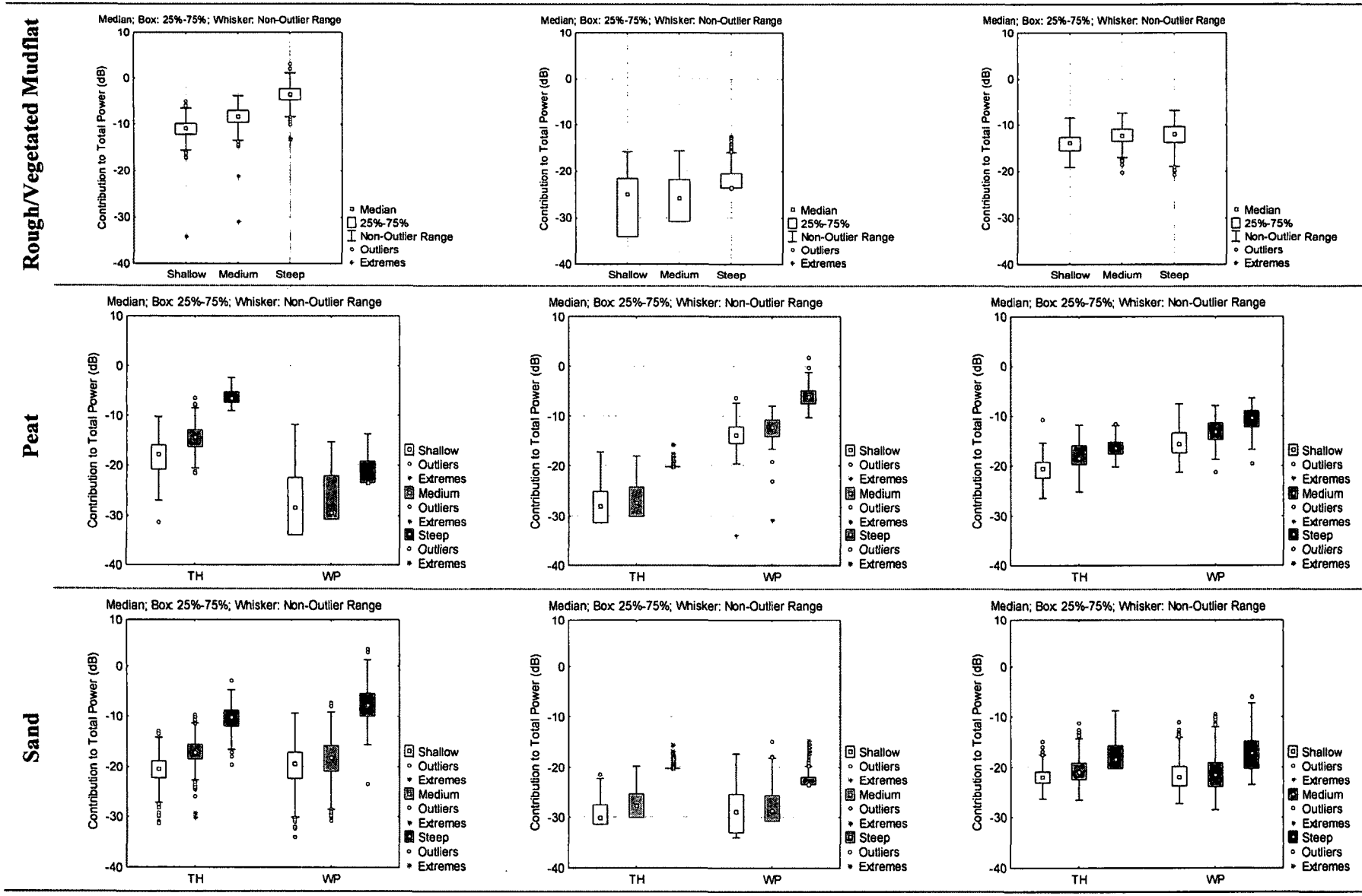
Rough/Vegetated Mudflat
Peat
Sand
Median; Box: 25%-75%; Whisker: Non-Outlier Range
Median; Box 25%-75%; Whisker: Non-Outlier Range
Contribution to Total Power (dB)
10
0
-10
-20
-30
-40
Shallow
Medium
Steep
TH
WP
Median
25%-75%
Non-Outlier Range
Outliers
Extremes

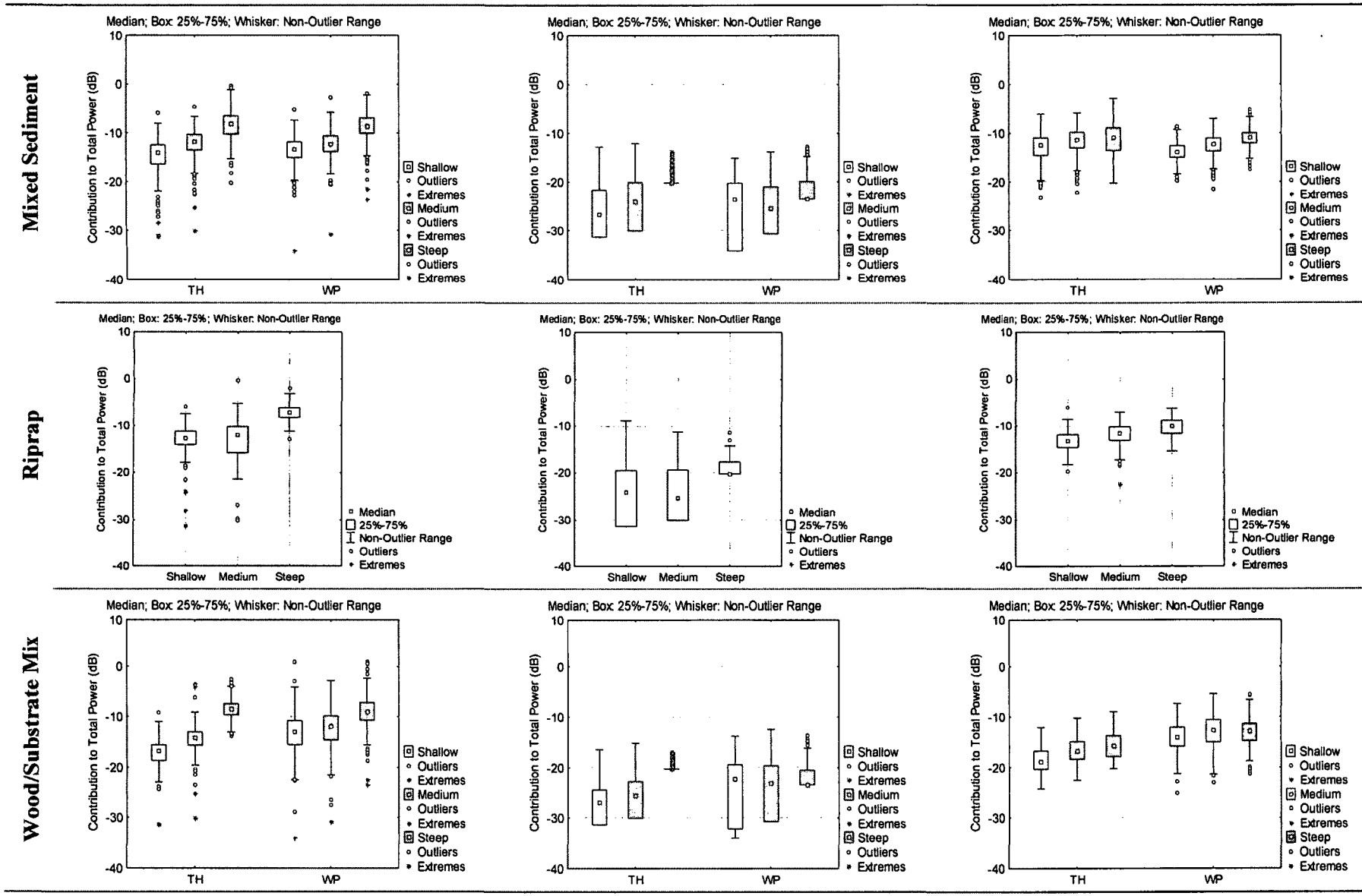
Mixed Sediment
Riprap
Wood/Substrate Mix
Median; Box 25%-75%; Whisker: Non-Outlier Range
Contribution to Total Power (dB)
10
0
-10
-20
-30
-40
TH
WP
Shallow
Outliers
Extremes
Medium
Outliers
Extremes
Steep
Outliers
Extremes
Median; Box: 25%-75%; Whisker: Non-Outlier Range
Shallow
Medium
Steep
Median
25%-75%
Non-Outlier Range
Outliers
Extremes

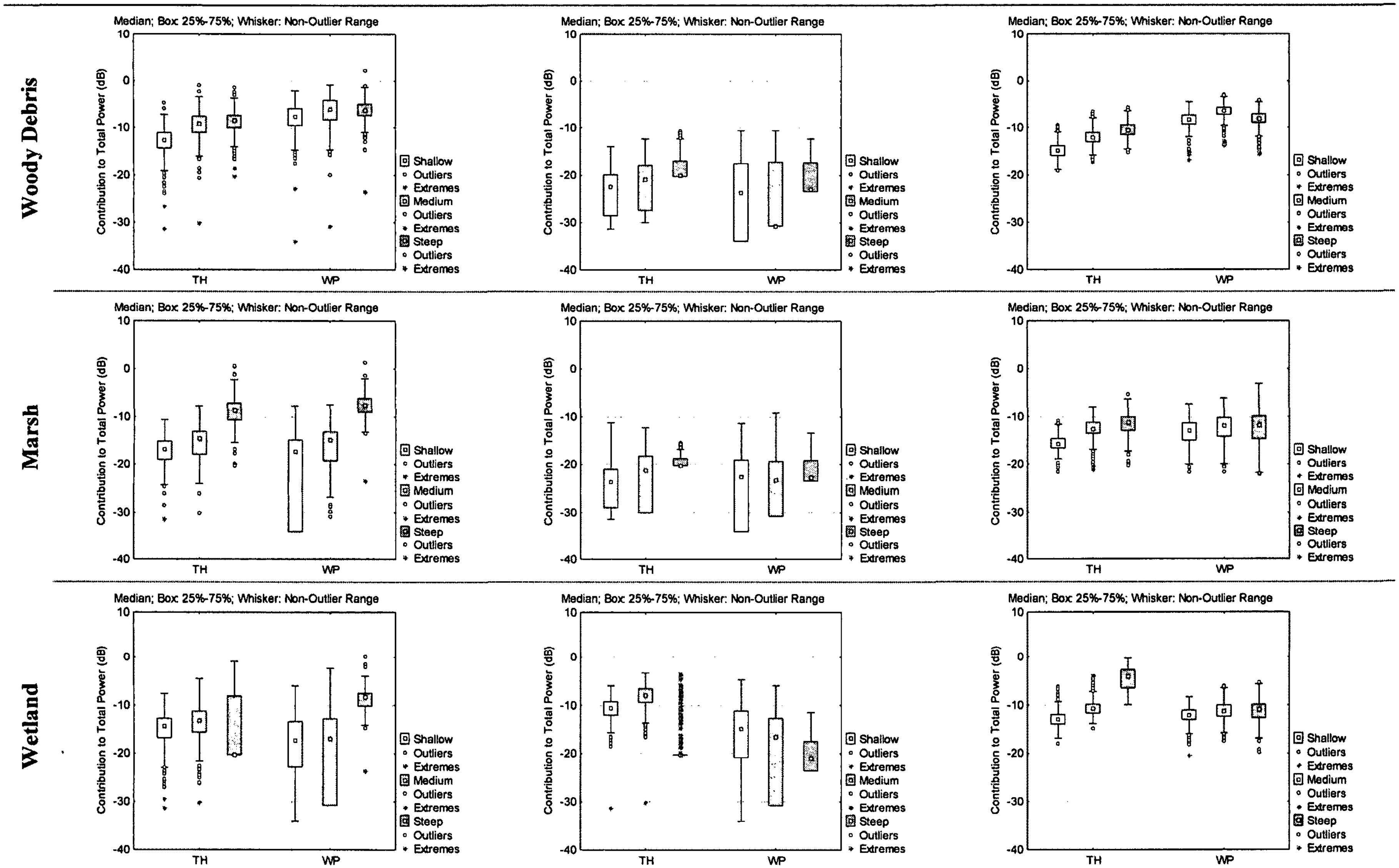
Woody Debris
Marsh
Wetland
Median; Box 25%-75%; Whisker: Non-Outlier Range
Contribution to Total Power (dB)
10
0
-10
-20
-30
-40
TH
WP
Shallow
Outliers
Extremes
Medium
Outliers
Extremes
Steep
Outliers
Extremes

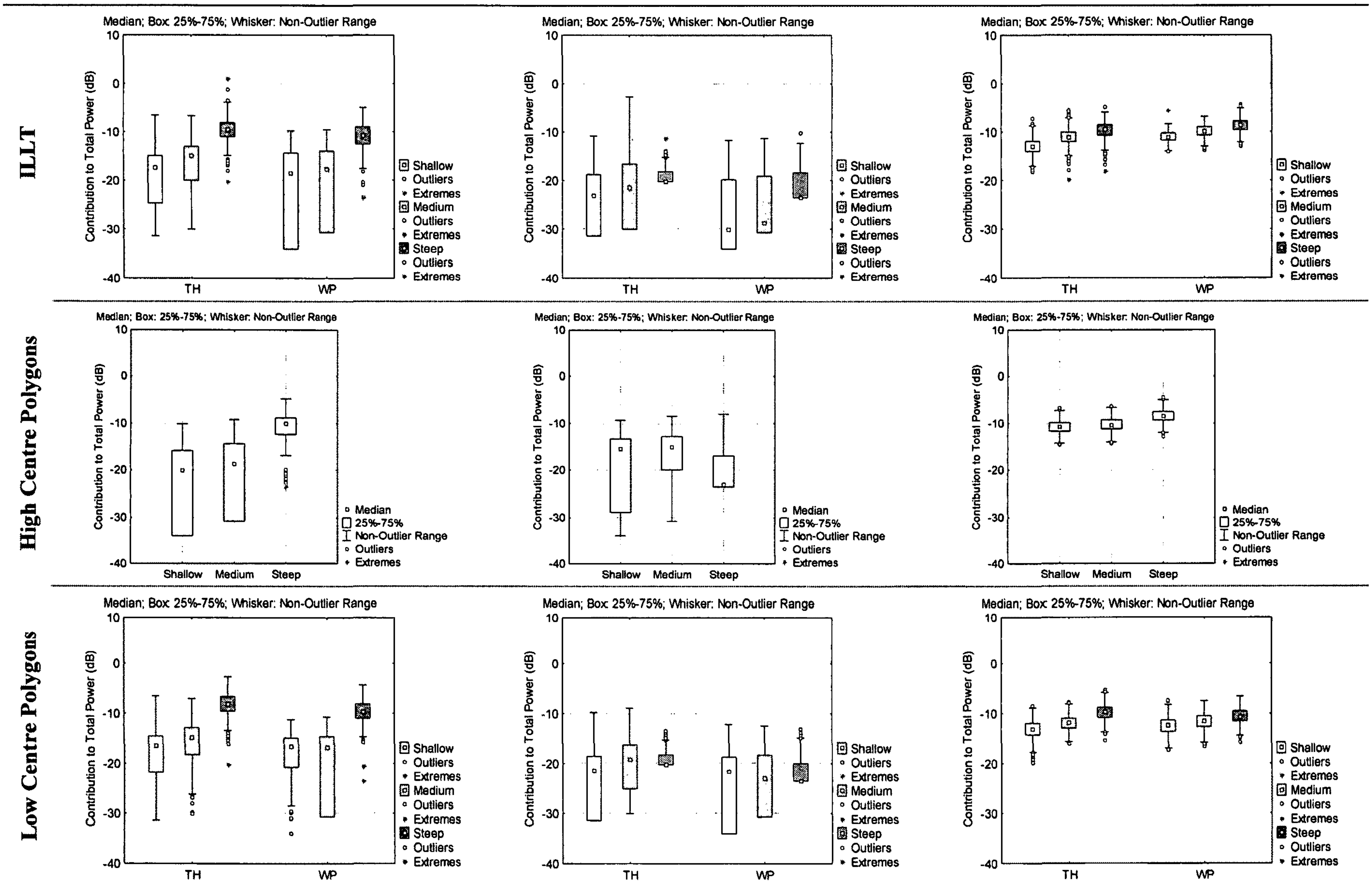
ILLT
High Centre Polygons
Low Centre Polygons
Median; Box 25%-75%; Whisker: Non-Outlier Range
Contribution to Total Power (dB)
TH
WP
Shallow
Medium
Steep
Outliers
Extremes
Median
25%-75%
Non-Outlier Range

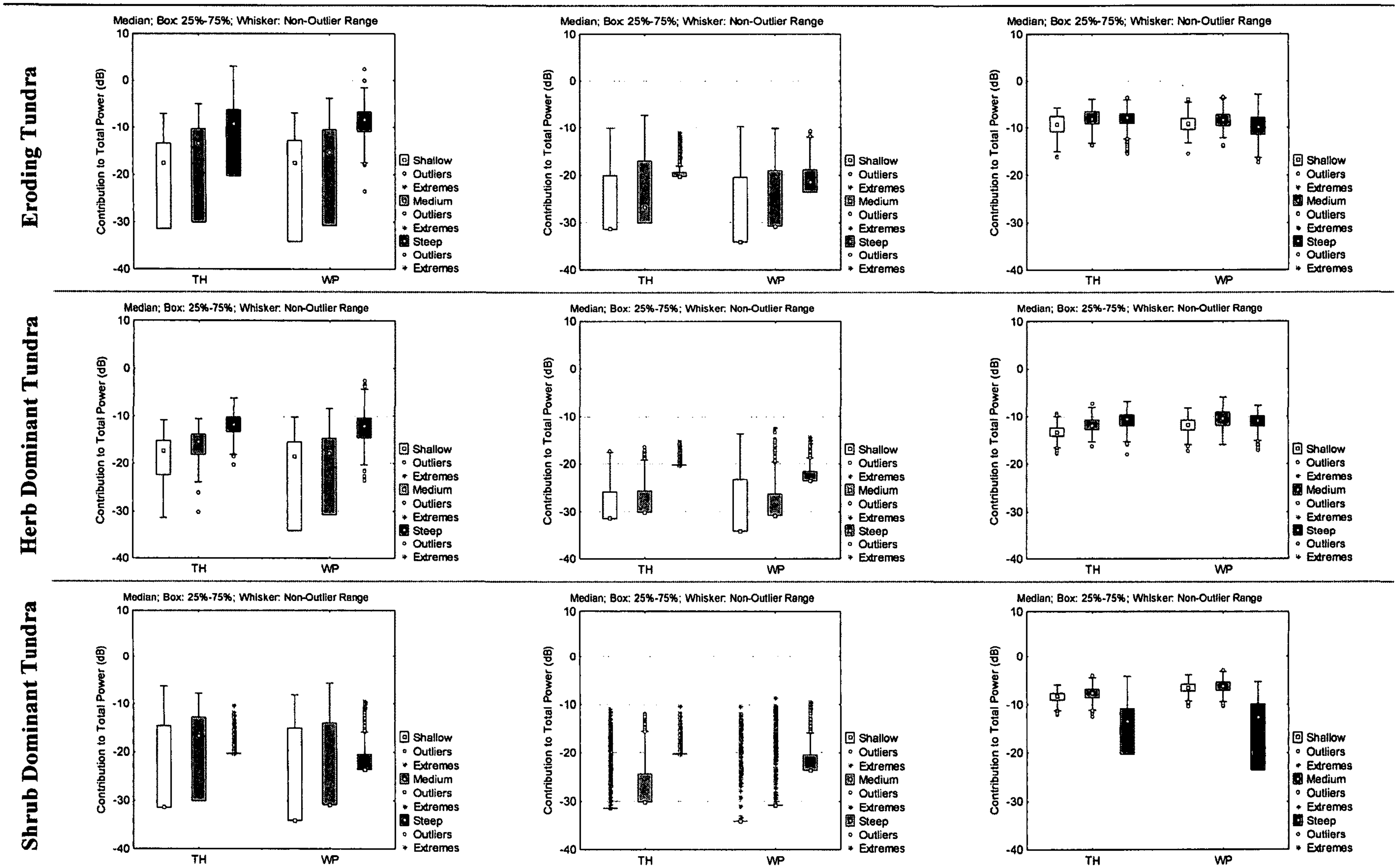
Eroding Tundra
Herb Dominant Tundra
Shrub Dominant Tundra
Median; Box: 25%-75%; Whisker: Non-Outlier Range
Contribution to Total Power (dB)
TH
WP
Shallow
Outliers
Extremes
Medium
Outliers
Extremes
Steep
Outliers
Extremes

Appendix 8.

Box and whisker plots to show consistency of sample distributions for the Cloude-Pottier decomposition parameters entropy, anisotropy and alpha between study areas and incidence angles.

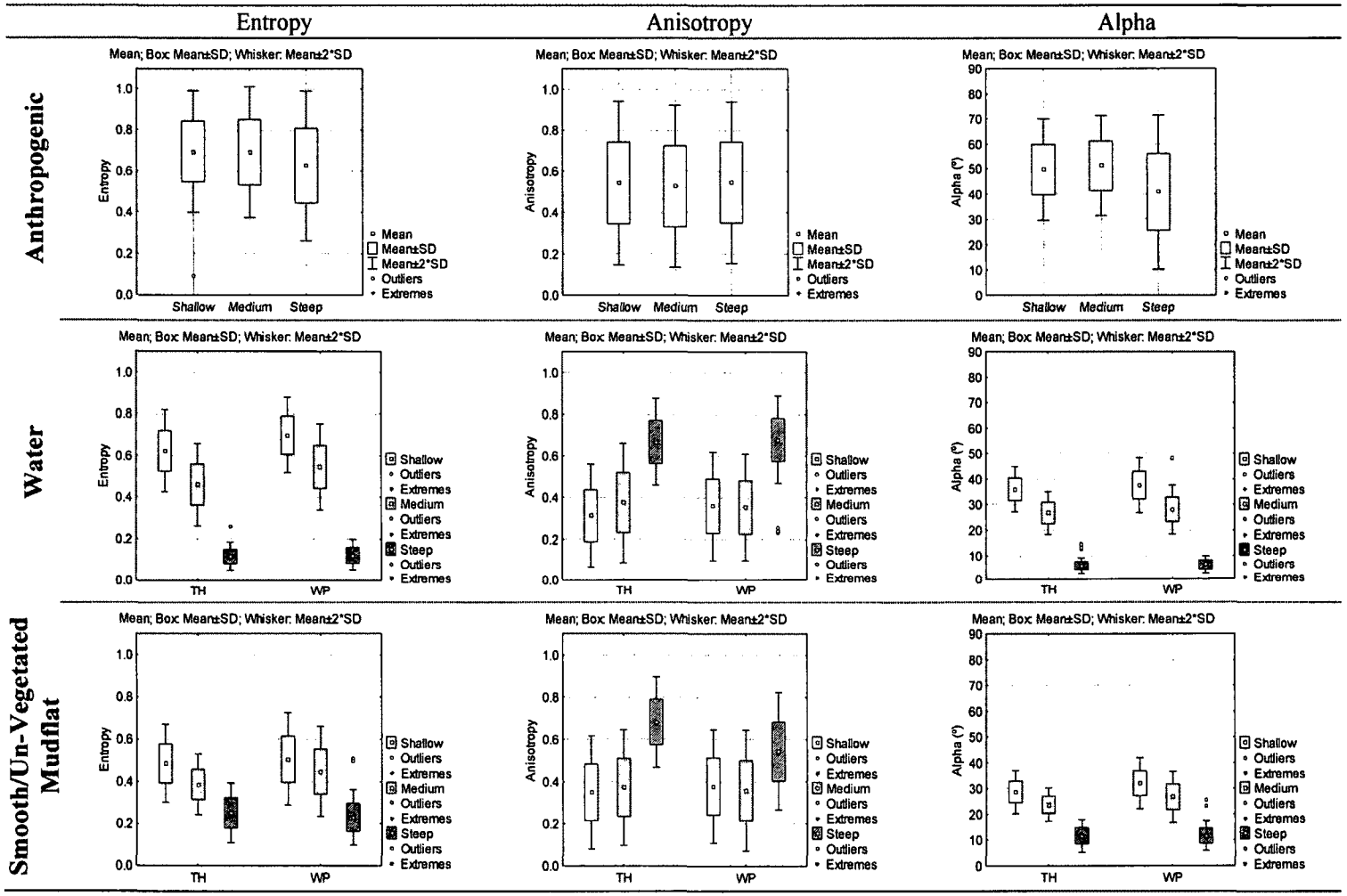

Rough/Vegetated Mudflat

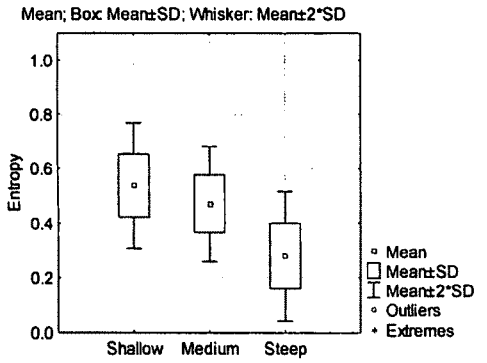

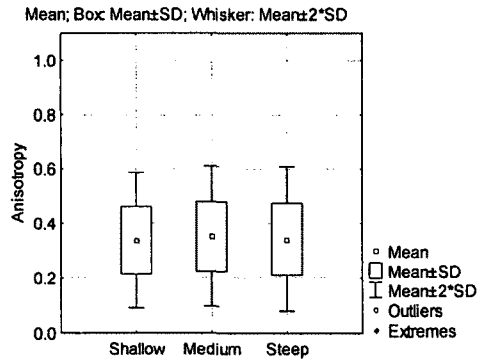

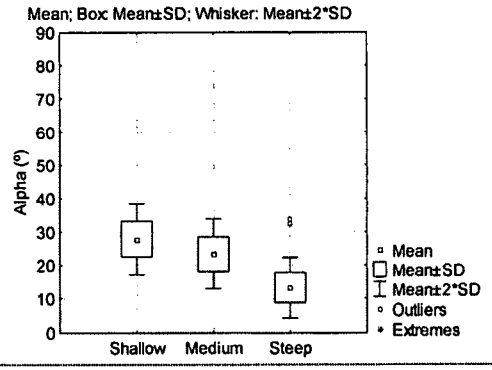

Peat

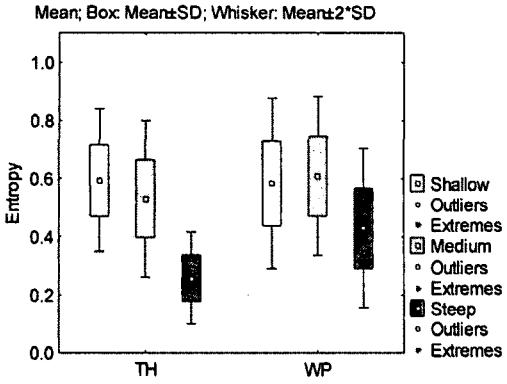

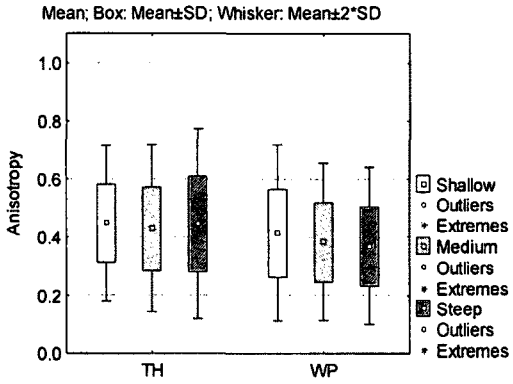

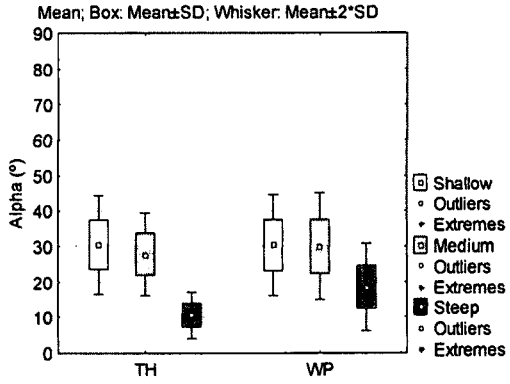

Sand

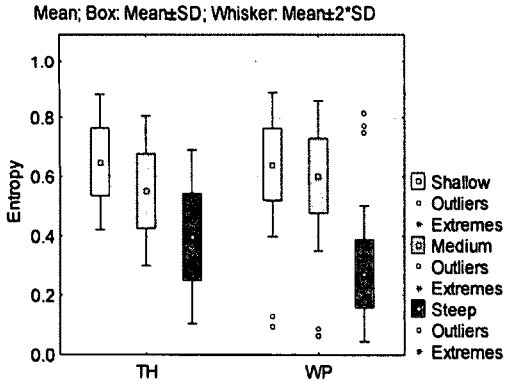

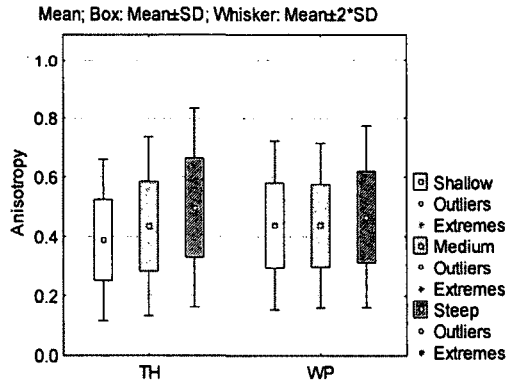

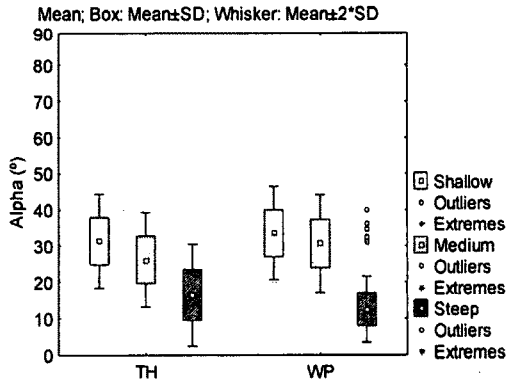

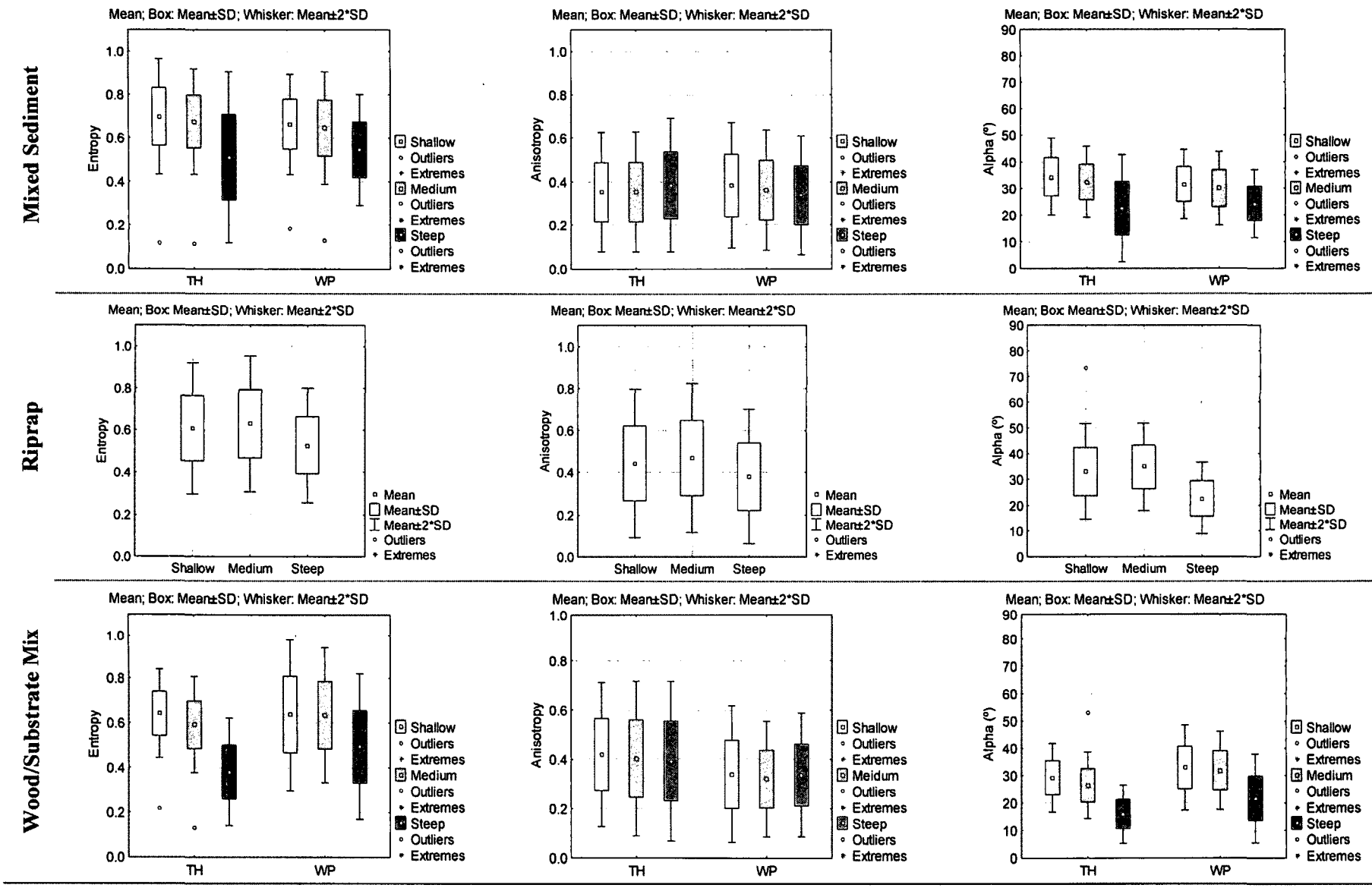
Mixed Sediment
Riprap
Wood/Substrate Mix
Mean; Box: Mean±SD; Whisker: Mean±2*SD
Entropy
Anisotropy
Alpha (°)
TH
WP
Shallow
Medium
Steep
Mean
Mean±SD
Mean±2*SD
Outliers
Extremes

Woody Debris

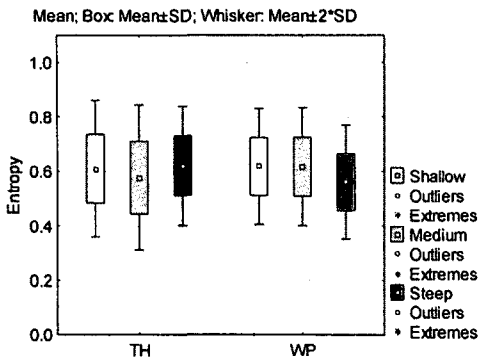

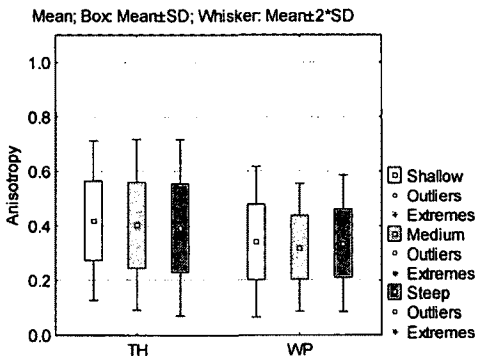

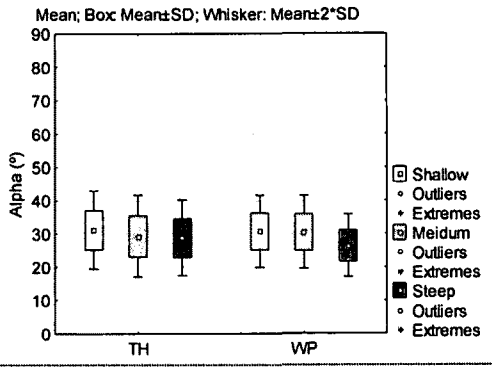

Marsh

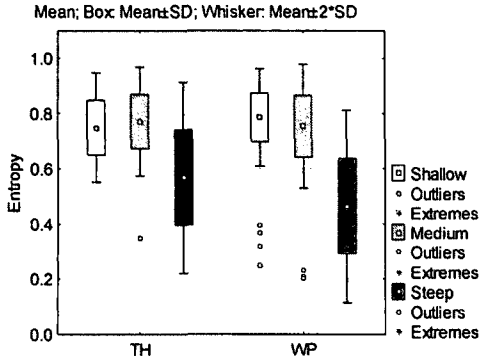

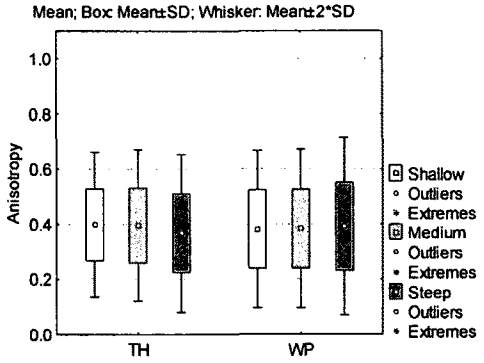

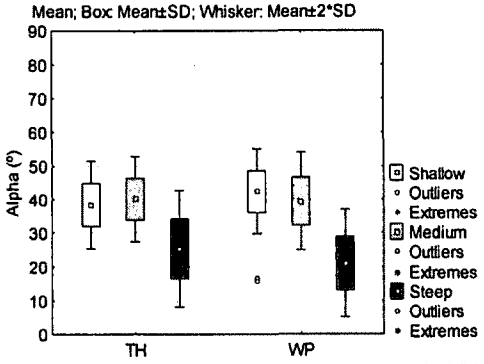

Wetland

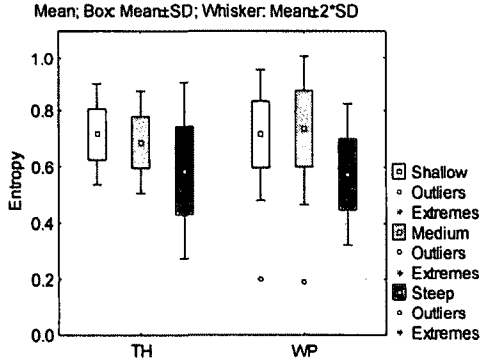

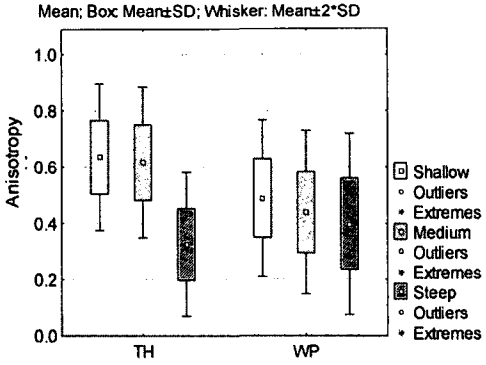

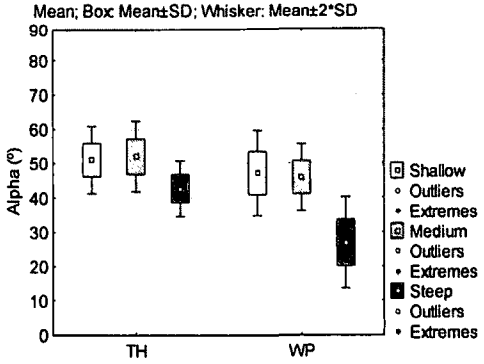

ILLT

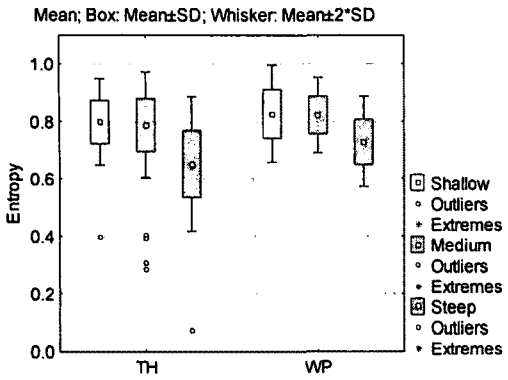

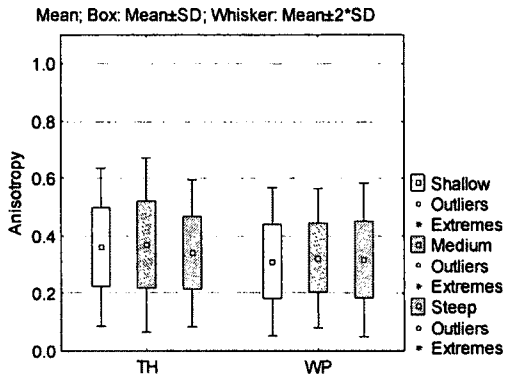

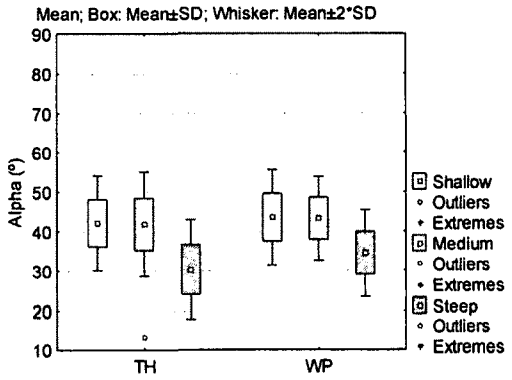

High Centre Polygons

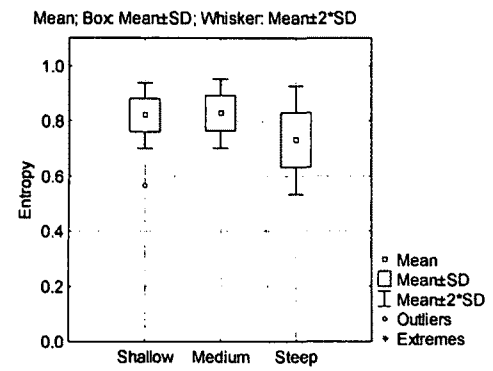

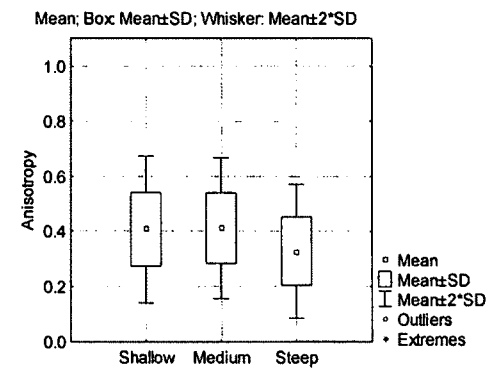

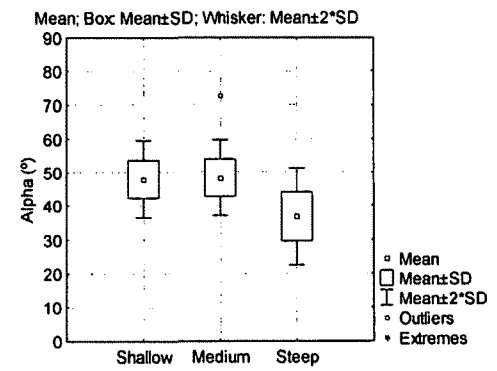

Low Centre Polygons

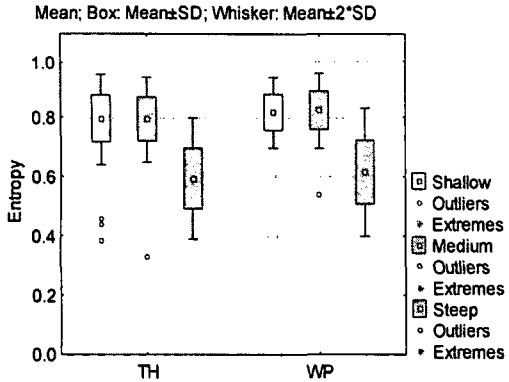

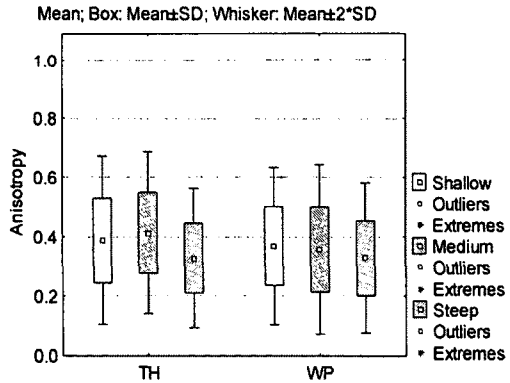

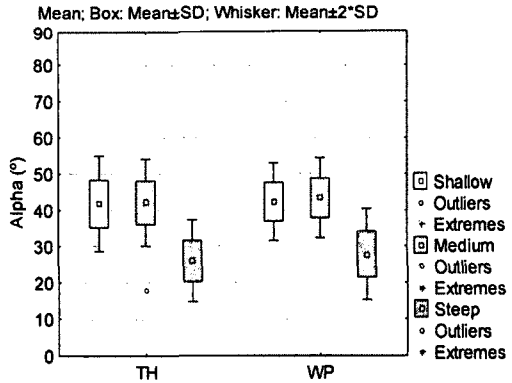

Eroding Tundra

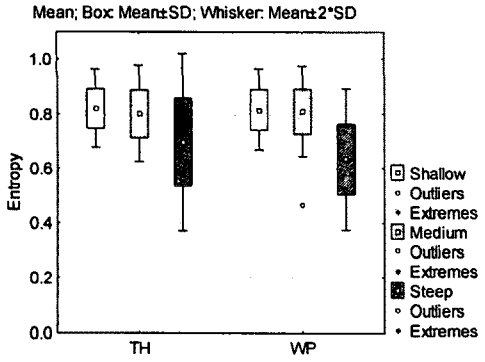

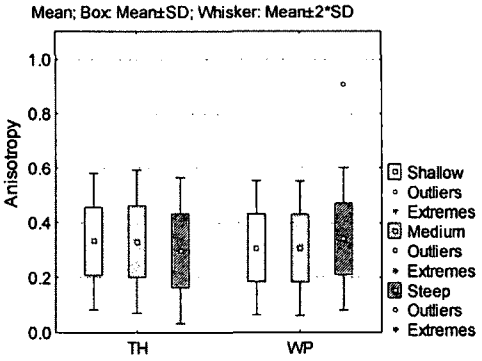

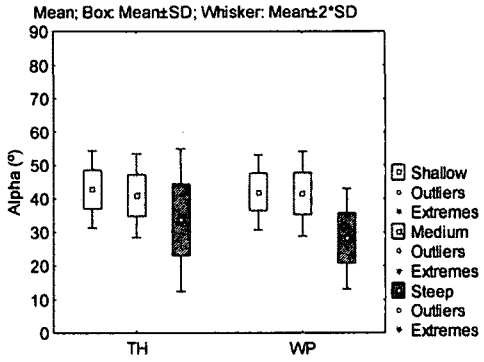

Herb Dominant Tundra

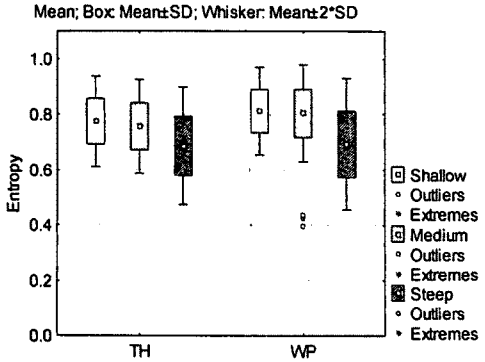

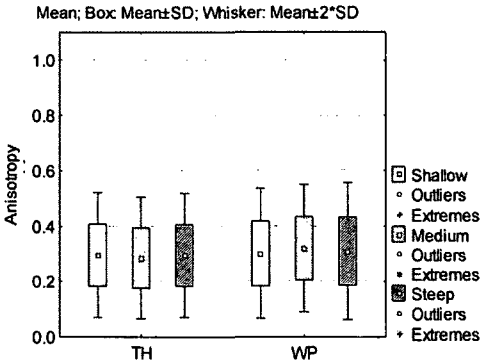

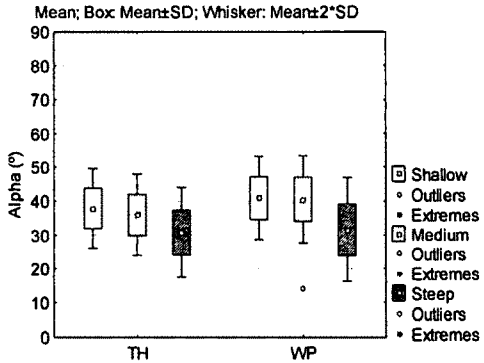

Shrub Dominant Tundra

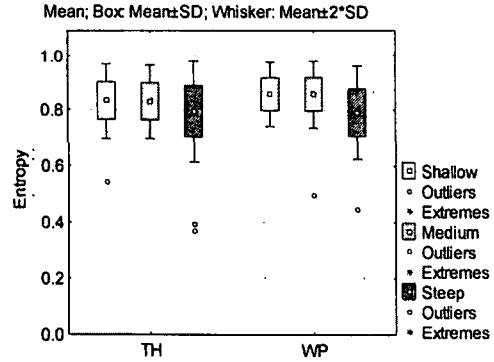

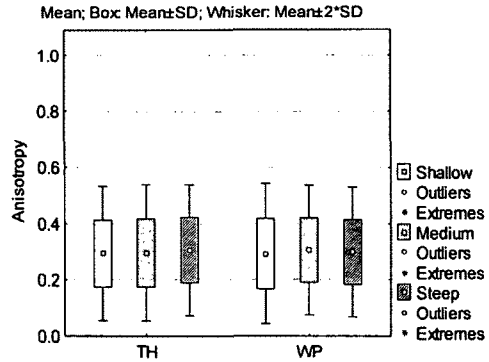

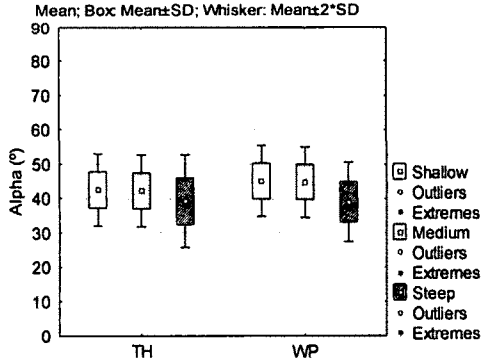

Appendix 9.

Results of the entropy-anisotropy feature space segmentations.

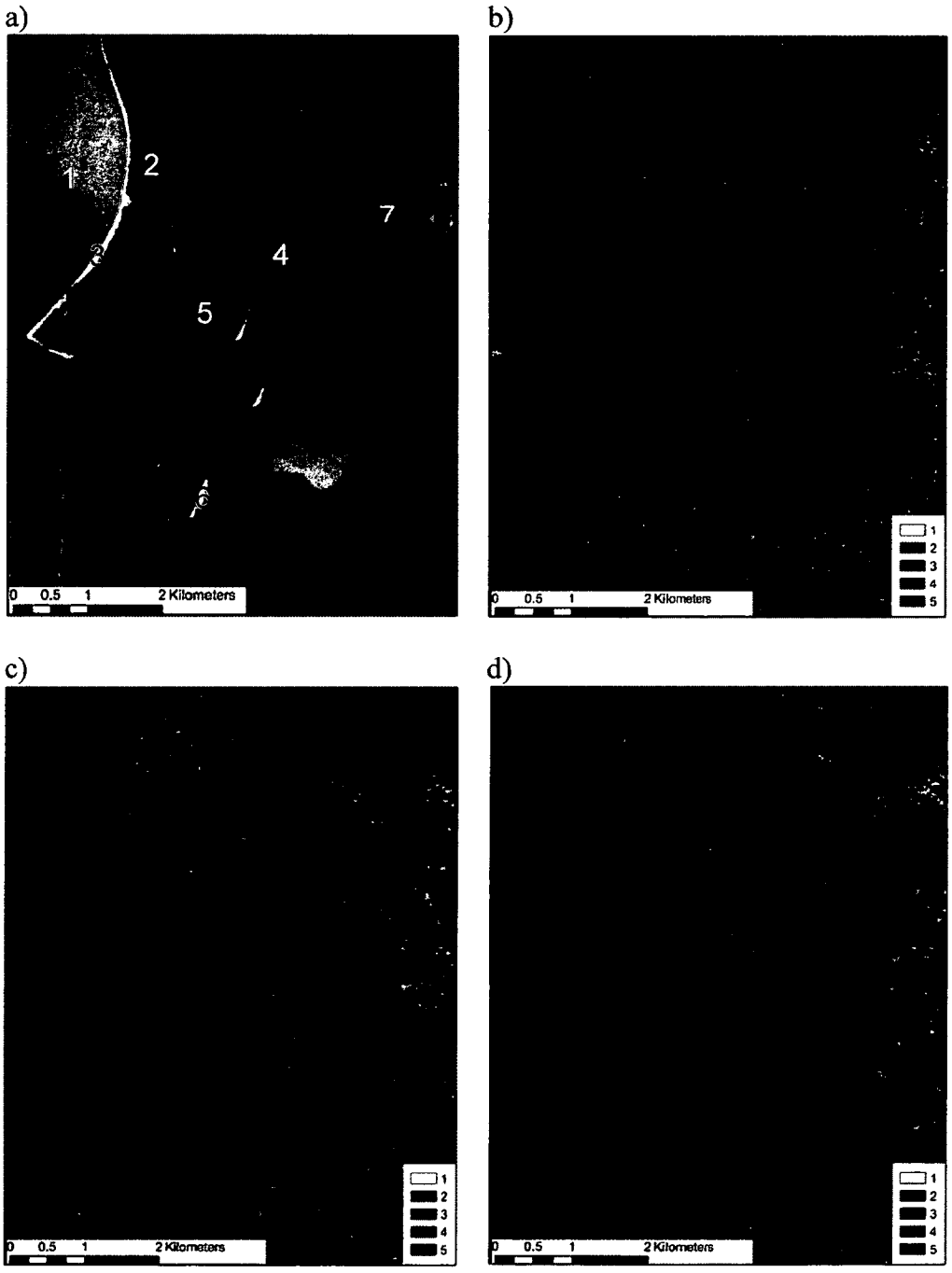

Figure 40: Ortho photo of TH study area (a), with numbers to represent areas where Water (1), Shrub Dominant Tundra (2), Sand (3), Herb Dominant Tundra (4), ILLT (5), Woody Debris (6), and Wetland (7) are present. Entropy-anisotropy segmentations for the same area are shown for shallow (b), medium (c) and steep angles (d).

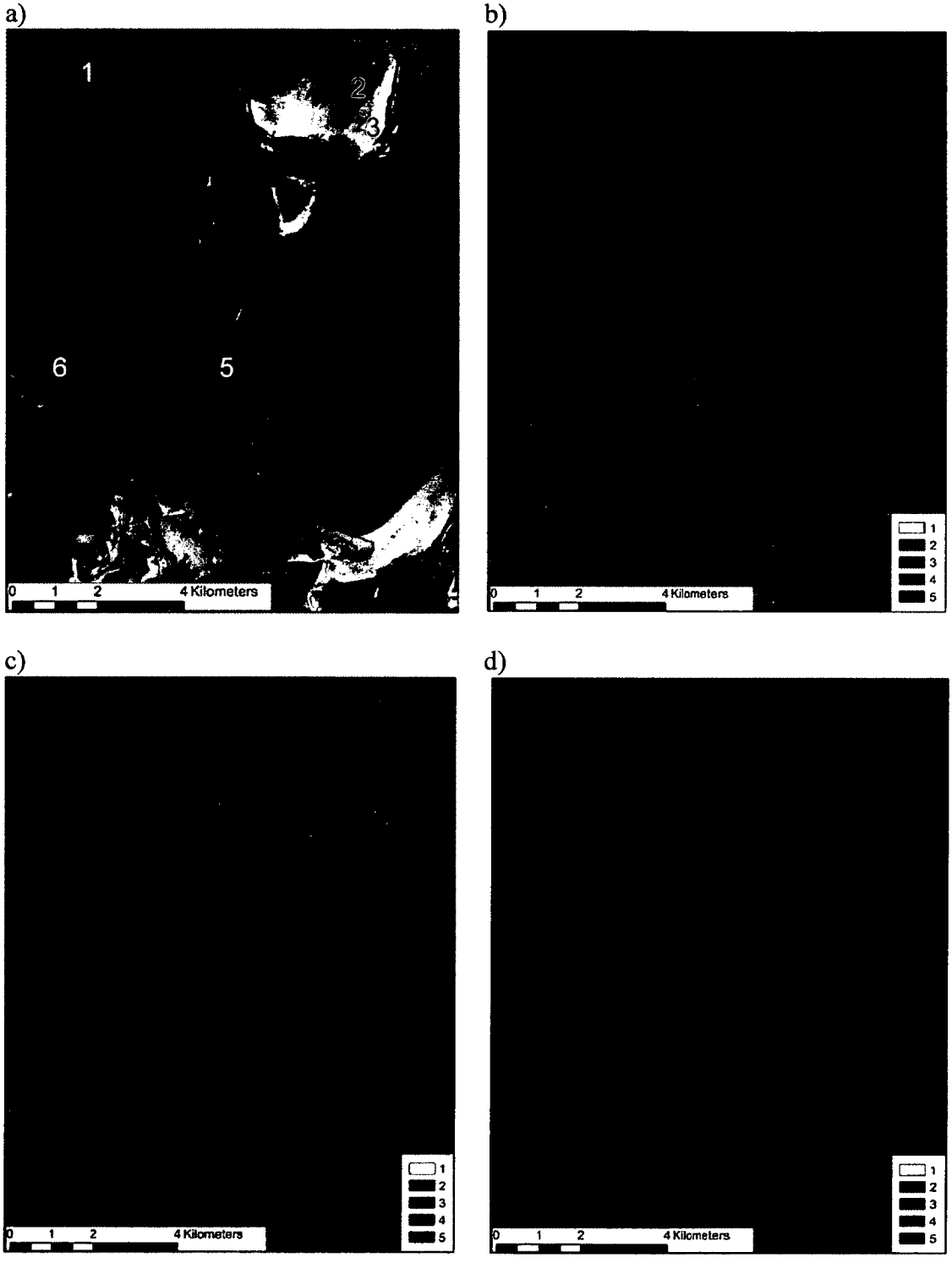

Figure 41: Ortho photo of WP study area (a), with numbers to represent areas where Water (1), Rough/Vegetated Mudflat (2) Smooth/Un-Vegetated Mudflat (3), Woody Debris (4), Shrub Dominant Tundra (5), and ILLT (6) are present. Entropy-anisotropy segmentations for the same area are shown for shallow (b), medium (c) and steep angles (d).

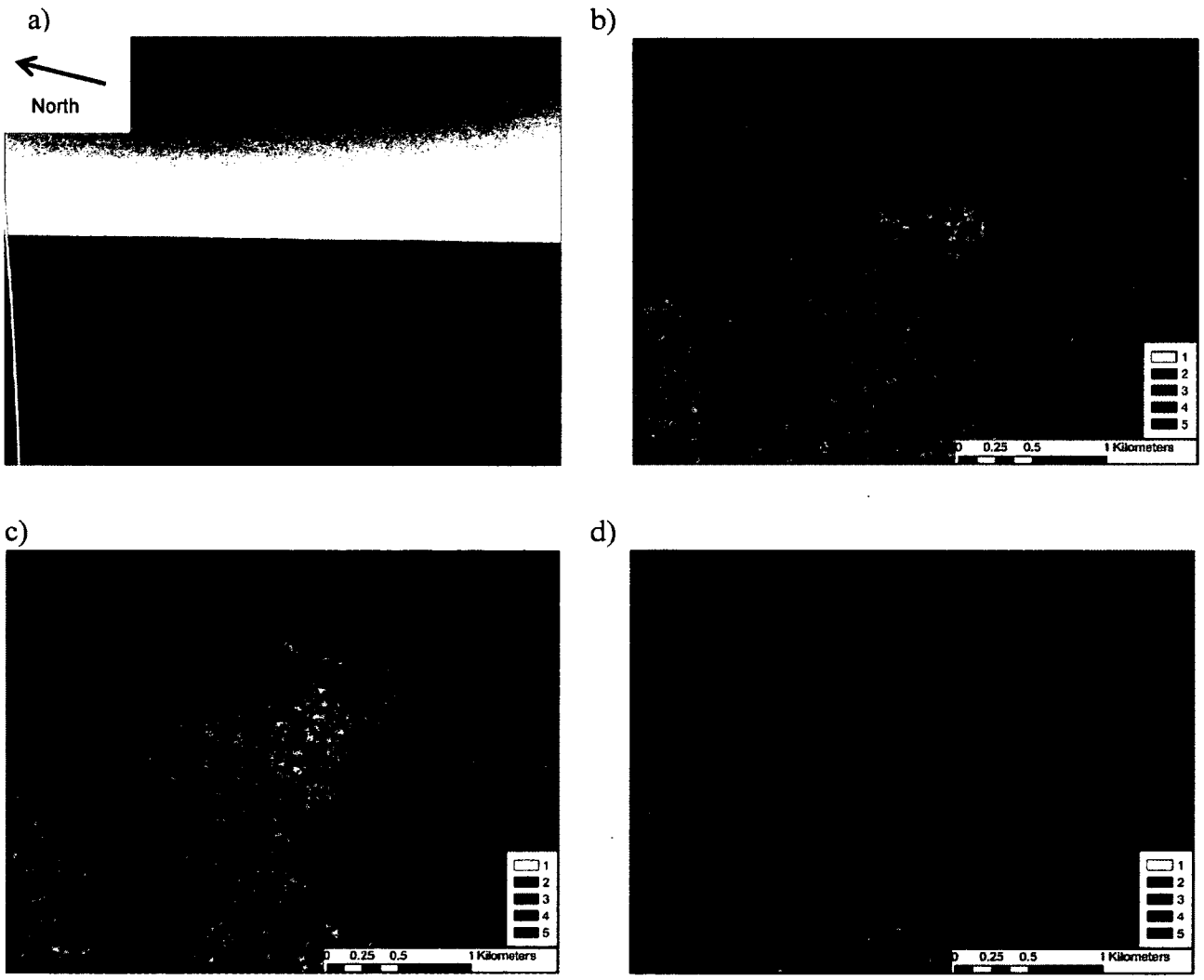

Figure 42: Snapshot from 2010 helicopter videography of a smooth and completley un-vegetated mudflat in the WP study area, as well as entropy-anisotropy segmentations of the same area for shallow (a), medium (b) and steep angles (c).

Appendix 10.

Confusion matrixes based on results of unsupervised Wishart-entropy/anisotropy/alpha classifiers.

Wishart-entropy/anisotropy/alpha (TH Shallow)

	Class	Sample Size	Class 1	2	3	4	5	6	7	8	10	11	12	13	14	15	16
	Anthropogenic	662	92	1	0	1	0	0	0	2	531	21	0	11	1	1	1
	Water	1960	0	0	1148	0	0	0	0	0	0	0	812	0	0	0	0
Substrates	Smooth/Un-vegetated Mudflat	268	0	0	22	0	0	77	0	0	0	0	161	2	1	5	0
	Peat	127	0	0	2	1	0	39	0	0	0	0	19	0	20	46	0
	Sand	834	0	0	7	1	0	456	0	0	0	0	213	0	9	147	1
	Mixed Sediment	760	56	172	0	40	104	0	26	89	26	76	0	6	141	12	12
	Riprap	140	3	48	0	10	20	0	0	9	7	28	0	6	9	0	0
	Wood/Substrate Mix	662	0	1	0	1	12	78	0	0	0	0	1	1	245	311	12
	Woody Debris	799	0	205	0	101	185	0	6	8	4	87	0	15	181	0	7
Vegetated Classes	Marsh	249	0	4	0	29	10	1	1	0	0	0	0	8	143	15	0
	Wetland	474	0	0	0	0	0	0	0	0	416	31	0	27	0	0	0
	ILLT	705	7	24	0	243	86	0	42	10	32	95	0	37	77	6	46
	Low Centre Polygons	813	0	68	0	240	69	0	33	31	10	126	0	81	89	0	66
	Eroding Tundra	489	216	21	0	13	7	0	22	72	64	72	0	0	2	0	0
	Herb Dominant Tundra	806	0	87	0	74	250	0	55	7	0	6	0	4	150	0	173
	Shrub Dominant Tundra	942	648	14	0	0	0	0	4	207	54	15	0	0	0	0	0

Wishart-entropy/anisotropy/alpha (TH Medium)

	Class	Sample Size	Class 1	2	3	4	5	6	7	8	10	11	12	13	14	15	16
	Anthropogenic	662	299	6	0	4	1	6	7	2	274	22	0	13	5	12	11
	Water	1960	0	0	1479	0	0	0	0	0	0	0	481	0	0	0	0
Substrates	**Smooth/Un-vegetated Mudflat**	268	0	0	161	0	0	0	0	0	0	0	92	0	0	15	0
	Peat	127	0	0	2	0	0	21	0	0	0	1	11	0	4	88	0
	Sand	834	0	0	39	0	0	15	0	0	0	0	326	1	0	453	0
	Mixed Sediment	760	8	92	0	21	49	203	15	51	0	35	1	23	235	20	7
	Riprap	140	1	11	0	12	8	25	1	9	2	12	0	16	38	3	2
	Wood/Substrate Mix	662	0	2	0	5	0	206	0	0	0	0	15	8	3	423	0
	Woody Debris	799	7	397	0	18	21	114	14	11	0	126	0	18	73	0	0
Vegetated Classes	**Marsh**	249	0	4	0	43	5	76	3	1	0	2	1	67	29	15	0
	Wetland	474	15	0	0	0	0	0	0	0	456	1	0	2	0	0	0
	ILLT	705	10	64	0	215	19	115	17	7	54	48	0	94	41	13	8
	Low Centre Polygons	813	0	31	0	178	5	135	14	2	9	112	0	219	87	7	14
	Eroding Tundra	489	199	58	0	8	20	4	39	88	24	34	0	0	11	0	4
	Herb Dominant Tundra	806	0	9	0	92	69	580	5	0	0	1	0	14	18	14	4
	Shrub Dominant Tundra	942	159	69	0	6	51	0	133	388	5	32	0	1	28	0	70

Wishart-entropy/anisotropy/alpha (TH Steep)

	Class	Sample Size	Class														
			1	2	3	4	5	6	7	8	10	11	12	13	14	15	16
	Anthropogenic	662	141	13	0	22	17	32	8	12	0	218	52	2	89	42	8
	Water	1960	0	0	674	0	0	0	0	0	0	0	1286	0	0	0	0
Substrates	Smooth/Un-vegetated Mudflat	268	0	0	264	0	0	0	0	0	0	0	0	3	0	0	1
	Peat	127	0	0	19	0	0	0	0	0	0	0	2	24	0	0	82
	Sand	834	0	0	445	0	0	13	0	20	0	0	0	27	0	0	329
	Mixed Sediment	760	0	19	39	19	55	151	13	52	0	0	81	8	14	45	247
	Riprap	140	0	13	0	2	5	44	0	3	0	0	32	0	3	14	24
	Wood/Substrate Mix	662	0	0	130	0	0	50	0	1	0	0	1	39	0	1	440
	Woody Debris	799	0	12	0	6	31	250	17	42	0	0	143	0	24	212	51
Vegetated Classes	Marsh	249	3	3	6	4	1	60	1	38	0	0	18	1	0	36	77
	Wetland	474	332	18	0	39	0	0	2	0	0	0	8	0	74	1	0
	ILLT	705	0	29	0	1	69	126	15	79	0	0	103	1	15	197	60
	Low Centre Polygons	813	1	42	0	5	83	205	0	36	0	0	221	0	8	137	71
	Eroding Tundra	489	54	48	0	2	48	41	133	12	0	0	62	0	10	45	18
	Herb Dominant Tundra	806	0	2	0	0	18	176	16	270	0	0	2	0	0	71	251
	Shrub Dominant Tundra	942	1	15	0	59	103	40	220	184	0	0	9	0	32	145	5

Wishart-entropy/anisotropy/alpha (WP Shallow)

	Class	Sample Size	Class 1	2	3	4	5	6	7	8	10	11	12	13	14	15	16
	Water	1056	0	0	448	0	0	0	0	0	0	0	608	0	0	0	0
Substrates	Smooth/Un-vegetated Mudflat	1050	0	0	0	0	1	804	0	0	0	0	100	0	35	110	0
	Rough/Vegetated Mudflat	937	0	9	0	1	403	0	0	63	1	419	0	0	7	0	34
	Peat	171	2	10	0	0	55	11	0	5	2	38	0	2	43	3	0
	Sand	1233	0	1	41	0	31	211	0	0	0	4	364	1	249	331	0
	Mixed Sediment	688	1	84	0	30	235	0	0	19	0	273	0	28	14	0	4
	Wood/Substrate Mix	425	31	26	0	9	48	0	4	23	14	139	0	49	48	2	32
	Woody Debris	724	0	0	0	0	0	0	14	3	0	2	0	0	0	0	705
Vegetated Classes	Marsh	923	138	34	0	156	84	0	3	15	27	97	0	225	137	6	1
	Wetland	198	61	1	0	6	0	0	0	0	98	11	0	19	1	1	0
	ILLT	725	246	101	0	204	1	0	1	32	41	88	0	8	0	0	3
	Low Centre Polygons	681	59	95	0	115	30	0	3	20	39	112	0	175	27	0	6
	High Centre Polygons	779	300	41	0	24	0	0	4	22	340	26	0	17	0	0	5
	Eroding Tundra	477	90	50	0	39	2	0	44	75	8	20	0	0	0	0	149
	Herb Dominant Tundra	989	55	210	0	264	156	0	3	109	11	72	0	94	15	0	0
	Shrub Dominant Tundra	818	1	0	0	0	0	0	268	14	0	0	0	0	0	0	535

Wishart-entropy/anisotropy/alpha (WP Medium)

	Class	Sample Size	Class														
			1	2	3	4	5	6	7	8	10	11	12	13	14	15	16
	Water	1056	0	857	0	0	0	0	0	0	0	199	0	0	0	0	0
Substrates	Smooth/Un-vegetated Mudflat	1050	0	0	5	0	0	128	0	0	0	0	126	0	0	791	0
	Rough/Vegetated Mudflat	937	0	2	0	0	8	101	0	179	0	3	0	20	624	0	0
	Peat	171	0	7	0	1	3	39	2	0	0	23	0	4	79	2	11
	Sand	1233	0	1	57	0	2	134	0	0	0	24	435	2	13	536	29
	Mixed Sediment	688	0	27	0	0	67	39	1	17	0	114	0	13	367	5	38
	Wood/Substrate Mix	425	5	58	0	2	23	23	3	50	1	65	0	23	78	29	65
	Woody Debris	724	0	6	0	2	0	0	0	716	0	0	0	0	0	0	0
Vegetated Classes	Marsh	923	18	109	0	92	11	80	42	10	10	188	0	43	107	59	154
	Wetland	198	64	27	0	18	1	0	1	2	40	21	0	13	1	1	9
	ILLT	725	16	276	0	84	47	0	89	13	17	59	0	43	33	0	48
	Low Centre Polygons	681	1	89	0	20	14	1	44	2	40	218	0	4	34	3	211
	High Centre Polygons	779	241	115	0	111	2	0	30	26	97	36	0	117	2	0	2
	Eroding Tundra	477	20	67	0	82	33	0	48	179	0	0	0	23	5	0	20
	Herb Dominant Tundra	989	3	104	0	26	134	6	120	67	0	82	0	14	118	0	315
	Shrub Dominant Tundra	818	1	1	0	13	10	0	20	757	0	0	0	16	0	0	0

Wishart-entropy/anisotropy/alpha (WP Steep)

	Class	Sample Size	Class 1	2	3	4	5	6	7	8	10	11	12	13	14	15	16
	Water	1056	0	0	304	0	0	0	0	0	0	0	752	0	0	0	0
Substrates	**Smooth/Un-vegetated Mudflat**	1050	0	0	507	0	0	2	0	0	430	0	16	0	0	95	0
	Rough/Vegetated Mudflat	937	1	0	0	0	1	78	0	0	0	0	0	502	28	327	0
	Peat	171	1	0	0	8	12	41	0	0	1	0	0	44	35	27	2
	Sand	1233	33	0	322	0	4	34	2	0	311	1	11	31	4	480	0
	Mixed Sediment	688	22	19	3	12	34	297	3	21	10	40	0	60	67	100	0
	Wood/Substrate Mix	425	52	11	5	0	21	104	8	1	56	8	0	26	19	109	5
	Woody Debris	724	6	0	0	415	67	12	0	0	7	0	0	115	87	4	11
Vegetated Classes	**Marsh**	923	33	36	57	29	62	186	18	8	132	29	5	17	142	162	7
	Wetland	198	14	19	0	26	9	27	7	5	1	39	0	4	39	5	3
	ILLT	725	0	37	0	57	118	5	121	62	0	48	0	2	151	0	124
	Low Centre Polygons	681	51	79	0	10	79	136	15	88	0	68	0	2	117	4	32
	High Centre Polygons	779	0	27	0	118	102	2	170	11	0	24	0	3	139	0	183
	Eroding Tundra	477	33	49	0	99	32	53	23	34	6	26	0	31	76	0	15
	Herb Dominant Tundra	989	316	203	0	0	22	89	31	132	5	103	0	8	65	6	9
	Shrub Dominant Tundra	818	0	19	0	131	66	0	235	14	0	1	0	0	67	0	285

Appendix 11.

Polarizations that showed the highest separability (bolded and italicized) for each class pair, where S = shallow, M = medium, and T = steep incidence angles. If more than one image achived moderate separability (BD > 1.5), it is also provided. Refer to Table 24 and Table 25 for the highest BD achieved for each pair.

TH Study Area

	Anthropogenic	Water	Smooth/Un-Vegetated Mudflats	Peat	Sand	Mixed Sediment	Riprap	Wood/ Substrate Mix	Woody Debris	Marsh	Wetland	ILLT	Low Centre Polygons	Eroding Tundra	Herb Dominant Tundra
Water	***S: HH*** HV VV M: HH HV VV T: HV														
Smooth/Un-Vegetated Mudflat	***S: HH*** HV VV M: HH HV VV T: HV	***T: HH***													
Peat	***S: HH*** HV	***M: HV***	***T: HV***												
Sand	***S: HH*** HV VV M: HH HV VV	***T: VV***	***T: HV***	***S:T: VV***											
Mixed Sediment	***S: HH***	***S: HH*** HV VV ***M: HH HV*** VV T: HV	S: HH HV VV ***M:*** HH ***HV*** VV T: HV	***S:T: HV***	***S: HH*** HV ***VV*** M: HV VV										
Riprap	***S: HH***	***S: HH HV*** VV M: HH HV VV T: HV	***S: HH*** HV M: HH HV T: HV	***S:T: HV***	***S: HH*** HV VV M: HV	***T: HV***									
Wood/ Substrate Mix	***S: HH*** HV VV	***S: HH*** HV M: HH HV	S: HH ***M: HH*** M: HV T: HV	***S:T: VV***	***S: HH***	***T: VV***	***S: HH***								
Woody Debris	***S: VV***	***S: HH HV*** VV ***M: HH HV*** VV ***S:T: HV***	S: HH HV ***M: HH HV*** VV ***S:T: HV***	***S: HH***	***S: HH*** HV VV M: HH HV VV	***M: HH***	***T: VV***	***M: HH***							
Marsh	***S: HH***	S: HH HV VV ***M: HH HV*** VV T: HV	S: HH HV ***M:*** HH ***HV*** T: HV	***S: HV***	S: HV ***M: HV***	***T: HH VV***	***S: HH***	***M: HV***	***M: HH***						
Wetland	***T: VV***	***S: HH HV VV M: HH HV VV T: HV***	***S: HH HV*** VV ***M: HH HV*** VV ***T: HV***	S: HH HV VV M: HH HV VV ***T: HV***	***S:*** HH HV ***VV*** M: HH HV VV T: HV	***T: HH***	***T: HH***	S: HH VV M: HH VV ***T:*** HH ***HV***	***S: VV***	***S:*** HH ***VV*** M: HH VV					
ILLT	***S: HH***	***S: HH HV*** VV ***M: HH HV*** VV ***T: HV***	S: HH HV ***M:*** HH ***HV*** ***T: HV***	***S: HV*** T: HV	***S:*** HH ***HV*** M: HV	***T: HV***	***T: VV***	***S: HV***	***M: HH***	***S: HV***	***M: VV***				
Low Centre Polygons	***S: HH***	***S: HH HV*** VV ***M: HH HV*** VV ***T: HV***	S: HH HV ***M:*** HH ***HV*** ***T: HV***	S: HV ***T: HV***	***S:*** HH ***HV*** M: HV	***T: HV***	***S: HH***	***T: HV***	***M: HH***	***S: HV***	***M: VV***	***S: VV***			
Eroding Tundra	***S: HH***	***S: HH HV*** VV ***M: HH HV*** VV ***T: HV***	***S: HH HV*** VV ***M:*** HH ***HV*** VV ***T: HV***	***S:*** HH ***HV*** M: HV T: HV	***S:*** HH ***HV*** VV M: HH HV VV T: HV	***M: HV***	***S: HV***	***S: HV*** M: HV	***S: HV***	***S: HV***	***S: HH***	***S: HV***	***M: HV***		
Herb Dominant Tundra	***S: HH***	***S: HH HV*** VV ***M: HH HV*** VV ***T: HV***	***S:*** HH ***HV*** ***M:*** HH ***HV*** ***T: HV***	***S: HV***	***S:*** HH ***HV*** M: HV	***M: VV***	***T: VV***	***S: HV***	***M: HH***	***S: HV***	***M:*** HH ***VV*** ***T: HH***	***S: HH***	***T: HH***	***M: VV***	
Shrub Dominant Tundra	***S: HH***	***S: HH HV VV M: HH HV VV T: HV***	***S: HH HV*** VV ***M: HH HV*** VV ***T: HV***	***S:*** HH ***HV*** VV M: HV T: HV	***S:*** HH ***HV*** VV M: HH HV VV T: HV	***S: HV***	***S: HV***	***S:*** HH ***HV*** VV M: HV T: HV	***S: HV***	***S: HV*** VV	***T: HH***	***S: HV***	***S: HV***	***T: HH***	***S: HV***

WP Study Area

	Water	Smooth/Un-Vegetated Mudflats	Rough/ Vegetated Mudflat	Peat	Sand	Mixed Sediment	Wood/ Substrate Mix	Woody Debris	Marsh	Wetland	ILLT	High Centre Polygons	Low Centre Polygons	Eroding Tundra	Herb Dominant Tundra
Smooth/Un-Vegetated Mudflats	***S: VV*** M: VV														
Rough/ Vegetated Mudflat	***S: HH HV VV*** ***M: HH HV VV*** ***T: HV*** VV	***S: HH*** HV VV M: HH HV VV T: HV													
Peat	S: HH HV VV ***M: HH*** HV ***VV*** ***T: HV***	M: HV ***T: HV***	***M: HV***												
Sand	***T: HV***	***M: VV***	S: VV ***M: HV*** VV	***M: HV***											
Mixed Sediment	***S: HH HV*** VV ***M: HH HV VV*** ***T: HV***	***S: HH*** HV M: HH HV T: HV	***T: VV***	***T: VV***	***S: HV***										
Wood/ Substrate Mix	***S: HH*** HV VV M: HH HV VV T: HV	***S: HH*** HV M: HH HV	***T: VV***	***T: VV***	***S: HH***	***T: HV***									
Wood Cover 100%	***S: HH HV VV*** ***M: HH HV VV*** ***T:*** HH ***HV***	***S: HH HV*** VV ***M: HH HV*** VV T: HH HV	***S: HH*** M: HV	S: HH ***M: HH*** HV	***S:*** HH ***HV*** VV ***M:*** HH ***HV*** VV T: HV	S: HH HV ***M: HH*** HV	***M: HV***								
Marsh	***S: HH*** HV VV M: HH HV VV T: HV	***S: HH HV*** M: HV	***M: VV***	***S: VV***	***S: HV***	***S: VV***	***S: VV***	***S:*** HH ***VV*** M: HH VV							
Wetland	***S: HH HV VV*** ***M: HH HV***VV ***T: HV***	***S: HH*** HV M: HH HV T: HV	***T: VV***	***S: HH***	***S: HH*** HV M: HH HV	***S: HH***	***S: HH***	***M: VV***	***S: HH***						
ILLT	***S: HH HV VV*** ***M: HH HV VV*** ***T: HV***	***S:*** HH ***HV*** ***M:*** HH ***HV*** T: HV	***T: VV***	***S: HV***	***S:*** HH ***HV*** M: HH HV T: HV	***S: HV***	***T: HV***	***M: HH*** VV M: HH VV	***T: HV***	***T: HV***					
High Centre Polygons	***S: HH HV VV*** ***M: HH HV VV*** ***T: HV***	***S: HH HV*** ***M:*** HH ***HV*** T: HV	***T: VV***	***S: HV***	***S:*** HH ***HV*** M: HH HV T: HV	***S: HV***	***T: HV***	***M: HH*** VV	***T: HV***	***T: HV***	***S: HH***				
Low Centre Polygons	S: HH HV VV ***M: HH HV*** VV ***T: HV***	***S:*** HH ***HV*** M: HH HV T: HV	***M: VV*** T: VV	***T: VV***	***S: HV*** M: HV	***M: VV***	***T: HV***	S: HH VV ***M: HH*** HV VV	***T: HV***	***S: HH***	***T: HV***	***S:M: HH***			
Eroding Tundra	***S: HH HV VV*** ***M: HH HV*** VV ***T: HV***	***S:*** HH ***HV*** ***M:*** HH ***HV*** T: HV	***S: HV***	***S: HV***	***S:*** HH ***HV*** M: HH HV	***S: HV***	***S: HV***	***M: HH***	***S: HV***	***S:M: HV***	***S: HV***	***S:M: HV***	***S:M: HV***		
Herb Dominant Tundra	***S: HH HV*** VV ***M: HH HV*** VV ***T: HV***	***S:*** HH ***HV*** M: HH HV T: HV	***T: VV***	***T: VV***	***S: HV*** M: HV	***T: VV***	***S: HV***	***S: HH*** VV M: HH VV	***T: VV***	***S: HH***	***T: HV***	***S: HH***	***T: VV***	***S: HH***	
Shrub Dominant Tundra	***S: HH HV VV*** ***M: HH HV VV*** ***T: HV***	***S: HH HV*** VV ***M:*** HH ***HV*** VV T: HV	***S: HV*** M: HV	***S: HV*** M: HV	***S:*** HH ***HV*** VV M: HH HV VV T: HV	***S: HV*** M: HV	***S: HV***	***M: HH***	***S: HV*** VV	***S: HV***	***S: HV***	***S: HV***	***S: HH***	***S: HV***	***S: HV***

Appendix 12.

Polarimetric images that showed the highest separability (bolded and italicized) for each class pair, where S = shallow, M = medium, and T = steep incidence angles. If more than one image achived moderate separability (BD > 1.5), it was also provided. Refer to Table 26 and 27 for the highest BD achieved for each pair.

TH Study Area

	Anthropogenic	Water	Smooth/Un-Vegetated Mudflats	Peat	Sand	Mixed Sediment	Riprap	Wood/Substrate Mix	Woody Debris	Marsh	Wetland	ILLT	Low Centre Polygons	Eroding Tundra	Herb Dominant Tundra
Water	***S*** ***M*** T														
Smooth/Un-Vegetated Mudflat	***S*** M T	***T***													
Peat	***S*** M T	***M*** T	***T***												
Sand	***S*** M T	M ***T***	***M***	***T***											
Mixed Sediment	***S***	***S*** ***M*** T	S ***M*** T	***S***	***S*** M										
Riprap	***S***	***S*** ***M*** ***T***	***S*** ***M*** ***T***	***S***	***S*** M T	***S***	***S***								
Wood/Substrate Mix	***S*** M	S ***M*** T	S ***M*** T	***T***	***S***	***S***	***T***	***M***							
Woody Debris	***S***	***S*** ***M*** ***T***	***S*** ***M*** ***T***	***S*** M ***T***	***S*** M T	***S***	***S***	***M***							
Marsh	***S***	***S*** ***M*** T	S ***M*** T	***S***	***S*** M	***S***	***T***	S M ***T***	***M***						
Wetland	***T***	***S*** ***M*** ***T***	***S*** ***M*** ***T***	S M ***T***	***S*** M T	***T***	***T***	***T***	S ***T***	***S*** M T					
ILLT	***S***	***S*** ***M*** ***T***	***S*** ***M*** ***T***	S M ***T***	***S*** M T	***T***	***S***	***T***	***S***	***S***	S M ***T***				
Low Centre Polygons	***S***	***S*** ***M*** ***T***	***S*** ***M*** ***T***	S M ***T***	***S*** M T	***T***	***M***	***S*** M T	***M***	***S***	S M ***T***	***M***			
Eroding Tundra	***S***	***S*** ***M*** ***T***	***S*** ***M*** ***T***	***S*** M T	***S*** M T	***M***	***M***	***S*** M T	***S***	***S***	***T***	***M***	***M***		
Herb Dominant Tundra	***S*** M	***S*** ***M*** ***T***	***S*** ***M*** ***T***	S M ***T***	***S*** M	***T***	***T***	***S***	***M***	***S***	S ***M*** T	***T***	***T***	***M***	
Shrub Dominant Tundra	***S***	***S*** ***M*** ***T***	***S*** ***M*** ***T***	***S*** M T	***S*** ***M*** T	***S***	***S***	***S*** M T	***S*** M	***S*** M	S M ***T***	***S***	***S*** M	***M***	***S*** M

WP Study Area

	Water	Smooth/Un-Vegetated Mudflat	Rough/Vegetated Mudflat	Peat	Sand	Mixed Sediment	Wood/Substrate Mix	Woody Debris	Marsh	Wetland	ILLT	High Centre Polygons	Low Centre Polygons	Eroding Tundra	Herb Dominant Tundra
Smooth/Un-Vegetated Mudflat	S ***M***														
Rough/Vegetated Mudflat	***S M T***	***S*** M T													
Peat	***S M T***	S ***M*** T	***M***												
Sand	***T***	***S***	S ***M***	***M***											
Mixed Sediment	***S M T***	***S*** M T	***T***	***S***	***S*** M										
Wood/Substrate Mix	***S*** M T	***S*** M T	***M***	***S***	***S***	***S***									
Woody Debris	***S M T***	***S M T***	***S*** M T	S ***M***	***S*** M T	***S M***	***M***								
Marsh	***S M*** T	***S*** M T	***M***	***S***	***S***	***S***	***M***	S ***M***							
Wetland	***S M T***	***S M*** T	***S*** M T	***S***	***S*** M	***S***	***M***	S ***M***	***M***						
ILLT	***S M T***	***S M T***	S ***M*** T	***S***	***S*** M T	***S***	***T***	S ***M***	***T***	***S***					
High Centre Polygons	***S M T***	***S M T***	S M ***T***	***S***	***S*** M T	***S***	***T***	S ***M***	***T***	***T***	***S***				
Low Centre Polygons	***S M T***	***S*** M T	S ***M*** T	***S***	***S*** M T	***M***	***M***	S ***M***	***T***	***S***	***S***	***M***			
Eroding Tundra	***S M T***	***S M*** T	S ***M***	***S***	***S*** M	***S***	***M***	***S***	***S***	***S***	***S***	***T***	***M***		
Herb Dominant Tundra	***S M T***	***S*** M T	M ***T***	***T***	***S*** M T	***S***	***S***	***S M*** T	***T***	***S***	***T***	***T***	***T***	***S***	
Shrub Dominant Tundra	***S M T***	***S M T***	***S*** M T	***S*** M	***S*** M T	***S*** M	***S*** M	***M***	***S*** M	***S*** M	***S*** M	***S*** M	***S***	***S***	***S***